The Electrochemistry Of Alcohols In Aqueous Phosphate Electrolytes Under Reducing Conditions.

A Thesis presented in partial fulfilment of the requirements for the degree of

Master of Philosophy

in

Chemistry

Massey University, Palmerston North,

New Zealand

Nessha M. Wise

2013

ABSTRACT

Few methods are available for the routine reduction of alcohols in synthetic chemistry. These few are dominated by reduction with HI/I_2, $LiAlH_4$ or Li/NH_3 and typically involve severe conditions for other functionalities and there is little research into less severe synthetic or electrochemical methods. There is also limited mechanistic or kinetic information available for these reduction methods. This leaves an interesting area for development within fundamental knowledge. The development of an effective process for the reduction of alcohols could have many applications in pharmaceutical and chemical industries along with many environmental and economical benefits.

A preliminary study on a range of electrodes established an electrochemical reduction response observed for a number of water-soluble alcohols on rotating disc copper, tin and lead electrodes in 0.1 M phosphate buffers.

A response was observed for ethanol, propanol, propan-2-ol and butanol on copper rotating disc electrodes in the 0.1 M phosphate buffer. Reduction of the alcohols at the copper disc electrodes was observed at pH 8.1 with the production of a limiting current plateau. The reduction was found to be continuous and reproducible. The observed limiting current was found to increase with both increasing concentration and increasing electrode rotation rate. A Koutecky-Levich study suggested the reduction of the alcohol occurred through both mass transport and kinetic processes.

A discrete, reproducible response was observed for ethanol, propanol and propan-2-ol on tin rotating disc electrodes in the 0.1 M phosphate buffer electrolyte at pH 7.3. A reductive peak was observed at –1.1 V vs Ag/AgCl in cyclic voltammetry. This formation of a reductive peak suggests that the reduction becomes progressively hindered, proposed to be due to a passivating layer forming on the surface of the electrode. The charge associated with the peak is relatively invariant with alcohol concentration (in the range 7–20 mM) and with scan rate (over the range 10–500 mV s^{-1}). In the case of ethanol, the peak charge is typically found to be in the range 2.9–3.6 C m^{-2} suggesting that a passivating layer of reaction products forms with an area of 8.8–10.8 $Å^2$ for each adsorbed molecule (assuming a 2-electron process and a surface roughness factor of one). This suggests formation of

a monolayer with sparsely located binding sites. The peak charge does not change with increasing electrode rotation rate, not inconsistent with the formation of a passivating layer on the surface of the electrode inhibiting any further reduction.

A discrete response was also observed for ethanol, propanol and propan-2-ol on lead rotating disc electrodes in the 0.1 M phosphate buffer electrolyte at pH 8.1. A reduction peak is observed at –0.9 V vs Ag/AgCl in cyclic voltammetry. This suggests that the reduction becomes progressively hindered due to a proposed passivating layer. The passivating layer is not permanent – employing a > 30 second open-circuit rest period or having an anodic limit more positive than –0.6 V will result in the new reduction peak for each subsequent voltammogram. Multiple-cycle voltammograms exhibit only the background response if these conditions are not met.

The charge associated with the peak decreases with scan rate (over the range 10–500 mV s^{-1}) but is relatively invariant with alcohol concentration (in the range 7–20 mM). In the case of ethanol, the peak charge is typically found to be in the range 0.5–4.0 C m^{-2} suggesting that a passivating layer of reaction products forms with an area of 19–58 $Å^2$ for each adsorbed molecule (assuming a 2–electron process and a surface roughness factor of one). This suggests formation of a monolayer with sparsely located binding sites.

The peak charge *decreases* with increasing electrode rotation rate. It is proposed that this is due to a surface chemical reaction following the electrochemical process – it is the product of this chemical reaction that results in a transient passivating monolayer. FT–IR analyses of the lead disc systems suggest possible products to be propandiol and butandiol.

ACKNOWLEDGEMENTS

First and foremost my thanks go to my supervisor, Prof. Simon Hall. Thank you for your encouragement, guidance, for always having time for me, and for clearing things up for me when I just kept confusing myself. Thank you also for you support and understanding for the life I have outside of Massey and the hard decisions I had to make. Thank you to my Co-supervisor Assoc. Prof. Mark Waterland. Thank you for your input and support over the past 4 years.

To all the IFS staff, for the help and support each of them has given me since returning to study. Whether academic assistance or personal support, they have all helped me get through the last few years. In particular, Colleen, Kat, Jenny and Adrian. To other students who understand what I am going through, particularly Shaune, Gaile and Doris, thanks for the listening ear and advice.

To my husband, Kent, for his support and encouragement and for having so much faith in my ability. When I needed it you would always gave me that little push but understood when everything was getting too much. To my three beautiful boys, having you around has made my time studying eventful and unpredictable, but I would not have made the choices I have or ended up where I am without you. Thank you to those close friends and family that have made these years go that little bit smoother, or gave me somewhere to escape to for a well needed break, just a cuppa and a chat goes a long way when you are stressed.

Lastly, thank you to my parents. Mum and Dad helped me get to where I am today, your support and encouragement over the years has been unfailing. My parents and my parents-in-law have been an immense help to me over the last few years supporting me with the transition from ‘at home mum’ to ‘career mum’. Thank you to my Mum’s for the continuous help with the smooth running of the household, the endless babysitting.

I know I could not have achieved this on my own and my gratitude goes out to all who supported me so faithfully.

TABLE OF CONTENTS

LIST OF TABLES

LIST OF FIGURES

LIST OF SYMBOLS

Symbol		Unit
A	area	m^2
A_N	area per molecule	nm^2
A1	first anodic peak	
Ag	Silver	
Au	Gold	
C1	first cathodic peak	
C2	second cathodic peak	
c_b	bulk concentration	mM
c_s	surface concentration	mM
Cu	Copper	
D	diffusion coefficient	$m^2\ s^{-1}$
δ	thickness of the Nernst diffusion layer	
E	potential	mV
E_1	initial potential	mV
E_2	final potential	mV
F	faraday constant	$C\ mol^{-1}$
h	thickness of the insulating layer	cm
I	current	A
I_L	limiting current	A
k_f	kinetic transfer rate constant	

m	mass of product	g
M	molar mass	g mol^{-1}
N_A	Avogadro's number	mol^{-1}
N_{C2}	number of molecules per unit area for peak C2	molecules m^{-2}
n_{C2}	moles of product per area for peak C2	mol m^{-2}
ρ	density	g cm^{-3}
Pb	Lead	
Pb_{BS}	Pb electrode binding site	
Pb_{surf}	Pb electrode surface	
Pb_{surf}-H_{ads}	H adsorbed to Pb electrode surface	
Pd	Palladium	
Pt	Platinum	
Q	charge	C
q	charge per unit area	C m^{-2}
Re	Reynold's number	
Sn	Tin	
r	radius	m
V	volume	cm^3
υ	kinematic viscosity of a fluid	m^2 s^{-1}
ω	electrode rotation rate	rad s^{-1}
z	number of electrons	

LIST OF ABBREVIATIONS

CA	Chronoamperometry
CE	Counter Electrode
Cu RDE	Copper Rotating Disc Electrode
CV	Cyclic Voltammetry
FT-IR	Fourier Transform Infrared spectroscopy
MS	Mass Spectrometry
MSCV	Mass Spectrometry Cyclic Voltammogram
Pb RDE	Lead Rotating Disc Electrode
RDE	Rotating Disc Electrode
RE	Reference Electrode
RHE	Reversible Hydrogen Electrode
rpm	revolutions per minute
SCE	Standard Calomel Electrode
SERS	Surface Enhanced Raman Spectroscopy
SHE	Standard Hydrogen Electrode
Sn RDE	Tin Rotating Disc Electrode
THF	Tetrahydrofuran
WE	Working Electrode

CHAPTER 1

Introduction

1.1 Introduction

This thesis is concerned with the electrochemical processes of simple alcohols in aqueous systems. This work was initially focused on the electrochemical reduction of alcohols. Synthetic methods for the reduction of alcohols typically have severe conditions and there is little research into less severe synthetic or electrochemical methods.[1-5] There have been some reports on the electrochemical reduction of a limited range of alcohols,[6-12] but there is little mechanistic or kinetic information. The development of an effective electrochemical process for the reduction of alcohols could have many applications in pharmaceutical and chemical industries, along with many environmental and economical benefits. The electrochemical reduction of five low-molecular weight alcohols were investigated; methanol, ethanol, propanol, propan-2-ol, butanol, in 0.1 M aqueous phosphate buffer solutions. However, experimental results suggest processes other than reduction are involved.

1.2 Reduction of alcohols

Alcohols are considered versatile organic reagents that are used as precursors for other organic molecules in synthetic chemistry. However, the hydroxyl group is a poor leaving group so generally requires activation before treating with a reducing agent.[13] A reducing agent is the element or compound in a redox reaction that reduces another species. In doing so, it becomes *oxidized*, and is therefore the electron donor in the redox. Strong reducing agents easily lose (or donate) electrons. Good reducing agents tend to consist of atoms with a low electronegativity, and species with relatively small ionization energies serve as good reducing agents also.[14,15] Examples of good reducing agents for alcohols are: the metal hydride reducing agents such as $NaBH_4$, NaH, LiH, $LiAlH_4$ and CaH_2, which act as hydride donors; phosphites and hypophosphoric acid; and active metals such as potassium, calcium, barium, sodium and magnesium.[14] Figure 1.1 provides some examples of reducing agents and their structures.

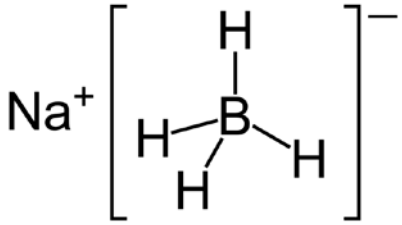

a) Sodium Borohydride, $NaBH_4$,

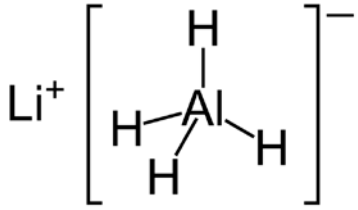

b) Lithium Aluminium Hydride, $LiAlH_4$,

c) Phosphite ion resonance structures

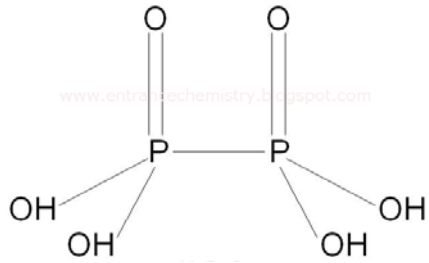

d) Hypophosphoric acid

Fig. 1.1 Examples of common reducing agents used in organic chemistry. a) sodium borohydride, b) lithium aluminium hydride, c) phosphites, and d) hypophosphoric acid.

Alcohols are readily produced by fermentation followed by distillation and are abundant in nature. Large alcohols exist in biological systems comprising up to 30 carbon atoms. They are found on the leaves of plants, the waxy surface of fruits and a wide array of other biological sources.[15,16,17] Polyfunctional or branched compounds with alcohol functionality are often isolated from volatile oils of plants by the process of steam distillation.[15,16] Substances such as cholesterol, found in most animal tissues (and abundant in egg yolks), and retinol (vitamin A alcohol), extracted from fish liver oils, are examples of naturally occurring sources of alcohol functionality. The common sugar alcohols – sorbitol, mannitol, maltitol, etc – can be manufactured from sources such as cornstarch, corn cobs, sugar cane bagasse (stalk residue remaining after sugar extraction), or birch wood waste.[15,16] Sugar alcohols are often referred to as polyols, a generic term that represents a family of different products, not a unique single compound. The polyol glycerol may be derived from triacylglycerides in fats and oils.

Figure 1.2 provides the structures and formulae for several alcohols found in biological systems.

An effective process for the reduction of these abundant alcohols to alkanes could have many applications in industry, providing important starting materials in many industries such as pharmaceuticals, manufacture of polythene, and the rubber industry, for fuels such as petrol, diesel, aviation fuel, and LPG, and for generating electricity, cooking and heating provided the cost of the processes was sufficiently low. [18]

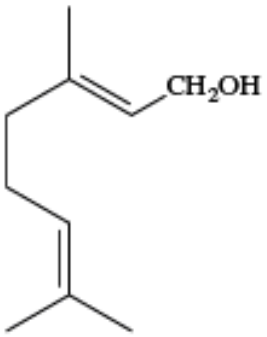

a) geraniol
geranium oil

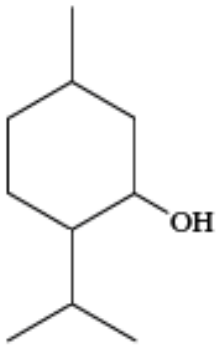

b) menthol
peppermint oil

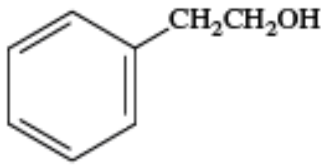

c) 2-phenylethanol,
rose oil

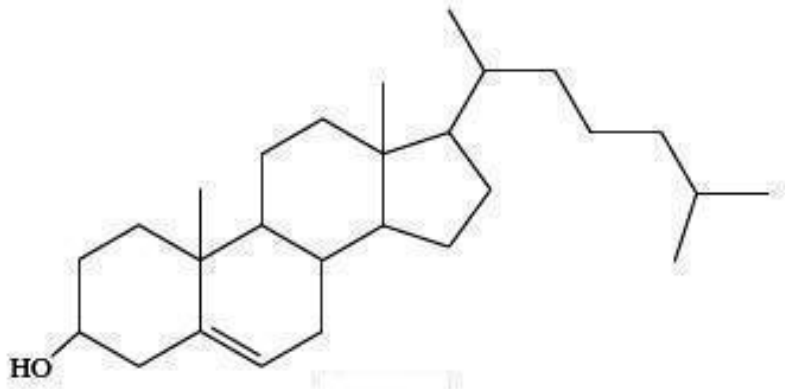

d) cholesterol (egg yolks)

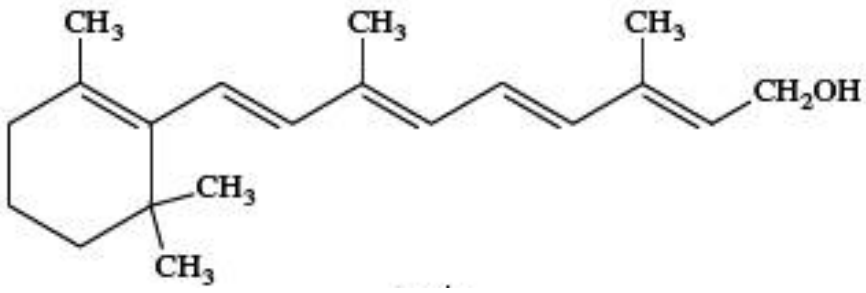

e) retinol (vitamin A alcohol)

Fig. 1.2 Structural formula of some alcohols found occurring naturally. a) geraniol, b) menthol, c) 2-phenylethanol, d) cholesterol, e) retinol.

1.3 Literature Review

1.3.1 Synthetic Reduction of Alcohols

There are relatively few bulk synthetic methods available for the reduction of alcohols. Three main methods HI/I_2, $LiAlH_4$ and Li/NH_3, together with a relatively recently reported method involving silanes and an $InCl_3$ catalyst are described below.

1.3.1.1 Iodine/Hydrogen Iodide method, HI/I_2

Hydrogen iodide, HI, is used in organic chemistry to convert primary alcohols into alkyl halides[1]. This reaction is initiated by an S_N2 substitution, in which the iodide ion replaces the 'activated' hydroxyl group. This activation process involves protonation of the OH group (to form a more favourable leaving group) followed by an S_N2 substitution by iodide forming the alkyl halide.

$$C_3H_7OH + HI \rightarrow C_3H_7OH_2^+ + I^- \xrightarrow[S_N2]{} C_3H_7I + H_2O \qquad (1.1)$$

Alkyl iodides are typically unstable, since iodide is a good leaving group. Therefore an elimination reaction follows to form the alkene or a substitution with further HI to form the corresponding alkane.

$$C_3H_7I \rightarrow C_3H_6 + HI \quad \text{(elimination)} \qquad (1.2)$$

$$C_3H_7I + HI \rightarrow C_3H_8 + I_2 \quad \text{(substitution)} \qquad (1.3)$$

The H^+---I^- interaction in hydrogen iodide facilitates dissociation of the proton from the anion making HI the strongest acid of the hydrohalides.[19] HI is preferred over other hydrogen halides in polar protic solvents since the iodide ion is a much better nucleophile than bromide or chloride, resulting in the reaction taking place at a reasonable rate without significant heating.[19] This is due to the large iodide anion being less solvated and more reactive in polar protic solvents than other smaller halides such as chloride. This causes the reaction to proceed faster for iodide because

of stronger partial bonds in the transition state. This method also reduces secondary and tertiary alcohols to alkanes, but here substitution occurs via an S_N1 pathway.[16]

The reduction of alcohols using HI is typically conducted in the presence of red phosphorus so that the iodine product can be reduced back to the iodide anion for use in further reduction of alcohol. This process has recently seen widespread and notorious use for the illegal production of methamphetamine.[20,21]

The iodine-sensitised decomposition of methanol has been extensively examined by Rollefson and Garrison where specific amounts of solid HI were introduced into a cell containing gaseous methanol at 325ºC.[21] This gas phase reaction reported by Rollefson and Garrison may have some relevance to the work reported in this thesis as the products obtained from the electrochemical processes in this work appear to be somewhat present in the gas phase. Rollefson and Garrison determined that optimal conditions for the reaction to occur are in the gas phase, where methane, iodine and water were produced according to:[22]

$$CH_3OH(g) + HI(s) \rightarrow CH_3I + H_2O(g) \quad (1.4)$$

$$CH_3I + HI(s) \rightarrow CH_4(g) + I_2 \quad (1.5)$$

Giving the overall reaction:

$$CH_3OH(g) + 2HI(s) \rightarrow CH_4(g) + I_2 + H_2O(g) \quad (1.6)$$

In this case of the simplest alcohol, methanol, the elimination process to form an alkene is not possible.

Mitchel and Williams[23] reported similar reactions for the reduction of alcohols by HI but state that complete reduction with HI/I_2 is difficult and the second substitution step may take place only partially giving a mixture of both the alkyl iodide and alkanes as final products.

1.3.1.2 Lithium Aluminium Hydride, $LiAlH_4$, method

The known reactions of $LiAlH_4$ with organic compounds consist essentially of the displacement of a strongly electronegative element, (such as oxygen, nitrogen or halides), on a carbon by a hydride ion. Reductions by $LiAlH_4$ involve a nucleophilic attack on the carbon by complex hydride ions.[24] While there are detailed mechanisms of the reduction of carboxylic acids or carbonyls by $LiAlH_4$ reported in

the literature, little mechanistic information is offered for the reduction of alcohols. However, the generally accepted overall process is as follows:[25]

$$LiAlH_4 + 2R{-}OH \rightarrow 2R{-}H + Li^+ + Al^{3+} + O_2 \qquad (1.7)$$

Here, the lithium aluminium hydride is thought to dissociate to Li^+ and AlH_4^-, and there is a nucleophilic attack by the hydride ion on the functional carbon.[26]

Ashby and Goel performed ESR studies on the reduction of alcohols with $LiAlH_4$ and deduced it to be a single electron transfer mechanism.[27] However, no detailed mechanistic information was provided. Further study into the mechanism of the reduction of alcohols by $LiAlH_4$ would be required for full understanding of the reduction process to be obtained.

1.3.1.3 Lithium/Ammonia, Li/NH_3, method

The reduction of a selection of benzyl alcohols has been studied in the Li/NH_3 reducing system by Small, Minella and Hall.[2] Li was present as 0.5 cm lengths of Li wire, and NH_3 in a 2:1 solution of NH_3:tetrahydrofuran (THF). This process involved the addition of a tetrahydrofuran solution of benzyl alcohol to the solution of Li in NH_3/THF, and the resultant reaction mixture was quenched rapidly with NH_4Cl to give typically > 80% yields for the corresponding aromatic hydrocarbon. A prime example of this relatively generic reduction of benzyl alcohols is given in eqn 1.8 for the reduction of 1,2,3,4-tetrahydro-1-naphthalenol to 1,2,3,4-tetrahydro-naphthalene.[2]

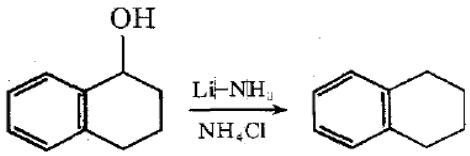

(1.8)

1.3.1.4 N-butylsilane with tris(pentafluorophenyl)borane

The reduction reaction employing *n*-butylsilane for the conversion of primary secondary and tertiary alcohols into alkanes together with a reaction mechanism has been reported by Nimmagadda and McRae.[3] Table 1.1 summarises the yields for

the alcohols studied by these workers. This method appears to be applicable for reduction of a wide range of alcohols to alkanes in high yields even in the presence of alkene functionalities.

The reduction of primary alcohols was illustrated with phenylmethanol and octadecanol with 2 equivalents of *n*-butylsilane obtaining yields of the corresponding alkanes, of 91-97%. Reduction of secondary and tertiary alcohols was demonstrated with norbornen-2-ol, 12-hydroxystearic acid, 2-isopropyl-5-methylcyclohexanol and 1-phenylethanol again with 2 equiv. of *n*-butylsilane and corresponding alkane yields of 81-97%. Carbon-carbon double bonds were shown to be unaffected during the reduction and high yields of corresponding alkanes were obtained in all cases studied. The proposed mechanism for the reduction of alcohols by *n*-butylsilane is shown in Scheme 1.

Scheme 1: Mechanism for the reduction of alcohols by *n*-butylsilane copied directly from Nimmagada and McRae.[3]

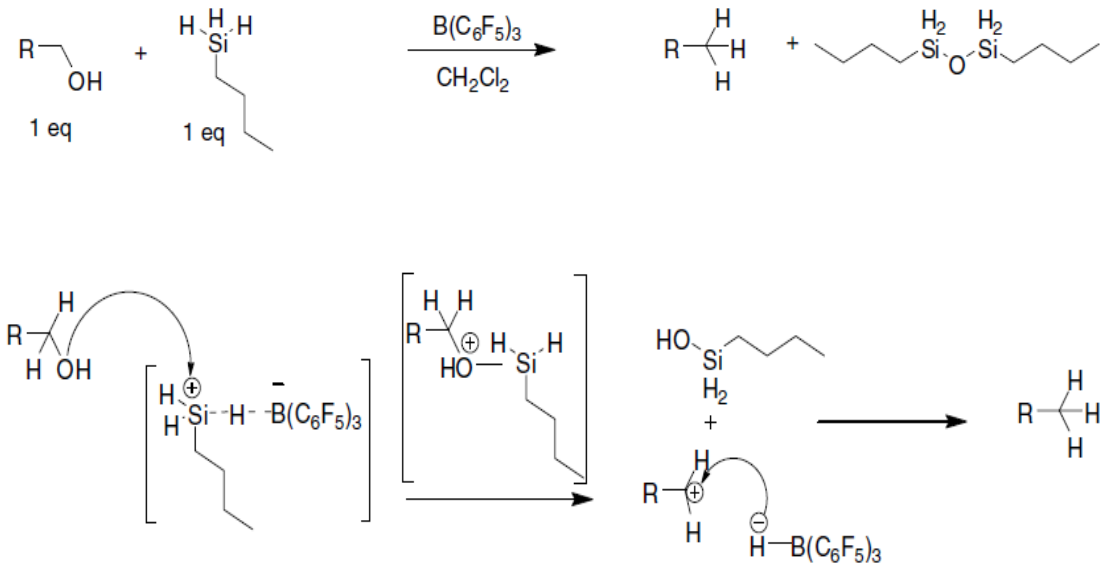

Table 1.1 Summary of the reduction of alcohols by *n*-butylsilane (*n*-BS) with tris(pentafluorophenyl)borane compared with diethylsilane (DES) discussed by Nimmagadda and McRae.[3]

Substrate	Product	% GC yield	
		n-BS	DES
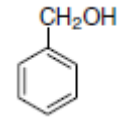	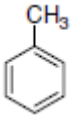	97	41
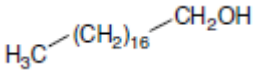	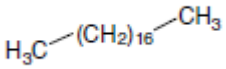	91	83
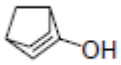		81	54
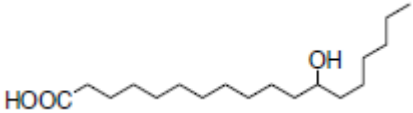	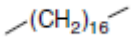	91	27
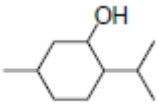	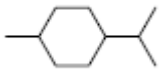	97	34
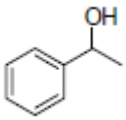	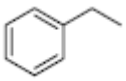	94	43
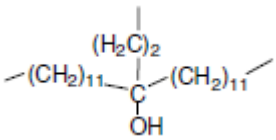	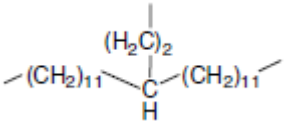	72	17
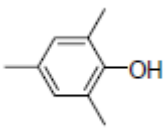	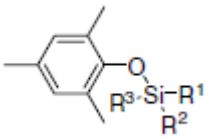	73	64
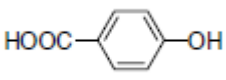	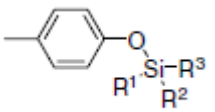	67	48
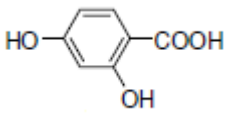	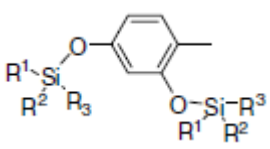	41	52

1.3.1.5 Direct borohydride reduction with phosphonium anhydride activation

In the direct borohydride reduction of alcohols to alkanes with phosphonium anhydride activation reported by Hendrickson,[4] the phosphonium anhydride reagent, $(Ph_3P^+)_2O$, $2CF_3SO_3^-$, initiates rapid reaction of the alcohols to form the activated phosphonium ether. This is followed by subsequent elimination or substitution with nucleophiles. The triflate counter ion is not nucleophilic, so allows substitution of the phosphonium ether through addition of exogenous nucleophiles with the absence of side reactions.

$$ROH + (Ph_3P^+)_2O \rightarrow Ph_3PO + ROP^+Ph_3 \rightarrow RNu \qquad (1.9)$$

In this case the added external nucleophile would be borohydride, presented as a slurry of sodium borohydride in dichloromethane. Table 1.2 lists the products obtained and yields for the 11 alcohols reported by Hendrickson.[4] While borohydride reduces primary and acyclic secondary alcohols activated as their phosphonium ethers, in the case of cyclic secondary alcohols the reaction appears severely limited by steric hindrance to the S_N2 reaction. The only product isolated in these cases (other than the unreacted alcohol) is the complex $Ph_3P.BH_3$. Presumably this arises from the initial attack of the hydride at the phosphorus end of the phosphonium ether resulting in the release of the starting alcohol and the complex $Ph_3P.BH_3$

$$ROPPh_3^+ + BH_4^- \rightarrow ROBH_3^- + Ph_3PH^+ \rightarrow ROH + Ph_3P{\cdot}BH_3 \qquad (1.10)$$

1.3.1.6 Chlorodiphenylsilane/$InCl_3$ method

Recently a direct reduction of alcohols to their corresponding alkanes using chlorodiphenylsilane as the hydride source in the presence of a catalytic amount of $InCl_3$ has been reported by Yasuda *et al.*[5] This new method demonstrated high chemoselectivity for benzylic alcohols, secondary alcohols and tertiary alcohols, while not reducing primary alcohols and functional groups that are readily reduced by standard methods such as esters, chloro, bromo, and nitro groups.[5] The reducing system used in the method involves 2 equivalents of Ph_2SiHCl and 5 mol % $InCl_3$ with CH_2Cl_2 at room temperature or $CH_3CH_2Cl_2$ at 80C. Using this reducing

system alcohols can be reduced to alkanes as described by the general eqn. (1.11), where R and R' represent aromatic or alkyl chains.

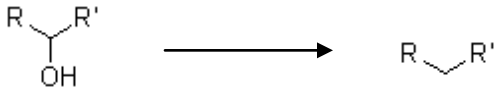

(1.11)

The simple aliphatic alcohol 2-decanol was used by these workers for an initial investigation of this reducing system.

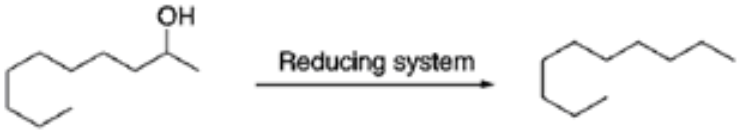

(1.12)

Table 1.3 lists the yield of the product decane with the hydrosilanes, Ph_2SiHCl, Ph_2SiH_2, Et_3SiH, and Me_2SiHCl, and catalysts, $InCl_3$, $AlCl_3$, and $BF_3.OEt_2$. The reactivity of hydrosilane strongly depends on the substituent on the silicon centre, chlorodiphenylsilane showed high activity with a catalytic amount of $InCl_3$ when refluxing in dicholoroethane. $InCl_3$ has the advantage over the other proposed catalysts, $AlCl_3$, and $BF_3.OEt_2$, in that it tolerates protic conditions and can be used even in water. However, the disadvantage is its expense given the geological scarcity of indium in any form. $InCl_3$ was not as effective with other hydrosilanes (Table 1.3) so a $Ph_2SiHCl/InCl_3$ system for direct reduction of alcohols was developed by these workers.

Table 1.4 summarises the direct reduction of the various alcohols that were then tested with this new reducing system. In the absence of $InCl_3$ the yields of the alkanes were significantly lowered. For example, 76% yield with 0.5 mmol of $InCl_3$ being present drops to 5% yield in the absence of $InCl_3$. When 1,1-diphenyl-2-propanol was used as a substrate only the phenyl-rearranged product 1,2-diphenyl-propane was obtained in high yield. This suggests that a carbocationic species may be present in the reduction process. When compared to other reducing systems such as $LiAlH_4$ and $Zn/CaCl_2$ where other functional groups present may be reduced, this $Ph_2SiHCl/InCl_3$ system is selective for the alcohol functional group as shown in Scheme 1. Therefore the $Ph_2SiHCl/InCl_3$ system provides an unusual and useful reducing reagent in selective organic synthesis, but may not see widespread use in bulk manufacturing operations given the expense associated with indium.

Table 1.2 Summary of the products and % yields from the borohydride reduction of alcohols with phosphonium anhydride activation as discussed by Hendrickson.[4]

Starting Material	Product	% yield
benzyl alcohol	Toluene	90
1-phenyl-2-ethanol	Ethylbenzene	87
1-phenyl-3-propanol	*n*-propylbenzene	90
1-phenyl-3-butanol	*n*-butylbenzene	89
Benzhydrol	Diphenylmethane	94
N-(-hyoxyethyl)aniline	N-ethylaniline	87
1-phenyl-1-ethanol	Styrene	85
1-phenyl-2-propanol	propenylbenzene + Allylbenzene	85

Table 1.3 % yields of decane from the reduction of 2-decanol with varying hydrosilanses, catalysts and solvents reported by Yasuda *et al.*[5]

Hydrosilane	Catalyst	Solvent	Temperature	% yield
2.0 mmol	1.0 mmol	1 mL	°C	0.05 mmol
Ph_2SiHCl	$InCl_3$	CH_2ClCH_2Cl	80	76
Ph_2SiHCl		CH_2ClCH_2Cl	80	5
Ph_2SiHCl	$AlCl_3$	CH_2ClCH_2Cl	80	23
Ph_2SiHCl	$BF_3.OEt_2$	CH_2ClCH_2Cl	80	trace
Ph_2SiH_2	$InCl_3$	CH_2ClCH_2Cl	80	19
Et_3SiH	$InCl_3$	CH_2ClCH_2Cl	80	0
Me_2SiHCl	$InCl_3$	CH_2ClCH_2Cl	room temp	0
Ph_2SiHCl	$InCl_3$	hexane	70	33
Ph_2SiHCl	$InCl_3$	benzene	80	20
Ph_2SiHCl	$InCl_3$	tetrahydrafuran	63	0
Ph_2SiHCl	$InCl_3$	acetonitrile	80	0

Table 1.4 Summary of the direct reduction of various alcohols with a $Ph_2SiHCl/InCl_3$ reducing system indicating reaction conditions, products and yields as reported by Yasuda *et al.*[5]

Alcohol	Solvent	Temperature	time	Product	Yield
	1 ml	°C	hour		%
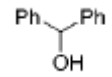	CH_2Cl_2	Room temp	2		87
	CH_2Cl_2	Room temp	1		88
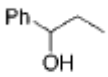	CH_2Cl_2	Room temp	1		90
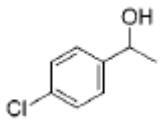	CH_2Cl_2	Room temp	2	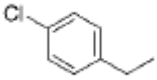	77
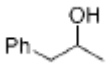	CH_2ClCH_2Cl	80	6		54
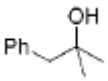	CH_2ClCH_2Cl	80	3	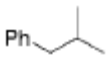	99
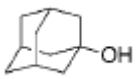	CH_2ClCH_2Cl	80	3		99
2-decanol	CH_2ClCH_2Cl	80	4	decane	76
4-decanol	CH_2ClCH_2Cl	80	4	decane	74
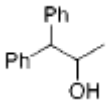	CH_2ClCH_2Cl	80	1	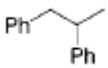	92
	CH_2ClCH_2Cl	80	5		0

The rate determining step was suggested by Yasuda *et al*.[5] to be the formation of the silyl ether from the alcohol and the chlorohydrosilane. The transformation of the silyl ether to the alkane appears to be facilitated by catalytic amounts of $InCl_3$. The $InCl_3$ is proposed to act as a Lewis acid to accelerate the desiloxylation through formation of an oxonium complex, (Scheme 2).

Table 1.5 summarises the techniques, conditions and products for the range of techniques described above. The development of an effective electrochemical process for the reduction of alcohols to alkanes may offer alternative pathways for reduction of alcohols which in turn may provide economical and environmental benefits over these complicated and severe synthetic processes.

Scheme 2: Mechanism for the reduction of alcohols in dicloromethane with the $Ph_2SiHCl/InCl_3$ reducing system copied directly from Yasuda *et al*.[5]

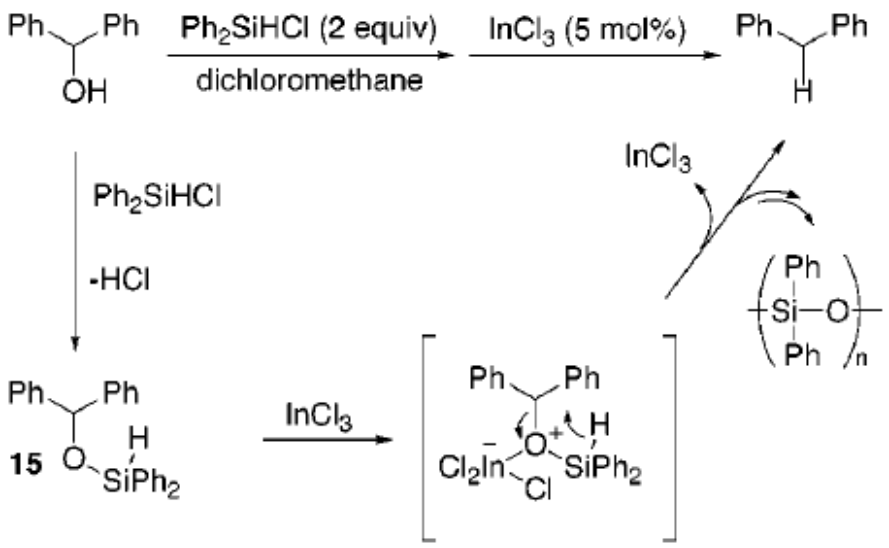

Table 1.5 Summary of the various synthetic techniques and their corresponding conditions and products as discussed in section 1.3.1.

Technique	Alcohols reduced	Conditions	Products	Ref
HI/I_2	Primary Secondary Tertiary	Aqueous HI, red phosphorus	Alkanes and alkenes	1, 16, 19, 20, 21, 22, 23
$LiAlH_4$		$Li^+ AlH_4^-$	Alkanes	24, 25, 26, 27
Li/NH_3	Benzyl	Li in 2:1 NH_3:THF solution, benzyl alcohol in THF, reaction quenched with NH_4Cl	Alkanes and alkenes	2
n-butylsilane	Primary Secondary Tertiary	2 equiv. of *n*-butylsilane in the presence of tris(pentafluorophenyl)borane,	Alkanes	3
Borohydride	Primary Acyclic secondary	Sodium borohydride in dichloromethane	Alkanes	4
Chlorodiphenylsilane $InCl_3$	Benzylic Secondary primary	2 equiv. Chlorodiphenyl silane 5 mol% $InCl_3$ as catalyst in dichloromethane at room temp.	Alkanes	5

1.3.2 Electrochemical Reduction of Alcohols

This research project addresses the question; can alcohols be readily reduced using electrochemical techniques? The electrochemically balanced equation for the reduction of alcohols to alkanes is as follows:

$$R–OH + 2e^- + 2H^+ \rightarrow R–H + H_2O \quad (1.13)$$

where R–OH is the alcohol in solution, H^+ is provided from the aqueous electrolyte and the two electrons are provided from the electrode surface at the electrolyte–electrode interface. However, because the nature of the electrode can

have significant effects on the process,[14] the kinetics of this reaction will likely depend greatly on the electrode material being used.

Electrochemical reduction experiments of secondary alcohols to corresponding alkanes have been performed by Horanyi *et al*. on platinum electrodes in 0.5 M solutions of the alcohols in aqueous $HClO_4$ electrolytes.[6] Yields of 87 – 96% of the corresponding alkanes were obtained.

A mechanism for the electrochemical reduction of allyl alcohol, (C_3H_5OH), at platinised Pt electrodes in acidic aqueous solution has been reported by Shukun *et al*.[7] and Arevalo *et al.*[8] The main products reported in each case being propene and propane. Electrochemical reduction of allyl alcohol in acidic solution takes place at −0.35 V *vs* SCE, more anodic than the potential for evolution of hydrogen in acidic aqueous solution (−0.42 V *vs* SCE). The electrochemical reduction of allyl alcohol has some irreversible characteristics where the cathodic peak potential shifts negatively with increasing sweep rate (and anodic peak shifts positively) and the difference between the cathodic and anodic peaks is greater than the ideal 0.059 V. By definition, the cathode is the electrode at which reduction occurs, while the anode is the electrode where oxidation takes place.[9] Therefore a cathodic potential is the potential at which reduction takes place, and an anodic potential is a potential at which oxidation takes place.[9] However, an anodic peak exists with a cathodic peak in the cyclic voltammogram so the electrode reaction being studied is not totally irreversible but partially irreversible or quasi-reversible.

The reaction order with respect to H^+ was found to be close to unity, indicating a preceding chemical reaction involving H^+, but was only 0.72 with respect to allyl alcohol.[8] This was taken to be due to the difference between the surface and bulk concentration of allyl alcohol together with an indication of an adsorption step involving allyl alcohol prior to the charge transfer steps. Allyl alcohol has an uneven charge distribution with the oxygen atom having the largest negative charge density. This leads to a substitution of the electrophilic H^+ on the oxygen to form the oxonium ion, $C_3H_5OH_2^+$, which may then dissociate and form $C_3H_5^+$. The product C_3H_5 is thought to form readily from the reduction of $C_3H_5^+$ at the electrode/solution interface, and then $C_3H_5^-$ is possibly formed in a further one−electron process at the electrode surface.[8] Propene is found to be the stable product and the overall reaction can be described as:

$$C_3H_5OH_{(aq)} + 2H^+_{(aq)} + 2e^- \rightarrow C_3H_{6\,(g)} + H_2O_{(aq)} \qquad (1.14)$$

The overall reaction is the combination of two reaction stages, the first forming $C_3H_5\bullet$ from allyl alcohol, the second producing propene from $C_3H_5\bullet$.

There are two possible pathways proposed for the formation of $C_3H_5\cdot$ from allyl alcohol, (Scheme 3a and 3b).[7] The allyl cation $C_3H_5^+$ has a lower unoccupied molecular orbital (LUMO) level than $C_3H_5OH\bullet^-_{ad}$ with the energy gap between the lowest unoccupied molecular orbital, LUMO, and the highest occupied molecular orbital (HOMO) is smaller for $C_3H_5^+$ than for $C_3H_5OH\bullet^-$.[7] Therefore the carbonium ion pathway requires less energy and will be the preferred pathway for this stage of the reaction.

Scheme 3: Mechanism for the formation of the $C_3H_5\cdot$ radical in the reduction of C_3H_5OH on platinised Pt electrode in acidic aqueous solution from Shukun *et al*.[7]

a) Anion radical pathway:

$$C_3H_5OH_{(aq)} + e^- \rightarrow C_3H_5OH\bullet^-_{(ad)}$$

$$C_3H_5OH\bullet_{(ad)} \rightarrow C_3H_5\bullet_{ad} + OH^-_{(aq)}$$

$$H^+_{(aq)} + OH^-_{(aq)} \rightarrow H_2O_{(aq)}$$

b) Carbonium ion pathway:

$$C_3H_5OH_{(aq)} + H^+_{(aq)} \rightarrow C_3H_5OH_2{}^+_{(aq)}$$

$$C_3H_5OH_2{}^+_{(aq)} \rightarrow C_3H_5{}^+_{(aq)} + H_2O_{(aq)}$$

$$C_3H_5{}^+_{(aq)} + e^- \rightarrow C_3H_5\bullet_{(ad)}$$

There are also two possibilities for the formation of propene from $C_3H_5\bullet$. (Scheme 4a and 4b).[7]

An analysis of the electrokinetic results indicated that the overall process followed a two-electron pathway involving two one-electron consecutive electrochemical steps in which the first step is the rate determining step.[7]

Scheme 4: Mechanism of the formation of propene from the $C_3H_5\cdot$ radical from Shukun *et al*.[7]

a) Carbanion pathway:

$C_3H_5\bullet_{(ad)} + e^- \rightarrow C_3H_5^-{}_{(ad)}$

$C_3H_5^-{}_{(ad)} + H^+_{(aq)} \rightarrow C_3H_{6(g)}$

b) Carbanion pathway with hydration

$C_3H_5\bullet_{(ad)} + e^- \rightarrow C_3H_5^-{}_{(ad)}$

$C_3H_5^-{}_{(ad)} + H_2O_{(aq)} \rightarrow C_3H_{6\,(g)} + OH^-_{(aq)}$

$H^+_{(aq)} + OH^-_{(aq)} \rightarrow H_2O_{(aq)}$

The overall electrode reaction was reported as:

$$C_3H_5OH_{(aq)} + 2H^+_{(aq)} + 2e^- \rightarrow C_3H_{6(g)} + H_2O_{(aq)} \qquad (1.15)$$

Electrochemical reactions of butanol isomers on platinum electrodes in aqueous 0.1 M $HClO_4$ has been studied by Rodríguez *et al*.[10] Four butanol isomers, 1-butanol, isobutyl alcohol, sec-butyl alcohol, and tert-butyl alcohol, all at 0.2 M concentration in aqueous 0.1 M $HClO_4$, were investigated. The electrochemical reduction of the butanol isomers takes place in the hydrogen adsorption potential range for platinum ($E < 0.2$ V *vs* the reversible hydrogen electrode (RHE)), with production of the corresponding butane isomer (butane or isobutene), together with a dissociative reaction leading to the formation of propane in all cases. All four butanol isomers are chemisorbed on platinum in a dehydration process that produces adsorbates with a carbon-carbon double bond. These then appear to be cleaved with anodic-cathodic cycling of the electrode potential.

Using a general formula for the butanol isomers, four reaction steps for the reduction of butanol isomers were proposed, dehydration, hydrogenation, fragmentation, and hydrogenolysis (Scheme 5).

Scheme 5: The general mechanism for the reduction of butanol isomers on platinum electrodes in $HClO_4$ copied from Rodríguez *et al*.[10]

General formula for butanol isomers:

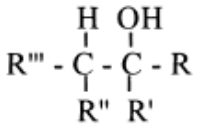

1 - butanol: R = R' = R" = H; R"' = CH_2-CH_3

sec- butyl alcohol: R = R"' = CH_3; R' = R" = H

isobutyl alcohol: R = R' = H; R" = R"' = CH_3

tert- butyl alcohol: R = R' = CH_3; R" = R"' = H

Dehydration

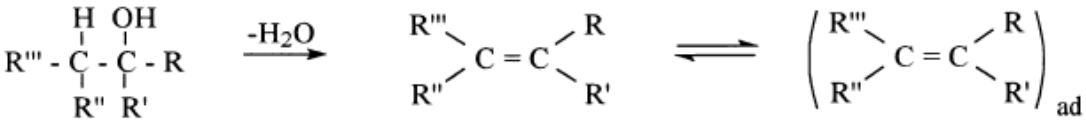

Hydrogenation

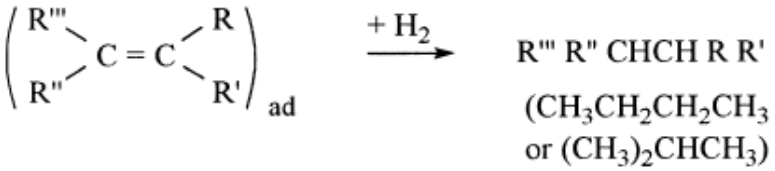

Fragmentation

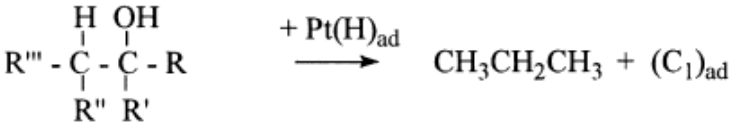

Hydrogenolysis

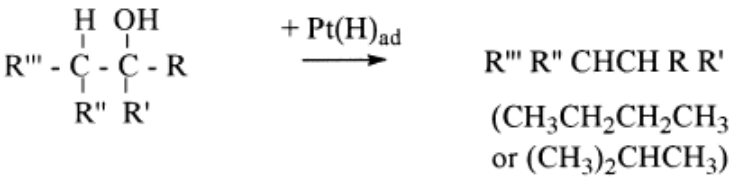

Dehydration leads to strongly adsorbed intermediates containing a carbon-carbon double bond. The adsorbed species can undergo hydrogenation through the addition of H_2 (generated at the Pt electrode) across the C=C bond of the adsorbates which leads to the formation of the corresponding butanes.

The detection of propane products can be accounted for by fragmentation where the C=C bond is broken into C_3 and C_1 species, (C_3 = propane), however, the lack of detection of methane as the C_1 species indicates that the C_1 species remains adsorbed to the electrode surface. The fourth reaction step reported is hydrogenolysis. The alcohol molecules in the bulk solution can react with adsorbed hydrogen, H_{ad}, on the electrode which may also lead to the formation of the butane isomers.

The electrochemical reactivity of benzyl alcohol at Pt and Pd electrodes using 2 mM benzyl alcohol in aqueous 0.1 M $HClO_4$ was investigated by Souto *et al*.[11] The significance of the two functionalities in benzyl alcohol, an aromatic and an alcohol group, was noted by these workers.[11] A porous metallic layer of platinum or palladium deposited on a porous Teflon™ membrane was the working electrode. Electrochemical reduction of benzyl alcohol occurs at these electrodes at potentials $E < 0.30$ V *vs* a reversible hydrogen electrode (RHE) during the cathodic sweep but after reversal at the cathodic limit the electrochemical reduction can be maintained up to 0.3 V. Mass spectrometry cyclic voltammograms (MSCV) were used to determine the products formed, and several compounds were observed, both aromatic and non-aromatic. On palladium electrodes, toluene and benzene were detected as reduction products, while on platinum, toluene and benzene were again detected together with cyclohexene, methyl-cyclohexene and methyl-cyclohexane. Hydrogenation of the aromatic ring appears to be hindered on Pd, with only very small amounts of cyclohexane and methyl-cyclohexadiene being produced. Benzene formation is favored on both electrodes as the potential becomes more negative, but this product can undergo hydrogenation of the aromatic ring to produce cyclohexene or cyclohexane in the potential range in which H_2 is formed through reduction of water, $E < 0.08$ V *vs* RHE. Toluene formation is observed from a more positive potential, $E = 0.28$ V, and continues to the cathodic limit. Hydrogenation of the aromatic ring occurs in a much narrower potential range than benzene and toluene formation due to the need for production of molecular H_2.

Possible reactions for the electrochemical reduction of benzyl alcohol on Pt and Pd electrodes were proposed based on these results. Reactions for the production of

benzene, cyclohexene, cyclohexane and toluene were proposed (Scheme 6). The production of cyclohexane coincides with a decrease of the benzene mass signal, therefore benzene can be regarded as being consumed through reaction with H_2. Toluene is only detected at potentials in the hydrogen adsorption region, E = 0.01 to 0.4 V, indicating H_{ad} is necessary for hydrogenolysis (Scheme 6b).

Scheme 6: Reactions for the reduction of benzyl alcohol to benzene, cyclohexene, cyclohexane and toluene reproduced from Souto *et al.*[11]

a) Dissociative adsorption of benzyl alcohol to form benzene:

$C_6H_5CH_2OH \rightarrow (C_6H_6)_{(ad)} + C_1$

where C_1 is a C_1 species originating from the $–CH_2OH$ group.

$(C_6H_6)_{ad} \leftrightarrow C_6H_6$

b) Cyclohexene/Cyclohexane formation:

$C_6H_6 + H_2 \rightarrow C_6H_8 + H_2 \rightarrow C_6H_{10} + H_2 \rightarrow C_6H_{12}$

c) Non-dissociative adsorption to form toluene:

$C_6H_5CH_2OH \leftrightarrow (C_6H_5CH_2OH)_{ad}$

$(C_6H_5CH_2OH)_{ad} + H_{ad} \rightarrow (C_6H_5CH_3)_{ad}$

$(C_6H_5CH_3)_{ad} \leftrightarrow C_6H_5CH_3$

d) Methylcyclohexene/methylcyclohexane formation:

$(C_6H_5CH_3)_{ad} + (H_2)_{ad} \rightarrow (C_6H_7CH_3)_{ad}$

$(C_6H_7CH_3)_{ad} + (H_2)_{ad} \rightarrow (C_6H_9CH_3)_{ad}$

$(C_6H_9CH_3)_{ad} + (H_2)_{ad} \rightarrow (C_6H_{11}CH_3)_{ad}$

The electrochemical reactivity of crotyl alcohol on platinum in acidic aqueous solutions of H_2SO_4 and $HClO_4$ has been investigated by Arévalo *et al.*[12] Crotyl alcohol is an unsaturated aliphatic alcohol with a double bond in the allyl position, CH_3-CH=CH-CH_2OH. Crotyl alcohol is isomerized in acidic media with the equilibrium shown in Scheme 7:[12]

Scheme 7: Isomerization of Crotyl Alcohol reported by Arévalo *et al.*[12]

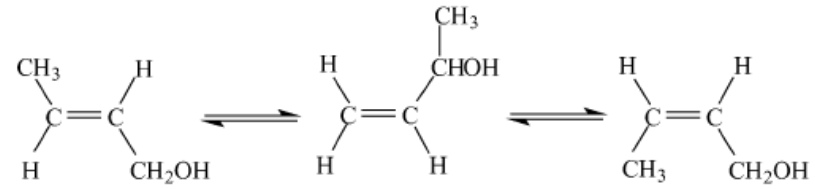

trans-crotyl alcohol α-methyl allyl alcohol *cis*-crotyl alcohol

All the isomers must be assumed to be present in solution in the work reported by Arévalo *et al.*[12] Structurally, crotyl alcohol has 2 functionalities, the double bond and the methyl alcohol group.

A Pt foil was used as the working electrode (WE) for the voltammetric and chronoamperometric experiments, a porous Pt layer sputtered on a micro-porous PTFE membrane for the online Mass Spectrometry experiments and a Pt disk for the Fourier Transform Infrared Spectroscopy (FTIR) experiments, with all experiments performed at room temperature and under Ar. Crotyl alcohol was adsorbed on the Pt electrode at controlled adsorption potentials, E_{ad}, ranging from 0.05 V to 0.80 V *vs* RHE, where the potential was stopped during the anodic scan at E_{ad} to prevent the oxidation of any reduction products obtained with the adsorption. Several reduction products were detected in the hydrogen evolution region, $E < 0.25$ V, propane, propene, 2-butene, butane, ethane, and methane, with no alcohols present. Possible electrochemical reactions were proposed considering all possible isomers for crotyl alcohol. Three possible interactions leading to adsorption were proposed, the first being the interaction between the electrode surface Pt and the carbon atom containing the OH group as shown in Scheme 8, and based on the different isomers this interaction will give A and B (Scheme 8a). Depending on E_{ad}, adsorbates A and B can experience further deprotonation or a fragmentation to give C, D and E (Scheme 8b). The second interactions leading to adsorption proposed was between the electrode surface and the double bond as shown in Scheme 8, giving products F and G. And thirdly a possible interaction between the π-system of crotyl alcohol and empty d orbitals of Pt was proposed. This third possible interaction is likely to be weaker than the other adspecies.

Scheme 8: The adsorption of crotyl alcohol to the platinum electrode due to the interaction of the electrode surface and the carbon containing the OH, copied from Arévalo *et al.*[12]

a) Adsorption of crotyl alcohol to Pt

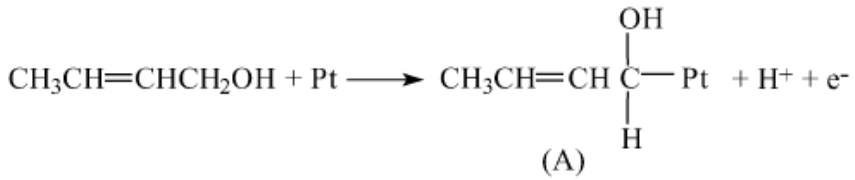

(A)

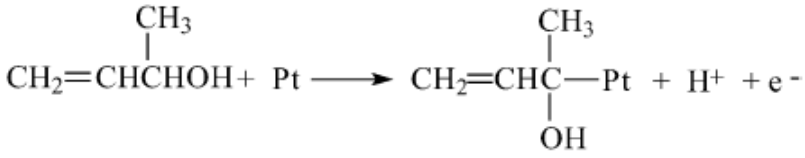

(B)

b) Deprotonation and fragmentation of A and B to form C, D and E

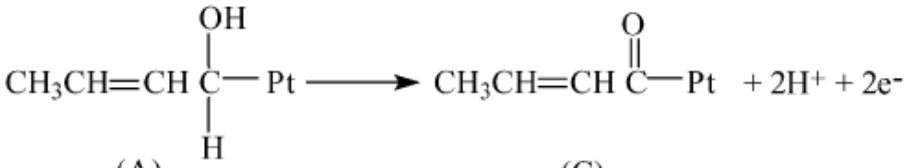

(A) (C)

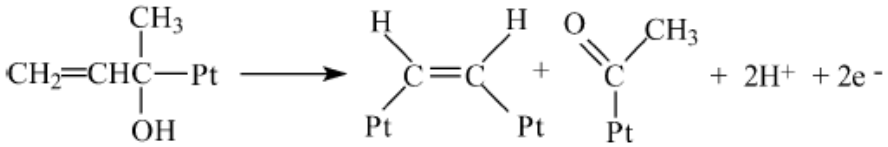

(B) (D) (E)

Scheme 9: The adsorption of crotyl alcohol to the platinum electrode due to the interaction between the electrode surface and the crotyl alcohol double bond copied from Arévalo *et al*.[12]

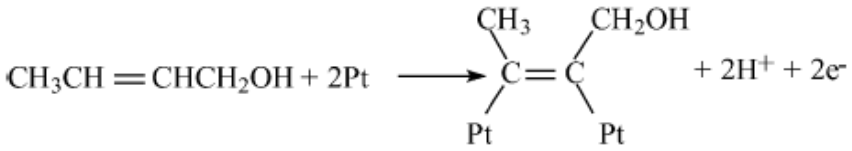

(F)

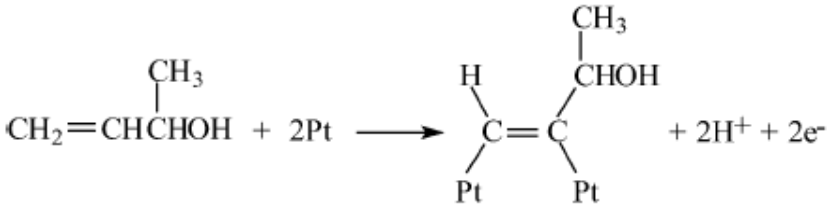

(G)

Arevalo *et al*.[12] state that the adsorbates A-G have to be responsible for the products detected by their online mass spectrometry and FTIR experiments and proposed reactions for the formation of the products, butane, butane, propene, propane, ethane and methane, from these adspecies only (Scheme 10). Hydrogenolysis and hydrogenation reactions were proposed for the production of butene and butane from A, F and G, assuming the 2 hydrocarbons probably proceed from different adsorbed species (Scheme 10a). In the cases of propene and propane, both products could originate from the same adsorbate C and the proposed reaction involves fragmentation of the adsorbate followed by hydrogenation with H_{ad}, with the formation of adsorbed CO indicated by the corresponding FTIR signal (Scheme 10b). Finally, ethane and methane are also detected and their formation is proposed via a hydrogenation process of D and E respectively (Scheme 10c).

Scheme 10: The reduction of adsorbed crotyl alcohol to butene, butane, propene, propane, ethane and methane on Pt electrode copied directly from Arévalo *et al.*[12]

a) Formation of butene and butane

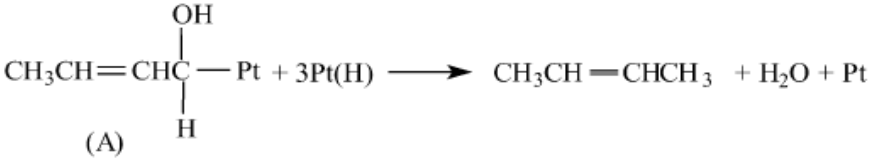

(A)

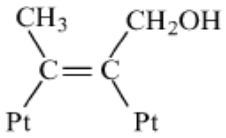

(F)

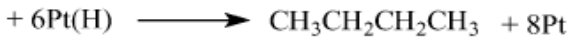

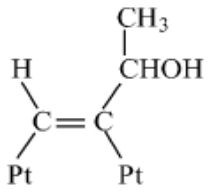

(G)

b) Formation of propene and propane

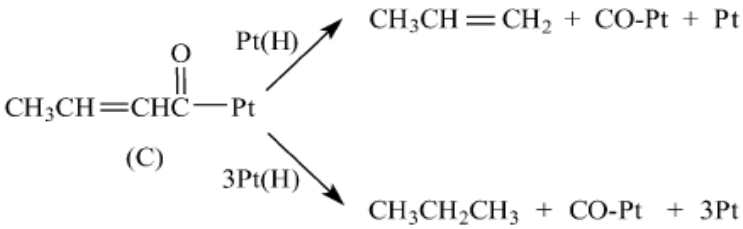

(C)

c) Formation of ethane and methane

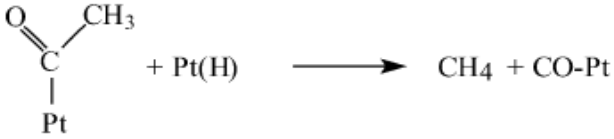

(E)

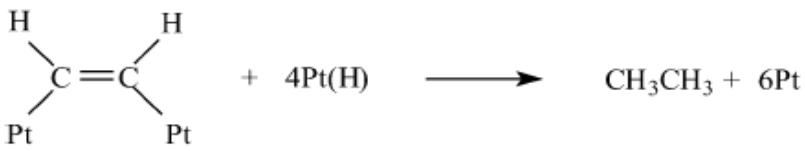

(D)

The limited amount of reported studies for the electrochemical reduction of alcohols provides little information on possible conditions. Due to this lack of relevant information, a literature search for studies of the electrochemical reduction of other simple carbon molecules, such as carbon dioxide, was completed to establish other possible experimental conditions for the electrochemical reduction of alcohols.

1.3.3 Electrochemical Reduction of Carbon Dioxide

Carbon dioxide is thought to be one of the largest contributors to the greenhouse effect.[28-30] The aim to decrease atmospheric CO_2 levels is a common theme in much research at present. Suggested methods include deposition as clathrates in deep ocean waters,[31,32] deposition as calcium carbonate, or capture and chemical reduction to form potentially valuable feed stocks for industrial processes.[33] The possibility exists that this reduction could be achieved electrochemically. Therefore this reaction has become of interest in studies of the environment, energy and natural resources, and has been studied extensively to aid the elimination of greenhouse gases.[28-30,34,35] Studies continue to be performed to elucidate the mechanism for the electrochemical reduction of CO_2.[36]

CO_2 is a very stable linear molecule in which the oxygen atoms are weak Lewis bases. Therefore reactions are dominated by nucleophilic attack on the electrophilic carbon resulting in bending of the O–C–O bond.[36] CO_2 may be electrochemically reduced to carbon monoxide, formic acid, hydrocarbons and alcohols on metal electrodes.[36]

The main electrochemical reactions involving CO_2 are as follows:[36]

$$CO_2 + H^+ + 2e^- \longrightarrow HCOO^- \qquad E^0 = -0.61V$$

$$CO_2 + 2H^+ + 2e^- \longrightarrow CO + H_2O \qquad E^0 = -0.53V$$

$$CO_2 + 6H^+ + 6e^- \longrightarrow CH_3OH + H_2O \qquad E^0 = -0.38V$$

$$CO_2 + 8H^+ + 8e^- \longrightarrow CH_4 + 2H_20 \qquad E^0 = -0.24V$$

All reported at pH 7 in aqueous solution at 25°C, 1 atm for gases and 1 M for other solutes.

When electrochemical reduction of CO_2 is performed in aqueous solution on metallic electrodes only carbon monoxide and formic acid is produced.[36] However,

copper has been found to be a suitable electrode for the formation of hydrocarbons, in particular methane and ethylene. In the latter case this must result from the formation of new carbon–carbon bonds. Using a polycrystalline Cu electrode and sulfuric or perchloric acid electrolytes CH_4, C_2H_6, CH_3OH and HCOOH have been produced.[36] The electrochemical reduction of CO_2 is thought to be a complex multi-step process involving adsorbed intermediates. Many different mechanisms have been offered to account for the process; this likely reflects the range of experimental conditions employed.

Jitaru proposed the following mechanism for the reduction of CO_2 to CH_4, C_2H_4, C_2H_6 and HCOOH (Scheme 11) on Cu electrodes in aqueous $NaHCO_3$.[36]

The generation of adsorbed hydrogen species competes with the CO_2 reaction in this aqueous media leading to additional processes accounting for some of the formation of formic acid and acetic acid (Scheme 12).[36]

Scheme 11: Mechanism for the reduction of CO_2 to CH_4, C_2H_4, C_2H_6, and HCOOH reported by Jitaru.[36]

$$CO_2 + e^- \rightarrow \bullet CO_2^-$$

$$\bullet CO_2^- + CO_2 \rightarrow CO + CO_3^-$$

$$\bullet CO_2^-{}_{ad} + e- + H^+ \rightarrow HCOO^-{}_{ad}$$

$$HCOO^-{}_{ad} + e^- \rightarrow HCOO^-$$

$$HCOO^-{}_{ad} + e^- \rightarrow CO_{ad} + OH^-{}_{ad}$$

$$HCOO^- + H^+ \rightarrow HCOOH$$

$$CO_{ad} + 4H^+ + 4e^- \rightarrow \bullet CH_2 + H_2O$$

$$\bullet CH_2 + \bullet CH_2 \rightarrow C_2H_4$$

$$\bullet CH_2 + \bullet CH_2 + 2e^- + 2H^+ \rightarrow C_2H_6$$

Scheme 12: The formation of formic acid and acetic acid from an adsorbed hydrogen and CO_2 as reported by Jitaru.[36]

$H^+ + e^- \rightarrow H_{ad}$

$CO_2 + H_{ad} \rightarrow HCOO^-_{ad}$

$HCOO^-_{ad} + H_{ad} \rightarrow HCOOH$

$HCOO_{ad} + CH_3OH \rightarrow CH_3COOH + OH_{ad}$

$OH_{ad} + H_{ad} \rightarrow H_2O$

Kaneco *et al*. also used Cu electrodes for the electrochemical reduction of CO_2 in aqueous 0.65 M $NaHCO_3$.[34] The temperature was constant at 271 K and cathodic potentials of −1.6 to −2.0 V, *vs* standard calomel electrode (SCE), were used to obtain CH_4 predominantly, with HCOOH and C_2H_4 also produced.[34]

These workers[34] referred to earlier work by Teeter and Van Rysselberghe[37] with the statement that only dissolved CO_2 molecules take part in the reduction, and not bicarbonate HCO_3^- or carbonate CO_3^{2-} ions formed from dissolution of CO_2. However, no evidence for this assertion was offered.

The results reported by Kaneco *et al.*[34] are consistent with those reported by Jitaru.[36] The pathway by which methane, ethylene and formic acid on Cu electrodes are formed was proposed by Kaneco *et al.* is shown in Scheme 13. This is based on: a one-electron reduction of CO_2, adsorption of this new $\bullet CO_2^-$ species, protonation and one electron reduction of adsorbed $\bullet CO_2^-$ radical anion to either form adsorbed formate (as a terminating step), or adsorbed CO, the latter being a key intermediate for further reduction. Through a succession of four protonation steps and accompanying reduction steps, an adsorbed reactive methylene group is thought to form. This reactive species stabilizes either through a two-proton, two-electron reduction to form methane, or by dimerization to form ethylene.

Scheme 12: Mechanism of the reduction of CO_2 to methane, ethylene and formic acid on Cu electrodes in $NaHCO_3$ reported directly from Kaneco *et al*.[34]

$CO_2 + e^- \rightarrow \bullet CO_2^-$

$\bullet CO_2^- + H^+ + e^- \rightarrow HCOO^-$

$\bullet CO_2^- + H^+ + e^- \rightarrow CO + {}^-OH$

$CO + {}^-OH + 4H^+ + 4e^- \rightarrow :CH_2 + H_2O$

$:CH_2 + H^+ + 2e^- \rightarrow CH_4$

$:CH2 + :CH_2 \rightarrow C_2H_4$

Azuma *et al*. investigated the electrochemical reduction of CO_2 on 32 types of electrodes in aqueous $KHCO_3$ media.[35] Formation of methane and ethylene was observed on almost all metal electrodes studied, although the efficiency (ratio of carbon-centered reduction process to all charge passed) is very low (typically < 1% coulometric efficiency at -2.2 V *vs* Ag/AgCl reference electrode) except for Cu (7-25%). Table 1.6 summarises the 32 electrodes types, experimental conditions and products investigated by these workers.[35] These workers offered two possible mechanisms for the reduction of CO_2 to HCOOH, either an electron transfer mechanism (Scheme 14a) or hydrogen adsorption mechanism (Scheme 14b).

Two alternative mechanisms for the formation of adsorbed CO were also offered (Scheme 15).[35]

Table 1.6 Summary of the electrode materials, conditions and % current efficiency of products from the electrochemical reduction of CO_2 discussed by Azuma *et al.*[35]

Metal	Conditions		% Current efficiency			
	Temperature	*E vs* SCE	CH_4	C_2H_4	C_2H_6	HCOOH
	C	V				
Cd	0.0	-2.0	0.015	0.002	0.00056	55.9
	20.0	-2.0	0.0073	0.001	0.0004	35.5
In	0.0	-2.0	0.001	0.00035	0.0006	70
	20.0	-2.0	0.05	0.0046	0.0067	33.3
Sn	0.0	-2.2	0.65	0.068	0.44	28.5
	0.0	-2.2	0.84	0.95	0.69	5.2
Pb	0.0	-2.0	0.39	0.008	0.0014	16.5
	20.0	-2.0	0.06	0.001	0.0003	9.9
Tl	0.0	-2.2	0.2	0.003	0.001	53.4
Hg	0.0	-2.2	0.0004	0	0	90.2
	20.0	-2.2	0.0035	0.0002	0.00006	87.6
Zn	0.0	-2.2	0.23	0	-	19.5
Pd	0.0	-2.0	0.083	0.011	0.014	16.1
	20.0	-2.0	0.31	0.061	0.078	8.6
Ti	0.0	-2.2	0	0	-	5.2
Ni	0.0	-2.2	0.71	0.069	0.18	13.7
	20.0	-2.2	0.13	0.010	0.021	0.1
Ag	0.0	-2.2	1.4	0.0052	0.013	20.5
	20.0	-2.2	1.1	0.009	0.0027	16
Au	0.0	-2.2	0	0	-	10.3
Cu	0.0	-2.2	24.7	6.5	0.015	30
	20.0	-2.2	17.8	12.7	0.039	10.2
C	0.0	-2.2	0.11	0.0064	0.007	0.31
Al	0.0	-2.2	0.012	0.00022	0.0004	0.78
Si	0.0	-2.2	0.025	0	0	1.6
V	0.0	-2.2	0.02	0	-	2.6
Cr	0.0	-2.2	0.74	0.05	0.18	0.15
Mn	0.0	-2.2	1.5	0.093	0.29	0.03
Fe	0.0	-2.2	0.07	0	-	1.1
Co	0.0	-2.2	0.13	0.0057	0.032	0.85
Zr	0.0	-2.2	0.49	0.021	0.05	0
Nb	0.0	-2.2	0.16	0.0088	0.042	0.03
Mo	0.0	-2.0	0.01	0.00028	0.0015	0.21
	20.0	-2.0	0.031	0.00077	0.0057	0.19
Ru	0.0	-2.2	0.043	0	0	0.08
Rh	0.0	-2.2	0.031	0.00067	0.0036	1.35
	20.0	-2.2	0.053	0.003	0.011	2.4

Table 1.6 cont.

Metal	Conditions		% Current efficiency			
	Temperature	*E vs* SCE	CH_4	C_2H_4	C_2H_6	HCOOH
	C	V				
Hf	0.0	-2.2	0.0046	0.00027	0.001	0.35
	20.0	-2.2	0.0073	0.00057	0.0005	0.21
Ta	0.0	-2.8	0.0015	0.0015	0.0002	0
	20.0	-0.3	0.0039	0.0039	0.0001	0
W	0.0	-2.0	0.015	0.0043	0.0022	1.3
	20.0	-2.0	0.055	0.0022	0.01	2.6
Re	0.0	-2.0	0.044	0.00022	0.0056	2
	20.0	-2.0	0.038	0.00024	0.0048	1.4
Ir	0.0	-2.2	0.051	0.0035	0.0072	1
	20.0	-2.2	0.086	0.0057	0.015	0.58
Pt	0.0	-2.2	0.029	0	-	5.5

Scheme 14: Mechanisms for the reduction of CO_2 to HCOOH in $KHCO_3$ from Azuma *et al*.[35]

a) Electron transfer mechanism

$CO_2 + e^- \rightarrow CO_2^-$

$CO_2^- + H^+ \rightarrow HCOO$

$HCOO + e^- \rightarrow HCOO^-$

$HCOO^- + H^+ \rightarrow HCOOH$

b) Hydrogen adsorption mechanism

$H^+ + e^- \rightarrow H_{ad}$

$H_{ad} + CO_2 \rightarrow HCOO^-_{ad}$

$HCOO^-_{ad} + H_{ad} \rightarrow HCOOH$

Scheme 15: Mechanisms of the reduction of CO_2 to CO in $KHCO_3$ from Azuma *et al.*[35]

$CO_2^-{}_{ad} + CO_2^-{}_{ad} \rightarrow CO_{ad} + CO_3^{2-}$

and

$CO_2^-{}_{ad} + H_{ad} \rightarrow CO_{ad} + {}^-OH$

Pettinicchi *et al*. investigated the use of Zn-Cu alloys (with Zn contents of 25 and 50%) in aqueous 0.5 M $KHCO_3$ and 0.5 M $NaClO_4$ electrolytes for the reduction of CO_2.[30] These studies demonstrated the effects of electrode microcrystalline structures on the selectivity, reversibility and reactivity for CO and HCOOH production.[30] The experiments on the Zn-Cu alloys were carried out at potentials ranging from –2.0 V to 1.5 V *vs* Hg/Hg_2SO_4 electrode with evidence of CO_2 reduction between –1.3 V and –2.0 V. In $KHCO_3$ electrolytes the reduction of CO_2 was studied in a –1.3 V to –1.60 V potential region and analysis shows the presence of alcohols and acetone. In contrast, experiments in 0.5 M $NaClO_4$ over the –1.90 V to –1.2 V potential region showed the presence of methane, ethane and ethylene. Full mechanisms of the formation of these products were not provided in this report.

Table 1.7 Summarises the various electrode metals, electrolyte solutions and corresponding products from the electrochemical reduction of CO_2 reported in the literature. Copper electrodes were found to be among the most promising options for hydrocarbon manufacturing.[30,34-36]

Table 1.7 Summary of electrode materials, electrolyte solutions and products from the electrochemical reduction of CO_2 reported in the literature.

Metal	Electrolyte	Products	Ref
Cu	aqueous $NaHCO_3$	CH_4, C_2H_4, C_2H_6, HCOOH	36
Cu	0.65 M $NaHCO_3$	HCOOH, CH_4, C_2H_4	34
Cu	$HClO_4$	CH_4, C_2H_4, C_2H_6, HCOOH	36
Cu	H2SO_4	CH_4, C_2H_4, C_2H_6, HCOOH	36
32 metals (see table 1.1 for details)	$KHCO_3$	CH_4, C_2H_4, C_2H_6, HCOOH	35
Zn-Cu alloy	0.5 M $KHCO_3$	alcohols and acetone	30
Zn-Cu alloy	0.5M $NaClO_4$	CH_4, C_2H_4, C_2H_6	30

1.3.3.1 Deactivation of the Cu electrode

Copper electrodes were found to be among the most promising options for hydrocarbon formation from CO_2 by most workers.[30,34-36,38] However, a difficulty reported for the use of Cu electrodes by several workers is the progressive deactivation of the Cu electrode. CO_2 reduction at high purity copper foil electrodes has been studied by several workers in 0.5 M $KHCO_3$ electrolyte.[30,34-36,38] The Faradaic efficiency for production of CH_4 and C_2H_4 could reach 65 % after 20 minutes of electrolysis but would then gradually decay to 0 % after 120 minutes. Copper foil electrode surfaces typically became blackened and elemental graphitic carbon was detected on the surface by X-ray photoelectron and Auger electron spectroscopy.[39] In these studies it was presumed that some products or intermediates formed in the CO_2 reduction process become irreversibly adsorbed to the electrode surface, suffered reduction to elemental carbon resulting in suppression of the reaction perhaps by occlusion of the copper surface. It was suggested that this deactivation of the electrode could be due to the deposition to the electrode surface of impurities originally contained in the electrolyte solution, although given the stated purity of the electrolytes this argument seems suspect.

Consistent with these findings, a later investigation of CO_2 reduction at a bulk Cu electrode coupled with simultaneous electrochemical mass spectrometry[40] showed that CH_4 and C_2H_4 formation declined during successive cathodic scans to −2.0 V *vs* SCE, for 10 minutes, also resulting in blackening of the electrode.

Several other workers have reported this poisoning or deactivation of the Cu electrode, together with other electrodes such as Au and Ag, in aqueous $NaHCO_3$ and $KHCO_3$ electrolytes.[41-43] It was however suggested that the poisoning of the Cu electrode could be suppressed by applying periodic anodic polarization pulses during the cathodic reduction of CO_2.[41,42] There was no discussion of what may take place at the electrode during these anodic excursions to prevent this apparent poisoning.

A summary of the proposed causes for the deactivation of the Cu electrode is as follows:[44]

1) Heavy metal impurities contained in reagent chemicals at extremely low levels cathodically reduced and deposited at the electrode during the CO_2 reduction. Deposited heavy metals other than Cu could deteriorate the electrocatalytic activity of Cu electrode for CO_2 reduction. However, this would not account for the change in electrode colour and detection of elemental carbon.

2) Very small amounts of organic substance are possibly contained in water, such as surface active reagents, and may be adsorbed on the electrode during CO_2 reduction. However, high purity electrolyte materials were reported to be used for preparing electrolyte solutions in all cases therefore it would be expected that impurity levels in the electrolytes would be too low for this significant deactivation.

3) Intermediate species or products formed during the CO_2 reduction may adsorb on the electrode.

The deactivation of the Cu electrode could be considered as a combination of all 3 possible causes, however, the possible adsorption of intermediate species is much more likely to have the largest contribution to the deactivation of the electrode.

Deactivated Cu electrodes recover their electrocatalytic activity for the electrochemical reduction of CO_2 by anodic polarization at -0.05 V *vs* standard hydrogen electrode (SHE), and the deactivation depends greatly on the individual

choice of electrolyte. It was also noted that purification of the electrolyte solution by pre-electrolysis with a Pt black electrode effectively prevented the deactivation of Cu electrodes.[44]

1.3.4 Reduction of Carbon Monoxide

The reduction of CO_2 to CO can be achieved on a variety of metal electrodes including: Au, Ag, Zn, Cu, Pd and Pt.[34-36,38] Among these metals Cu can effectively reduce CO further to hydrocarbons and alcohols.[34,36] Therefore the reduction of gaseous CO at Cu electrodes is also of interest.[38] The electrochemical processes involved in the reduction of CO to CH_4, C_2H_4 and alcohols at Cu electrodes as functions of the pH and electrode material have been examined by Hori *et al*.[38] Concentrations of $KHCO_3$ used ranged from 0.03 to 0.3 M, with potentials of CO_2 reduction occurring from -1.35 to -1.38 V *vs* Ag/AgCl electrode on the Cu electrodes. Table 1.8 shows the faradaic yields of CH_4, C_2H_4 and C_2H_5OH at each concentration of $KHCO_3$, and corresponding potentials at which reduction was achieved. Results show that Faradaic yields for production of C_2H_4 and C_2H_5OH were higher in dilute $KHCO_3$ solutions on a copper electrode, decreasing with increasing $KHCO_3$ concentration, whereas the CH_4 yield increases with increasing $KHCO_3$ concentration.

These workers[38] also compared Cu electrodes with Fe and Ni electrodes in both 0.1 M $KHCO_3$ and a 0.1 M KH_2PO_4/0.1 M K_2HPO_4 electrolyte. Results for Cu electrodes, as listed in Table 1.9, show lower Faradaic yields for C_2H_4 and C_2H_5OH yield in the KH_2PO_4/K_2HPO_4 electrolyte when compared to the yields in $KHCO_3$. In contrast, the CH_4 yield was not substantially altered. Both Fe and Ni electrodes were found to be much less active, only producing CH_4, C_2H_6, C_2H_4, C_2H_3OH, and C_2H_5OH, in small Faradaic efficiencies of 0.1 to 2.6%.

The proposed mechanism for the reduction of adsorbed CO on Cu is as outlined in Scheme 16:[38]

Table 1.8 Concentration of $KHCO_3$, reduction potential of CO and the % Faradaic efficiencies for products reported by Hori *et al.*[38]

$KHCO_3$ conc.	Potential E vs SHE	% Faradaic Efficiencies CH_4	C_2H_4	C_2H_5OH
mol L^{-1}	V			
0.03	-1.38	16.2	28.1	13.1
0.05	-1.36	18.5	19.1	7.6
0.1	-1.36	22.3	21.7	7.1
0.2	-1.35	23.2	15.8	7.1
0.3	-1.35	32.4	15.3	6.3

Table 1.9 Summary of the activity of Cu, Fe, Ni electrodes in $KHCO_3$ and K_2HPO_4/KH_2PO_4 electrolytes for the reduction of CO as discussed by Hori *et al.*[38]

Metal	Electrolyte	Potential *E vs* SHE	% Faradaic yields CH4	C2H4	C2H5OH
	0.1 M	V			
Cu	$KHCO_3$	-1.36	22.3	21.7	7.1
	KH_2PO_4/K_2HPO_4	-1.24	15.6	4.1	0.3
Fe	$KHCO_3$	-1.38	1.1	0.1	Trace
	KH_2PO_4/K_2HPO_4	-1.32	2.6	0.2	0.2
Ni	$KHCO_3$	-1.49	1.1	0.2	Trace
	KH_2PO_4/K_2HPO_4	-1.14	1.5	0.1	0.1

Scheme 15: Mechanism for the reduction of adsorbed CO on Cu electrodes in $KHCO_3$ copied directly from Hori *et al.*[38]

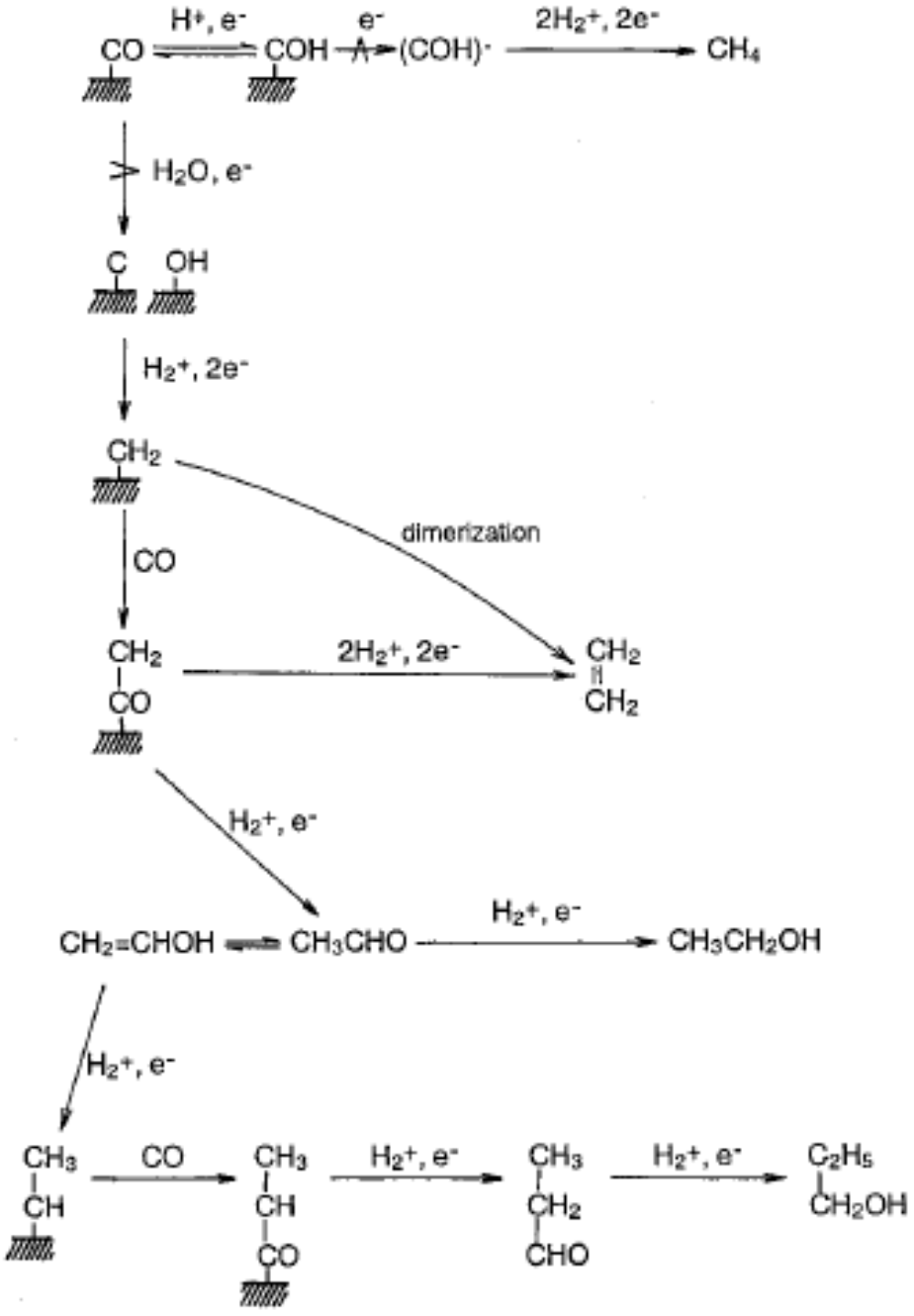

Where C represents an adsorbed species to the electrode surface.

The proposed mechanisms for the reduction of CO_2 and CO summarised in this section show strong evidence of alcohol contribution in some proposed mechanisms, with CO_2 reduced to alcohols, alcohols as intermediates to the reduction of CO_2 to alkanes or the reduction to alcohols as adjacent reduction processes to that of the reduction to alkanes. There is, therefore, evidence here to suggest that alcohols could be reduced to alkanes in similar conditions to the proposed mechanisms for the electrochemical reduction of CO_2. Surely bulk alcohol introduced into an electrolyte and a suitable electrode could be directly reduced to an alkane in a similar process to some of the CO_2 processes reported above?

1.4 Rationale for this work

The use of a number of electrodes for reduction of alcohols has been reported throughout the literature. The literature indicates suitable electrodes for the electrochemical reduction of alcohols, such as, Cu and Pt, therefore these metals are candidate electrode materials for this work. A variety of electrolyte solutions were indicated also, aqueous solutions of $NaHCO_3$, $KHCO_3$, and $NaClO_3$, dilute acidic solutions such as $HClO_4$, H_2SO_4 and aqueous phosphate buffer solutions prepared from K_2HPO_4 and KH_2PO_4. The phosphate buffers were considered initially as the supporting electrolyte in the work undertaken in this project.

Many areas of the literature report the occurrence of adsorbed species on the electrode, whether it is the product, the intermediate or H adsorption, adsorbates are a common thread and it will be important to consider this possibility within the studies undertaken here.

Previous studies in the area of electrochemical reduction of alcohols have been limited. The reduction of alcohols is performed by relatively few synthetic methods involving severe conditions.[28,38,40,44] The electrochemical reduction of alcohols is implicitly involved in the electrochemical reduction of CO_2, where the CO_2 was found to be able to be reduced to alcohols and alkanes and the alcohol possibly being an intermediate to the reduction to alkanes.[36,38]

Although there has been some research into the area of electrochemical reduction of alcohols the range of alcohols studied is limited and there is little mechanistic or kinetic information provided from the current research. A general mechanism has

not yet been provided. This leaves an interesting area for development within fundamental knowledge.

The present study, introduced in this report, is concerned with

a) establishing whether alcohols may be readily electrochemically reduced

b) determining the products of these reduction processes, and

c) establishing the mechanisms for the reduction

The conditions for reproducibility, for a variety of experimental parameters, of the reduction process will be demonstrated.

From the data obtained in this research a mechanism for the electrochemical processes of alcohol on the Pb electrode was developed.

1.5 Organisation of this Thesis

The format of this thesis has combined the results and discussion. Chapter 3 reports the results and discussion for the cyclic voltammetry of the rotating disc electrode and Chapter 4 reports the product identification and discussion of the Pb rotating disc electrode system. Chapter 2 provides details of the experimental conditions and equipment.

Figures are displayed two figures to one page when possible due to the extensive amount of figures presented in this work. However, FT-IR spectra included in chapter 4 are displayed in landscape orientation, one spectra to one page for easier interpretation.

CHAPTER 2

Experimental Methods and Materials

2.1 Introduction

This chapter provides an overview of the electrochemical methods and experimental conditions used to study the electrochemical reduction of alcohols in aqueous systems. Cyclic voltammetry (CV) was performed in aqueous phosphate buffer solutions over a range of alcohol concentrations, potential scan rates and electrode rotation rates. The analytical techniques used were Mass Spectrometry and gas phase Fourier Transform Infrared Spectroscopy (FT–IR).

2.2 Instrumentation

2.2.1 Potentiostat

An Autolab Potentiostat Galvanostat PGSTAT30 ADC 164 accompanied by Autolab GPES software (Eco Chemie B. V. Utrecht, The Netherlands, Ver. 4.9) was used to control the electrochemical experiments in this study.

The Autolab Potentiostat allows the control of the potential for the cyclic voltammetry.

2.2.2 Analytical Rotator

A MSRX speed control (PINE Instrument Company, NC, USA) controlled the rotation speed of the shaft in the analytical rotator (model AFMSRXE 1402, PINE Instrument Company, NC, USA). The analytical rotator also permits the changing of disc types, size and models for versatility in experiments. PINE Instrument Company provides electrodes of high purity metals typically > 99.9%.

2.2.3 Electronic Magnetic Stirrer

A Global Science electronic magnetic stirrer (IKA Colour squid) was used for the experiments where a rotating disc was not employed. The stirrer ensured good hydrodynamic flow to the electrode.

2.2.4 Mass Spectrometer

A Bruker 9.4T FT–ICR Mass Spectrometer was used for the Mass Spectrometry investigations. The sample was ionized with electron impact ionization.

2.2.5 FT–IR Analyser

A Nicolet 5700 FT–IR analyzer (Thermo Electron Corporation) was used for the FT–IR spectroscopy experiments, accompanied by OMNIC Software Version 7.3 (©1992-2006 Thermo Electron Corporation). A 200 mL gas cell was used for gas analysis.

2.3 Mechanistic Electrochemistry

Electroanalytical techniques are used to study chemical reactions taking place at the interface between an electrode (a metal or a semiconductor) and an electrolyte. These reactions involve electron transfer between electrode and electrolyte, or species in solution. Electroanalysis is concerned with the interrelation between electrical response and chemistry: measurements of electrical quantities, i.e. current, potential, and charge; and the relationship of these electrical quantities to chemical parameters.[13,14,18] There is a vast range of applications for electroanalytical techniques such as environmental monitoring, industrial quality control and biomedical analysis.[1,14,18,45] In contrast to many chemical measurements, electrochemical processes take place at the electrode-solution interface rather than in bulk phases or mixtures.

Electroanalytical methods are based on the measurement of either the current in an electrochemical cell at a fixed or varying potential (potentiostatic and potentiodynamic respectively), or the potential of a cell while the current is fixed at

some constant level (galvanostatic).[9,46] In general, choosing to control one variable precludes any independent control of the other. Control of the potential or current is achieved by the use of a potentiostat/galvanostat instrument. These instruments have the electronic hardware to control the electrochemical cell and perform a variety of electroanalytical experiments. The potentiostat maintains/controls the potential of the working electrode at a constant or varying level with respect to a reference electrode by adjusting the current flowing between the working and the counter electrodes. In galvanostatic mode the current is maintained at a constant level through the working and counter electrodes by varying the working electrode potential with respect to the reference electrode.

2.4 Analytical Techniques

2.4.1 Cyclic Voltammetry

Voltammetry is a technique in electrochemistry where information about an analyte is obtained by measuring the current of a system as the potential is varied. Voltammetric methods can study reaction kinetics and mechanisms. Some examples of how this can be achieved are: changing the solution flow rate at a channel or wall-jet electrode, changing the angular speed of a rotating disk electrode, or by the use of microelectrodes.[1,3,9,14,18,45-48]

Cyclic Voltammetry is the most widely used technique for acquiring initial information about electrochemical reactions.[9,14,46] It rapidly provides considerable information on the thermodynamics of the redox processes and the kinetics of the heterogeneous electron transfer reactions and on coupled chemical reactions of adsorption processes.[9,46] It is often the first experiment performed in an electroanalytical study; it offers prompt location of redox potentials of the electroactive species and convenient evaluation of the effect of the media on the redox process.[9,14,46] The potential of a stationary working electrode (WE) is scanned linearly using a triangular potential waveform and during the potential sweep the potentiostat measures the current resulting, producing the cyclic voltammogram.[9,13,14,46] The cyclic voltammogram is a current-potential plot, a display of the current signal versus the potential. The shape and magnitude of the cyclic voltammogram is governed by the processes involved in the electron

reaction.[1,9,13,14,18,45,46] Quantitative applications require establishment of a reliable baseline for accurate observations and conclusions.[13,18,45,46]

Characteristic peaks in a voltammogram are caused by the formation of a diffusion layer near the electrode surface.[13,18,45-48] Changes in the shape of the cyclic voltammogram can result from chemical competition for the electrochemical reactant or product.[9,46] This can be extremely useful for elucidating reaction pathways and providing reliable chemical information about: reactive intermediates, adsorption and desorption processes, and interfacial behavior, gradual increase of cathodic and anodic peak currents, and progressive adsorptive accumulation at the surface.[45]

Cyclic Voltammetry will be used in the present study to provide information about for the processes taking place for the electrochemical reduction of alcohols.

2.4.2 Mass Spectrometry

Mass spectrometry (MS) measures the masses of molecules and their fragments. It is used for determining the elemental composition of a sample, the masses of particles and of molecules, and for elucidating the chemical structures of molecules, such as peptides and other chemical compounds.[9,49,50] Mass spectrometry works by ionizing chemical compounds to generate charged molecules or molecule fragments and measuring their mass-to-charge ratios.[9,50] A vaporized sample passes into the ionization chamber where the ions are separated according to their mass-to-charge ratio.[9,50,51] The ions are detected and the signal is processed into the spectrum of the masses of the particles of that sample. Correlating known masses with the identified masses identifies the elements or molecules.[9,50,51]

Quadrupole mass analyzers use oscillating electrical fields to selectively stabilize or destabilize the paths of ions passing through a radio frequency (RF) quadrupole field created between 4 parallel rods.[50,51] Only the ions in a certain range of mass/charge ratio are passed through the system at any time, but changes to the potentials on the rods allow a wide range of m/z values to be swept rapidly, either continuously or in a succession of discrete hops. A quadrupole mass analyzer acts as a mass-selective filter and is designed to pass untrapped ions.[50,51] It is important that the mass spectrometer has a vacuum so that the ions produced in the ionization chamber can pass through the instrument avoiding collisions with other gas phase species.[50]

Mass Spectrometry can detect to a minimum molar mass of 28 g mol^{-1}, and can be used for liquid or gas samples.[50] For testing a solution, previous studies have used a membrane as the WE; however, this introduces a new interface and is difficult to set up.[52] Another option is a capillary in the solution or a simple injection into the Mass spectrometer. Gas samples can be collected in a headspace above the reaction with capillary transfer to the Mass Spectrometer or an injection of the sample into a carrier gas stream in the Mass Spectrometer.[52]

2.4.3 Fourier Transform Infrared Spectroscopy (FT-IR)

Infrared spectroscopy is the measurement of the wavelength and intensity of the absorption of infrared light by a sample.[9,16,53] Infrared light is energetic enough to excite molecular vibrations to higher energy levels. The wavelength of the infrared absorption bands are characteristic of specific types of chemical bonds, and infrared spectroscopy finds its greatest utility for identification of organic and organometallic molecules, and can be used for the analysis of gas, liquid or solid samples.[9,53]

This method involves examination of the twisting, bending, rotating and vibrating motions of atoms in a molecule. Virtually all organic compounds will absorb infrared radiation due to characteristic normal mode frequencies of their component atoms.[9,53]

Molecular vibrations have characteristic frequencies in the Infrared region of the electromagnetic spectrum.[9,53] Molecular vibrations generally involve highly coupled, and therefore delocalised, motion of the atoms in a molecule, making detailed interpretation of most bands in an infrared spectrum a challenging task. These bands are known collectively as the finger-print bands in vibrational spectroscopy, as the complex pattern of band intensities and frequencies provide a virtually unique identifier for each molecule. Functional groups of atoms with either different masses or bond strengths from the molecular “backbone” do, however, display characteristic frequencies and modes, that are independent of the molecular structure, and for this reason Infrared spectroscopy has been used extensively for the identification of functional groups in organic compounds.[53,54]

2.5 Electrochemical Cells

A three electrode cell is commonly used in controlled potential experiments and was employed for the purposes of this work. The three electrodes are the working electrode, WE, the reference electrode, RE, and the counter electrode, CE, all of which are immersed in the sample solution.[1,9,13,14,18,45-48] The potential of the WE is controlled by the use of a potentiostat that fixes, in the case of chronoamperometry, or scans in the case of cyclic voltammetry, the potential difference between the WE and the RE by altering the current flowing through the WE and CE.[13,14,18,45,48] The RE provides a reference potential and does not pass current.[13,14,48]

By definition, the cathode is the electrode at which reduction occurs, while the anode is the electrode where oxidation takes place.[9] Therefore, in this work, the WE is the cathode and the CE is the anode as we are examining a reduction of interest at our WE. A current where electrons cross the interface from the electrode to the species in solution is a cathodic current, and electron flow from the solution species into the electrode is an anodic current.[13]

The RDE experiments were conducted in a 30 mL (internal volume) water-jacketed glass cell and thermally controlled at 25.0°C ± 0.5°C by an LKB Bromma 2219 Multitemp II Thermostat Circulator (initial experiments in this work, without the RDE, were not thermally controlled). A fritted gas bubbler 25–50 µm (Bioanalytical Systems Inc. Indiana, USA, model MW 4145) was immersed in the electrochemical cell for deoxygenation of the electrolyte (see deoxygenation, Section 2.6). Prior to conducting any electrochemical experiments the gas flow was terminated.

2.5.1 Working Electrodes

The WE is the electrode at which the reaction of interest occurs. [1,13,14,18,48] The potential of the WE is observed or controlled with respect to the RE. This is equivalent to controlling the energy of the electrons within the WE.

The analyte is usually dissolved in an electrolyte solution.[13,48] At the surface of the WE, the dissolved electrochemically-active species alter their charges by exchanging one or more electrons with the electrode. The performance of a voltammetric procedure is strongly influenced by the working electrode material.[1,13,14,18,48] The working electrode should provide high signal to noise characteristics, as well as a reproducible result. Selection depends on the redox behaviour of the target analyte

and the background current over the potential region required for measurement. Other considerations are the potential window (for the electrolyte and solvent reduction and oxidation on that WE), electrical conductivity, surface reproducibility, mechanical properties, cost, availability and toxicity.[9,13,14,18,45,46]

Electrochemical reduction of alcohols

$$R{-}OH + 2e^{-} + 2H^{+} \rightarrow R{-}H + H_2O \qquad (1.13)$$

occurs at the WE with the generation of a Faradaic current due to the electron transfer processes.[55-63] The Faradaic current is defined as the portion of the current flowing through the working electrode generated by the reduction or oxidation of some chemical substance at the electrode. [55-63]

For the preliminary investigations 10 electrode materials in a range of presentations (based on immediate availability) were used as the WE: lead sheet, copper wire, tin sheet, silver wire, gold microelectrode, platinum microelectrode, titanium oxide block, aluminium sheet, nickel disc electrode and a glassy carbon microelectrode.

The second phase of experiments involved the use of the RDE, containing a lead, copper or tin disc as the WE.

Subsequently, experiments on larger surface area electrodes for the WE were performed to aid product determination.

2.5.2 Rotating Disc Electrodes (RDE)

RDEs are a controlled mass-transport electrode system for which hydrodynamic equations and convective-diffusion equations have been solved rigorously for the steady state.[13] RDEs consist of a disk of material of interest embedded in a cylinder of insulating material with only the circular surface exposed to the solution as illustrated in Fig. 2.1. The electrode is rotated in the solution under study. In this work rotation speeds were in the range 0-50 Hz. RDEs are typically vertically mounted (with the electrode disk forming the lower face) in the shaft of a synchronous controllable speed motor and rotated with constant angular velocity, ω, about an axis perpendicular to the planar disc surface.[1,14,46]

a)

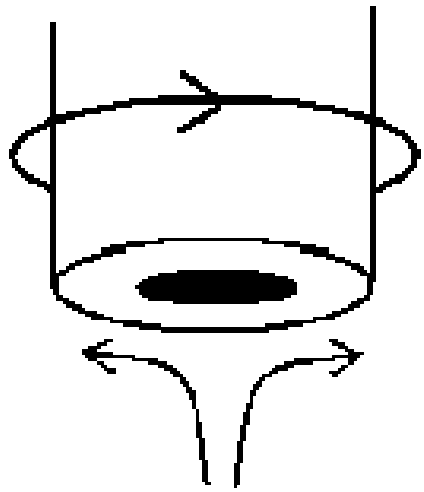

b)

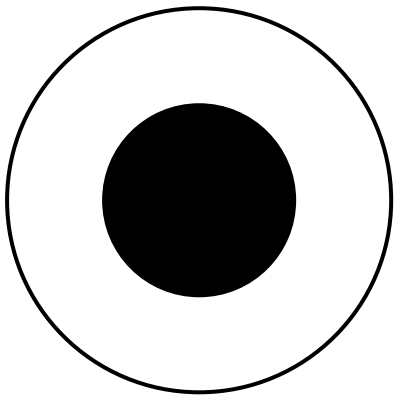

Fig. 2.1(a) A schematic diagram of a RDE with the upper circular arrow depicting the rotation of the shaft. The darkened circle in the centre of the bottom is indicative of the disc surface of the end of a cylinder of electrode material and the arrows up and out at the bottom of this cylinder show the direction of the induced flow of the electrolyte.
Fig. 2.1(b) Bottom view of the RDE where the central darkened circle is again the disc surface.

As the electrode rotates it induces a flow of electrolyte rising perpendicular to the disc from the bulk of the solution that then flows uniformly across the face of the disk due to centrifugal forces.[13] This continually replenishes the supply of the electroactive species in the solution at the surface of the electrode.

Reversal techniques, such as examining the immediate reoxidation of a reduced product by a reverse anodic sweep, are not available with RDEs as the product of the electrode reaction is continuously swept away from the disk.[13]

In the RDE experiments in this work a lead, copper or tin RDE with a geometric area of $1.97 \times 10^{-5}\ m^2$ was used as the WE. The RDE was held at constant rotation speeds of 500, 675, 750, 1000, 1250, 1500, and 2000 rpm. The RDE employed in this work has a maximum rotation rate of 3000 rpm.

2.5.2.1 Mass Transport and the Rotating Disc Electrode

An electrode reaction is an interfacial reaction involving mass transport of the electroactive species to the electrode surface and a charge transfer step at the surface. Diffusion, migration and convection are three possible mass transport processes.[56] The rate of the electrode process depends on the most hindered step in the process. Stirring of an electrolyte solution results in the bulk concentration being maintained at a distance and a diffusion layer is established.[56] This stirring can be achieved with the help of a RDE. The diffusion layer thickness is a crucial parameter in the system. This is the thickness from the electrode surface where no hydrodynamic motion of the solution is assumed and thus mass transport occurs mostly by diffusion. Diffusion is induced by concentration gradients arising between the electrode surface and the bulk solution.[56] Forced convection can also be achieved by stirring the solution.[56] Under laminar flow conditions the thickness of the diffusion layer decreases with increasing electrode angular velocity; thickness of the diffusion layer is independent of the diameter of the disc electrode which gives a uniform layer across the surface of the electrode. The decrease in the diffusion layer thickness provides a sharper concentration gradient and forced convection of the electroactive species to the electrode surface. This provides efficient and reproducible mass transport and allows analytical measurements to be made with high sensitivity and precision, simplifying the interpretation of the measurement.[13,14,18,45,46]

Rotation of the RDE takes place at an angular velocity, ω, in rad s^{-1} resulting in well-defined transport of the electroactive species to the electrode surface by forced convection.[45,56] Therefore when using a RDE, material is transported to the electrode surface by a combination of diffusion and force convection. Considering Fick's first law and the Nernst Diffusion layer concept, the current response is expressed in eqn. 2.1.

$$I = \frac{nFD(c_b - c_s)}{\delta} \qquad (2.1)$$

Where I is the current density, A cm^{-2}, n the number of electrons transferred during the reaction, F is the Faraday constant, 96,485.3 C mol^{-1}, D is the diffusion coefficient of the electroactive species, m s^{-1}, c_b and c_s are the bulk and surface

concentrations of the electroactive species respectively, mol L^{-1}, and δ is the thickness of the Nernst diffusion layer.[47,56]

A limiting current, I_L, is reached when the surface concentration of the electroactive species of interest becomes effectively zero, $c_s = 0$. Substitution of $c_s = 0$ into eqn 2.1 provides the relationship for the limiting current given in eqn 2.2.[13,14,47,56]

$$I_L = \frac{nFDc_b}{\delta} \qquad (2.2)$$

However this relationship does not take into account the hydrodynamics of the process, being the electrode rotation rate. Under laminar flow conditions, in a liquid medium of kinematic viscosity, ν, the thickness of the diffusion layer decreases with increasing angular velocity according to the quantitative treatment described by Levich.[47]

$$\delta = 1.61D^{1/3}\omega^{-0.5}\nu^{1/6} \qquad (2.3)$$

The combination of eqn. 2.2 and 2.3 then give the Levich equation, eqn. 2.4, for the hydrodynamic processes at the RDE under mass-transport conditions.

$$I_L = 0.620nFD^{2/3}\omega^{0.5}\nu^{-1/6}c_b \qquad (2.4)$$

From this it is evident that under mass transport the limiting current should be proportional to the square root of the angular velocity.[47]

2.5.2.2 Turbulent and Laminar Flow and the Reynolds Number

Laminar flow in the vicinity of the disk electrode is essential to interpret electrode kinetics and is the flow rate of interest in this work. The point at which the transition from laminar flow to turbulent flow occurs is predicted using the Reynolds number, *Re*, defined by

$$Re = \omega r^2/\upsilon \qquad (2.5)$$

where ω is the electrode rotation rate in rad s^{-1}, υ is the kinematic viscosity of the fluid in m^2/s and r is the radius of the rotating cylinder in m ($r = 7.5 \times 10^{-3}$ m for this study). The critical *Re* number represents the upper limit for laminar flow over ideal smooth planar surfaces.[56] Equation 2.5 can be rearranged to give the maximum rotation rate before turbulent flow is likely to occur.

$$\omega = \upsilon Re/r^2 \quad (2.6)$$

υ is likely to be close to that for pure water at the maximum ω obtainable by the RDE. Provided the Reynolds number is not exceeded, laminar flow will occur and the mass transport of the species in solution may be determined. The critical Reynolds number is 2×10^{-5}.[56] Therefore, the maximum rotation rate possible for maintenance of laminar flow based on this critical Reynolds number of 2×10^{-5} is 3364 rpm. This is higher than the maximum rotation rate of 2500 rpm used in this work. Therefore, in this work laminar flow is consistently achieved.

2.5.3 Large Surface Area Electrodes

A large surface area electrode was employed to obtain larger volumes of reduced material in order to aid the product determination analysis of the Pb electrode system due to the interesting phenomenon observed.

A large surface area lead electrode was obtained by extracting a lead plate from a lead acid battery. With careful washing to remove all acid residues and full charging to ensure the lead plate was completely in the Pb^0 state, the plate was suitable to be used with a surface area of $> 1 \times 10^{-3}$ m^2. The exact surface area is unable to be determined due to the surface texture of the plate.

2.5.4 Counter Electrode

The current carrying CE is usually a non-reactive high surface area electrode of inert conducting material such as platinum wire or graphite rod.[1,2,7,45,56] The CE is driven by the potentiostatic circuit to balance the Faradaic process at the WE, *i.e.* current flows between the WE and CE.[1,13,14,45,56] Processes occurring at the CE are typically of no interest; any electrolytic products at the CE have no influence on the processes occurring at the WE, and this was assumed to be the case here.[13,14,56]

It is recommended that the area of the CE is substantially larger than that of the WE. If the area is larger than the WE, the CE should not effect the current measurement due to passivation, deactivation or blocking.[1,13,14,56]

A platinum static disc electrode with diameter 1.6 mm (Bioanalytical Systems Inc., Indiana, USA, model MF-2013) was used as the CE for all preliminary and RDE

experiments with a Ni mesh used as the CE for all large surface area WE experiments.

2.5.5 Reference Electrode

The RE provides a stable and reproducible potential (independent of the sample composition), against which the potential of the WE is compared.[14,18] The potential of the RE is fixed; any changes in the cell are ascribable to the WE. In a three electrode system, as used here, a very small current only, of the order of pA, charges the RE.[14,18] Such small currents do not affect the species that determine the potential of the RE.[14,18]

2.5.5.1 Silver/Silver Chloride (Ag/AgCl) Reference Electrode

The Ag/AgCl reference electrode is the most frequently used RE because its construction is very simple, the potential is very reproducible and importantly it is also free of mercury.[1,13,14,18,45,56] The construction is usually of a silver wire covered with a layer of solid AgCl, formed electrochemically or thermally, in contact with an electrolyte solution typically of saturated KCl. [14,18,24,56] The electrode reaction is given by:

$$Ag^0 + Cl^- \leftrightarrow AgCl + e^- \qquad (2.3)$$

The Ag/AgCl electrode allows measurements to be taken in high temperature and changing pressure conditions.

Frits are typically used to provide physical separation between the saturated KCl reference electrode solution and the electrolyte employed in the three-electrode cell. The chloride concentration is usually higher in the reference electrode solution forming diffusive fluxes across the frit and therefore potentially leading to contamination of the three-electrode test solution. Incorporation of an intermediate bridge, known as a Luggin tube, with a further frit, minimizes this potential for contamination.[14,18,56]

An Ag/AgCl gel electrode with a saturated KCl internal electrolyte (Koslow Scientific Company, New Jersey, USA, model 1004) was used as the RE in all experiments. The RE was mounted in a Luggin tube fitted with a Vycor tip

(Vycor^{TM}, tip length 3.5 mm, Koslow Scientific company, New Jersey, USA, model 5011), in turn immersed in the electrochemical cell. The Luggin tube was filled with identical electrolyte solution to that used in the three-electrode cell.

The potential of the Ag/AgCl gel electrode is 197 mV *vs.* the standard Hydrogen Electrode.[56] The potential of the WE is quoted with respect to this Ag/AgCl RE throughout this work.

2.6 Supporting Electrolyte

Electrochemical measurements are commonly carried out in a medium that consists of solvent containing a supporting electrolyte. The choice of solvent is usually based on the solubility of the electroactive species, the redox activity of the analyte and the solvent properties such as electrical conductivity, chemical reactivity, and electrochemical activity.[1,9,14,46,47] The supporting electrolyte should be prepared from highly purified reagents and not be easily oxidized or reduced or react with the electroactive species or products. When there is a need for pH control, buffer solutions are used as electrolytes. Aqueous and non-aqueous solvents can be used, and mixed solvents may be used for certain applications.[1,9,18,45]

In most experimental situations it is common to work with a large quantity of supporting electrolyte. A high concentration of supporting electrolyte can aid in the elimination of electromigration effects and will decrease the cell resistance. Additionally it will minimize the potential drop across the cell as current flows.[1,9,18,45] Electron transfer between the electrode and solution species is located within a distance of some 10–20 Å of the electrode surface, and with sufficient supporting electrolyte the electrical double layer can be of comparable thickness. Typical concentrations for the supporting electrolyte are $> 10^{-1}$ M and electrolytes are chosen for their electrochemical inertness at the potentials of interest.

The electrical double layer is the array of charged particles and/or oriented dipoles that exist at every material interface.[13,56] The charging of the double layer is responsible for the background current. It occurs when a potential is applied across the double layer or when the electrode area or capacitances are charging.[13,56] Electrons are not transferred across the electrode-solution interface in a background current.

Aqueous 0.1 M Phosphate buffer solutions were selected as the electrolyte for the reported work. The initial aim of this study was to investigate the electrochemical reduction of alcohols in aqueous systems, which requires an aqueous electrolyte. Phosphate buffers provide pH control, are simple and easy to use, and do not add any complexity to the investigation.

2.7 Reagents

All chemicals used in the preparation of this work were > 99% purity and all electrolyte solutions were prepared in millipore water (Millipore^{TM}, Milli-Q type I Reagent water system).

2.7.1 Alcohols

Absolute ethanol (99.9% pure, HPLC grade), propanol (99.5% pure, AnalaR), propan-2-ol (99% pure, AnalaR) butanol (99.5% pure, AnalaR) and methanol (99% pure, AnalaR) were used in this work.

2.7.2 Phosphate Buffers

The experiments in this thesis were performed in 0.10 mol L^{-1} phosphate buffer solutions of varying pH. These phosphate buffer solutions were prepared using K_2HPO_4, (Analytical UNIVAR Reagent, 2221, AJAX Chemicals, Australia, > 99% purity.) and KH_2PO_4, (AnalaR BDH Laboratory Supplies, Product 102034B, England, > 99% purity.)[57] in Millipore water (Millipore^{TM}, Milli-Q type I Reagent water system) as reported in Table 2.1 maintaining a constant 0.100 molL^{-1} total phosphate concentration, [PO_4^{3-}].

Four candidate 0.10 M phosphate buffers, of pH 5.3, 6.0, 7.3, and 8.1, were tested in the preliminary studies with two determined to be used in the RDE experiments, those at pH 7.3 and 8.1, with the three selected electrode materials.

Table 2.1 Composition of 0.1 M Phosphate buffer solutions over the pH range 5.3 – 8.1.[57]

Composition of Standard 0.1M Phosphate Buffer Solutions		
	$[K_2HPO_4]$	$[KH_2PO_4]$
pH	mol L^{-1}	mol L^{-1}
5.3	0.0975	0.0025
6.0	0.0875	0.0125
7.3	0.0250	0.0750
8.1	0.0040	0.0960

2.8 Deoxygenation of Electrolyte

Under normal atmospheric conditions at room temperature oxygen dissolves in aqueous solutions up to 10^{-3} M.[1] In this work the concentrations of C_2H_5OH were in the range 7–15 mM; this potential concentration of dissolved oxygen is comparable and may be significant, either through participating in reoxidation of a material just formed, or by giving rise to a background current due to O_2 reduction. This work was performed in slightly acidic to slightly basic pH 5.0–8.0 electrolytes.

Dissolved oxygen may be reduced in acidic media according to [1]

$$O_2(aq) + 2H^+(aq) + 2e^- \rightarrow H_2O_2(aq) \quad (2.4)$$

followed by

$$H_2O_2(aq) + 2H^+(aq) + 2e^- \rightarrow 2H_2O(l) \quad (2.5)$$

And in neutral or basic media as

$$O_2(aq) + 2H_2O(aq) + 2e^- \rightarrow H_2O_2(aq) + 2OH^-(aq) \quad (2.6)$$

followed by

$$H_2O_2(aq) + 2e^- \rightarrow 2OH^-(aq) \quad (2.7)$$

To avoid the possibility of interference by dissolved oxygen in this work, deoxygenation of the electrolyte was employed for all experiments. A fritted gas bubbler 25-50 µm (Bioanalytical Systems Inc. Indiana, USA, model MW 4145) was immersed in the electrochemical cell for deoxygenation of the electrolyte. Prior to conducting any electrochemical experiments the gas flow was terminated.

2.9 Data Analysis

The Autolab GPES software was used for all electrochemical data acquisition. Although Autolab software is well organized and can acquire and can record data to excellent resolution, the software is capable of only relatively routine deconvolution and interpretation of data. The Autolab software can be used to determine peak parameters, perform basic convolution and linear regressions, and perform baseline corrections. It also performs fitting and simulation processes based on predetermined models.

As this study is not just obtaining new data, but also applying a range of mathematical models, the Autolab interpretation capabilities are insufficient. Consequently, there was a need for offline data analysis. Excel™ was employed to assemble spreadsheets that can encapsulate proposed models, optimize the kinetic parameters using the Excel™ Solver routine, and prepare the plots for presentation in this report.

The OMNIC software was used for all FT-IR spectroscopy data acquisition. The OMNIC software was used to determine absorbance and transmittance of samples, and specify peak positions, however, Excel™ was again employed to assemble spreadsheets and compare collected spectra data.

Chapter 3

Rotating Disc Electrode Cyclic Voltammetry Results and Discussion

3.1 Introduction

The objective of this project was to investigate the electrochemical reduction of alcohols using a selection of electrode materials and aqueous supporting electrolytes and to establish possible conditions for the electrochemical reduction of alcohols. Ten different electrode materials; lead, copper, tin, silver, gold, platinum, aluminium, titanium oxide, glassy carbon, and nickel, were investigated with four 0.1 M aqueous phosphate buffers (ranging from pH 5.3 – 8.1, see Table 2.1) as supporting electrolytes. This was to provide an initial appraisal of electrode/electrolyte combinations affording a response for ethanol reduction.

The main focus of this chapter is to interpret and discuss the observations of the rotating disc electrode (RDE) cyclic voltammetry of the electrode materials determined to have a reductive response due to the presence of alcohol. Different aspects of the RDE cyclic voltammetry studies are focused on, such as, concentration dependence, scan rate dependence, and rotation rate dependence.

The experiments were carried out with the digitally-controlled potentiostat where both potential and current within the cell can be controlled as described in Section 2.1.

3.2 Cyclic Voltammetry

Cyclic voltammetry rapidly provides considerable information on the thermodynamics of the redox processes, the kinetics of the heterogeneous electron transfer reactions and on coupled chemical reactions of adsorption processes.[1,2,6,7,24] The potential of the WE is scanned linearly using a triangular potential waveform and the potentiostat measures the current resulting, producing the cyclic voltammogram.[1,2,24,46] The cyclic voltammogram is a current-potential plot, a display of the current signal versus the potential, where the shape and magnitude of the cyclic voltammogram is governed by the processes involved in the electron reaction.[1,2,6,7,24,45,46] Cyclic Voltammetry was

the main electrochemical technique employed in this study for the purpose of providing an overview of the electrochemical processes of the alcohols taking place in the system.

3.3 Preliminary Results

Several electrode materials and electrolyte solutions were tested to establish suitable conditions for the possible electrochemical reduction of alcohol. Evidence of a reductive response in the presence of ethanol in the supporting electrolytes of varying pH was established. The preliminary results indicated that there was significant electrochemical activity due to the addition of ethanol associated with three particular electrode materials, copper and lead in the pH 8.1 phosphate buffer and tin in the pH 7.3 phosphate buffer. The results for the other combinations of candidate electrodes and buffers are not reported here. Discs of the three promising metals for the RDE were obtained for the next phase of experiments. Five low molecular weight alcohols, all having appreciable solubility in the aqueous system, were selected for investigating on the RDE, methanol, ethanol, propanol, propan-2-ol and butanol.

The following sections of this chapter detail the observations for the cyclic voltammetry studies for each of the three metal discs.

3.4 Copper Rotating Disc Electrode Cyclic Voltammetry

The electrochemical reduction of the five alcohols, methanol, ethanol, propanol, propan-2-ol and butanol on a Cu RDE in the aqueous phosphate buffer of pH 8.1 was examined. An electrochemical response on the copper disc electrode was observed with the addition of ethanol, propanol, propan-2-ol and butanol; but no electrochemical response was observed with the addition of methanol. This section discusses the cyclic voltammetry responses on the copper rotating disc electrode due to the presence of ethanol, propanol, propan-2-ol and butanol.

The electrode material utilized here, copper, is not an inert substance and has its own electrochemistry within the system. Therefore, it is important to first establish the electrochemistry of the electrode within the electrolyte system before attempting to establish the electrochemistry specifically associated with the alcohol reduction.

Figure 3.1 shows the cyclic voltammograms for the copper disc electrode in 0.1 M pH 8.1 phosphate buffer with and without the presence of 10 mM ethanol. For the cyclic voltammogram in the absence of ethanol an oxidation current is observed when commencing at an anodic limit more positive than −100 mV, assumed to be associated with the oxidation process of $Cu^0 \rightarrow Cu^{2+}$. A reductive wave, C1, is also present when the potential is swept progressively more cathodic due to the reduction process, $Cu^{2+} \rightarrow Cu^0$. On the return anodic sweep a anodic wave, A1, is observed again for the oxidation process of $Cu^0 \rightarrow Cu^{2+}$.

Upon the addition of the 10 mM ethanol the oxidative and reductive waves assigned to the electrochemistry of copper in this electrolyte are retained. However, there appears to be a limiting current plateau at more cathodic potentials than C1. This plateau, identified in Fig. 3.1 as C2, provides evidence of the behavior that would be expected in rotating disc electrochemistry. When both the reactant and the product are soluble, and there is a continual replenishment of reactant at the electrode surface, an increase in the reductive current is observed, until the surface concentration reaches zero, followed by a limiting current plateau due to the diffusion from the bulk electrolyte. Continuous replenishment of reactant toward the surface of the reactant leads to a continual reduction response.

The limiting current plateau observed at potentials more cathodic than −300 mV appears to be associated with the addition of the alcohol. The onset of the reduction occurs at a potential of −0.2 V and reaches the limiting current plateau at approximately −0.3 V, more than 200 mV more cathodic than C1. However, there is a possibility that a new copper product is responsible for the plateau rather than the alcohol itself. This possibility must be eliminated to accurately interpret the alcohol response. Therefore the potential range was limited to a region where the copper would be maintained in the reduced Cu^0 state through the range. The new anodic limit and starting potential for the cyclic voltammogram was set at −0.1 V, more cathodic than the cessation of Cu^0 oxidation on the cathodic scan. The cathodic limit was maintained at −1.2 V. This new potential range of −0.1 to −1.2 V was used for all subsequent copper scans. Figure 3.2 shows the resulting voltammogram when performing cyclic voltammetry within the potential range of −0.1 to −1.2 V. A limiting current plateau is observed with no evidence of the electrochemistry of copper that was observed in the previous larger potential range.

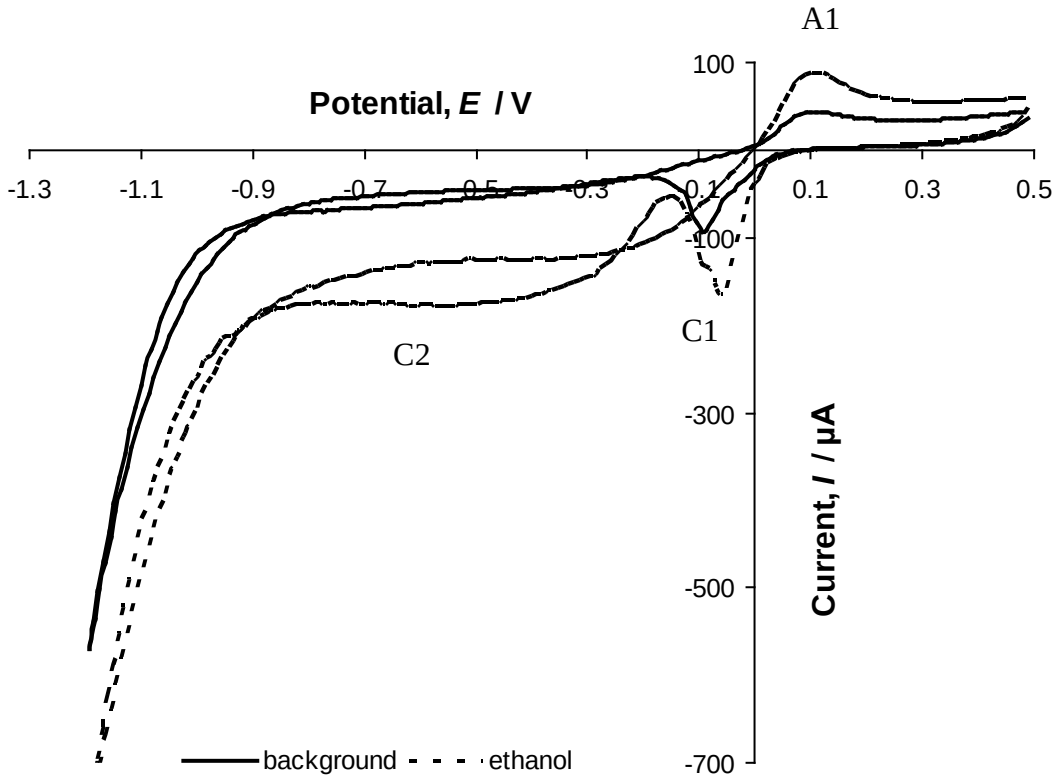

Fig. 3.1 Cyclic voltammograms for the copper disc electrode in pH 8.1, 0.1 M Phosphate buffer with and without the presence of 10 mM bulk ethanol concentration, collected at 50 mV s^{-1} potential scan rate and 1000 rpm electrode rotation rate.

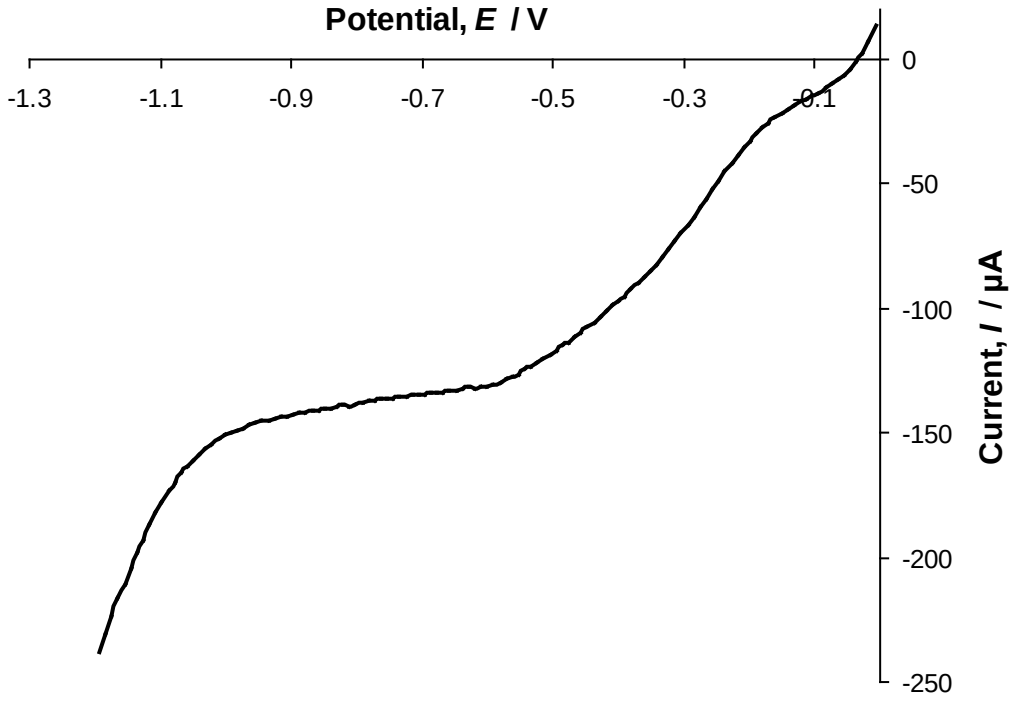

Fig. 3.2 Cyclic Voltammogram for the copper disc electrode in pH 8.1, 0.1 M phosphate buffer in the presence of 10 mM ethanol, at 50 mV s^{-1} potential scan rate and 1000 rpm electrode rotation rate confined to the potential range −0.05 to −1.2 V.

This observation is consistent with the hypothesis that the presence of ethanol is responsible for the plateau. The limiting current plateau was found to be reproducible with cycling and the anodic wave followed the already scribed cathodic wave. Therefore, as long as the potential was less cathodic than the onset of the reduction current, I_{ons}, approximately –0.3 V, the reduction was continuous.

3.4.1 Data Analysis

The background cyclic voltammograms of the phosphate buffer solution electrolyte fit well to the beginning of the cyclic voltammograms in the presence of the alcohols. As such, it was assumed that the addition of the alcohol has very little effect on the underlying Cu electrochemistry, in this potential range, -0.1 to -1.2 V. Therefore the background voltammograms were suitable to use as the baseline without requiring any scaling or fitting of trendlines.

The limited current was determined and compared for all scan rates, rotation rates, and alcohol concentrations to determine trends in the data. The background current was subtracted from the alcohol data to obtain a current response associated with the addition of the alcohol, therefore eliminating any response due to the reduction of the electrolyte.

3.4.2 Effect of Alcohol Concentration

Four of the primary alcohols initially examined; ethanol, propanol, propan-2-ol and butanol, provided significant electrochemical response with the Cu disc electrode. The effect of the bulk concentration of these four alcohols in the 0.1 M phosphate buffer electrolyte, pH 8.1, was investigated.

Voltammograms for a range of bulk alcohol concentration were examined. The bulk alcohol concentration in the 0.1 M phosphate buffer electrolyte was increased from 7 mM to 10, 15 and 20 mM. Figures 3.3 – 3.6 show the voltammograms of the four bulk ethanol, $[C_2H_5OH]_{bulk}$, propanol, $[C_3H_7OH]_{bulk}$, propan-2-ol, $[CH_3CH(OH)CH_3]_{bulk}$ and butanol $[C_2H_5OH]_{bulk}$ concentrations respectively.

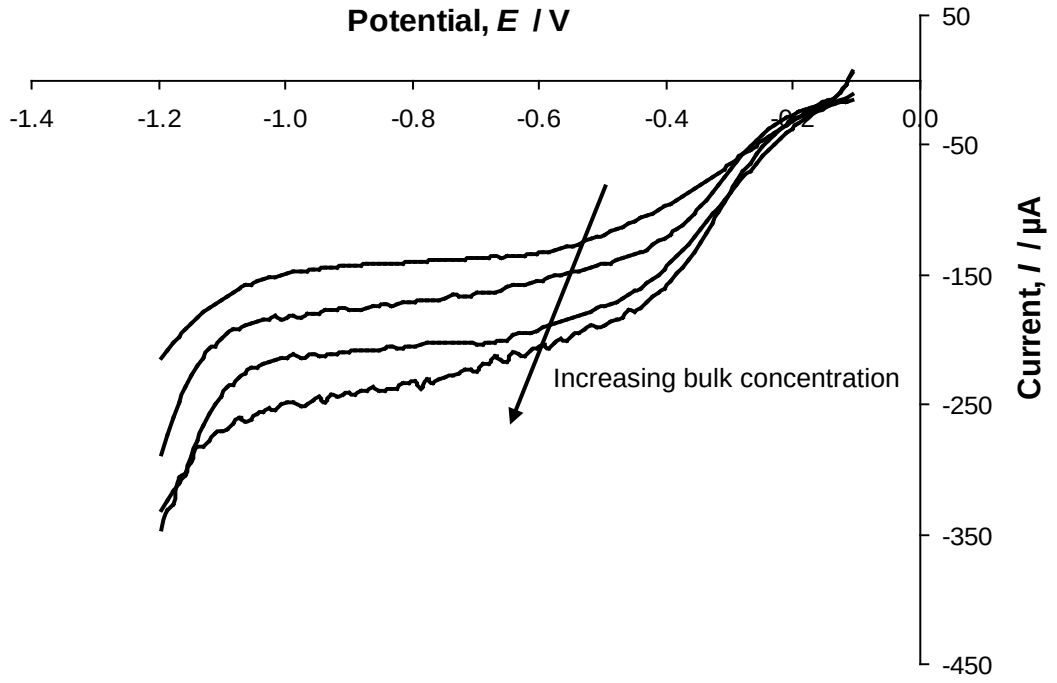

Fig. 3.3 Cathodic sweeps of the cyclic voltammograms for the Cu RDE, at 7, 10, 15 and 20 mM bulk ethanol concentrations, showing increase in limiting current plateau with increasing concentration, collected at 1000 rpm electrode rotation rate, and 50 mV s^{-1} potential scan rate.

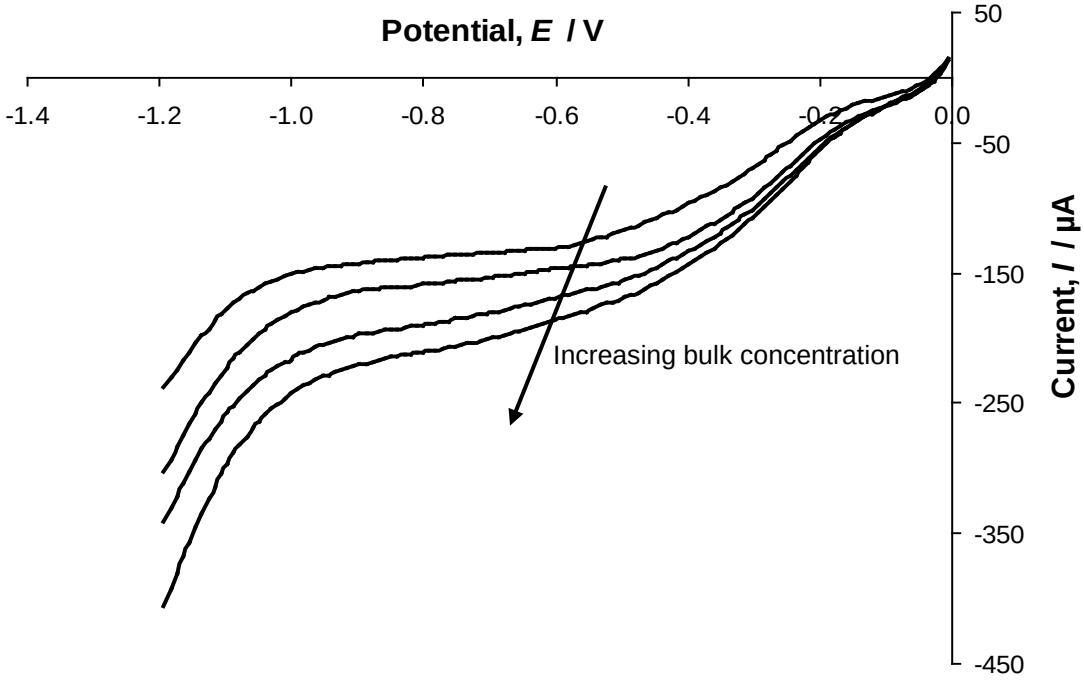

Fig. 3.4 Cathodic sweeps of the cyclic voltammograms for the Cu RDE, at 7, 10, 15 and 20 mM bulk propanol concentrations, showing increase in limiting current plateau with increasing concentration, collected at 1000 rpm electrode rotation rate, and 50 mV s^{-1} potential scan rate.

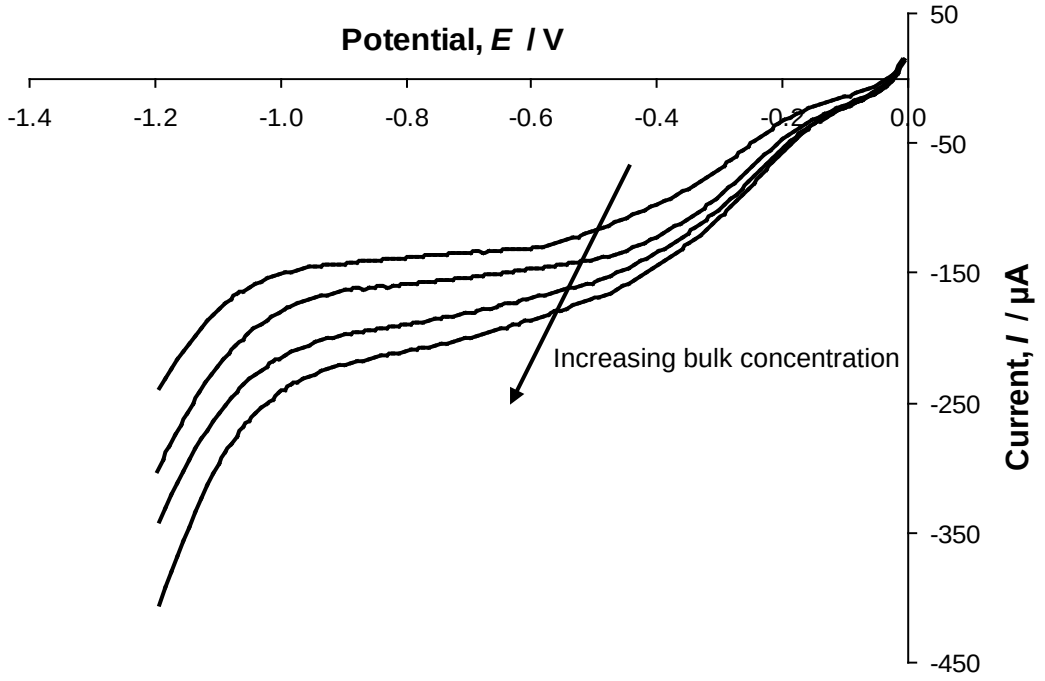

Fig. 3.5 Cathodic sweeps of the cyclic voltammograms for the Cu RDE, at 7, 10, 15 and 20 mM bulk propan-2-ol concentrations, showing increase in limiting current plateau with increasing concentration, collected at 1000 rpm electrode rotation rate, and 50 mV s^{-1} potential scan rate.

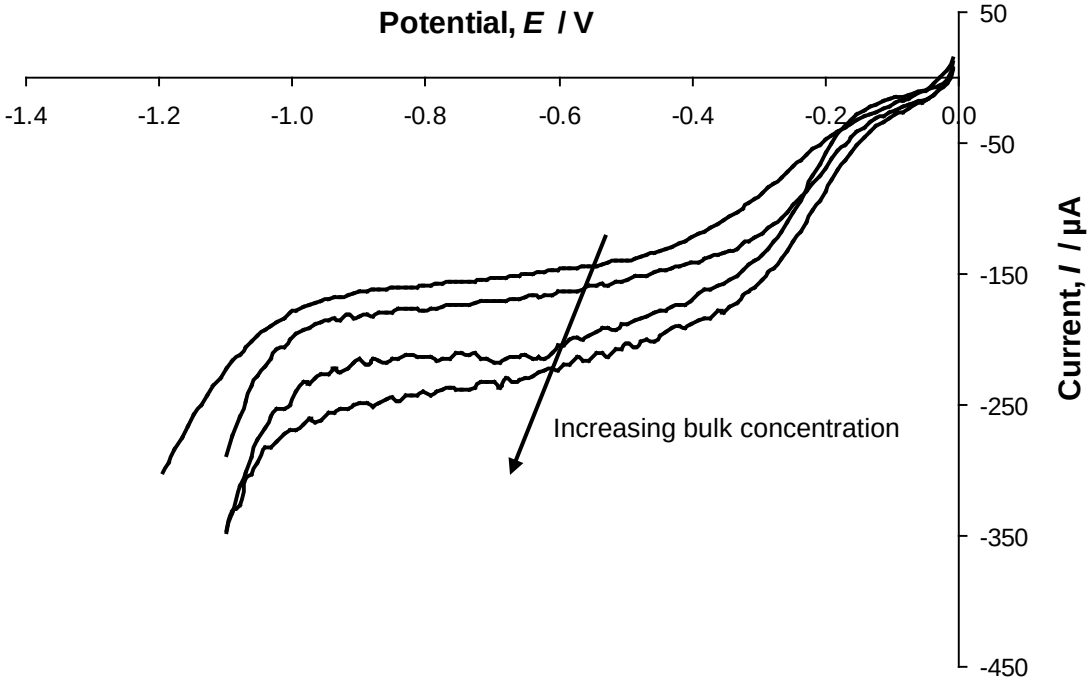

Fig. 3.6 Cathodic sweeps of the cyclic voltammograms for the Cu RDE, at 7, 10, 15 and 20 mM bulk butanol concentrations, showing increase in limiting current plateau with increasing concentration, collected at 1000 rpm electrode rotation rate, and 50 mV s^{-1} potential scan rate.

The voltammograms were collected in the potential range −0.1 to −1.2 V at 1000 rpm electron rotation rate and 50 mV s^{-1} potential scan rate. An increase in limiting current is observed with increasing alcohol concentration.

Table 3.1 shows the observed limiting currents for the three alcohols at each concentration. These values show a progressive increase in the limiting current for each alcohol as the bulk alcohol concentration is increased. The three alcohols appear to behave similarly, at any one concentration the 3 alcohols limiting current values agree within an uncertainty of ± 10 μA and the progressive increases exhibited by each alcohol follow similar trends.

This progressive increase in limiting current is exhibited by all four of the alcohols that provided a response and is consistent with the reduction of the alcohol being a diffusion-controlled reduction process. Reduction can only occur when the analyte is in the vicinity of the electrode surface, but as the experiments are being performed on a RDE the laminar flow induced by the rotation of the electrode will help to provide a continuous replenishment of the alcohol at the surface allowing continuous reduction. An increase in concentration of the alcohol in the bulk electrolyte leads to a larger amount of alcohol being replenished at the surface of the electrode at any one time. This larger amount of alcohol present allows for a larger reduction current to be produced. In these experiments the rotation rate is unchanged so the reactant is replenished at the surface at the same flow rate in each experiment, the diffusion coefficient is the same for each experiment with the same alcohol, however, with an increase in concentration there is more analyte available at any time to diffuse to the surface and an increase in reduction response with increasing concentration would be expected if the process is diffusion-controlled.

When the concentration of any of the 3 alcohols is approximately doubled from 7 to 15 or 10 to 20 mM the current is observed to increase < 1.5 times. For example at 7 mM the limiting current produced is approximately 1.4×10^{-4} A, and when the concentration is increased to 15 mM the limiting current is observed to be approximately 2.0×10^{-4} A. When the concentration is approximately tripled from 7 mM to 20 mM the current is then observed to less than double (from ~1.4×10^{-4} A to ~2.2×10^{-4} A respectively). If the process was completely diffusion controlled an increase in reduction current proportional to the increase in concentration would be expected, i.e. doubling the concentration would double the reduction current response.

Table 3.1 Limiting current observed on the Cu RDE for 7, 10, 15, and 20 mM bulk concentrations of ethanol, propanol, propan-2-ol and butanol at 1000 rpm electrode rotation rate and 50 mV s^{-1} potential scan rate.

	Limiting Current, I_L / μA			
	Bulk Alcohol Concentration / mM			
Alcohol	7	10	15	20
Ethanol	142	165	201	229
Propanol	136	153	189	214
Propan-2-ol	136	162	189	220
Butanol	156	166	221	233

The results reported here suggest the rate of reaction may not be entirely diffusion-controlled and other processes such as electron transfer kinetics may have an effect on the rate of the reaction.

3.4.3 Effect of Potential Scan Rate

The scan rate is the rate at which the cyclic voltammogram is swept through the potential range, in all cases thus far this has been set at 50 mV s^{-1}. Each scan rate will have a different time scale associated with it, which often needs to be considered when analyzing the data. Although the *x*-axis in the voltammograms is presented as a potential axis in all voltammograms, it can also be represented as a time axis. Peak charges arise from time integrals so peak currents are not ready comparisons with changing potential scan rates.

In a typical voltammogram, by observing how the peaks appear and disappear as the scan rate is varied and noting the difference between the first cycle and the subsequent cycles it may be possible to determine how processes represented by the peaks are related. From scan rate dependence of peak amplitudes or areas the role of adsorption, diffusion and chemical reactions may be identified. However, in rotating disc electrochemistry continuous replenishment of the reactant at the surface of the electrode can produce a limiting current plateau. This limiting current plateau shows the maximum current response available from the amount of reactant at the surface, which may be unchanged regardless of scan rate.

Figures 3.7, 3.8, 3.9 and 3.10 show the voltammograms at five potential scan rates (10, 20, 50, 100, and 200 mV s^{-1}), at 1000 rpm electron rotation rate, for the 10 mM ethanol, propanol, propan-2-ol and butanol responses respectively, in the 0.1 M phosphate buffer electrolyte. The voltammograms and the observed limiting currents across the five scan rates examined for each of the 4 alcohols are very similar.

Table 3.2 shows the observed limiting current for the 10 mM response of the three alcohols at each scan rate. The observed limiting current for each scan rate shows close agreement within a small range of (1.52–1.73) $\times 10^{-4}$ A for all scan rates tested. There is a very small trend of increasing limiting current with increasing scan rate observed for these results, however, this increase is well within a 10 % experimental error in each alcohol case.

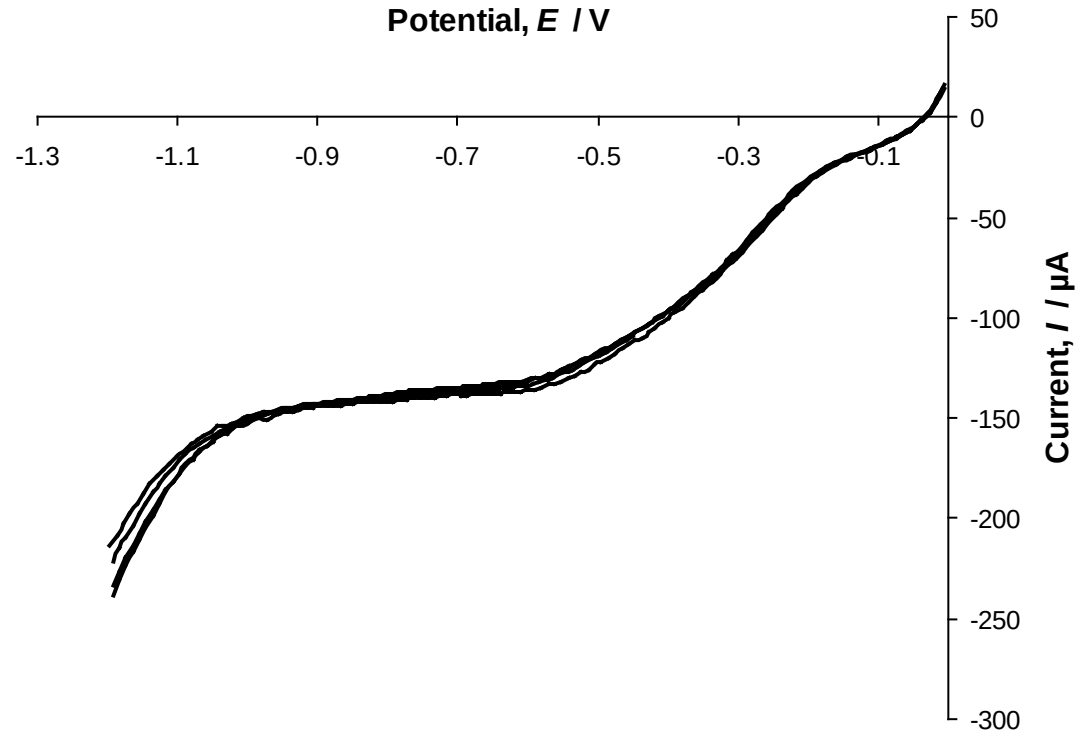

Fig. 3.7 Cathodic sweeps of the cyclic voltammograms for the Cu RDE in the presence of 10 mM ethanol at 1000 rpm electrode rotation rate and varying potential scan rates; 10 – 200 mV s^{-1}.

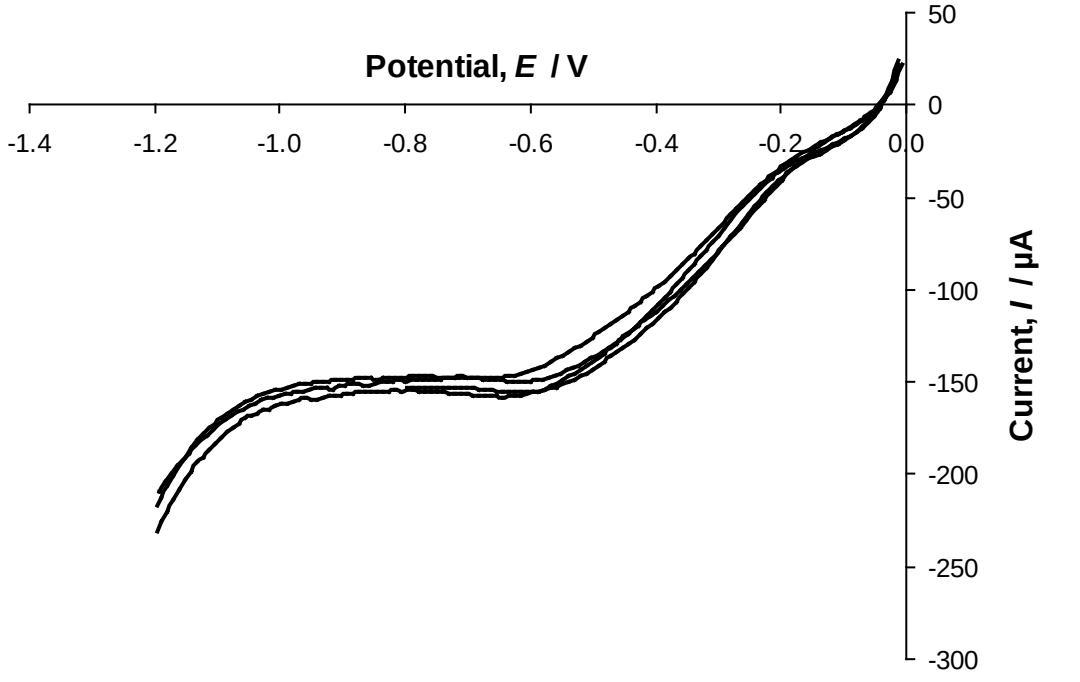

Fig. 3.8 Cathodic sweeps of the cyclic voltammograms for the Cu RDE in the presence of 10 mM propanol at 1000 rpm electrode rotation rate and varying potential scan rates; 10 – 200 mV s^{-1}.

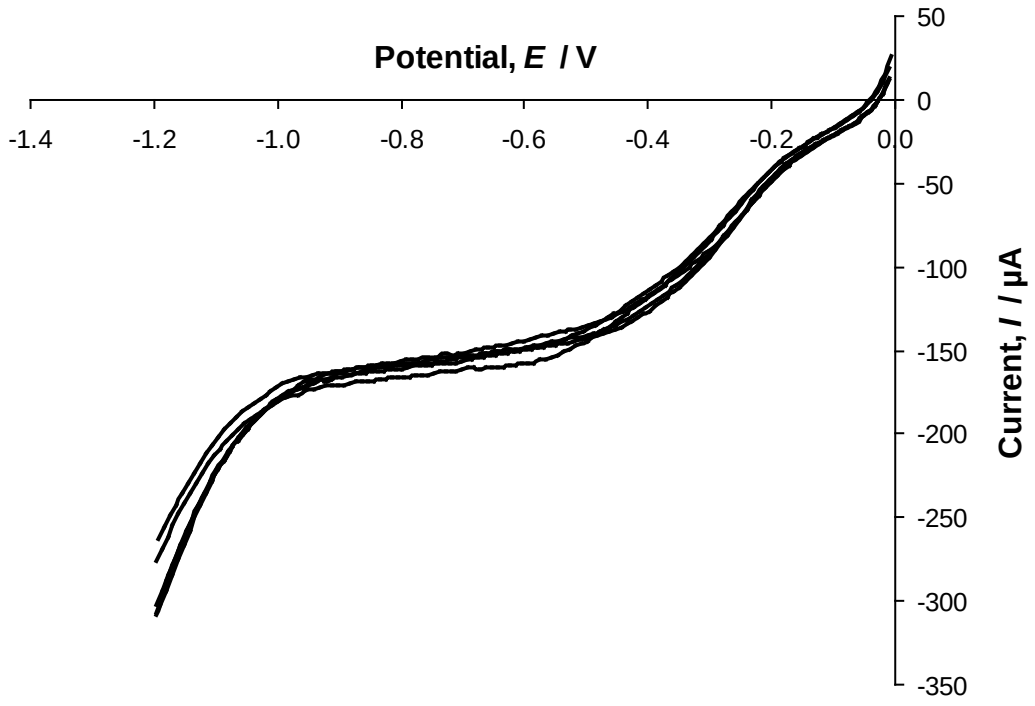

Fig. 3.9 Cathodic sweeps of the cyclic voltammograms for the Cu RDE in the presence of 10 mM propan-2-ol at 1000 rpm electrode rotation rate and varying potential scan rates; 10 – 200 mV s^{-1}.

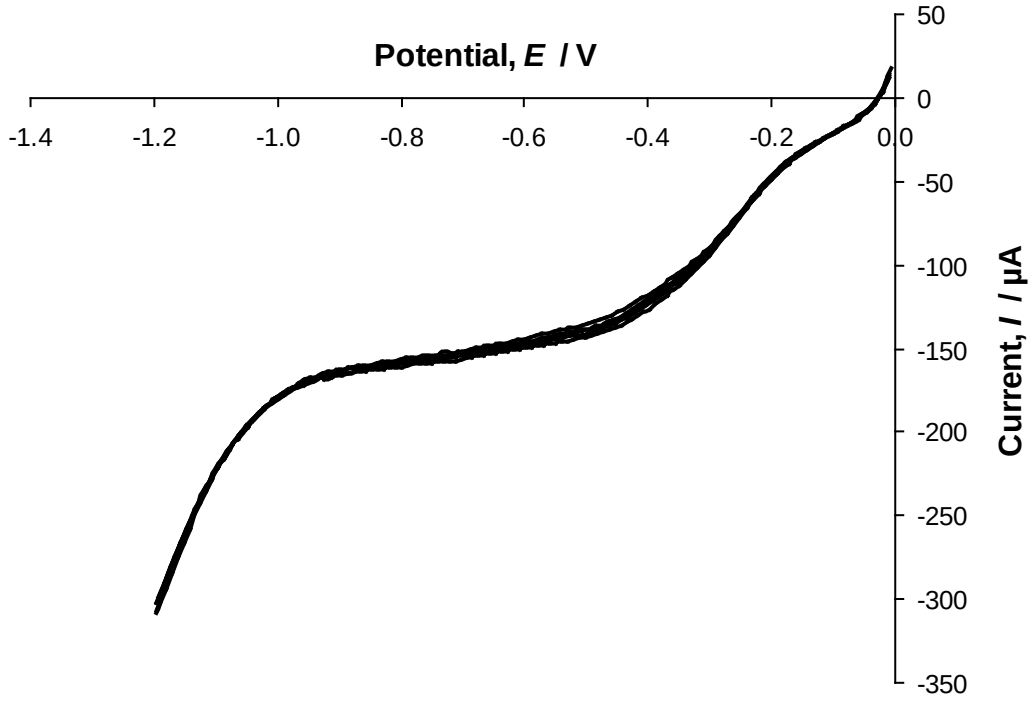

Fig. 3.10 Cathodic sweeps of the cyclic voltammograms for the Cu RDE in the presence of 10 mM butanol at 1000 rpm electrode rotation rate and varying potential scan rates; 10 – 200 mV s^{-1}

Table 3.2 Limiting currents observed on the Cu RDE at each of the potential scan rates; 10, 20, 50, 100, and 200 mV $s^{-1}$with 10 mM bulk concentrations of ethanol, propanol, propan-2-ol and butanol at 1000 rpm electrode rotation rate.

Limiting Current, I_L / μA					
	Potential Scan Rate / mV s^{-1}				
	10	20	50	100	200
Alcohol					
Ethanol	159	162	165	170	172
Propanol	152	152	153	160	163
Propan-2-ol	153	159	162	165	168
Butanol	157	161	166	169	173

If the processes are completely diffusion-controlled the limiting current plateau would not change with scan rate as the maximum current able to be produced will be dependent only on the diffusion to the surface and the amount of reactant available to do so. If not completely diffusion controlled a change in the response with changing scan rate may be observed. Increasing the scan rate for the experiments appears to have a small effect on the limiting current produced. This is consistent with the suggestion that the processes observed may be largely diffusion-controlled with a small kinetic effect.

3.4.4 Effect of Electrode Rotation Rate

The rotation rate is the rate, in revolutions per minute (rpm), at which the rotating disc electrode is rotated in the electrolyte. This rotation induces the characteristic laminar flow of the electrolyte toward the surface of the electrode as seen in rotating disc electrochemistry. Examining the changes in a voltammogram when varying the rotation rate can give insight to what processes are taking place, mass transport, oxidation and reduction, reversibility and irreversibility.

The rotation rates of 500, 675, 750, 100, 1250, 1500 and 2000 rpm were chosen for investigation of the rotation dependence in this work. The reductive response at these rotation rates was examined for all alcohols. Peak C2 was present at each rotation rate.

Figures 3.11, 3.12, 3.13 and 3.14 show the cathodic sweeps of the cyclic voltammograms for the Copper RDE in the presence of 10 mM ethanol, propanol, propan-2-ol and butanol respectively at each of the seven rotation rates examined at a potential scan rate of 50 mV s^{-1}, in the 0.1 M phosphate buffer electrolyte. Table 3.3 lists the limiting currents observed for each rotation rate in the presence of 10 mM ethanol, propanol, propan-2-ol or butanol.

The observed voltammograms for each alcohol show that as the rotation rate is increased, the limiting current plateau response is observed at a larger reductive current. In rotating disc electrochemistry where the rotation of the electrode induces a flow of electrolyte toward the electrode surface providing a continuing replenishment of analyte to the surface there is continual reduction hence leading to the limiting current. As the rotation rate is increased the analyte is replenished at a greater rate to the surface of the electrode so an increase in the reductive limiting current is expected.

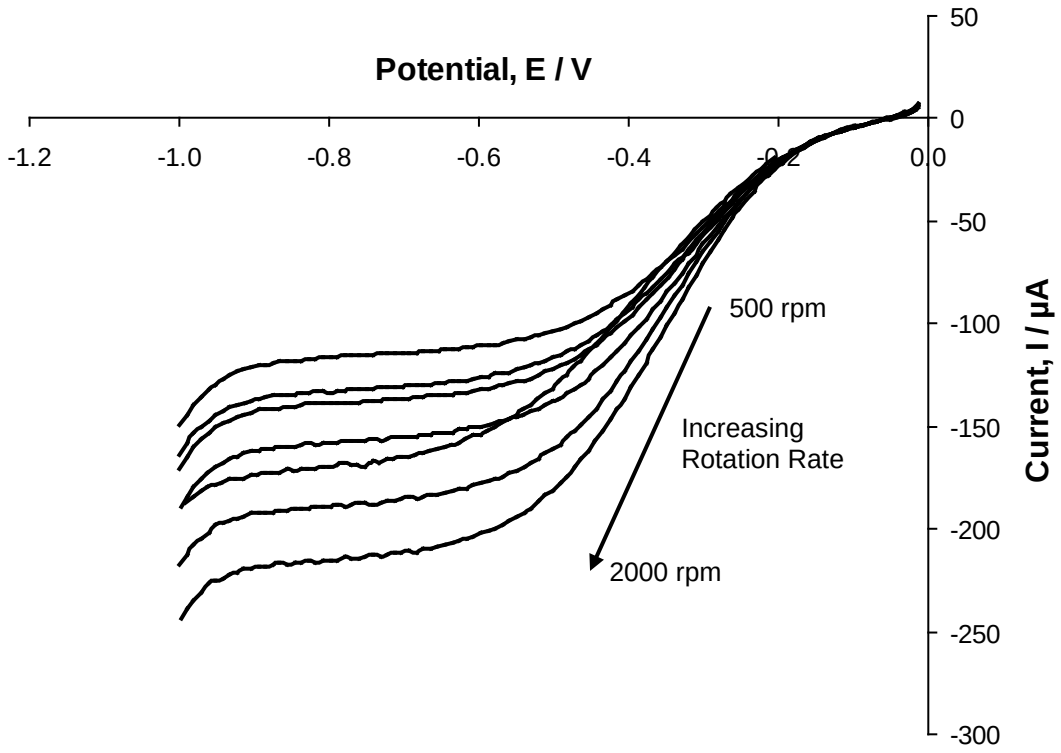

Fig. 3.11 Cathodic sweeps of the cyclic voltammograms for the Cu RDE in the presence of 10 mM ethanol at 50 mV s^{-1} potential scan rate and varying electrode rotation rate; 500 – 2000 rpm.

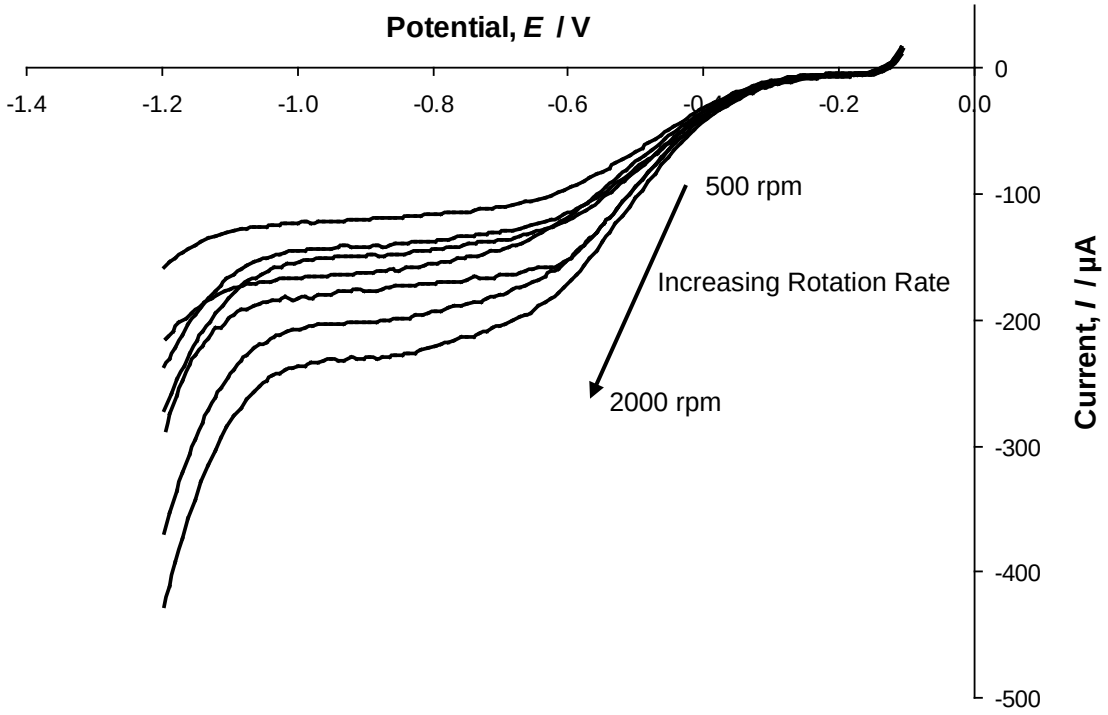

Fig. 3.12 Cathodic sweeps of the cyclic voltammograms for the Cu RDE in the presence of 10 mM propanol at 50 mV s^{-1} potential scan rate and varying electrode rotation rate 500 – 2000 rpm.

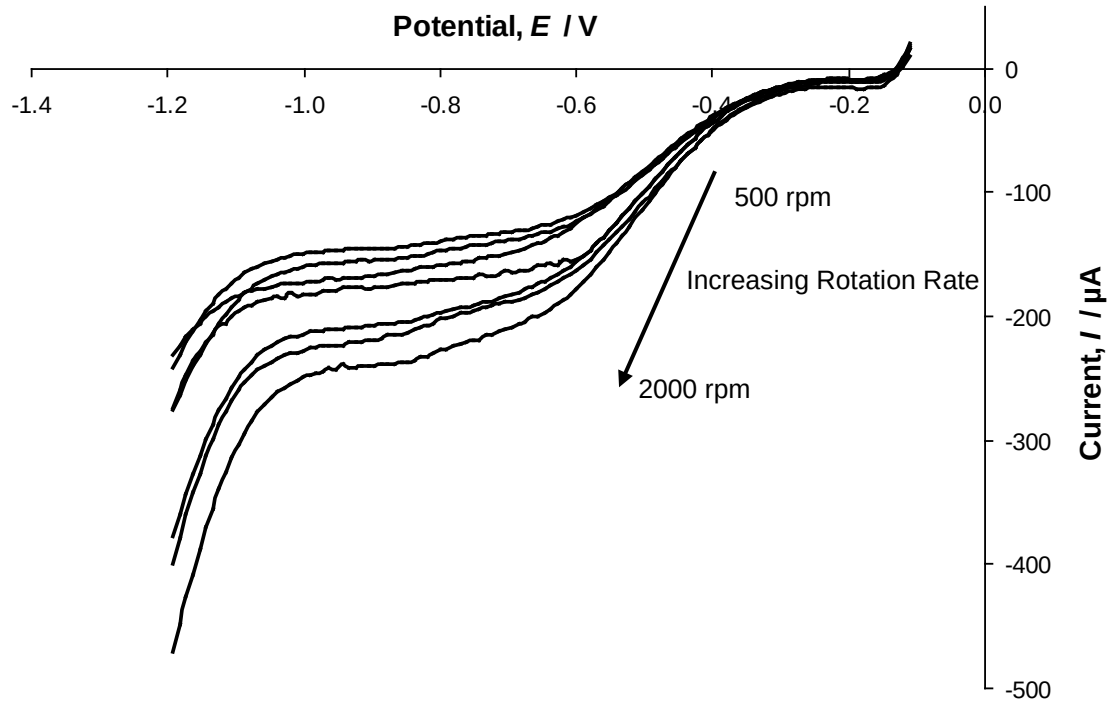

Fig. 3.13 Cathodic sweeps of the cyclic voltammograms for the Cu RDE in the presence of 10 mM propan-2-ol at 50 mV s^{-1} potential scan rate and varying electrode rotation rate; 500 – 2000 rpm.

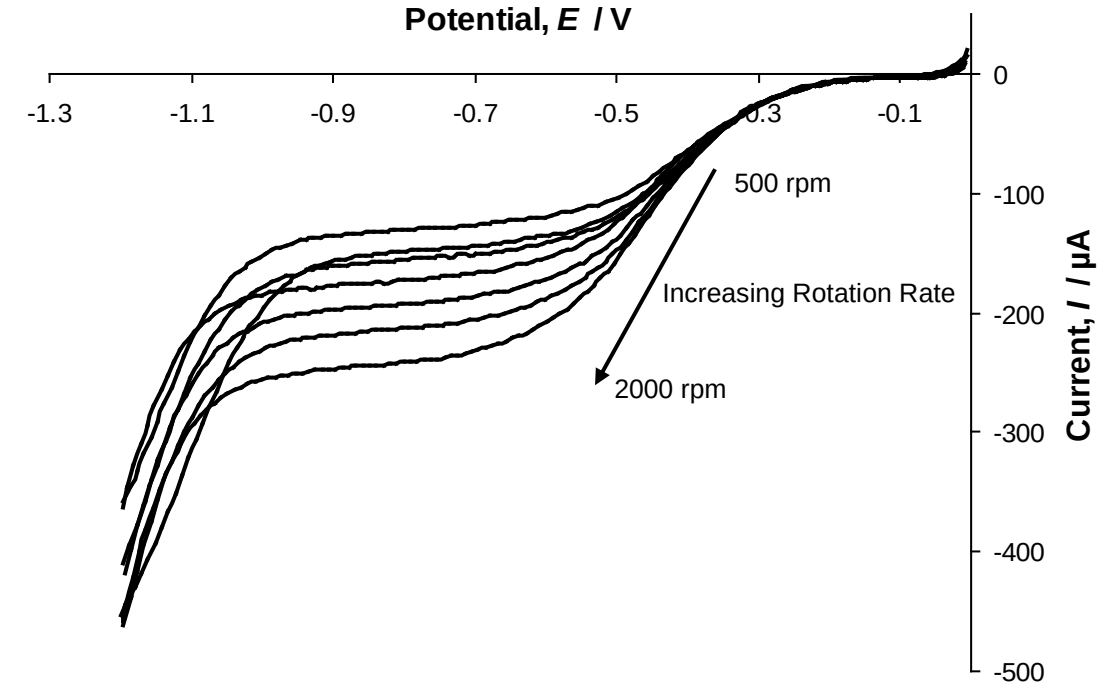

Fig. 3.14 Cathodic sweeps of the cyclic voltammograms for the Cu RDE in the presence of 10 mM butanol at 50 mV s^{-1} potential scan rate and varying electrode rotation rate; 500 – 2000 rpm.

Table 3.3 Limiting currents observed at each of the electrode rotation rates, 500, 675, 750, 1000, 1250, 1500, and 2000 rpm of the Cu RDE with 10 mM bulk concentrations of ethanol, propanol, propan-2-ol and butanol at 50 mV s^{-1} potential scan rate.

	Limiting Current, I_L / μA						
	Electrode rotation rate / rpm						
Alcohol	500	675	750	1000	1250	1500	2000
Ethanol	130	146	153	165	191	210	240
Propanol	114	131	137	153	170	190	217
Propan-2-ol	120	140	160	162	177	202	231
Butanol	132	148	155	166	190	219	237

The observed voltammograms for the Cu disc electrode reported here show this expected increase in limiting current with increasing rotation rate. The values listed in table 3.3 show a progressive increase in limiting current with the increasing electrode rotation rate for each alcohol as expected and similar values between alcohols at constant rotation rate.

An increase in bulk alcohol concentration or electrode rotation rate leads to an increase in the limiting current produced suggesting mass transport control of the reduction of alcohols. However, the increase in current is not proportional to the increase in concentration or rotation. To determine whether the processes occurring are completely mass transport controlled a Levich study was conducted.

3.4.4.1 Levich Study

The Levich method is the simplest model involving mass transport processes.[1,2,47] Where the surface concentration of an electroactive species is zero, a relationship between the current density and the rotation rate can be given by the Levich equation[1,2,47] (eqn 2.4).

$$I_L = 0.620nFD^{2/3}\omega^{1/2}\nu^{-1/6}c_b \qquad (2.4)$$

This equation shows that the limiting current I_L is proportional to the bulk concentration, c_b, of the electroactive species and is entirely mass transport controlled.[45] In this case, a plot of I_L vs $\omega^{1/2}$ should be linear and pass through the origin. The slope may then be used to estimate the diffusion coefficient of the electroactive species.

Figure 3.15 shows the plots of the current, I_L, as a function of the square root of the angular velocity, $\omega^{1/2}$, for the bulk 10 mM concentrations of the 4 alcohols showing reductive response: ethanol, propanol, propan-2-ol and butanol. Figures 3.16 – 3.19 show I_L, for a selection of bulk alcohol concentrations as a function of $\omega^{1/2}$, for each of the alcohols examined, ethanol, propanol, propan-2-ol and butanol, respectively.

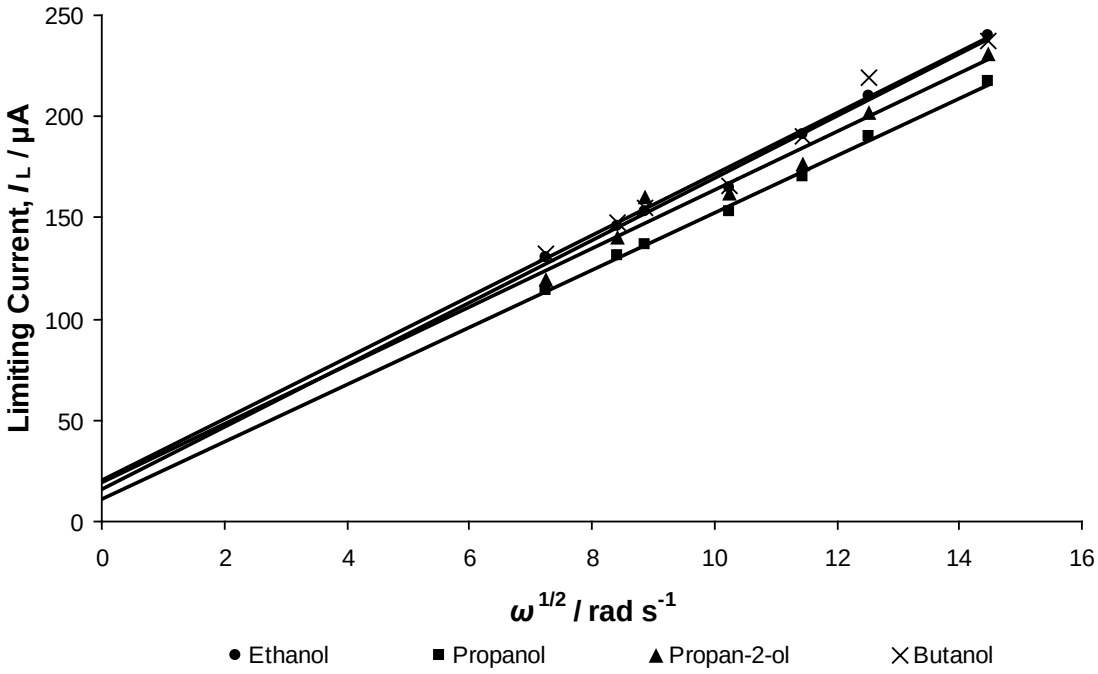

Fig. 3.15 Levich study for 10 mM bulk ethanol, propanol, propan-2-ol and butanol concentrations at the Cu RDE, showing the linear relationship between I_L and $\omega^{½}$.

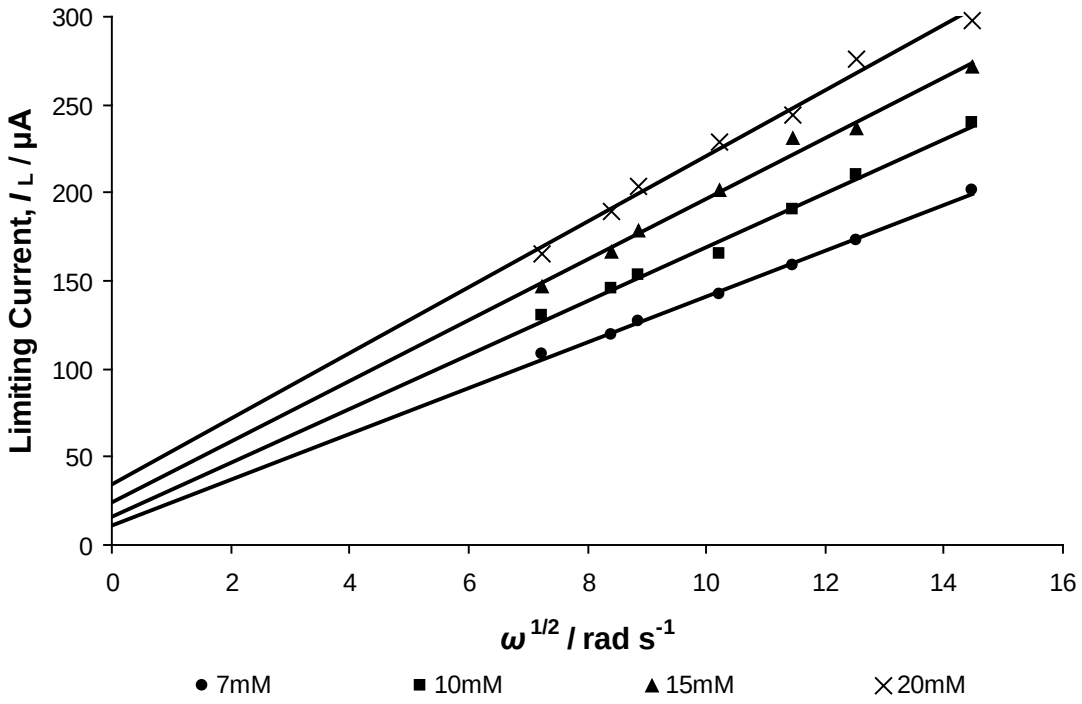

Fig. 3.16 Levich study for 7, 10, 15 and 20 mM bulk ethanol concentrations at the Cu RDE. Showing linear relationship between I_L and $\omega^{½}$ and the increasing slope with increasing concentration.

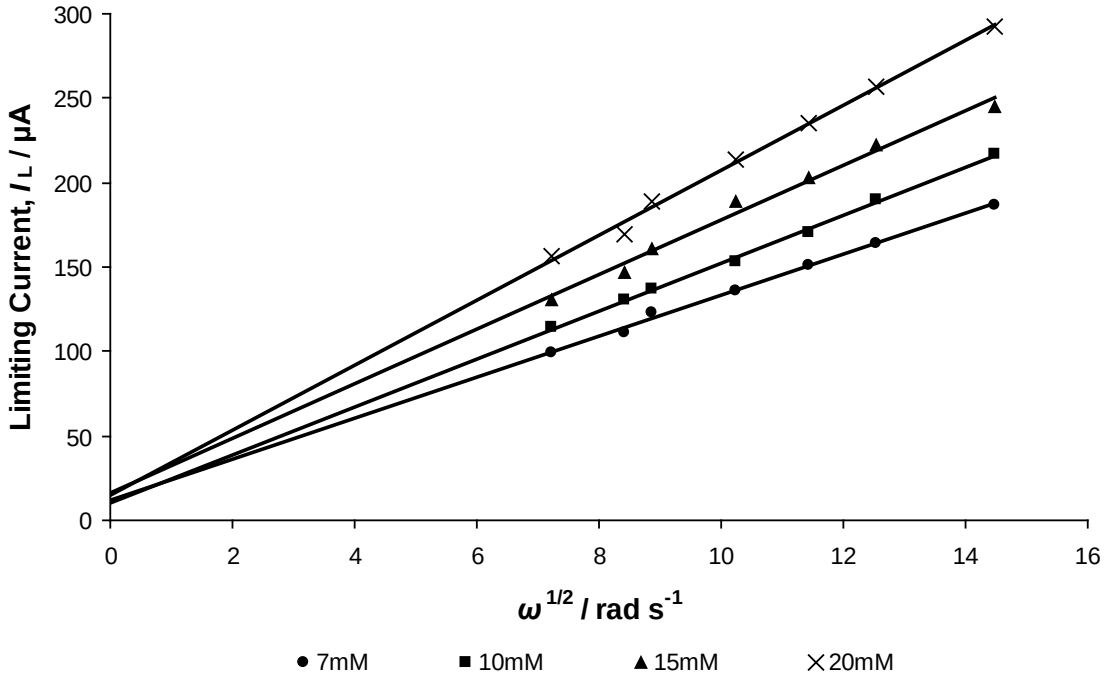

Fig. 3.17 Levich study for 7, 10, 15 and 20 mM bulk propanol concentrations at the Cu RDE. Showing linear relationship between I_L and $\omega^{½}$ and the increasing slope with increasing concentration.

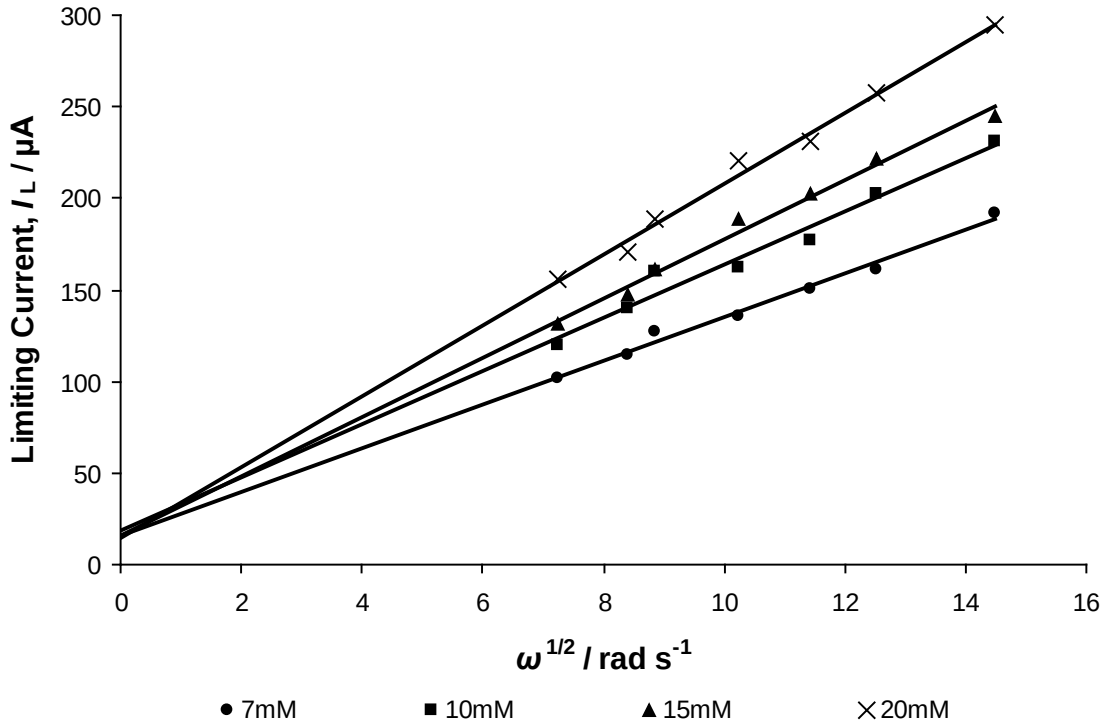

Fig. 3.18 Levich study for 7, 10, 15 and 20 mM bulk propan-2-ol concentrations at the Cu RDE. Showing linear relationship between I_L and $\omega^{½}$ and the increasing slope with increasing concentration.

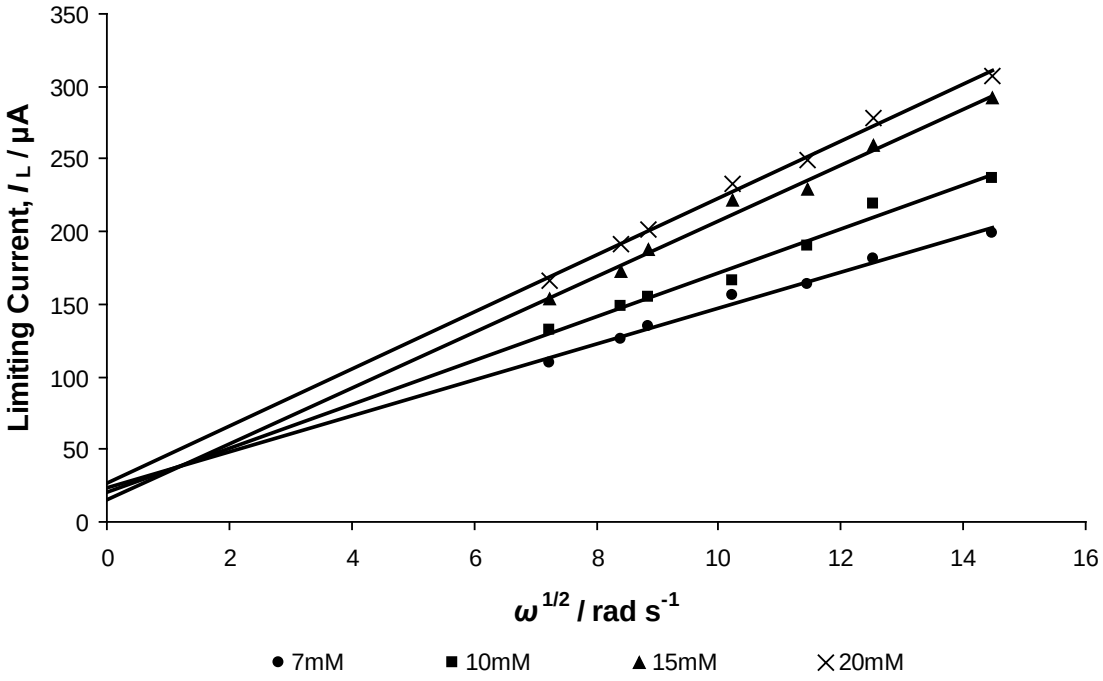

Fig. 3.19 Levich study for 7, 10, 15 and 20 mM bulk butanol concentrations at the Cu RDE. Showing linear relationship between I_L and $\omega^{½}$ and the increasing slope with increasing concentration.

The data was observed to be approximately linear suggesting that the process is largely controlled by mass transport. However, when the data is extrapolated back to zero it is noted that in this case the line does not pass through the origin as would be expected if the process was completely mass-transport controlled. This model is therefore inappropriate to use to evaluate the Diffusion coefficient of the species and does not fully interpret the data. Hence, the Koutecky-Levich model was studied.

3.4.4.2 Koutecky-Levich Study

The Koutecky-Levich model is a modification on the Levich model, which takes into account the control of the rate of reaction through a combination of both mass transport and electron transfer processes.[1,2,47]

For an irreversible electrode process the current-potential wave can be divided into three sections;

1) the limiting current plateau where the current density depends only on the rate of mass transport, $I \propto \omega^{1/2}$;

2) very low current density, where the current is totally determined by electron transfer. I is independent of ω; and,

3) mixed control region, an intermediate zone where the current is controlled by both the electron transfer and the mass transport process. I must vary with ω.

In the mixed control region, the current at any potential is given by both mass transport and electron transfer kinetics.[1,2,47,64] The current density due to the electron transfer kinetics is given by the equation;

$$I = nFk_f c_s \tag{3.1}$$

where k_f is the heterogeneous electron transfer constant and c_s is the surface concentration of the electroactive species. The current can also be related to the bulk concentration, c_b, and the thickness of the Nernst diffusion layer[64] described by eqn 2.1,

$$I = \frac{nFD(c_b - c_s)}{\delta} \tag{2.1}$$

By combining eqn 3.1 and 2.1 to eliminate I an expression for c_s can be obtained;

$$c_s = \frac{Dc_b}{k_f\delta + D} \tag{3.2}$$

This expression for c_s can be substituted into eqn 3.1 to give;

$$\frac{1}{I} = \frac{\delta}{nFDc_b} + \frac{1}{nFk_f c_b} \tag{3.3}$$

The variation in the diffusion layer thickness with rotation rate is expressed in eqn 2.3;

$$\delta = 1.61D^{1/3}\omega^{-1/2}\nu^{1/6} \tag{2.3}$$

substituting this expression into eqn. 3.2 gives the Koutecky Levich equation,

$$\frac{1}{I} = \frac{1}{nFk_f c_b} + \frac{1}{0.620nFD^{2/3}\nu^{-1/6}c_b} \cdot \frac{1}{\omega^{1/2}} \tag{3.4}$$

This gives a graphical means for separating the contribution from the kinetics and the mass transport. A general relationship for the process can be written by the following;

$$\frac{1}{I} = \frac{1}{I_k} + \frac{1}{I_d}.\frac{1}{\omega^{1/2}} \tag{3.5}$$

where the kinetic current, I_k, and the diffusion current, I_d are given by;

$$I_k = nFk_f c_b \tag{3.6}$$

$$I_d = 0.620nFD^{2/3}\nu^{1/6}c_b \tag{3.7}$$

Therefore a Koutecky-Levich plot of $1/I$ vs $1/\omega^{1/2}$ should provide a linear relationship with the intercept equal to $1/I_k$ and slope equal to $1/I_d$, from which the electron transfer rate constant k_f and diffusion coefficient D can be calculated as follows.

$$k_f = \frac{I_k}{nFc_b} \tag{3.8}$$

$$D = \left(\frac{I_d}{0.620nF\nu^{1/3}c_b}\right)^{-2/3} \tag{3.9}$$

where ν is assumed to be 1×10^{-6} m^2 s^{-1}, the kinematic viscosity of water at 25°C.[65,66] The mole fraction of alcohol in the electrolyte is less than 0.01 hence will have very little effect on the overall kinematic viscosity of the solution.

Figure 3.20 shows the Koutecky-Levich plot of the $1/I$ vs $1/\omega^{1/2}$ of the 4 alcohols, ethanol, propanol, propan-2-ol and butanol at bulk concentrations of 10 mM. Linear relationships are observed for each of the alcohols with similar slopes and intercepts at the $1/I$ axis. This indicates that the kinetic electron transfer constant, k_f, and the diffusion coefficient for the three alcohols are likely to be similar in value.

Figures 3.21 to 3.24 show $1/I$, for a selection of bulk alcohol concentrations as a function of $1/\omega^{1/2}$, for each of the 4 alcohols examined, ethanol, propanol, propan-2-ol and butanol, respectively.

Again linear relationships are observed with slopes decreasing with increasing bulk concentrations consistent with that expected with the Koutecky-Levich relationship. The intercepts appear to be close in value at the $1/I$ axis.

Table 3.4 lists the values for the intercept and the slope of each line present in Figs. 3.20, and the calculated values for k_f and D for each alcohol at each bulk concentration. Tables 3.5 – 3.7 list the values for the intercept and the slope of each alcohol at each concentration present in Figs. 3.21 – 3.24 respectively, along with the corresponding calculated values for k_f and D.

The calculated values for D across the four alcohols at each concentration are in good agreement; however, there is an apparent increase in D with increasing bulk alcohol concentration. The structure/size of the alcohol appears to have little effect on the diffusion coefficient, whereas, the bulk alcohol concentrations appears to affect it. At 10 mM bulk alcohol concentration, the four alcohols are within a range of $(1.04–1.17) \times 10^{-9}$ m^2 s^{-1} for D. This is a little low when compared to the values for the diffusion coefficient of ethanol in water reported in the literature as 1.6×10^{-9} m^2 s^{-1}.[67] However as the bulk concentration of the alcohol is increased the value of D approaches this literature value where at 20 mM bulk alcohol concentration the four alcohols diffusion coefficients are within the small range of $(1.41–1.53) \times 10^{-9}$ m^2 s^{-1}. It appears that as the bulk alcohol concentration is increased, within the range of this experiment, the diffusion-control becomes more prominent.

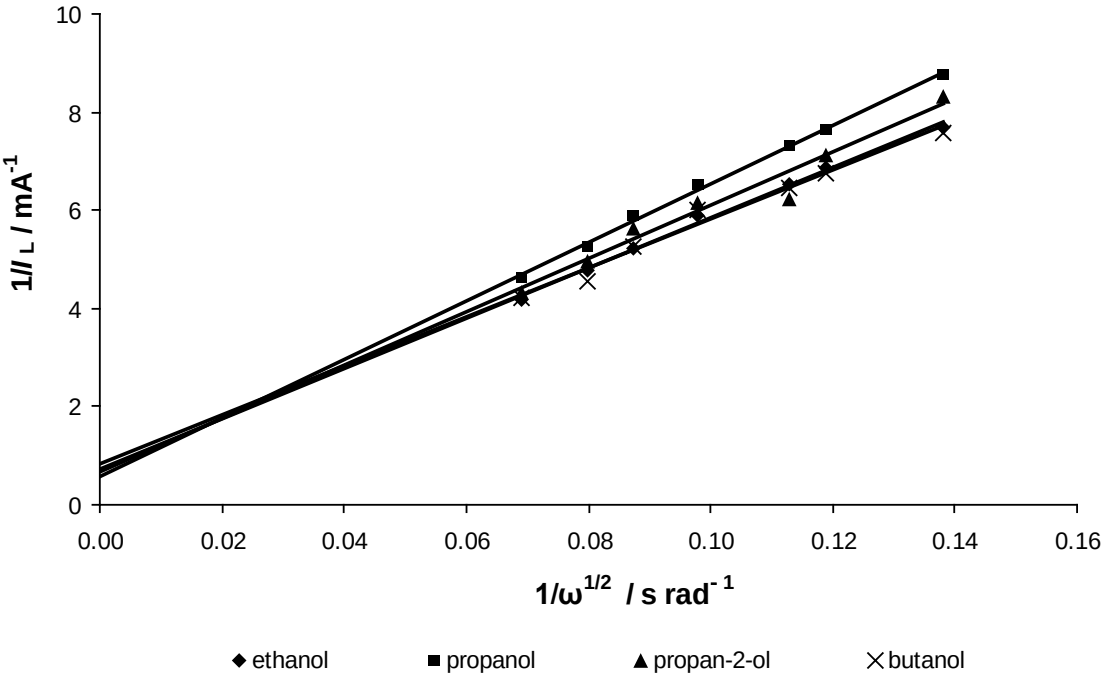

Fig. 3.20 Koutecky-Levich Study for 10 mM bulk ethanol, propanol, propan-2-ol and butanol concentrations at Cu RDE, showing the linear relationship between $1/I_L$ and $1/\omega^{1/2}$.

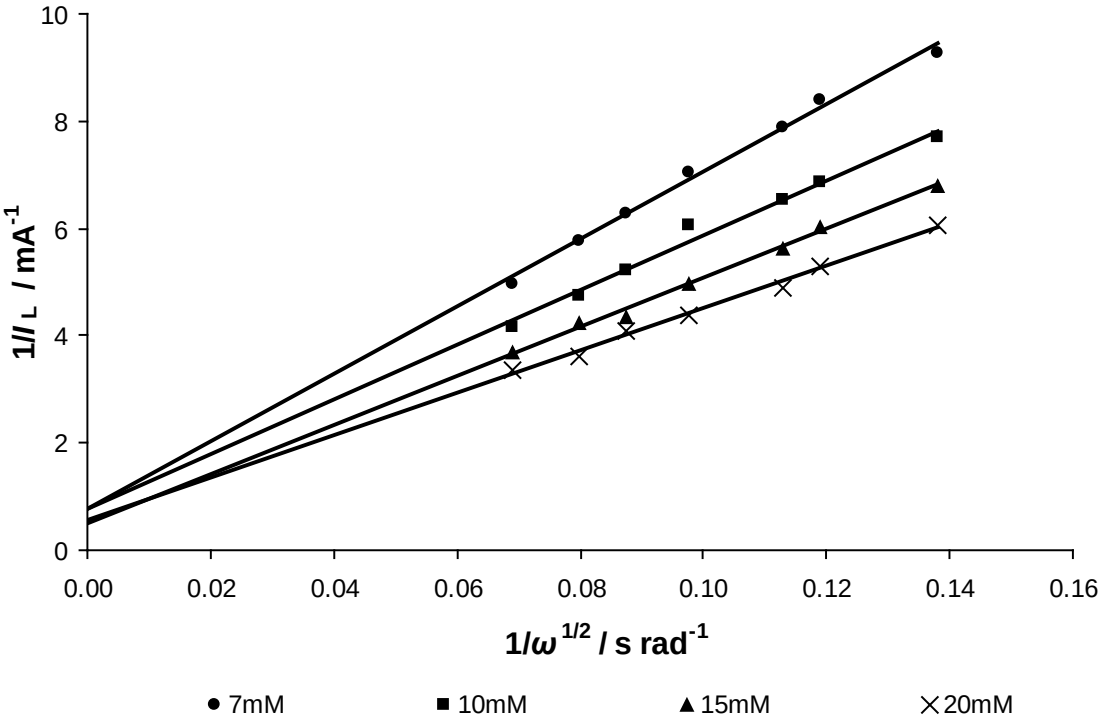

Fig. 3.21 Koutecky-Levich Study for 7, 10, 15 and 20 mM bulk ethanol concentrations at Cu RDE, showing the linear relationship between $1/I_L$ and $1/\omega^{1/2}$ and the decrease in slope with increasing bulk concentration.

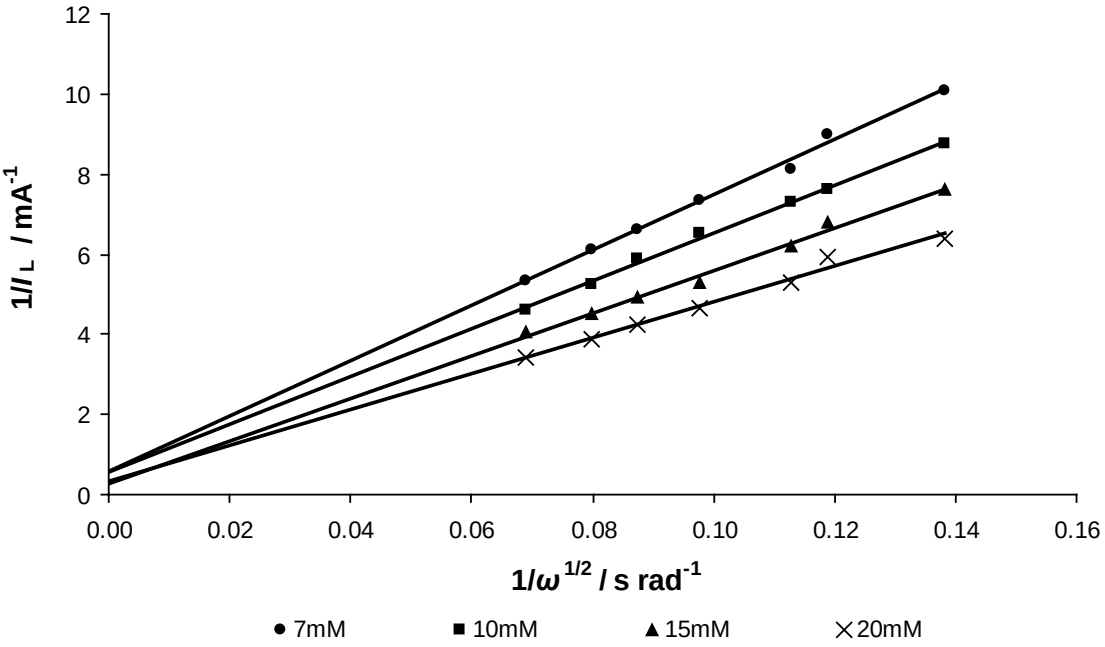

Fig. 3.22 Koutecky-Levich Study for 7, 10, 15 and 20 mM bulk propanol concentrations at Cu RDE, showing the linear relationship between $1/I_L$ and $1/\omega^{1/2}$ and the decrease in slope with increasing bulk concentration.

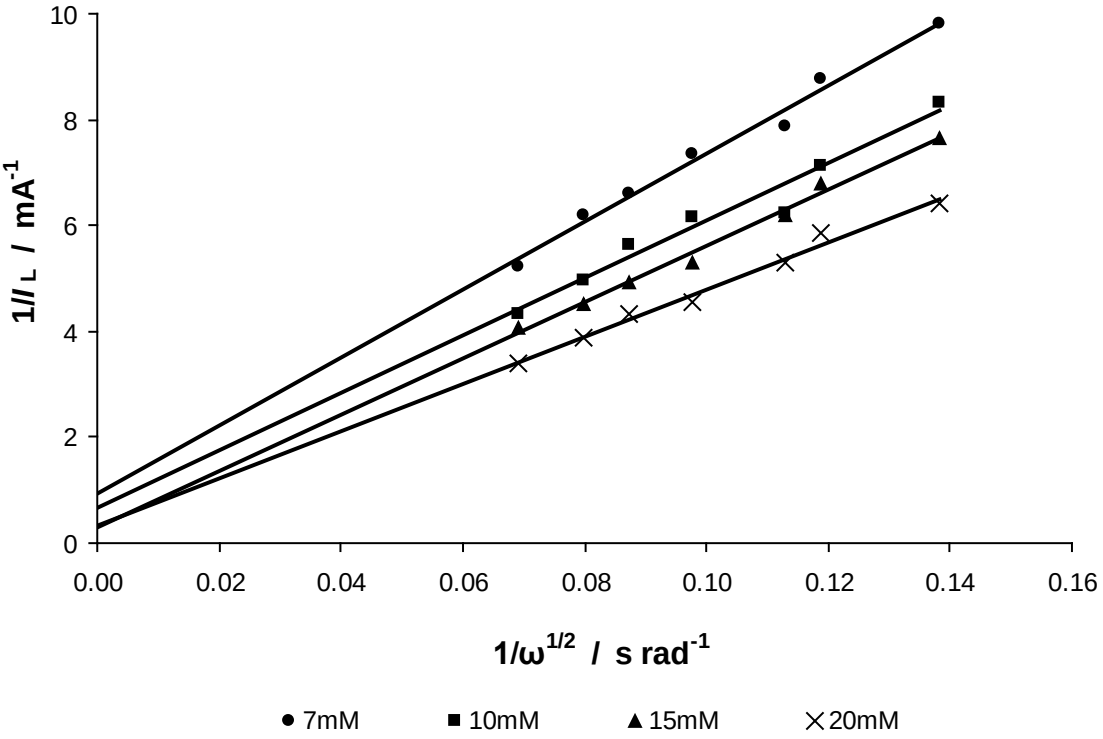

Fig. 3.23 Koutecky-Levich Study for 7, 10, 15 and 20 mM bulk propan-2-ol concentrations at Cu RDE, showing the linear relationship between $1/I_L$ and $1/\omega^{1/2}$ and the decrease in slope with increasing bulk concentration.

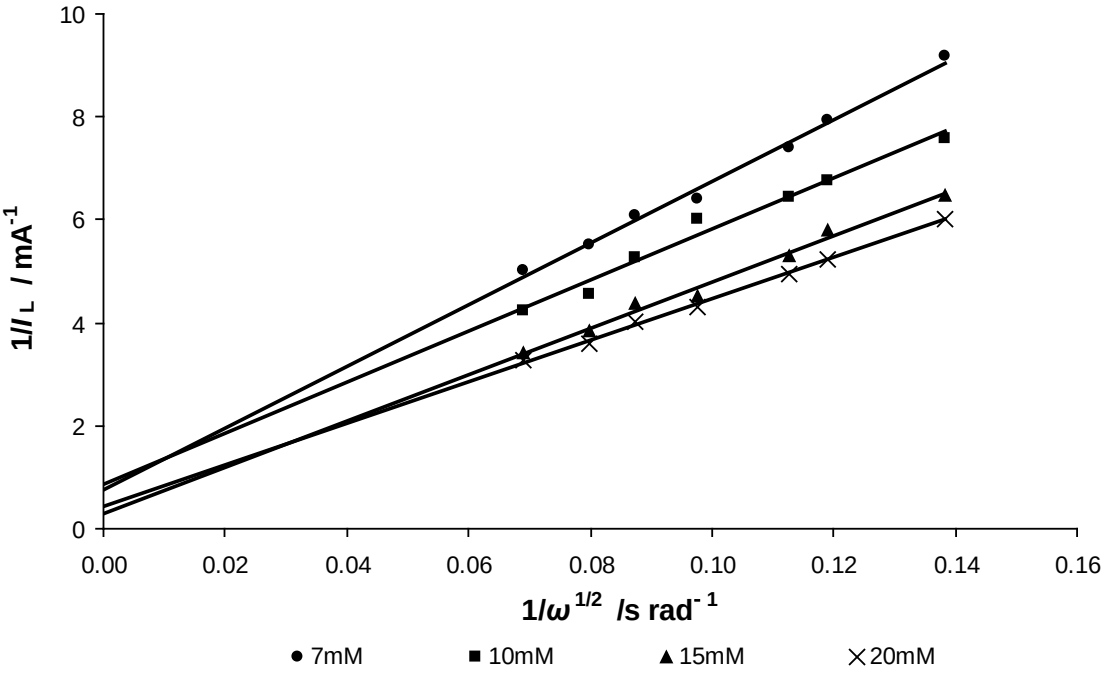

Fig. 3.24 Koutecky-Levich Study for 7, 10, 15 and 20 mM bulk butanol concentrations at Cu RDE. Showing the linear relationship between $1/I_L$ and $1/\omega^{1/2}$ and the decrease in slope with increasing bulk concentration.

Table 3.4 Slope and intercept for Fig. 3.20 Koutecky-Levich plot along with the calculated diffusion coefficient and electron kinetic transfer rate constant values for 10 mM concentrations of ethanol, propanol, propan-2-ol and butanol.

Alcohol	Slope $mA^{-1}\ rad^{-1}\ s$	Intercept mA^{-1}	D $10^{-9}\ m^2\ s^{-1}$	k_f $10^{9}\ m\ s^{-1}$
Ethanol	51.2	0.763	1.06	1.36
Propanol	59.7	0.57	1.17	1.82
Propan-2-ol	54.3	0.66	1.10	1.57
Butanol	49.7	0.84	1.04	1.23

Table 3.5 Slope and intercept for Fig. 3.21 Koutecky-Levich plot along with the calculated diffusion coefficient and electron kinetic transfer rate constant values for 7, 10, 15 and 20 mM bulk ethanol.

Ethanol Concentration, mM	Slope $mA^{-1}\ rad^{-1}\ s$	Intercept mA^{-1}	D $10^{-9}\ m^2\ s^{-1}$	k_f $10^9\ m\ s^{-1}$
7	62.9	0.761	0.96	1.95
10	51.2	0.763	1.06	1.36
15	45.7	0.503	1.28	1.37
20	39.4	0.569	1.41	0.91

Table 3.6 Slope and intercept for Fig. 3.22 Koutecky-Levich plot along with the calculated diffusion coefficient and electron kinetic transfer rate constant values for 7, 10, 15 and 20 mM bulk propanol concentration.

Propanol Concentration, mM	Slope $mA^{-1}\ rad^{-1}\ s$	Intercept mA^{-1}	D $10^{-9}\ m^2\ s^{-1}$	k_f $10^9\ m\ s^{-1}$
7	69.0	0.579	1.02	2.56
10	59.7	0.567	1.17	1.83
15	53.1	0.291	1.42	2.37
20	44.7	0.341	1.53	1.52

Table 3.7 Slope and intercept for Fig. 3.23 Koutecky-Levich plot along with the calculated diffusion coefficient and electron kinetic transfer rate constant values for 7, 10, 15 and 20 mM bulk propan-2-ol concentration.

Propan-2-ol Concentration, mM	Slope $mA^{-1}\ rad^{-1}\ s$	Intercept mA^{-1}	D $10^{-9}\ m^2\ s^{-1}$	k_f $10^9\ m\ s^{-1}$
7	64.3	0.940	0.97	1.58
10	54.3	0.660	1.10	1.57
15	53.1	0.291	1.42	2.37
20	44.5	0.329	1.53	1.58

Table 3.8 Slope and intercept for Fig. 3.24 Koutecky-Levich plot along with the calculated diffusion coefficient and electron kinetic transfer rate constant values for 7, 10, 15 and 20 mM bulk butanol concentration.

Butanol Concentration, mM	Slope $mA^{-1}\ rad^{-1}\ s$	Intercept mA^{-1}	D $10^{-9}\ m^2\ s^{-1}$	k_f $10^9\ m\ s^{-1}$
7	60.0	0.76	0.927	1.95
10	49.7	0.842	1.04	1.23
15	45.0	0.299	1.27	2.31
20	40.2	0.433	1.43	1.20

A considerable variation is noted in the k_f values for the four alcohols with no apparent trend to the variation. The calculated values of k_f, ranging $(0.91 - 2.37) \times 10^9$ m s^{-1}, shows that there is some kinetic control over the processes involved in the reduction of alcohols on Cu electrodes. There may be an indication of a decrease in k_f with the increase in D associated with increasing bulk alcohol concentration, however, the variation in the calculated values of k_f leads to some data values not fitting this possible trend and is challenging to provide further interpretation.

The results of the Koutecky-Levich and Levich analysis suggest that the steady state current being reached is due to both mass transport control and electron transfer processes. If the steady state current was not due to only mass transport then a change in scan rate should give a change in the value of the observed steady state current.

In Section 3.4.3 it was assumed that there was no change in the limiting current with changing scan rate. However, it is possible, a small change may not be obvious over the uncertainty of the experiment.

3.4.5 Copper Disc Summary

In this section the electrochemical processes on the Cu disc electrode in pH 8.1 phosphate buffer electrolyte in the presence of ethanol, propanol, propan-2-ol and butanol has been discussed. A reductive limiting current plateau is observed in association with the presence of the alcohols. The limiting current plateau observed is evident of behavior which is expected when employing rotating disc electrochemistry techniques. An initial increase of current is observed when the electroactive species at the surface of the electrode is being consumed. When the surface concentration of the electroactive species (in this case the alcohol) becomes zero a limiting current is established. As there is a limiting current plateau the electrochemical processes occurring, thought to be the reduction of the alcohol, can be determined to be continuous. The plateau was found to be reproducible with cycling and the anodic limit was assumed to have no significant effect on the plateau. The processes remain continuous provided the potential is more cathodic than the initial onset of the reduction current, I_{ons}. The presence of a limiting current plateau also indicates the probability that the processes of interest are diffusion controlled. This limiting current was found to be controlled predominantly by the mass transport of the electroactive species from the

bulk electrolyte through the Nernst diffusion layer to the surface of the electrode and to a small extent the electron transfer at the surface of the electrode.

The effect on the limiting current plateau of the bulk alcohol concentration, potential scan rate and rotation rate were examined. An increase in the bulk alcohol concentration was observed to cause an increase in the limiting current produced. This was expected, as an increase in concentration would mean that a larger amount of electroactive species is available to travel to the surface of the electrode at any point in time allowing for a larger amount of current to be produced. This observed increase in the limiting current with increasing concentration is also consistent with the suggestion that the process is diffusion controlled.

When the potential scan rate was increased through the range 10-200 mV s^{-1} there was very little change to the limiting current. Therefore, it was assumed that regardless of the scan rate applied on the system the limiting current is constant. This observation is consistent with the processes being diffusion controlled as the potential scan rate has no effect on the limiting current.

Increasing the electrode rotation rate created an increase in the limiting current. In rotating disc electrochemistry a continual replenishment of analyte to the surface is produced by the flow of electrolyte allowing continual reduction leading to an observed limiting current. As the rotation rate is increased a greater rate of flow of electrolyte is induced increasing the rate at which the analyte is replenished to the surface of the electrode and hence producing an increase in the reductive limiting current. As rotation rate is increased the Nernst diffusion layer thickness is decreased and diffusion can take place at a higher overall rate.

To confirm the mass-transport control of the process and determine the diffusion coefficient the Levich model was first employed. This is the simplest model involving mass transport and states that I_L is proportional to c_b when a process is shown to be entirely mass transport controlled.[45] The Levich equation gave data that appeared linear as required to use the model to determine D. However, when extrapolated the data obtained did not provide an intercept through the origin. The Levich model was therefore inadequate to use for the determination of D and the Koutecky-Levich Model was then employed.

The Koutecky-Levich model considered a mixed control region where the current may be controlled by both electron transfer and mass transport effects.[1,2,47] A plot of $1/I$ as

a function of $1/\omega^{1/2}$ provided a linear relationship and from the intercept and slope of the relationship, the electron transfer constant, k_f, and the diffusion coefficient, D, were calculated.

The calculated values for D across the four alcohols at each concentration were within good agreement (~12 %), however, there is an apparent increase in D with increasing bulk alcohol concentration. The structure/size of the alcohol appears to have little effect, whereas the bulk alcohol concentrations do have an affect on D.

At 10 mM bulk alcohol concentration the four alcohols examined, ethanol, propanol, propan-2-ol and butanol, are within the small range of $(1.04–1.17) \times 10^{-9}$ m^2 s^{-1} for D. This value of D is lower than the value for the Diffusion coefficient of ethanol in water reported in the literature, 1.6×10^{-9} m^2 s^{-1}.[67] However, as the bulk concentration of the alcohol is increased the value of D approaches this literature value where at 20 mM bulk alcohol concentration the four alcohols diffusion coefficients are within the small range of $(1.41–1.53) \times 10^{-9}$ m^2 s^{-1}. It appears that as the bulk alcohol concentration is increased, within the range of this experiment, that diffusion becomes more prominent.

A considerable variation was noted in the k_f values for the four alcohols with no apparent trend to the variation. The calculated values of k_f, $(0.91 – 2.37) \times 10^9$ m s^{-1}, shows that there is some kinetic control over the processes involved in the reduction of alcohols on Cu electrodes. But gives no specific indication of the extent of this kinetic control.

The observations of the cyclic voltammetry; the limiting current plateau, bulk alcohol concentration-dependence, potential scan rate-independence, electrode rotation rate-dependence and the Koutecky-Levich study, are not inconsistent with a simple 2 e$^-$ reduction process forming alkanes, which would likely be escaping as gaseous products. The results reported here show that there is a definite irreversible reduction process occurring associated with the presence of the alcohol with dependencies as expected with rotating disc electrochemistry. It was therefore assumed that ethanol was reduced to ethane, propanol and propan-2-ol were reduced to propane and butanol was reduced to butane.

3.5 Tin Disc Rotating Disc Electrode Cyclic Voltammetry

In the preliminary studies, tin metal electrodes showed a reductive response to the addition of ethanol, however this response was observed in the pH 7.3 phosphate buffer rather than the pH 8.1 as with the copper electrode. The five alcohols, methanol, ethanol, propanol, propan-2-ol and butanol were tested for an electrochemical response on the tin disc RDE. A response was observed with the addition of ethanol, propanol and propan-2-ol in the form of a reductive peak at a potential of approximately –1.1 V. No response from methanol or butanol was observed under these conditions. The focus of this section is to discuss the response and resulting analysis of the response on the tin electrode in the presence of ethanol, propanol and propan-2-ol.

The electrochemistry of the tin was examined to ensure the response can be associated with the addition of the alcohol and not the electrochemistry of the tin. Figure 3.25 shows the cyclic voltammogram of the tin disc electrode in the pH 7.3 phosphate buffer, with and without the presence of 10 mM ethanol. When commencing at an anodic limit more positive than -500 mV an oxidation current is observed this is assumed to be due to the oxidation of metallic Sn^0 to Sn^{2+}. As the potential is swept progressively more cathodic than -500 mV, a reductive wave assigned to the reduction of Sn^{2+} to Sn^0 is observed. This peak is identified as C1. During the return sweep of the potential an oxidation wave (identified as peak A1) is observed which is assumed to be due to the oxidation of Sn^0 to Sn^{2+}.

Upon the introduction of 10 mM of ethanol to the cell and repeating the cyclic voltammogram experiment a number of observations are made:

i) Peaks A1 and C1 assigned to the electrochemistry of tin in this electrolyte are maintained.

ii) A slight change to the general background of the voltammogram is observed in the presence of ethanol, with larger currents when compared to the ethanol-free voltammogram.

iii) There is an additional peak, C2, observed in the presence of ethanol background.

The change to the general background is assumed to be the small extent of reduction of H_2O on tin metal under these conditions. The presence of ethanol appears to enhance

this process. The new C2 peak is found at −1.1 V, some 400 mV more cathodic that C1. No new anodic wave accompanies the C2 peak, suggesting an irreversible reduction process over the potential range of the experiment. The possibility of a new tin product being responsible for reduction peak C2 must be eliminated, therefore the potential range was limited to a region where the tin remains in the Sn^0 state throughout. The new anodic limit and starting potential was set at −0.7 V, more cathodic than the cessation of Sn^0 oxidation on a cathodic scan in the absence of ethanol. The cathodic limit was maintained at −1.40 V.

Figure 3.26 shows the resulting voltammogram when performing cyclic voltammetry within this more confined potential range of −0.7 to −1.30 V. The C2 peak is also observed in this voltammogram and a reducing current is maintained throughout the voltammogram, with no evidence for reduction of Sn^{2+}. This observation is consistent with the hypothesis that the presence of ethanol is responsible for this peak. Again, no accompanying anodic wave is associated with C2 on the reverse sweep indicating that the reduction process is irreversible over the potential range of the experiment.

As discussed in Section 3.4 with the copper results in rotating disc electrochemistry, an increase in the reductive current followed by a limiting current plateau is expected. In this case, however, there is an initial increase in the reduction current and then the current decreases again, forming peak C2. This is consistent with what is observed in the case of static electrodes in quiescent solutions in classical cyclic voltammetry where peaks arise from progressive exhaustion of supply of the electroactive species to the electrode due to mass-transport limitations.

The formation of a peak is thus indicative of the reduction being unable to continue, but in this case it cannot be attributed to a decrease in availability of the reactant in the Nernst diffusion layer immediately adjacent to the electrode. Here, electrode rotation continuously replenishes this zone. The formation of this peak may suggest the presence of an insoluble and insulating product on the surface of the electrode, forming a passivating layer preventing continuation of the reduction process.

The balanced electrochemical equation for the presumed reduction process

$$R{-}OH + 2e^- + 2H^+ \rightarrow R{-}H + H_2O \qquad (1.13)$$

suggests the presence of an insoluble and insulating product is not unlikely if alkanes are being produced, since alkanes are not substantially soluble in aqueous systems.

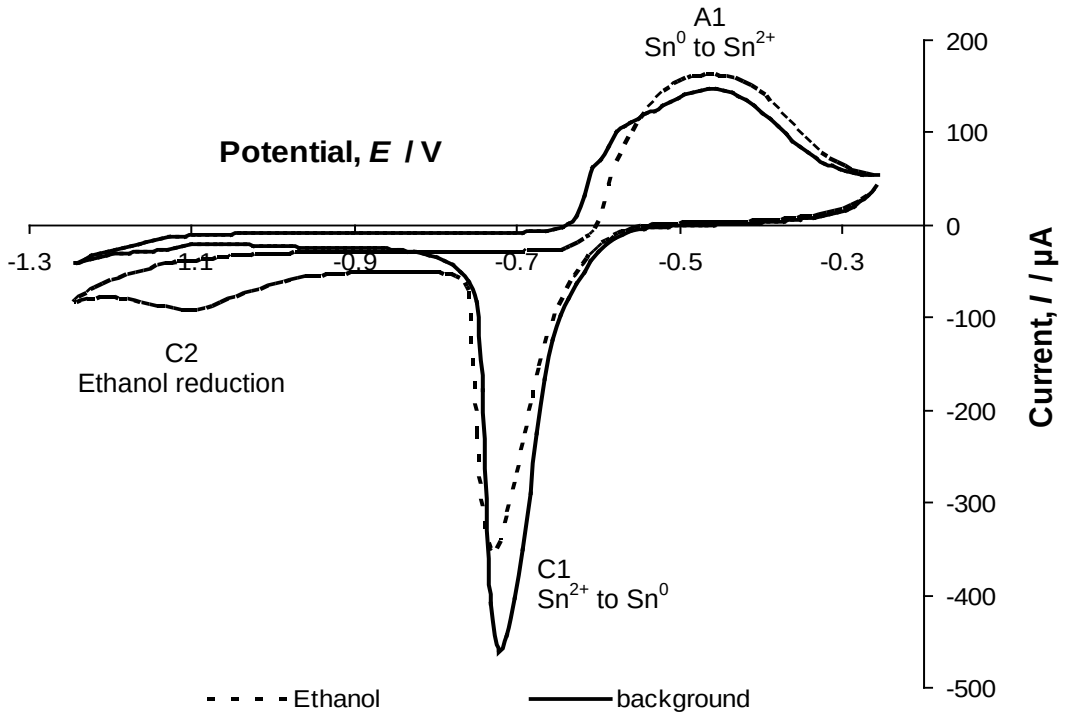

Fig. 3.25 Cyclic voltammograms of the current response of a Sn RDE in 0.1 M phosphate buffer, pH 7.3, with and without the presence of 10 mM bulk ethanol concentration, at 1000 rpm electrode rotation rate and 50 mV s^{-1} potential scan rate. Displaying peaks A1, and C1 and C2.

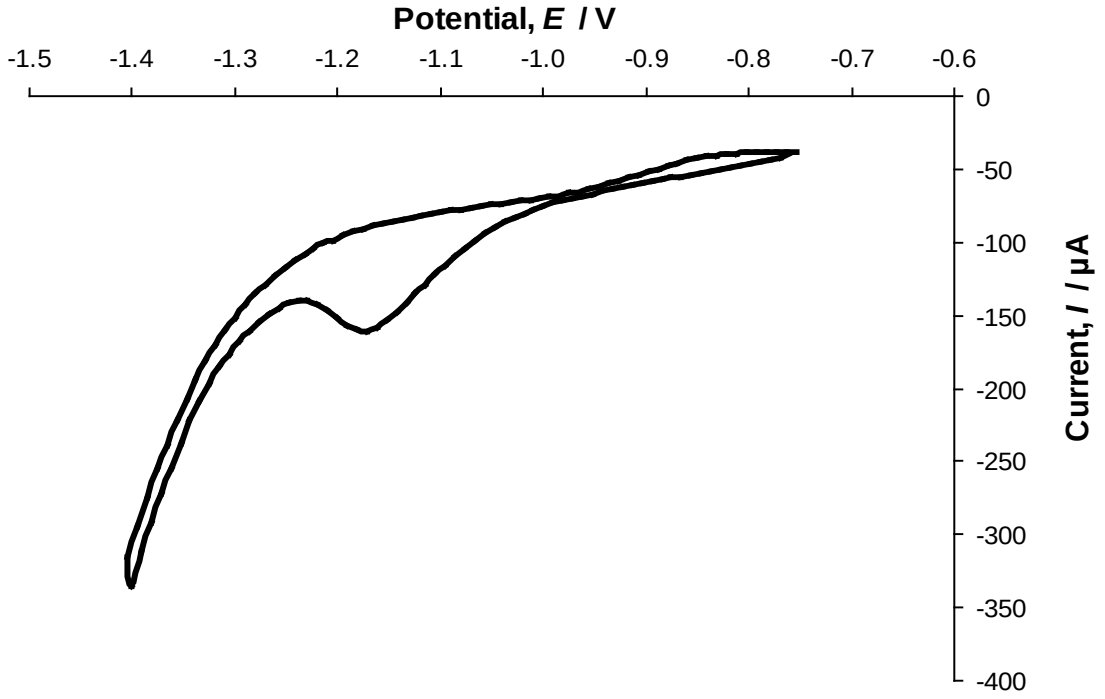

Fig. 3.26 Cyclic voltammogram of the current response of a Sn RDE in 0.1 M phosphate buffer, pH 7.3, in the presence of 10 mM bulk ethanol concentration for the potential range –0.7 to –1.4 V, at 1000 rpm electrode rotation rate and 50 m s^{-1} potential scan rate, displaying only peak C2 for the response associated with the addition of ethanol.

However, it should be noted that in this case the product of ethanol reduction according to eqn. (1.13) would be ethane. This would be expected to be a gas under these conditions (b.p. (ethane) = −89°C), as was concluded with the Cu investigation in section 3.4. Consequently, in this case, if ethane were forming a passivating layer, then it must be presented as a persistent (presumably chemisorbed) layer on the electrode surface, where the gaseous alkane cannot escape from the surface of the electrode.

The absence of any accompanying oxidative wave on the anodic sweep of these cyclic voltammograms strongly indicates that the reduction product is not being oxidised back to the alcohol (or to any other species). This suggests that, with a Sn disc electrode in a 0.1 M phosphate buffer, at pH 7.3, an irreversible process for the reduction of the alcohol is occurring.

3.5.1 Effect of Anodic Limit

The anodic limit was set at −0.7 V to ensure that the observed currents could be associated with the presence of the alcohol and any possible Sn electrochemistry effects were removed. The effect of the anodic limit on the reduction process was tested by holding the cathodic limit constant at −1.30 V while changing the anodic limit. Figure 3.27 shows the cyclic voltammograms of four different potential ranges with a constant cathodic limit of −1.30 V and the anodic limits of −0.65 to −0.80 V. The voltammograms displayed in Fig. 3.27 demonstrate that variation of the anodic limit has little effect on the size and shape of the observed peak C2. The peak is reproducible regardless of the starting anodic limit. For consistency in the results, and due to the observation that the change in anodic limit has no effect on the peak C2 of interest, only one potential range, −0.7 to −1.30 V, was selected for the following investigation on the Sn disc electrode.

3.5.2 Reproducibility of peak C2

The voltammograms presented here are confined to single cycle experiments with commencement at the selected anodic limit. The reproducibility of the voltammograms with further cycling was also tested. Figure 3.28 shows two consecutive scans (with no intervening potential pause) for the potential range −0.65 to −1.30 V at 1000 rpm

electrode rotation rate and 50 mV s^{-1} potential scan rate. Under these conditions there is good reproducibility of the C2 peak. This suggests that the putative insoluble layer proposed due to the formation of a peak, cannot be permanent. If this is an irreversible electrochemical reaction then there must be some form of detachment of the product layer from the surface occurring *via* a non-electrochemical process so that further reduction may take place in subsequent cycles.

3.5.3 Data Analysis

The charge, *Q*, in coulombs, C, associated with peak C2 can be calculated by subtracting a background baseline from the curve with the reductive peak and integrating the resulting voltammetric curve with respect to time.

An appropriate background baseline is required in order for the data analysis to be carried out with any confidence. However, the complicating factor in determining the baseline is that, as noted in Section 3.2, the addition of the ethanol to the electrolyte solution appears to alter the ability of Sn to reduce H_2O; background curves for the Sn electrode in the pH 7.3 0.1 M phosphate buffer electrolyte in absence of ethanol are not coincident with those in the presence of ethanol response (Fig. 3.25). Therefore the response in the absence of ethanol is not suitable as a baseline when ethanol is present.

The ethanol-free background cyclic voltammogram may be scaled arithmetically to fit to the curve immediately either side of the C2 peak observed in cyclic voltammograms in the presence of ethanol providing a possible baseline. An alternative option for establishing a baseline is to consider sections of the cyclic voltammogram in the presence of ethanol immediately either side of peak C2. Fitting a polynomial trendline to these sections may then be used to determine an assumed baseline.

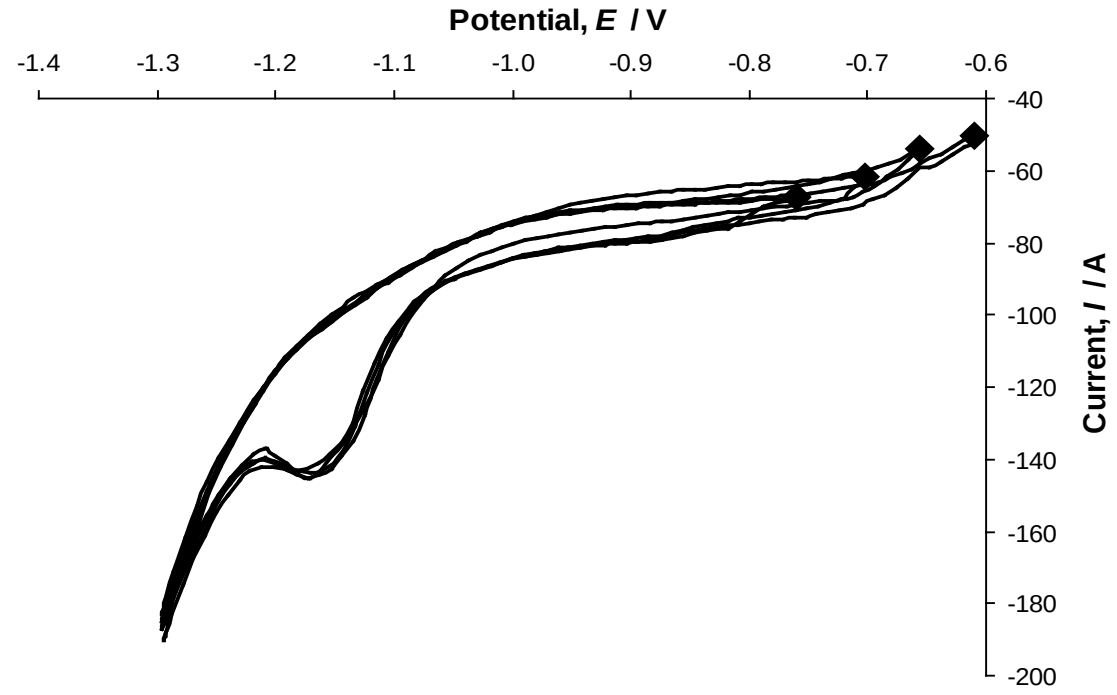

Fig. 3.27 Cyclic voltammograms of the current response on a Sn RDE in the presence of 10 mM bulk ethanol concentration, at 1000 rpm electrode rotation rate and 50 mV s^{-1} potential scan rate, with cathodic limit held constant at –1.3 V, and anodic limit varied between –0.6, –0.65, –0.7 and –0.75 V.

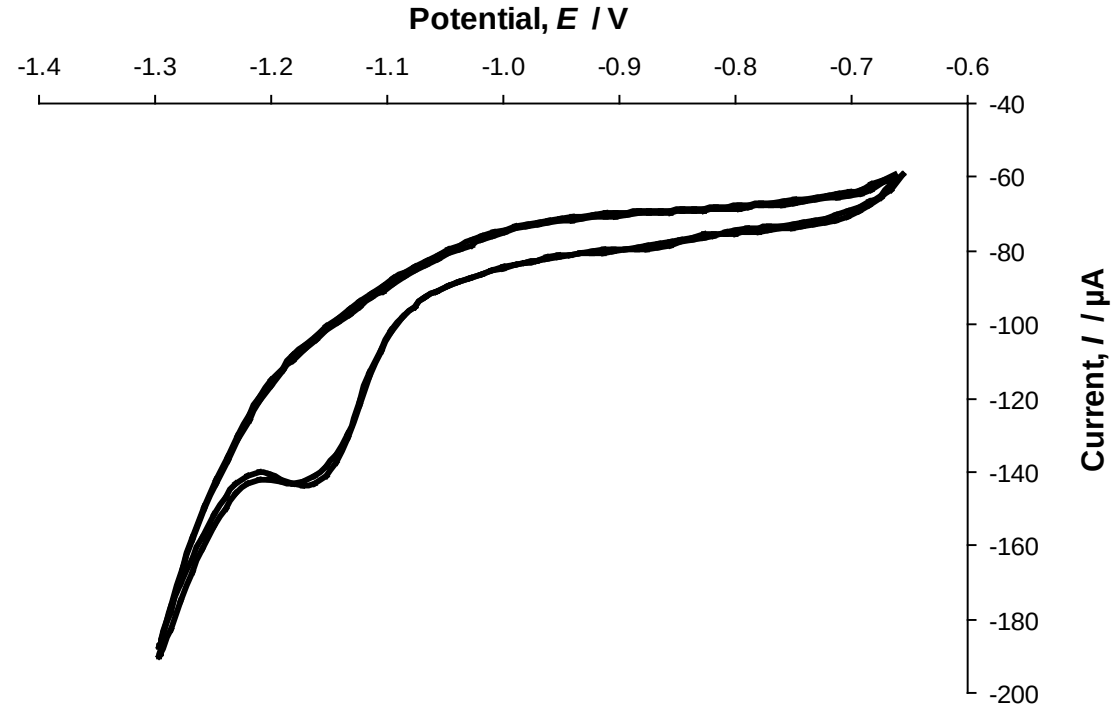

Fig. 3.28 Cyclic voltammograms of 2 subsequent scans for the same experiment in the potential range –0.65 to –1.3 V, showing reproducibility of the C2 peak, with a Sn RDE in the presence of 10 mM ethanol, at 1000 rpm electrode rotation rate and 50 mV s^{-1} potential scan rate.

Figure 3.29 shows cyclic voltammograms collected at 1000 rpm electrode rotation rate and 50 mV s^{-1} potential scan rate, for 10 mM bulk ethanol concentration with each of the three possible baseline cyclic voltammograms described:

(a) the collected background cyclic voltammogram,

(b) the scaled background, in this case the collected background current multiplied by a factor of 1.2 at each potential, and

(c) the baseline calculated from the polynomial trendline fitted to the cyclic voltammograms in the presence of ethanol.

The polynomial trendline showed a good fit for the baseline compared to the collected background and was used for all baseline corrections reported in sections 3.5.4 – 3.5.6. Once the assumed baseline was determined the charge of the peak was calculated. The assumed baseline was subtracted from the ethanol curve and the resulting voltammetric curve was integrated with respect to time giving a charge, *Q*, in coulombs, C, associated with the peak C2.

The charge of the peak is converted to a specific charge (charge per unit area), q_{C2},

$$q_{C2} = Q/A \tag{3.9}$$

where *Q* is the charge associated with the reduction peak, *A* is the surface area of the disc electrode, 1.96×10^{-5} m^2, and q_{C2} is the charge per area of the electrode. As the electrode is a circular disc the surface area of the electrode is given by;

$$A = \pi r^2 \tag{3.10}$$

where *r* is the radius of the electrode, 2 mm.

The number of moles of product per area, n_{C2}, can then be calculated by Faraday's law.

$$n_{C2} = q_{C2}/zF \tag{3.11}$$

where *F* is Faraday's constant, and *z* is the number of electrons in the process. This is assumed to be a two electron process in this instance (eqn (1.13)).

The number of molecules per unit area, $N_{C2,}$ of the electrode can then be calculated from the moles of product using Avogadro's number, N_A.

$$N_{C2} = n \times N_A \tag{3.12}$$

The data analysis described here, including the polynomial fitting method for the baseline, is followed for all subsequent cyclic voltammetry work on the tin disc RDE.

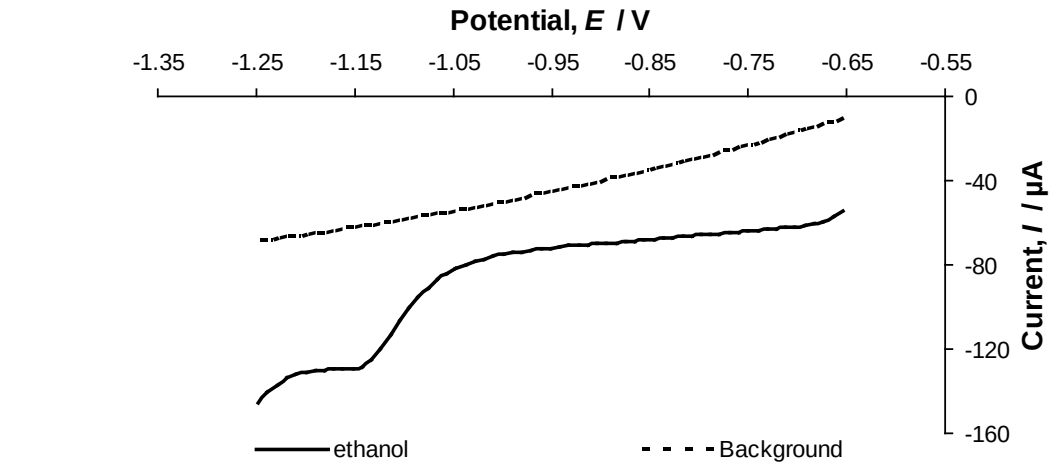

(a)

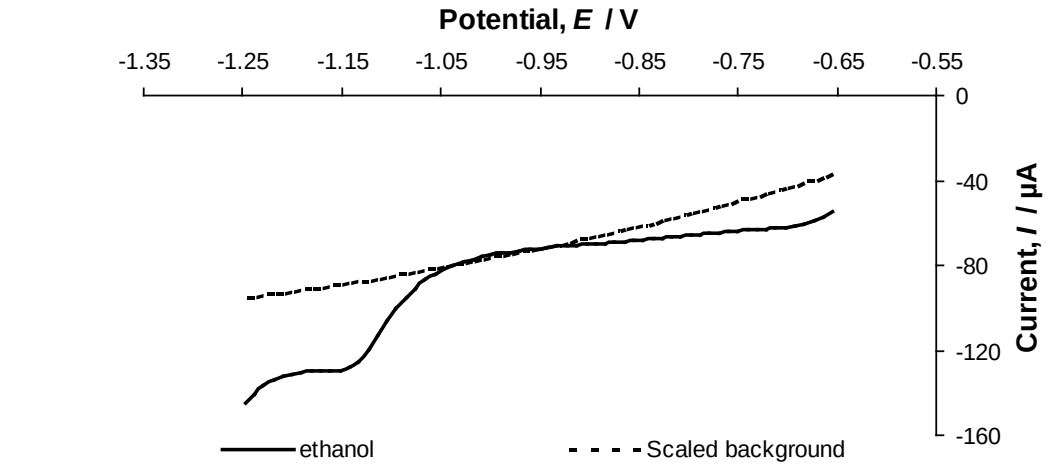

(b)

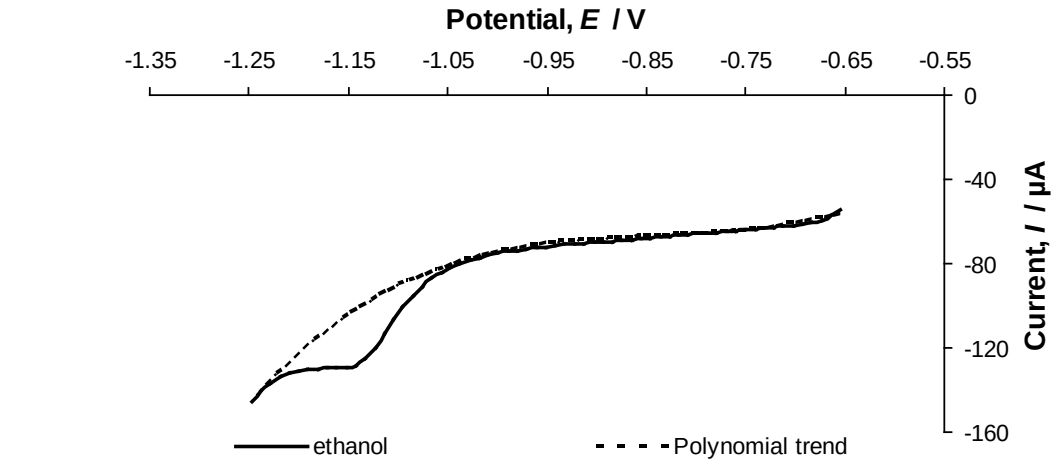

(c)

Fig. 3.29 Cathodic scans of cyclic voltammograms of (a) 7 mM ethanol and background, (b) 7 mM ethanol and background (multiplied by 1.2), and (c) 7 mM ethanol and baseline calculated from curve before and after ethanol peak, all collected at 1000 rpm electrode rotation rate and 50 mV s^{-1} potential scan rate.

3.5.4 Effect of Alcohol Concentration

The bulk ethanol concentration, $[C_2H_5OH]_{bulk}$ was increased from 7 mM to 10, 15 and 20 mM. Figure 3.30 shows the voltammograms for each of the four concentrations and from these voltammograms it is evident that the increase in concentration has no effect on the peak size. The charge of the reductive peak, C2, was calculated and amount of product and molecules per area were calculated from the charge of the peak. These values are recorded in Table 3.9.

Examining the values in Table 3.9, it is noted that the values of N_{C2}, all being within the small range $(0.95 - 1.15) \times 10^{19}$ molecules m^{-2}, are considered to be effectively equivalent. This suggests that the increase in the ethanol concentration does not have any substantial influence on the amount of reduction of the alcohol.

Propanol and propan-2-ol also provided a reductive response on the tin disc electrode in pH 7.3 phosphate buffer. Therefore, the effect on the reductive response of the bulk propanol concentration, $[C_3H_5OH]_{bulk}$, and the bulk propan-2-ol concentration, $[CH_3CH(OH)CH_3]_{bulk}$, was also examined at 7, 10, 15 and 20 mM. Figures 3.31 and 3.32 show the voltammograms for each of the four concentrations, for propanol and propan-2-ol respectively, showing that an increase in concentration does not affect the peak size. The charge for each peak was calculated following the data analysis described earlier along with the moles and molecules/m^2. These values are recorded in Table 3.10 for propanol and Table 3.11 for propan-2-ol.

The values of N_{C2} recorded, $(0.45 - 0.60) \times 10^{19}$ molecules m^{-2}, are also effectively equivalent suggesting that the increase in propanol concentration does not alter the amount of reduction. This is consistent with the observations in the ethanol investigation for the tin electrode. It is noted that there is no significant difference between the responses from propanol and propan-2-ol observed for the electrochemical reduction of the alcohol. Therefore the processes are likely the same for the propanol and propan-2-ol molecules.

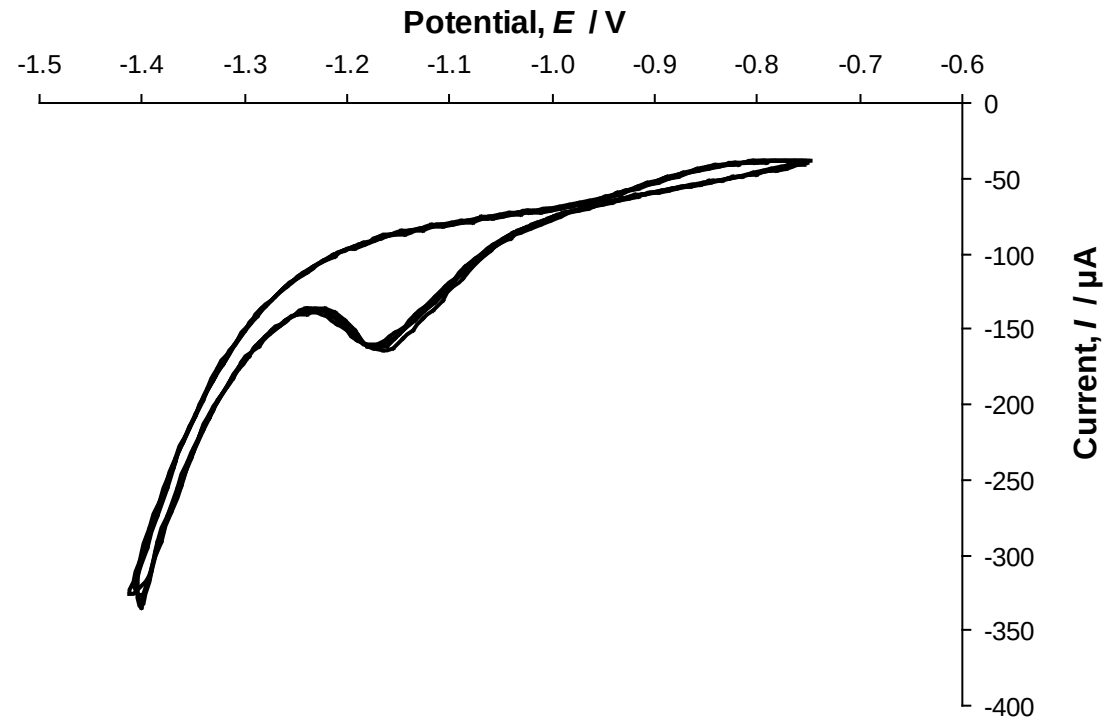

Fig. 3.30 Cyclic voltammograms with a Sn RDE at four bulk ethanol concentrations; 7, 10, 15 and 20 mM, collected at 1000 rpm electrode rotation rate and 50 mV s^{-1} potential scan rate, showing the similarity of the C2 peak for all concentrations studied.

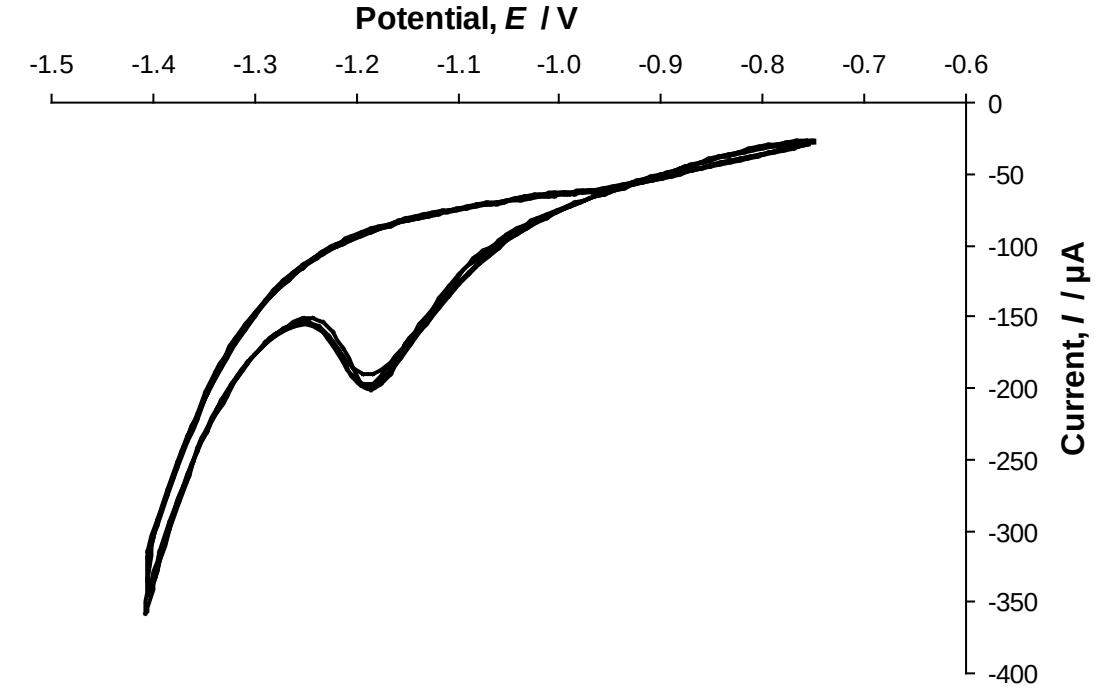

Fig. 3.31 Cyclic voltammograms with a Sn RDE at four bulk propanol concentrations; 7, 10, 15 and 20 mM, collected at 1000 rpm electrode rotation rate and 50 mV s^{-1} potential scan rate, showing the similarity of the C2 peak for all concentrations studied.

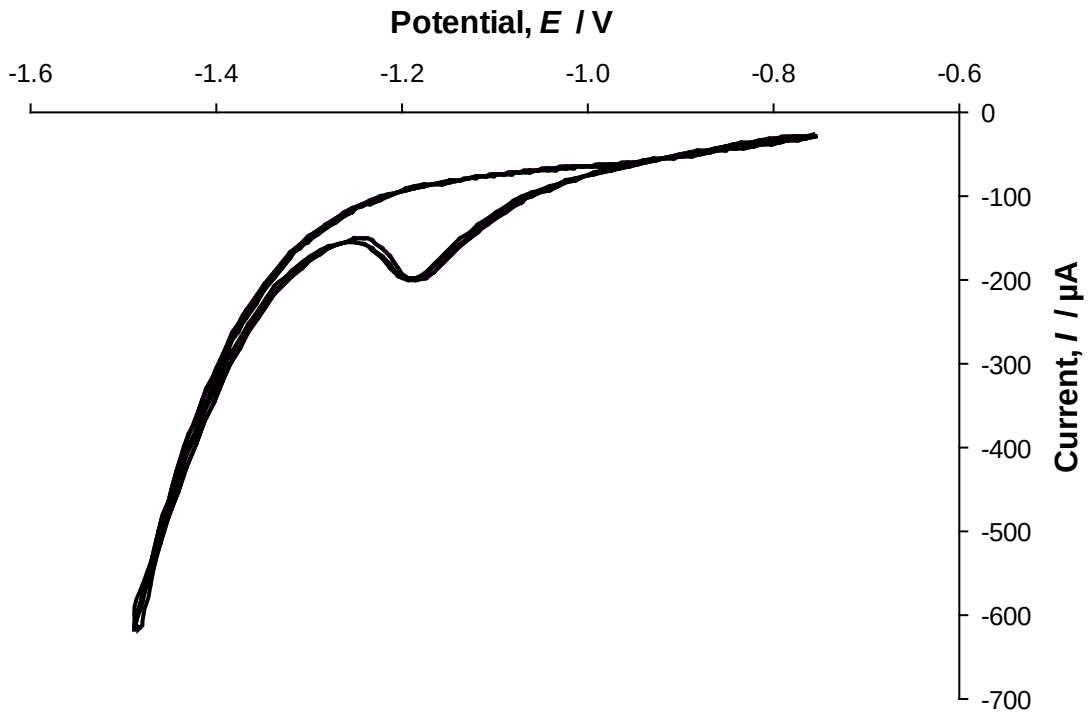

Fig. 3.32 Cyclic voltammograms with a Sn RDE at four bulk propan-2-ol concentrations; 7, 10, 15 and 20 mM, collected at 1000 rpm electrode rotation rate and 50 mV s^{-1} potential scan rate, showing the similarity of the C2 peak for all concentrations studied.

Table 3.9 Analysis for the effect of bulk ethanol concentration on the current response on the Sn RDE at 50 mV s^{-1} potential scan rate and 1000rpm electrode rotation rate. Listing the charge, Q, from the reduction peak, charge per area, q_{C2}, moles of material, n_{C2}, molecules per area, N_{C2}, and area per molecule, A_N, as a function of $[C_2H_5OH]_{bulk}$.

	Bulk Ethanol Concentration / mM			
	7	10	15	20
Charge of Peak Q / μC	63.6	61.0	69.9	62.3
Charge per area q_{C2} / C m^{-2}	3.24	3.11	3.56	3.17
Moles per area n_{C2} / 10^{-6} mol m^{-2}	16.8	16.1	18.4	16.4
molecules per area N_{C2} / 10^{19} m^{-2}	1.01	0.970	1.11	0.990
area per molecule A_N / nm^2	0.99	1.03	0.90	1.01

Table 3.10 Analysis for the effect of bulk propanol concentration on the current response on the Sn RDE at 50 mV s^{-1} potential scan rate and 1000rpm electrode rotation rate. Listing the charge, Q, from the reduction peak, charge per area, q_{C2}, moles of material, n_{C2}, molecules per area, N_{C2}, and area per molecule, A_N, as a function of $[C_2H_5OH]_{bulk}$.

	Bulk Propanol Concentration / mM			
	7	10	15	20
Charge of Peak Q / μC	32.3	34.5	30.8	37.5
Charge per area q_{C2} / C m^{-2}	1.65	1.76	1.57	1.91
moles per area n_{C2} / 10^{-6} mol m^{-2}	8.52	9.11	8.13	9.90
molecules per area N_{C2} / 10^{19} m^{-2}	0.513	0.548	0.490	0.596
area per molecule A_N / nm^2	1.94	1.82	2.04	1.67

Table 3.11 Analysis for the effect of bulk propan-2-ol concentration on the current response on the Sn RDE at 50 mV s^{-1} potential scan rate and 1000rpm electrode rotation rate. Listing the charge, Q, from the reduction peak, charge per area, q_{C2}, moles of material, n_{C2}, molecules per area, N_{C2}, and area per molecule, A_N, as a function of $[C_2H_5OH]_{bulk}$.

	Bulk Propan-2-ol Concentration / mM			
	7	10	15	20
Charge of Peak Q / μC	30.8	33.3	28.3	37.4
Charge per area q_{C2} / C m^{-2}	1.57	1.70	1.44	1.90
moles per area n_{C2} / 10^{-6} mol m^{-2}	8.13	8.79	7.46	9.86
molecules per area N_{C2} / 10^{19} m^{-2}	0.490	0.529	0.449	0.594
area per molecule A_N / nm^2	2.04	1.89	2.22	1.68

Two points can now be considered:

1.) In rotating disc electrochemistry the rotation of the electrode induces a flow of the electrolyte (and therefore the dissolved electroactive species) towards the electrode, replenishing the analyte at the surface of the electrode. This replenishment of analyte would normally provide a continual reduction process. In this case, the reduction was observed to not be maintained as expected. This suggests that there may be an insulating layer being produced on the surface of the electrode.

2.) When the concentration of an electroactive species in solution is increased, the normal response in rotating disc electrochemistry would be for the reductive current to also increase. This is due to the analyte being replenished at the surface at a larger amount when the concentration in the bulk electrolyte is increased, providing more reduction to take place. In this case the concentration of the analyte has no effect on the reduction, which is consistent with a suggested insulating layer on the surface inhibiting any further reduction.

Regardless of how much analyte is being replenished at the surface, once the electrode surface is sufficiently covered no more reduction can occur. The size of the electrode surface is constant, the amount of reduction required to sufficiently cover the electrode surface is constant, and therefore there is a constant amount of reduction occurring at all concentrations.

Another interesting observation is the small difference in the range of the ethanol N_{C2} values compared with the propanol and propan-2-ol values. This difference in N_{C2} values cannot be explained by the experimental error of ± 12 % in the data collection and analysis alone. It should be considered that adsorption to the surface of the electrode appears to be required for reduction to occur; thus forming a layer on the surface inhibiting any further reduction and causing the observed peak in the cyclic voltammogram. It is possible that, as propanol is a slightly larger molecule than ethanol, fewer molecules of propanol (than ethanol) might be packed onto the surface of the electrode before the electrode is sufficiently covered to inhibit the reduction. The amount of molecules packed onto the surface is dependent on where the adsorption takes place on the molecule, oxygen or carbon, and how the molecule is orientated affecting the area of the electrode surface that one molecule effectively covers.

3.5.5 Effect of Potential Scan Rate

The cathodic sweeps of the voltammograms for the Sn disc in pH 7.3 phosphate buffer in the presence of 10 mM ethanol at the 5 different scan rates (10, 20, 50, 100, and 200 mV s^{-1}) are shown in Fig. 3.33. The reductive peak C2 observed in the voltammogram increases in size when the scan rate is increased. Due to the differing time scales associated with the potential scan rates, this increase in peak size must be evaluated in terms of charge before comparisons are made. An increase in peak current with increasing scan rate may be attributable to a constant amount of reduction. A constant peak charge over all scan rates may indicate a scan rate-independence of the reduction process. A constant amount of product forming on the electrode surface would be consistent with the proposed formation of an insulating layer. Following the calculations described in Section 3.4.3, the Q, q_{C2}, n_{C2} and N_{C2} were calculated for the peak C2 for the Sn disc at the five scan rates and are recorded in Table 3.12.

The cathodic sweeps of the voltammograms in the presence of 10 mM propanol and propan-2-ol bulk concentration at 5 different scan rates are presented in Fig. 3.34 and 3.35 respectively. The reductive peak, C2, observed in these voltammograms also increases in size when the scan rate is increased. Again, an increase in size could be indicative of a constant amount of product forming on the electrode. The values for Q, q_{C2}, n_{C2} and N_{C2} for the propanol and propan-2-ol systems were calculated at the five different scan rates and are recorded in Tables 3.13 and 3.14 respectively.

Some irregularity of peak shape is observed within Figs. 3.33 – 3.35, where some potential scan rates appear to have a more obvious peak shape. However, the charge of the peaks at each potential scan rate are reproducible within ± 10 μC, as shown in the alcohol concentration dependence investigations, section 3.5.4. The irregularities in the shape of the peaks may be indicative that the onset of reduction is not instantaneous but may require time to induce reduction, giving rise to an initial increase of current that varies depending in this initial onset of reduction and hence the peak shape varies.

The values of N_{C2} for the experiments in the presence of ethanol are all within a small range of $(0.92 - 1.13) \times 10^{19}$ molecules m^{-2}, those in the presence of propanol are within $(0.48 - 0.60) \times 10^{19}$ molecules m^{-2} and those in the presence of propan-2-ol are within the $(0.44 - 0.63) \times 10^{19}$ molecules m^{-2}. It is proposed, as in the concentration section 3.4.4, that there may be a formation of a constant amount of insulating reaction product in each case.

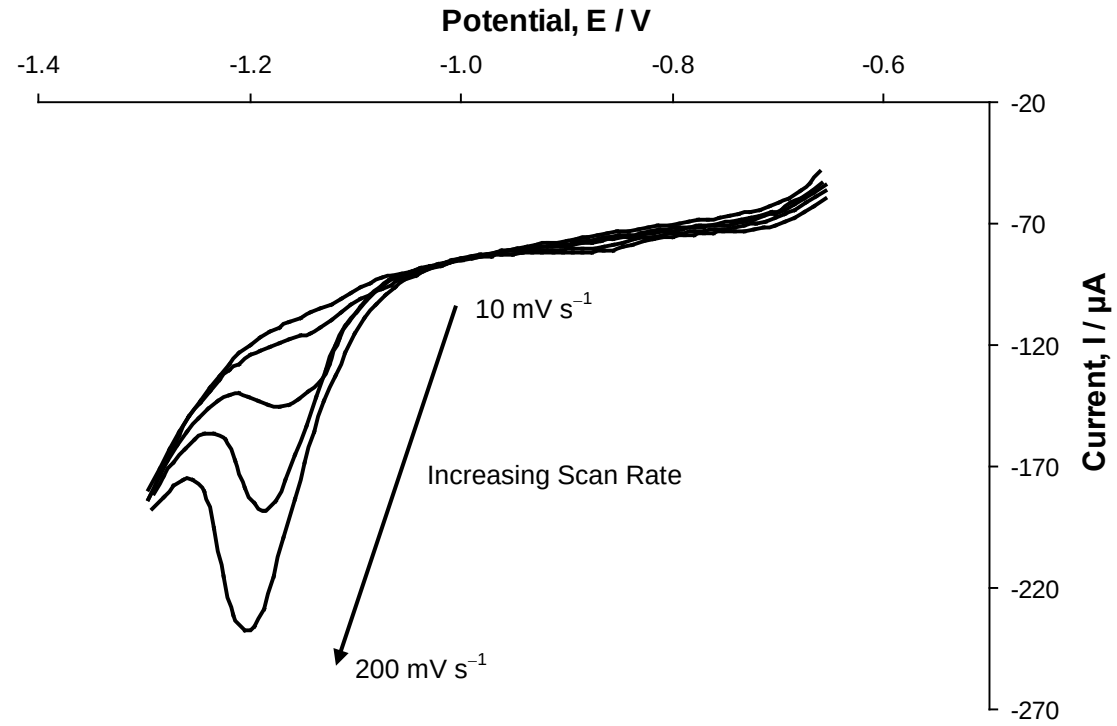

Fig. 3.33 Cathodic scans of cyclic voltammograms for a Sn RDE with 10 mM bulk ethanol concentrations, at 1000 rpm electrode rotation rate and varying potential scan rate; 10 – 200 mV s^{-1} showing the increase of the size of the C2 peak with increasing potential scan rate.

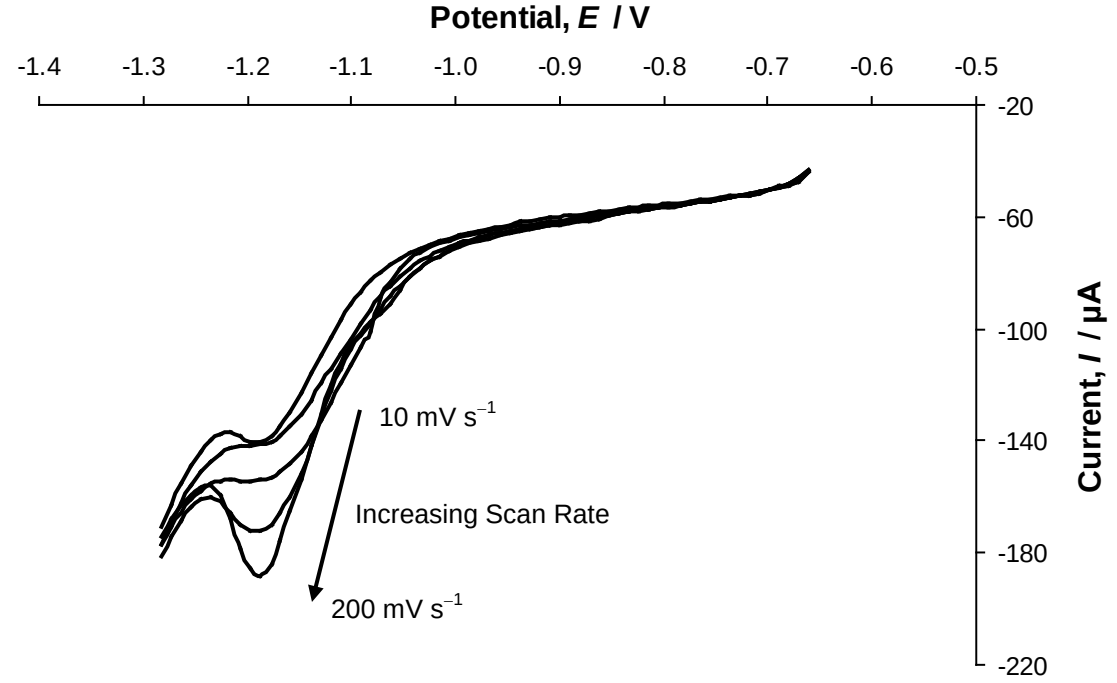

Fig. 3.34 Cathodic scans of cyclic voltammograms for a Sn RDE with 10 mM bulk propanol concentrations, at 1000 rpm electrode rotation rate and varying potential scan rate; 10 – 200 mV s^{-1} showing the increase of the size of the C2 peak with increasing potential scan rate.

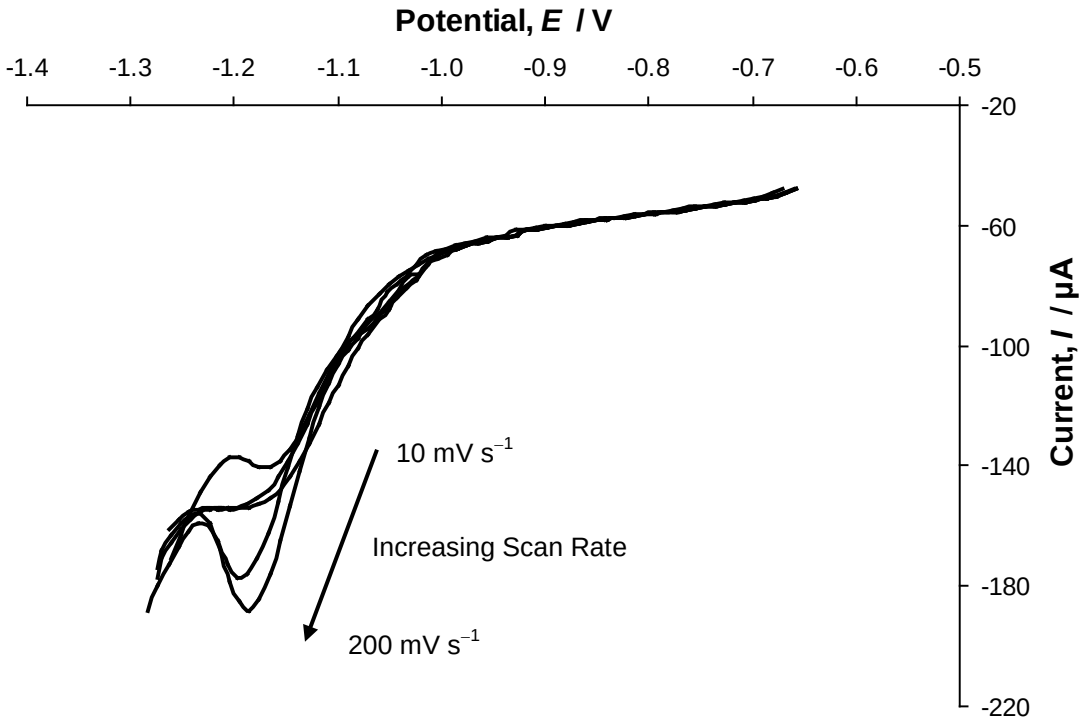

Fig. 3.35 Cathodic scans of cyclic voltammograms for a Sn RDE with 10 mM bulk propan-2-ol concentrations, at 1000 rpm electrode rotation rate and varying potential scan rate; 10 – 200 mV s^{-1}. Showing the increase of the size of the C2 peak with increasing scan rate.

Table 3.12 Analysis for the effect of potential scan rate of voltammograms on the Sn RDE with 10 mM bulk ethanol concentration, at 1000 rpm electrode rotation rate and varying potential scan rate; 10 – 200 mV s^{-1}. Listing the charge, Q, from the reduction peak, charge per area, q, moles of material, n_{C2}, molecules per area, N_{C2}, and area per molecule, A_N, as a function of potential scan rate.

	Potential scan rate / mV s^{-1}				
	10	20	50	100	200
Charge of Peak Q / μC	58.4	66.7	61.0	71.1	59.1
Charge per area q_{C2}/ C m^{-2}	2.98	3.40	3.11	3.62	3.01
Moles per area n_{C2} / 10^{-6} mol m^{-2}	15.4	17.6	16.1	18.8	15.6
Molecules per area N_{C2} / 10^{19} m^{-2}	0.929	1.06	0.970	1.13	0.94
area per molecule A_N / nm^2	1.08	0.94	1.03	0.88	1.06

Table 3.13 Analysis for the effect of potential scan rate of voltammograms on the Sn RDE with 10 mM bulk propanol concentration, at 1000 rpm electrode rotation rate and varying potential scan rate; 10 – 200 mV s^{-1}. Listing the charge, Q, from the reduction peak, charge per area, q, moles of material, n_{C2}, molecules per area, N_{C2}, and area per molecule, A_N, as a function of potential scan rate.

	Potential scan rate / mV s^{-1}				
	10	20	50	100	200
Charge of Peak Q / μC	30.2	37.4	34.5	34.7	31.8
Charge per area q_{C2}/ C m^{-2}	1.54	1.90	1.76	1.77	1.62
Moles per area n_{C2} / 10^{-6} mol m^{-2}	7.97	9.86	9.11	9.15	8.39
Molecules per area N_{C2} / 10^{19} m^{-2}	0.480	0.594	0.548	0.551	0.505
area per molecule A_N / nm^2	0.208	0.168	0.182	0.181	0.198

Table 3.14 Analysis for the effect of potential scan rate of voltammograms on the Sn RDE with 10 mM bulk propan-2-ol concentration, at 1000 rpm electrode rotation rate and varying potential scan rate; 10 – 200 mV s^{-1}. Listing the charge, Q, from the reduction peak, charge per area, q, moles of material, n_{C2}, molecules per area, N_{C2}, and area per molecule, A_N, as a function of potential scan rate.

	Potential scan rate / mV s^{-1}				
	10	20	50	100	200
Charge of Peak Q / μC	28.3	39.6	33.3	34.2	31.9
Charge per area q_{C2}/ C m^{-2}	1.44	2.01	1.70	1.74	1.62
Moles per area n_{C2} / 10^{-6} mol m^{-2}	7.46	10.4	8.79	9.03	8.41
Molecules per area N_{C2} / 10^{19} m^{-2}	0.449	0.629	0.529	0.544	0.507
area per molecule A_N / nm^2	0.222	0.159	0.189	0.184	0.197

This constant peak charge over all scan rates indicates a possible scan rate-independence of the reduction process. However, to fully assess this scan rate-independence, experiments varying scan rate at all of the bulk alcohol concentrations previously examined were completed. Tables 3.15, 3.16 and 3.17 show the values of N_{C2} calculated for each of the four concentrations at each scan rate to further examine the possibility of the amount of reduction occurring being scan rate – independent. The values of N_{C2} recorded in Tables 3.15 – 3.17 are still within the ranges reported earlier, $(0.92 – 1.13) \times 10^{19}$ molecules m^{-2} (ethanol) and $(0.44 – 0.63) \times 10^{19}$ molecules m^{-2} (propanol and propan-2-ol), supporting the proposal that there is a constant amount of insulating reaction product being produced at each scan rate. This is consistent with the nature of the peak being scan rate-independent.

Table 3.15 Average molecules per area, N_{C2}, at each bulk ethanol concentration 7, 10, 15, 20 mM, as a function of potential scan rate, on a Sn RDE, at 1000 rpm electrode rotation rate.

Molecules per area, N_{C2} / 10^{19} m^{-2}					
	Potential scan rate / mV s^{-1}				
Ethanol Concentration / mM	10	20	50	100	200
7	0.990	1.02	1.01	0.973	0.942
10	0.929	1.06	0.970	1.13	0.940
15	0.935	1.01	1.11	0.984	1.03
20	1.08	0.951	0.990	1.11	1.09

Table 3.16 Average molecules per area, N_{C2}, at bulk propanol concentrations 7, 10, 15, 20 mM, as a function of potential scan rate, on the Sn RDE, at 1000 rpm electrode rotation rate.

Molecules per area, N_{C2} / 10^{19} m^{-2}					
	Potential scan rate / mV s^{-1}				
	10	20	50	100	200
Propanol Concentration / mM					
7	0.507	0.529	0.513	0.601	0.461
10	0.480	0.594	0.548	0.551	0.505
15	0.529	0.484	0.490	0.449	0.544
20	0.581	0.564	0.596	0.469	0.493

Table 3.17 Average molecules per area, N_{C2}, at bulk propan-2-ol concentrations 7, 10, 15, 20 mM, as a function of potential scan rate, on the Sn RDE, at 1000 rpm electrode rotation rate.

Molecules per area, N_{C2} / 10^{19} m^{-2}					
	Potential scan rate / mV s^{-1}				
	10	20	50	100	200
Propan-2-ol Concentration / mM					
7	0.529	0.511	0.490	0.504	0.486
10	0.449	0.629	0.529	0.544	0.507
15	0.548	0.499	0.449	0.564	0.524
20	0.588	0.505	0.594	0.484	0.456

3.5.5.1 Insulating Layer Thickness

The responses observed for ethanol, propanol and propan-2-ol at varying bulk concentrations and varying scan rate all support the proposed insulating layer. The thickness of this proposed insulating layer thought to be forming is now considered. The calculations described earlier gave values for the moles of product per area and these values can be used to calculate the possible thickness of the insulating layer. The mass of the product, *m*, can be calculated using the molar mass, *M* and the number of moles from eqn (3.3).

$$m = n_{C2}M \tag{3.13}$$

where *m* is the mass of the product in g, and *M* is the molar mass in g mol^{-1}.

Considering the ethanol investigation, and assuming the product is ethane, the molar mass of ethane (30 g mol^{-1}) can be used to obtain values for the mass of ethane at the electrode surface of $(0.95 – 1.10) \times 10^{-8}$ g. The density of the product with the calculated mass can provide the volume of product, *V*, at the surface.

$$V = m/\rho \tag{3.14}$$

where *V* is the volume of the product in cm^3 and ρ is the assumed density of the product in g cm^{-3}.

As ethane is typically a gas at standard conditions, the density of ethane in the aqueous solution of the experiment is unknown and can only be assumed to be approximately 0.65 g cm^{-3} (density of hexane at standard conditions). This was chosen as the assumed density of ethane as hexane is the smallest alkane present in the liquid phase at room temperature and would therefore give the best approximation of the density of the assumed ethane in the system. Values obtained for the volume of product at the surface of the electrode are approximately 1.46×10^{-8} cm^3.

As the product is possibly an insulating layer forming on the surface, the product can be considered to form a disc shape, where the end of a cylinder is coincident with the circular surface of the disc electrode forming a layer covering the surface and the height of the insulating disc corresponds to the thickness of the layer. The volume of an insulating disc is given in Eqn. (3.14).

$$V = \pi r^2 h \tag{3.15}$$

where r is the radius of the circular cross section of the cylinder in cm, equivalent to the radius of the disc electrode (2.5 mm), and h is the height of the cylinder in cm. Rearranging Eqn. 3.13, the thickness of the insulating layer, h, can be calculated from the volume of product on the surface of the electrode.

$$h = V/\pi r^2 \tag{3.16}$$

These calculations provide values for the thickness of the layer of approximately 0.74 nm, consistent with only a very thin layer forming before the reduction process is stifled. Similar calculations were also carried out for the propanol and propan-2-ol investigations. Assuming the product is propane, using the molar mass and assumed density of propane as 44.1 g mol^{-1} and 0.65 g L^{-1} respectively; values for the thickness of the layer on the surface of the electrode were calculated. The values were found to be approximately 1.4 nm, also indicative of a very thin layer forming before reduction is stifled. The size of molecules such as those considered as products in this work is typically only a few angstroms. Here the calculated thickness of the layer forming is only 8 A, therefore there is a possibility that a monolayer of product is forming on the surface of the electrode.

The number of sites on a metal surface available for adsorption of electroactive species is typically 1.3×10^{19} sites m^{-2}.[52] If a monolayer of product is forming, with one molecule of product adsorbing to each of these sites on the electrode surface, the monolayer would typically require 1.3×10^{19} molecules m^{-2}. The data reported in this section gives values of $(0.92 - 1.13) \times 10^{19}$ molecules m^{-2} for the ethanol reduction product and $(0.44 - 0.63) \times 10^{19}$ molecules m^{-2} for the propanol and propan-2-ol reduction products. These values are lower than the typical value of 1.3×10^{19} molecules m^{-2}, suggesting that not all possible sites on the electrode surface are occupied before the surface is sufficiently covered to inhibit any further reduction. This could be indicative of the available binding sites being mutually widely spaced on the electrode surface.

3.5.6 Effect of Electrode Rotation Rate

Figure 3.36 shows the cathodic sweeps of the voltammograms for the response on the Sn disc electrode due to the addition of ethanol in 0.1 M Phosphate buffer of pH 7.3 at the seven electrode rotation rates (500, 675, 750, 1000, 1250, 1500 and 2000 rpm). The peak C2 is observed to remain very similar in size with increasing rotation rate.

It was observed from Fig. 3.36 that the effective baseline appears to move slightly with increasing rotation rate. The baseline of the voltammograms shows the small extent of reduction of H_2O in the electrolyte occurring on tin metal under these conditions. The shift observed in the baseline of the ethanol cyclic voltammograms was also observed in the background voltammograms, (not shown here), this suggests that the shift is not associated with the ethanol but instead with the reduction of the electrolyte. The baseline from the background cyclic voltammograms does not coincide with that of the ethanol cyclic voltammograms, (as shown in Fig. 3.29), as the presence of ethanol appears to enhance the reduction of H_2O. As the electrode rotation rate is increased the baseline shifts to a larger negative current indicating that the increase in flow rate facilitates more reduction of the electrolyte.

However, when considering this shift in baseline it appears that the actual peak size, and therefore amount of reduction, may remain largely similar. Figure 3.37 shows the cathodic sweeps of the voltammograms of the seven electrode rotation rates with the baselines adjusted to show the alignment of the peaks indicating the similarity of the actual peak size. This could also be consistent with the formation of an insulating layer being formed. In normal rotating disc electrochemistry the rotation of the electrode induces a laminar flow of electrolyte to the surface of the electrode providing a continued supply of more analyte to the electrode for reduction. As the electrode rotation rate of the electrode increases the flow rate of the electrolyte increases therefore analyte is replenished at the electrode surface at a greater rate. More analyte at the surface allows more reduction. Normally it is also observed that increased rotation rate will facilitate the removal of some of the reduced product from the surface of the electrode therefore allowing for more reduction to occur. However, if the reduced product remains on the surface of the electrode as an insulating layer the continuation of reduction is inhibited regardless of more analyte provided to the surface. Even though as the electrode rotation rate increases it can be assumed that more analyte is available at the surface; at any point in time the reduction will still be restricted by the size of the

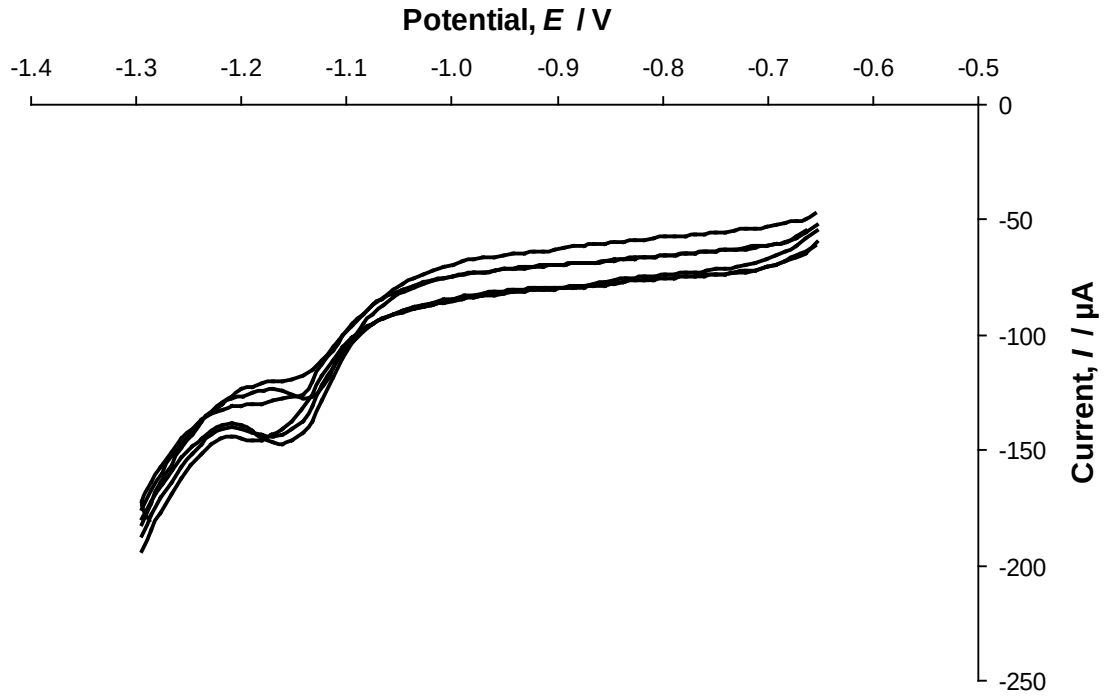

Fig. 3.36 Cathodic scans of cyclic voltammograms with a Sn RDE with 10 mM bulk ethanol concentration, at 50 mV s^{-1} potential scan rate and varying electrode rotation rates; 500 – 2000 rpm.

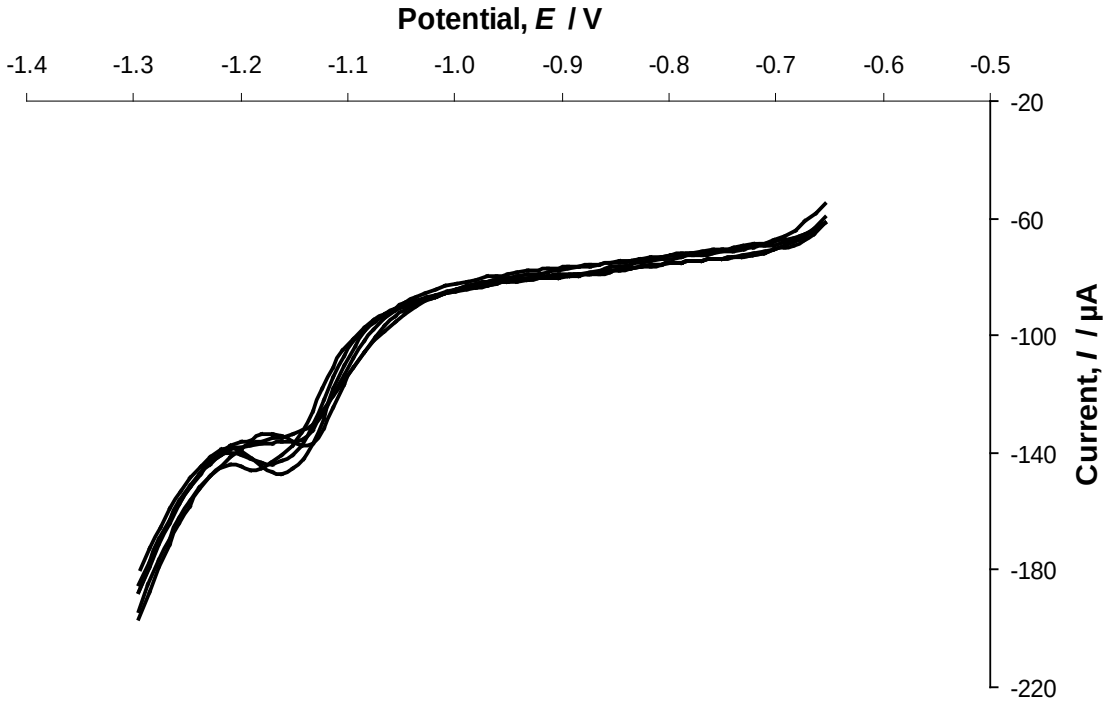

Fig. 3.37 Cathodic scans of cyclic voltammograms in Fig. 3.36 after baseline correction, showing the similarity of the size of the C2 peak at all rotation rates studied.

electrode rather than the amount of analyte and maximum reduction is reached when the insulating layer sufficiently covers the surface of the electrode.

Figures 3.38 and 3.39 shows the cathodic sweeps of the voltammograms for the response due to the addition of 10 mM propanol and propan-2-ol respectively, on the Sn disc electrode in the 0.1 M Phosphate buffer at the seven electrode rotation rates (500, 675, 750, 1000, 1250, 1500 and 2000 rpm).

As with the ethanol studies the effective baseline is observed to shift with increasing rotation rate and when considering this shift in baseline the actual size of the peak C2 and consequently the amount of reduction is observed to remain largely similar at each rotation rate. Thus the reduction must still be restricted by the size of the electrode rather than the amount of analyte and maximum reduction is reached when the insulating layer sufficiently covers the surface of the electrode. There is the same amount of material reducing regardless of the rotation rate.

The charge, Q, of the peak, C2, for all three alcohols at each rotation rate was calculated and, along with q_{C2}, n_{C2} and $N_{C2,}$ is recorded in Tables 3.18 (ethanol), 3.19 (propanol) and 3.20 (propan-2-ol). From these values, it is observed that the charge of the peak is very similar, giving rise to values of N_{C2} which are within the small range of $(0.90 – 1.10) \times 10^{19}$ molecules m^{-2} in the presence of ethanol and the range of $(0.45 – 0.60) \times 10^{19}$ molecules m^{-2} in the presence of propanol. These small ranges are consistent with the suggestion that the amount of reduction occurring is effectively equivalent across all rotation rates. This is different to what would be expected in rotating disc electrode chemistry where an increase in rotation would be expected to facilitate the removal of some of the insulating layer assumed to be forming on the electrode and the replenishment of analyte at the surface of the electrode, therefore providing the ability for more reduction to occur. In this case it appears that the increase in rotation rate does not aid in the removal of the product and maximum reduction remains at the point at which the electrode becomes sufficiently covered by the assumed insulating layer.

The effect of rotation rate was also examined at all four bulk concentrations previously reported. Tables 3.21, 3.22 and 3.23 list the values of N_{C2} for each rotation rate at bulk ethanol, propanol and propan-2-ol concentrations respectively. These values are consistent with a similar amount of reduction occurring for each alcohol regardless of electrode rotation rate or concentration of the alcohol.

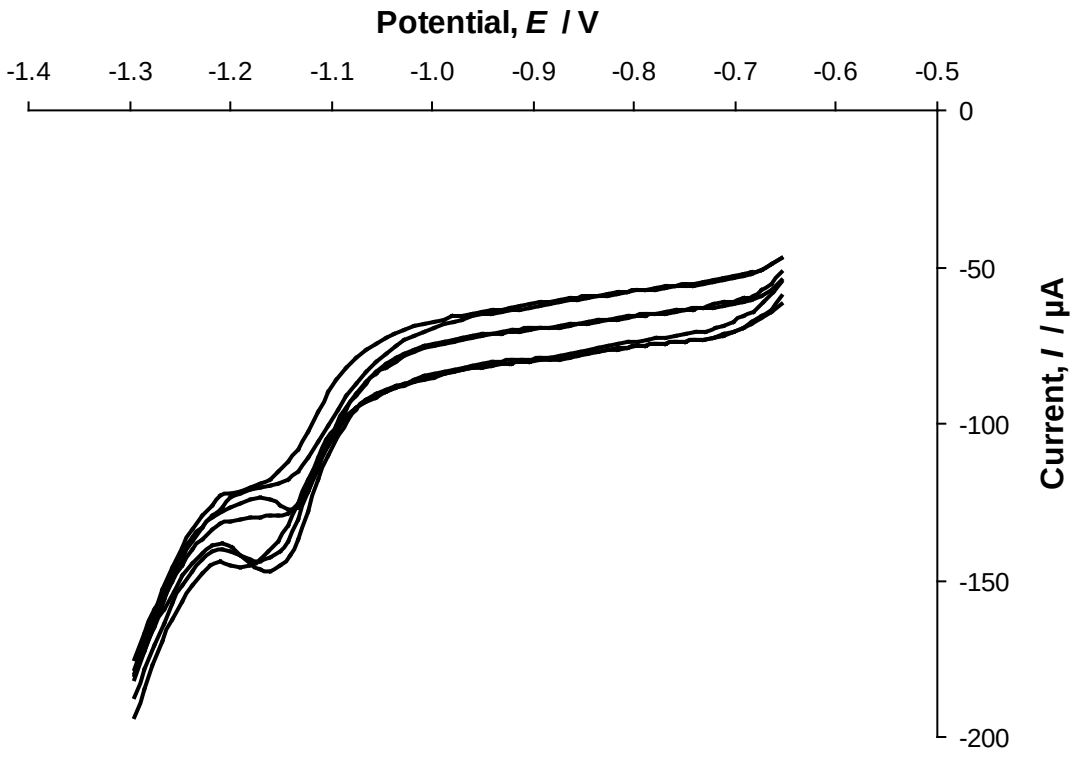

Fig. 3.38 Cathodic scans of cyclic voltammograms with a Sn RDE with 10 mM bulk propanol concentrations, 50 mV s^{-1} potential scan rate and varying electrode rotation rate; 500 – 2000 rpm.

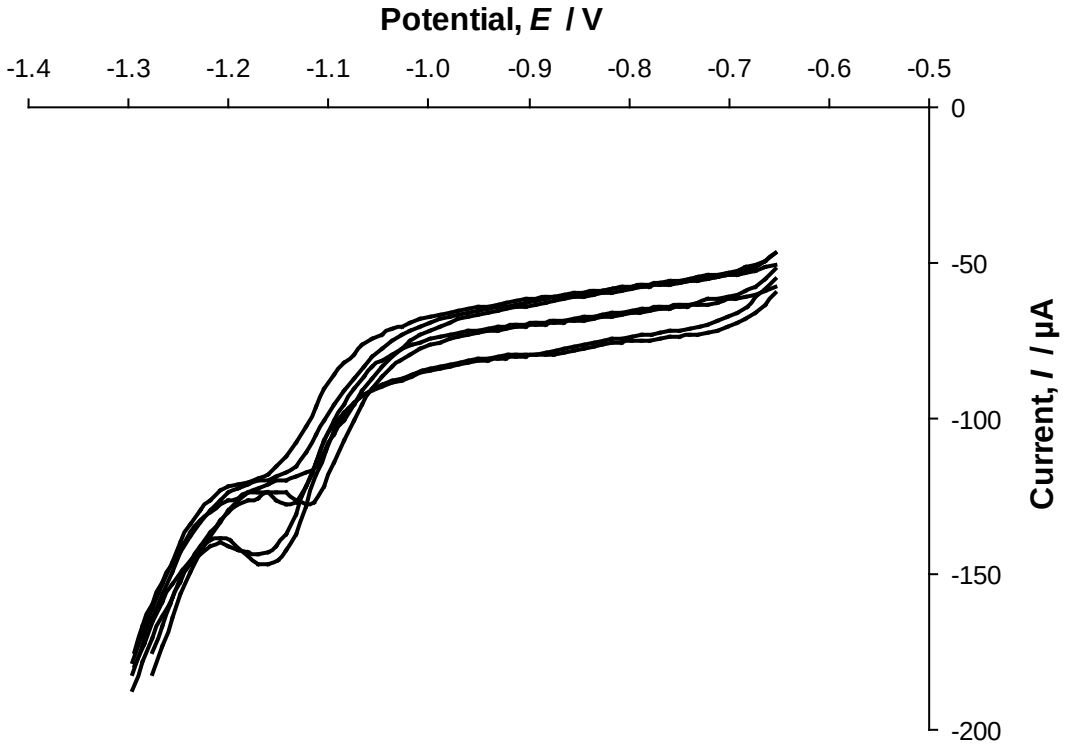

Fig. 3.39 Cathodic scans of cyclic voltammograms with a Sn RDE with 10 mM bulk propan-2-ol concentrations, 50 mV s^{-1} potential scan rate and varying electrode rotation rate; 500 – 2000 rpm.

Table 3.18 Analysis for the effect of the electrode rotation rate of the Sn RDE with 10 mM bulk ethanol concentration. Listing the charge, Q, from the reduction peak, charge per area, q_{C2}, moles of material, n_{C2}, molecules per area, N_{C2}, and area per molecule, A_N, as a function of electrode rotation rate.

	Electrode rotation rate / rpm						
	500	675	750	1000	1250	1500	2000
Charge of Peak Q / μC	72.0	58.4	58.4	61.0	53.2	62.0	67.3
Charge per area q_{C2} / C m^{-2}	3.67	2.97	2.98	3.11	2.71	3.16	3.43
Moles per area n_{C2} / 10^{-6} mol m^{-2}	19.0	15.4	15.4	16.1	14.0	16.4	17.8
molecules per area N_{C2} / 10^{19} m^{-2}	1.14	0.928	0.929	0.970	0.848	0.985	1.07
Area per molecule A_N / nm^2	0.87	1.08	1.08	1.03	1.18	1.01	0.93

Table 3.19 Analysis for the effect of the electrode rotation rate of the Sn RDE with 10 mM bulk propanol concentration. Listing the charge, Q, from the reduction peak, charge per area, q_{C2}, moles of material, n_{C2}, molecules per area, N_{C2}, and area per molecule, A_N, as a function of electrode rotation rate.

	Electrode rotation rate / rpm						
	500	675	750	1000	1200	1500	2000
Charge of Peak Q / μC	33.3	36.0	28.3	34.5	37.4	30.4	31.9
Charge per area q_{C2} / C m^{-2}	1.70	1.84	1.44	1.76	1.90	1.55	1.62
Moles per area n_{C2} / 10^{-6} mol m^{-2}	8.79	9.5	7.46	9.11	9.86	8.03	8.41
molecules per area N_{C2} / 10^{19} m^{-2}	0.529	0.573	0.449	0.548	0.594	0.484	0.507
Area per molecule A_N / nm^2	1.89	1.75	2.22	1.82	1.68	2.07	1.97

Table 3.20 Analysis for the effect of the electrode rotation rate of the Sn RDE with 10 mM bulk propan-2-ol concentration. Listing the charge, Q, from the reduction peak, charge per area, q_{C2}, moles of material, n_{C2}, molecules per area, N_{C2}, and area per molecule, A_N, as a function of electrode rotation rate.

	Electrode rotation rate / rpm						
	500	675	750	1000	1200	1500	2000
Charge of Peak Q / μC	24.6	34.5	28.3	33.3	36.0	37.4	30.4
Charge per area q_{C2} / C m^{-2}	1.26	1.76	1.44	1.70	1.84	1.9	1.55
Moles per area n_{C2} / 10^{-6} mol m^{-2}	6.50	9.11	7.46	8.79	9.52	9.86	8.03
molecules per area N_{C2} / 10^{19} m^{-2}	0.392	0.548	0.449	0.529	0.573	0.594	0.484
Area per molecule A_N / nm^2	2.55	1.82	2.22	1.89	1.75	1.68	2.07

Table 3.21 Average molecules per area, N_{C2}, as a function of electrode rotation rate of the Sn RDE at four bulk ethanol concentrations.

Molecules per area, N_{C2} / 10^{19} m^{-2}							
	Electrode rotation rate / rpm						
Ethanol Concentration / mM	500	675	750	1000	1200	1500	2000
7	0.954	1.092	0.946	1.014	1.031	0.997	0.925
10	1.140	0.928	0.929	0.970	0.846	0.985	1.077
15	0.924	0.995	1.02	1.111	0.977	0.981	0.974
20	0.984	0.889	0.988	0.990	1.018	1.041	0.955

Table 3.22 Average molecules per area, N_{C2}, as a function of electrode rotation rate of the Sn RDE with four bulk propanol concentrations.

Molecules per area, N_{C2} / 10^{19} m^{-2}							
	Rotation rate / rpm						
Propanol Concentration / mM	500	675	750	1000	1200	1500	2000
7	0.392	0.556	0.507	0.513	0.573	0.579	0.549
10	0.529	0.573	0.449	0.548	0.594	0.484	0.507
15	0.595	0.484	0.572	0.490	0.457	0.360	0.586
20	0.488	0.598	0.486	0.596	0.601	0.515	0.448

Table 3.23 Average molecules per area, N_{C2}, as a function of electrode rotation rate of the Sn RDE with four bulk propan-2-ol concentrations.

Molecules per area, N_{C2} / 10^{19} m^{-2}							
	Electrode rotation rate / rpm						
Propan-2-ol Concentration / mM	500	675	750	1000	1200	1500	2000
7	0.457	0.579	0.507	0.490	0.578	0.488	0.546
10	0.392	0.548	0.449	0.529	0.573	0.594	0.484
15	0.572	0.488	0.556	0.449	0.544	0.577	0.515
20	0.552	0.596	0.588	0.594	0.457	0.524	0.493

Values of N_{C2} are within a small range of (0.84–1.14) × 10^{19} molecules m^{-2} in the presence of ethanol and (0.36–0.60) × 10^{19} molecules m^{-2} with propanol or propan-2-ol. These small ranges show that the amount of reduction occurring remains similar in each alcohol case, indicating a rotation-rate-independence for the system.

As has been noted earlier there is still a small difference in values between the two alcohols which is proposed to be due to the small difference in size of the alcohol molecule. This leads to there being fewer propanol than ethanol molecules required to sufficiently cover the electrode surface before reduction can no longer continue therefore less reduction occurs.

3.5.7 Tin Disc Summary

The conditions for the reproduction of the reduction of peak C2 using the Sn disc electrode were established along with the effect on the reduction of the bulk alcohol concentration, potential scan rate, and electrode rotation rate. The possible products of this reduction process include alkanes and ethers however a working hypothesis of the reduction of alcohols in this system producing alkanes has been used thus far and the data was examined.

A reductive peak was observed on the cathodic sweeps of the cyclic voltammograms with no accompanying oxidative peak, indicating an irreversible reduction occurring in the presence of the alcohol. The formation of a peak is counter to what is typically observed with rotating disc electrochemistry. In normal rotating disc electrochemistry an initial increase in reduction current is observed followed by a limiting current plateau similar to that observed in the Cu disc systems. The formation of a peak is indicative of the reduction being unable to continue which may indicate the presence of an insoluble product forming and insulating layer on the surface of the electrode inhibiting further reduction. The presence of an insoluble product is not inconsistent with the hypothesis that an alkane is forming from the reduction of the alcohol as alkane are not significantly soluble in aqueous solutions.

When the anodic limit of the cyclic voltammogram for the Sn disc electrode is shifted the reductive peak is unchanged. The peak C2 is reproducible, remaining in subsequent cycles, maintaining a similar size, shape and charge associated with it. Therefore any anodic limit from –650 mV to –800 mV is suitable and provides a reproducible

reductive peak, C2, at approximately −1.1 V. So, providing the anodic limit is maintained at a potential that is more positive than the onset of peak C2, ~ –950 mV and less positive than the potential where the electrochemistry of the Sn becomes a factor, ~ –600 mV, there appears to be the same amount of material reducing and forming on the surface.

The amount of charge produced within peak C2 may suggest a monolayer is being formed on the surface of the electrode within the conditions considered in this work. The studies of the effect of the alcohol concentration on the reductive response of the system found that increasing the concentration of the alcohol, be it ethanol or propanol, has no significant effect on the total charge produced. This supports the proposal that the reduction process is being progressively inhibited by the formation of an insoluble insulating layer.

Investigating the effect of the potential scan rate of the experiment also showed no significant effect on the total charge produced from peak C2, with the same amount of material reducing regardless of the potential scan rate applied. The peak was found to show scan rate-independence across all bulk concentrations tested. Therefore, irrespective of the concentration of the alcohol in the system and the potential scan rate applied to the system, (in the range 10 - 200 mV s^{-1}), the same amount of material appears to be reducing and forming on the surface.

The electrode rotation rate of the Sn disc electrode also appears to have an effect on the reduction processes. There is a shift in the baseline observed when the rotation rate is increased. This shift is apparent in the background experiments without the presence of ethanol suggesting it is an effect from the reduction of the electrolyte occurring.

When considering this observed shift in baseline the actual peak size and hence the charge associated with the peak remains largely similar with increasing rotation rate. Values of N_{C2} for the ethanol experiments were in the range of $(0.9–1.2) \times 10^{19}$ molecules m^{-2} and for the propanol experiments were $(0.5–0.9) \times 10^{19}$ molecules m^{-2}. This is not inconsistent with the proposed formation of an insulating layer being formed. As the rotation rate of the electrode increases the flow rate of the electrolyte toward the electrode surface increases therefore replenishing analyte at the electrode surface at a greater rate. As the rotation rate increases it can be assumed that more analyte is available at the surface at any point in time. However, if the reduced product remains on the surface of the electrode as an insulating layer the

continuation of reduction is inhibited regardless of how much more analyte is provided to the surface. Therefore, the amount of reduction observed is still restricted by the size of the electrode and maximum reduction is reached when the surface of the electrode is sufficiently covered by the insulating layer.

The thickness of the proposed insulating layer forming was calculated using eqns. 3.11 to 3.14. The working hypothesis assumed the product was the alkane in each case, i.e ethanol reduces to ethane, and the density of the alkanes was assumed to be 0.65 g mL^{-1}, the density of hexane at 25°C, as hexane is the smallest alkane in liquid phase at 25°C. For the ethanol investigation the thickness of the proposed layer was calculated to be approximately 0.30 nm, and for the propanol and propan-2-ol investigations approximately 0.45 nm.

The results presented here provide evidence of a reduction process associated with the presence of the alcohols in the electrolyte. The most likely reduction occurring is the reduction of the alcohol to the corresponding alkane. The concentration, scan rate and rotation rate independences determined provide no indication of any further processes occurring, therefore are not inconsistent with this initial working hypothesis that alkanes are being produced. The bulk alcohol concentration, potential scan rate and rotation rate independence support the suggestion that an insoluble product is forming an insulating layer on the surface of the electrode.

Alkanes are typically insoluble in aqueous solutions and could be this proposed insoluble product. However, the alcohol reduction process may involve the formation of a Sn-C bond, where an alkyl chain bonds to a binding site on the surface of the Sn electrode, supporting the formation of a persistent insulating layer on the surface of the electrode.

It was assumed from the results of these Sn investigations and the lack of any contradicting information thus far, that the reduction of alcohols to alkanes (eqn. 2.11) may be occurring in these experiments; ethanol is reduced to ethane, propanol and propan-2-ol to propane.

3.6 Lead Disc Rotating Disc Electrode Cyclic Voltammetry

The third electrode material that exhibited an electrochemical response due to the addition of ethanol was lead. The electrochemical reduction of the five alcohols on the lead disc RDE with the supporting electrolyte of aqueous phosphate buffer of pH 8.1 was examined. An electrochemical response was observed due to the addition of ethanol, propanol and propan-2-ol with this lead disc electrode. The cyclic voltammetry of the Pb disc electrode in 0.1 M aqueous phosphate buffer of pH 8.1 in the presence of ethanol, propanol and propan-2-ol was examined and is described in Sections 3.6.1 - 3.6.5.

Again, the electrochemistry of the electrode within the system must be established before the electrochemistry specifically associated with alcohol reduction can be determined. Figure 3.40 shows the cyclic voltammogram of the lead disc electrode in the phosphate buffer, pH 8.1, with and without the presence of 10 mM ethanol. Considering the voltammogram in the absence of ethanol, when commencing at an anodic limit more positive than −520 mV an oxidation current is observed. This is assumed to be due to the oxidation of metallic Pb^0 to Pb^{2+}. As the potential is swept progressively more cathodic than −520 mV a reductive wave assigned to the reduction of Pb^{2+} to Pb^0 is observed. This peak is identified as C1. During the return sweep of the potential the oxidation wave, Pb^0 to Pb^{2+}, identified as peak A1 is observed.

Repeating the cyclic voltammogram experiment after the introduction of 10 mM of ethanol to the cell leads to a number of similar observations to those made with the Sn system:

i) Peaks A1 and C1 assigned to the electrochemistry of lead in this electrolyte are maintained although altered in both position and magnitude.

ii) There is a change to the general background of the voltammogram in the presence of ethanol, with larger currents observed when compared to the ethanol-free voltammogram.

iv) There is an additional peak, C2, observed in the presence of ethanol background.

No new anodic wave accompanies the new C2 peak suggesting that the reduction process is irreversible over the potential range of the experiment.

The background is assumed, as with the Sn, to be the small extent of reduction of H_2O on lead metal under these conditions. The presence of ethanol appears to also enhance this process. It is also noted that the C1 and A1 peaks, Pb^{2+} to Pb^0 and Pb^0 to Pb^{2+} respectively, are less well defined in the presence of ethanol, with both position and magnitude affected.

The new C2 peak is found at –1.02 V some 300 mV more cathodic than C1. In order to eliminate the possibility of a new lead product being responsible for reduction peak C2, the potential range was limited to a region where lead was maintained in the Pb^0 state throughout. Consequently the new anodic limit and starting potential was set at –0.60 V, approximately 100 mV more cathodic than the potential for the cessation of Pb^0 oxidation on a cathodic scan in the absence of ethanol. The cathodic limit was maintained at –1.3 V.

Figure 3.41 shows the resulting voltammogram when performing cyclic voltammetry within this more confined potential range of –0.6 to –1.30 V. A reducing current is maintained throughout the voltammogram, with no evidence for reduction of Pb^{2+} as anticipated and the C2 peak is apparent in this voltammogram at a potential of –0.93 V.

This is consistent with the hypothesis that the presence of ethanol is responsible for this peak. Again, no accompanying anodic wave is associated with C2 on the reverse sweep indicating that the reduction process is irreversible over the potential range of the experiment.

As was discussed with respect to the tin electrode in section 3.5, in normal rotating disc electrochemistry an increase in the reductive current is observed followed by a limiting current plateau. In this case, as with the tin disc, there is an initial increase in the reduction current, then the current decreases again, forming peak C2. The formation of this peak is indicative of the reduction being unable to continue. This may suggest the possible presence of an insoluble and insulating product forming on the surface of the electrode, preventing continuation of the reduction process.

Considering the balanced electrochemical equation for the presumed process, eqn 1.13,

$$R\text{-}OH + 2e^- + 2H^+ \rightarrow R\text{-}H + H_2O \qquad (1.13)$$

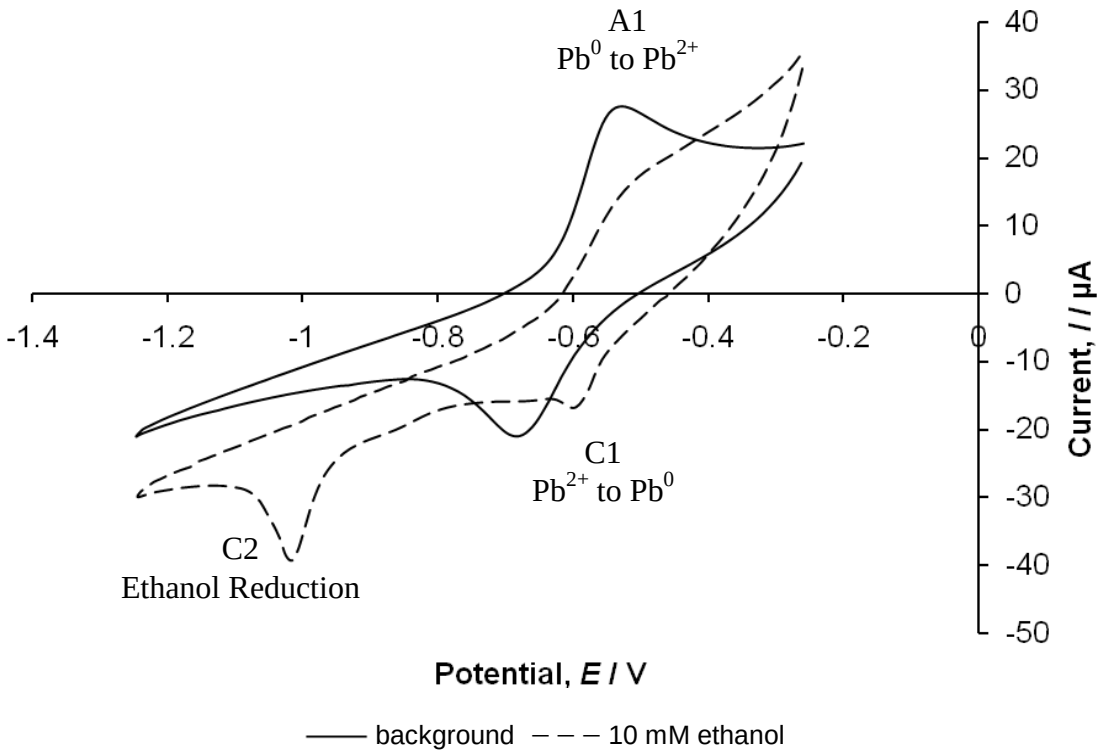

Fig. 3.40 Cyclic voltammograms for the Pb RDE in 0.1 M phosphate buffer, pH 8.1, with and without the presence of 10 mM ethanol at 1000 rpm electrode rotation rate and 50 mV s^{-1} potential scan rate displaying peaks A1, C1 and C2.

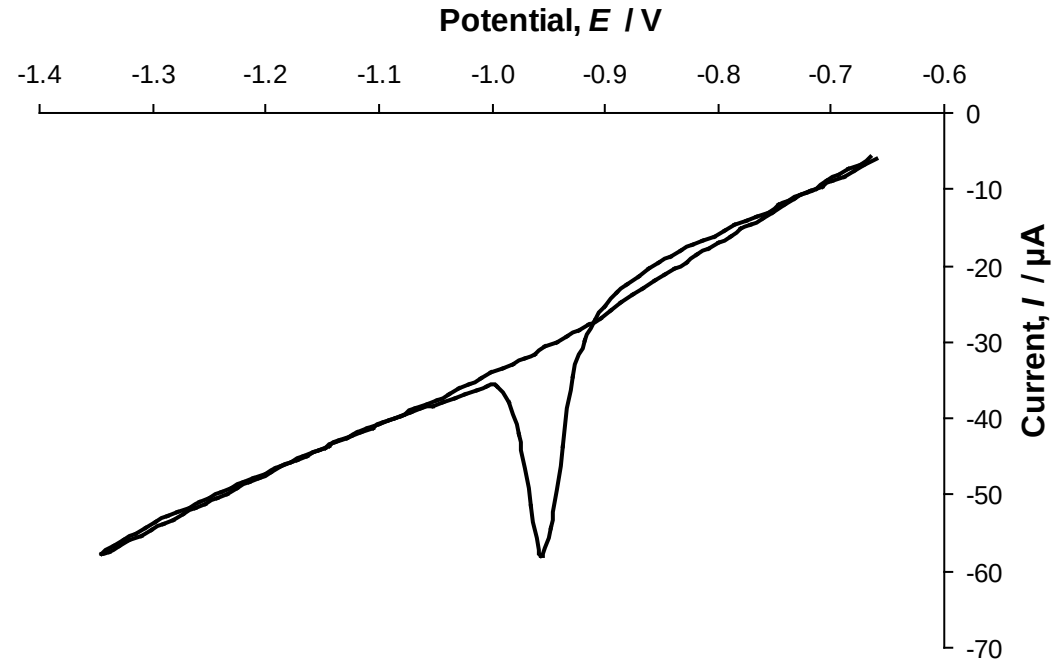

Fig. 3.41 Cyclic voltammogram for the Pb RDE in 0.1 M phosphate buffer, pH 8.1, in the presence of 10 mM ethanol for the potential range –0.6 to –1.3 V, collected at 1000 rpm electrode rotation rate and 50 m s^{-1} potential scan rate, displaying only peak C2 for the response associated with the addition of ethanol.

suggests alkanes may be being produced. Since alkanes are not substantially soluble in aqueous systems it is not unlikely that there may be an insoluble insulating product present. As identified in studies on tin and copper, if the product of the ethanol reduction were to be ethane, it would be expected to be a gas under these conditions (b.p. = –89°C). Consequently, it must be noted that if ethane was forming a passivating layer then it must be present as a persistent layer (*i.e.* chemisorbed) on the electrode surface as was specified for the tin investigation in section 3.2.

3.6.1 Effect of anodic limit

The anodic limit was set at −0.6 V to ensure that the electrode response could be attributed to the addition of the alcohol and that any possible Pb electrochemistry effects were removed. Figure 3.42 shows the cyclic voltammograms of four different potential ranges with the cathodic limit held constant and the anodic limits progressively shifted more negative. The change in the cathodic wave between the anodic limit of –0.65 V and –0.70 V is pronounced where the reductive peak becomes smaller. The previously noted absence of an accompanying oxidative wave on the anodic sweep of these cyclic voltammograms strongly indicates that the reduction product is not being oxidised back to the alcohol (or any other species) suggesting an irreversible electrode process. There appears to be some decrease in reduction on the electrode surface for the cyclic voltammograms with anodic limit $E < -0.70$ V, while this decrease is absent for those with anodic limit $E > -0.65$ V (note that any anodic limits > -0.52 V can not be undertaken without introducing artifacts associated with the chemistry of lead). This behaviour could be accounted for by either a time-dependent phenomenon or a potential-dependent phenomenon.

3.6.2 Reproducibility of peak C2

The voltammograms presented so far have been confined to single cycle experiments with commencement at the selected anodic limit. The issue to be addressed in this section is the reproducibility of the voltammograms upon further cycling. Figure 3.43 shows two consecutive scans (with no intervening potential pause) in the potential range –0.60 to –1.30 V, at 1000 rpm electrode rotation rate and 50 mV s^{-1} potential scan rate.

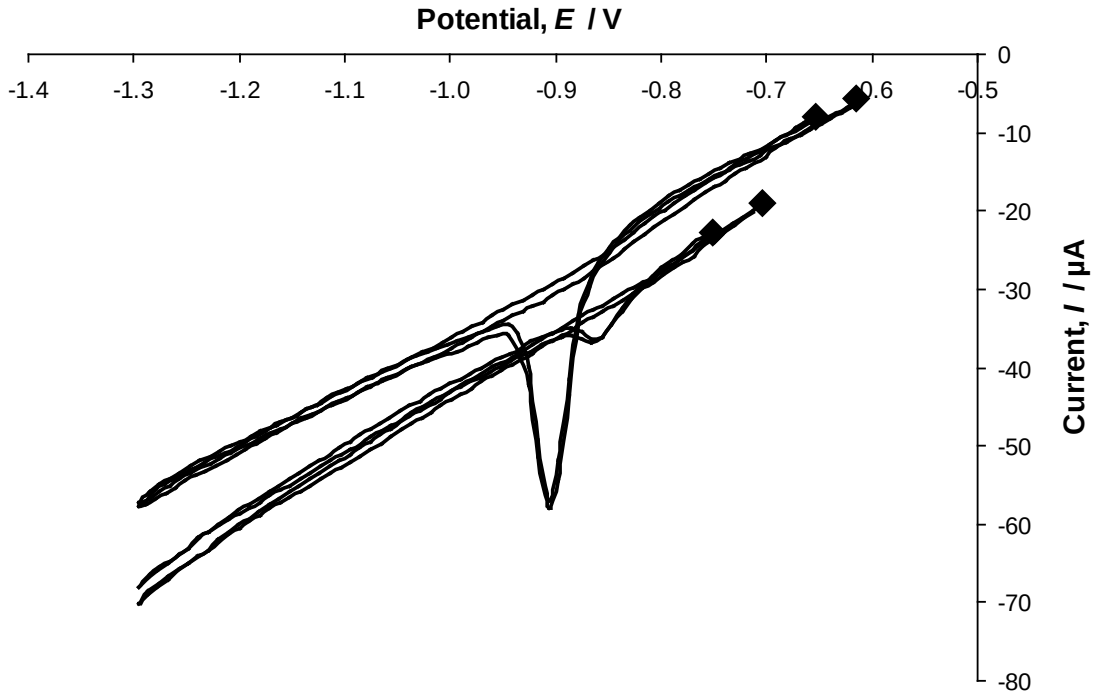

Fig. 3.42 Cyclic voltammograms for the Pb RDE in 0.1 M phosphate buffer pH 8.1, in the presence of 10 mM ethanol, at 1000 rpm electrode rotation rate and 50 mV s^{-1} potential scan rate, with cathodic limit held constant at –1.3 V, and anodic limit varied between –0.6, –0.65, –0.7 and –0.75 V.

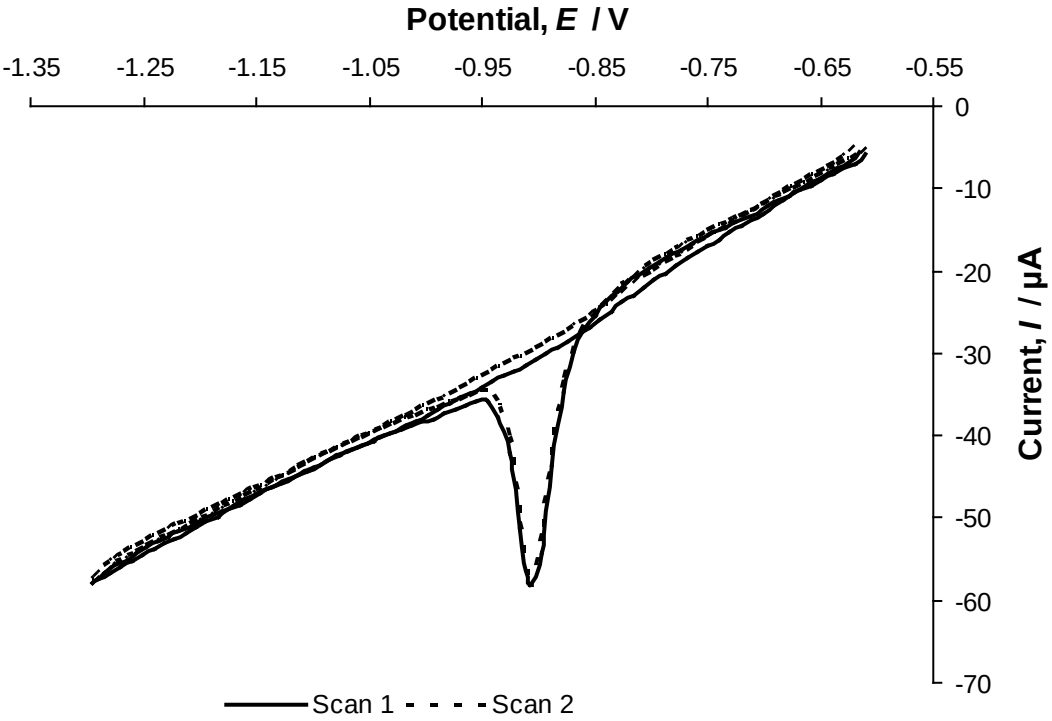

Fig. 3.43 Cyclic voltammograms of 2 subsequent scans for the same experiment in the potential range –0.6 to –1.3 V, with a Pb RDE in the presence of 10 mM ethanol, at 1000 rpm electrode rotation rate and 50 mV s^{-1} potential scan rate, showing reproducibility of the C2 peak.

Under these conditions there is good reproducibility of the C2 peak. This suggests that the putative insoluble layer cannot be permanent. As considered above, if this is an irreversible electrochemical reaction then there must be some form of detachment of the product layer from the surface occurring *via* a non-electrochemical process so that further reduction may take place in subsequent cycles.

Figure 3.44 shows two subsequent scans in the potential range –0.75 to –1.30 V at 1000 rpm electrode rotation rate and 50 mV s^{-1} potential scan rate. Under these conditions with a 0.1 V more negative anodic potential limit (together with 6 seconds/cycle less time spent at potentials more positive than –0.75 V) a smaller peak is observed in the first scan and then subsequent scans return to only the baseline curve. Consequently, the reproducibility of the peak, C2, is lost by merely shifting the anodic limit from –0.60 V to –0.75 V. Any detachment of the product that appears to be occurring in the scans with the more positive anodic limits of E = –0.60 V and –0.65 V is not evident here. In this case, if an insoluble and insulating layer exists then it appears to remain on the electrode surface.

Further experimentation was undertaken to test the time- or potential-dependence of this phenomenon by performing potential hold experiments using the potentiostat. Cyclic voltammograms with an anodic limit of –0.75 V were recorded; after the first scan has completed and returned to the –0.75 V anodic limit, the potential was held at this anodic limit for a time period equivalent to the time taken to scan to an anodic limit of –0.65 V and back to –0.75 V before continuing with the second scan. For example, at a scan rate of 50 mV s^{-1}, as shown in Fig. 3.45, the potential was held at –0.75 V for 4 seconds, the time required to scan 200 mV from –0.75 V to –0.65 V and then back to –0.75 V, before the second scan was collected. As seen in Fig. 3.45, the reductive peak is now present in the second scan of the voltammograms. This suggests that the reproducibility of the peak C2, for voltammograms with anodic limits < –0.7 V, may be a time-dependent phenomenon; when the voltammograms with anodic limits < –0.7 V are held at the anodic limit for a period of time the peak is present on the subsequent scan with good reproducibility of the peak observed for the initial scan. However, the size of the C2 peaks produced at anodic limits < –0.7 V are still observed to be smaller than the size of the peak produced at anodic limits > –0.65 V, suggesting this decrease in observed reductive current may be time-independent. Consequently a combination of

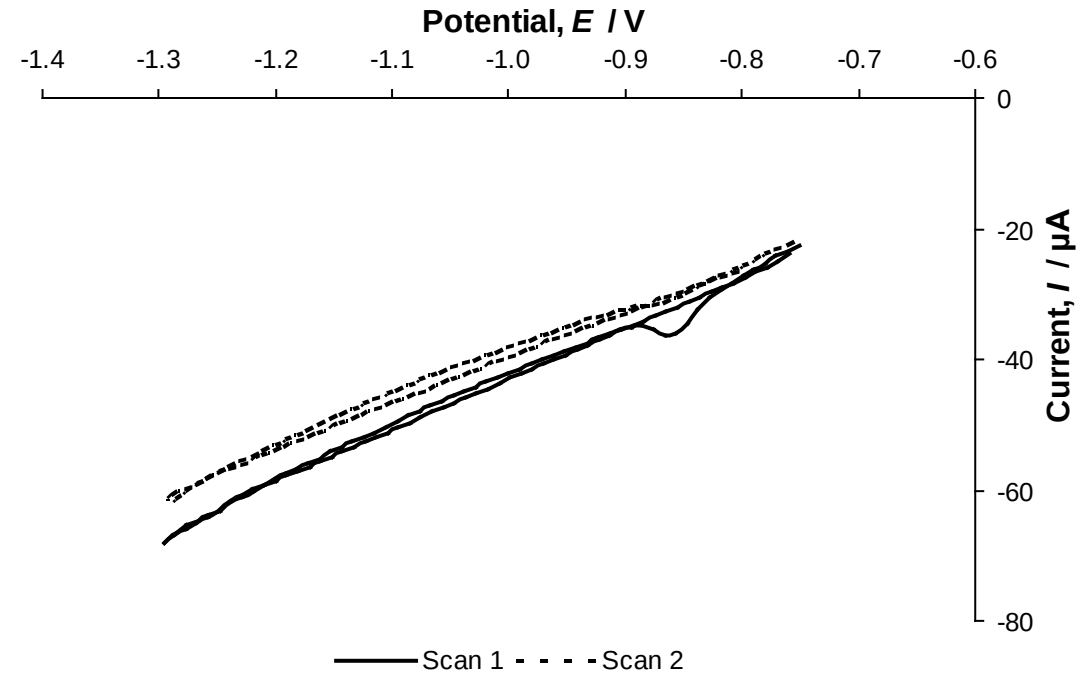

Fig. 3.44 Cyclic voltammograms of 2 subsequent scans for the same experiment in the potential range –0.75 to –1.3 V, with a Pb RDE in the presence of 10 mM ethanol, at 1000 rpm electrode rotation rate and 50 mV s^{-1} potential scan rate, showing removal of the C2 peak on the subsequent run.

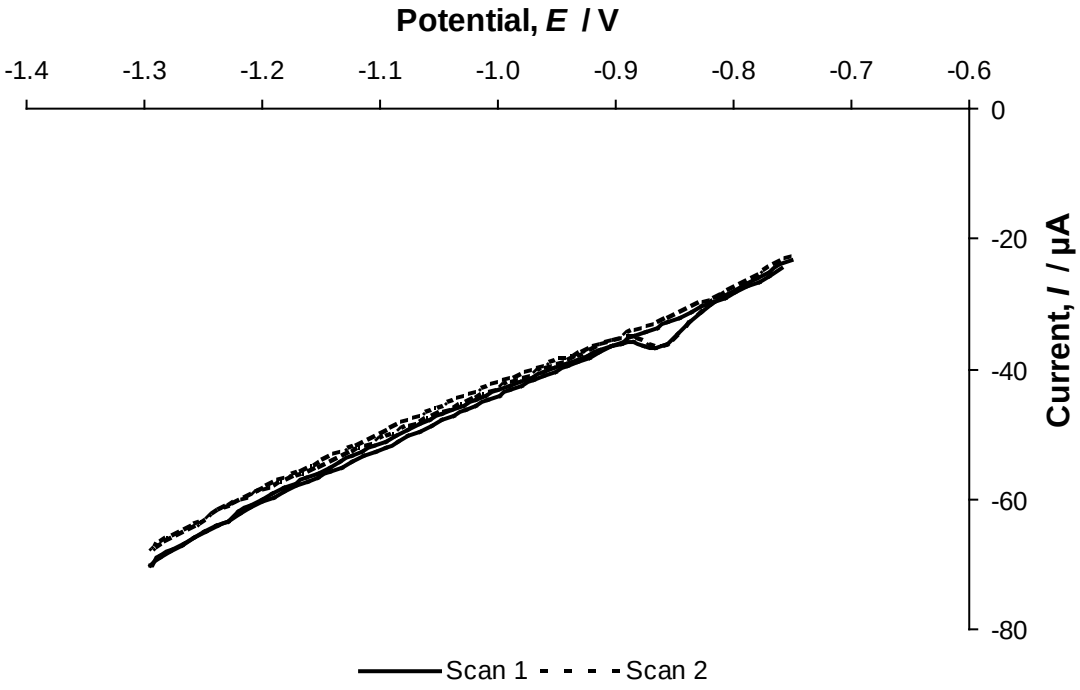

Fig. 3.45 Cyclic voltammograms of 2 subsequent scans for the same experiment in the potential range –0.75 to –1.3 V, holding the potential constant at the anodic limit for 4 seconds, with a Pb RDE in the presence of 10 mM ethanol, at 1000 rpm electrode rotation rate and 50 mV s^{-1} potential scan rate, showing the return of the C2 peak on the subsequent run.

time-dependent and potential-dependent behaviour may be responsible for these observations.

3.6.3 Data Analysis

The charge, *Q*, in coulombs, C, associated with the peak, C2, can be calculated by subtracting a background baseline from the curve with the reductive peak and integrating the resulting voltammetric curve with respect to time.

As with electrochemistry on tin electrodes, the addition of the ethanol to the electrolyte solution appears to alter the background baseline of the Pb electrode. The background curves for the Pb electrode in the pH 8.1 phosphate buffer electrolyte in absence of ethanol are not coincident with those in the presence of ethanol (Fig. 3.40). Thus the response in the absence of ethanol is not suitable as a baseline when ethanol is present and a more suitable baseline must be established to accurately determine the results. Baseline curves are generated using methods similar to the Sn experiments;

1) to scale the ethanol-free background arithmetically, or
2) to consider fitting a polynomial trendline immediately either side of the peak C2 of the cyclic voltammograms in the presence of alcohol providing an assumed baseline.

Figure 3.46 shows cyclic voltammograms collected at 1000 rpm and 50 mV s^{-1}, depicting the cyclic voltammogram of a 10 mM ethanol concentration with each of the three possible baseline cyclic voltammograms described,

(a) the collected background cyclic voltammogram,

(b) the scaled background multiplied by a factor of 1.3 at each potential, and

(c) the polynomial trendline calculated from the cyclic voltammograms in the presence of ethanol.

The polynomial trendline (c) was considered the best fit for the baseline of the experiments and was used in this work as the assumed baseline. This assumed baseline was subtracted from the ethanol curve and the charge of the peak, *Q*, was calculated. The data analysis then followed that described in section 3.5.3 for the tin electrode following eqns 3.9 – 3.12 to give q_{C2}, n_{C2}, and N_{C2}.

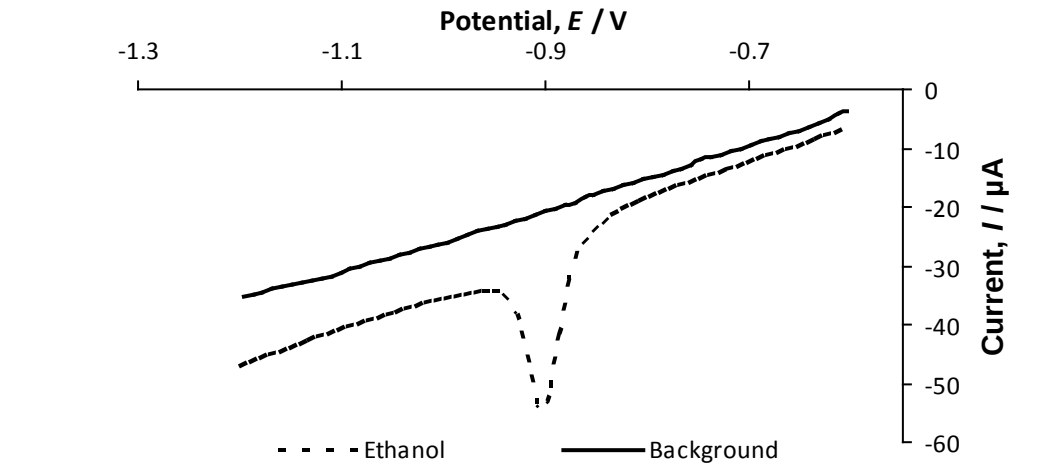

(a)

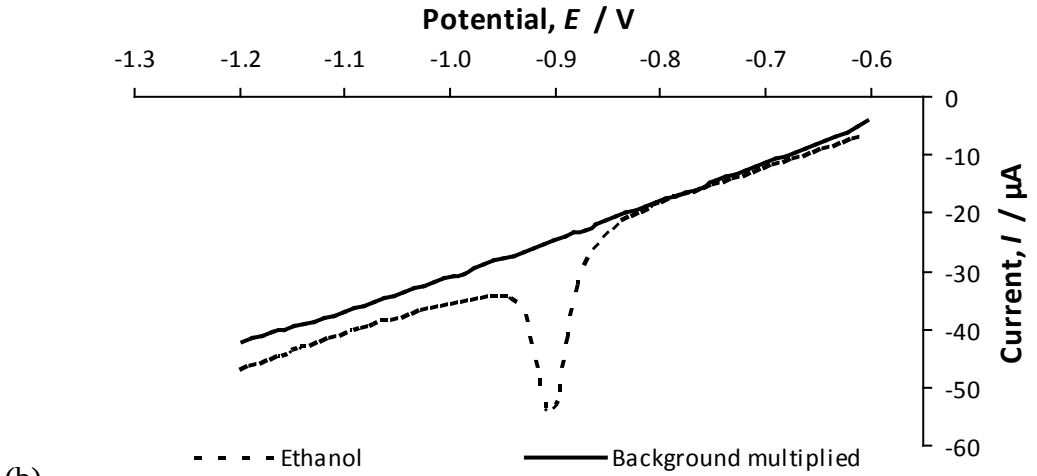

(b)

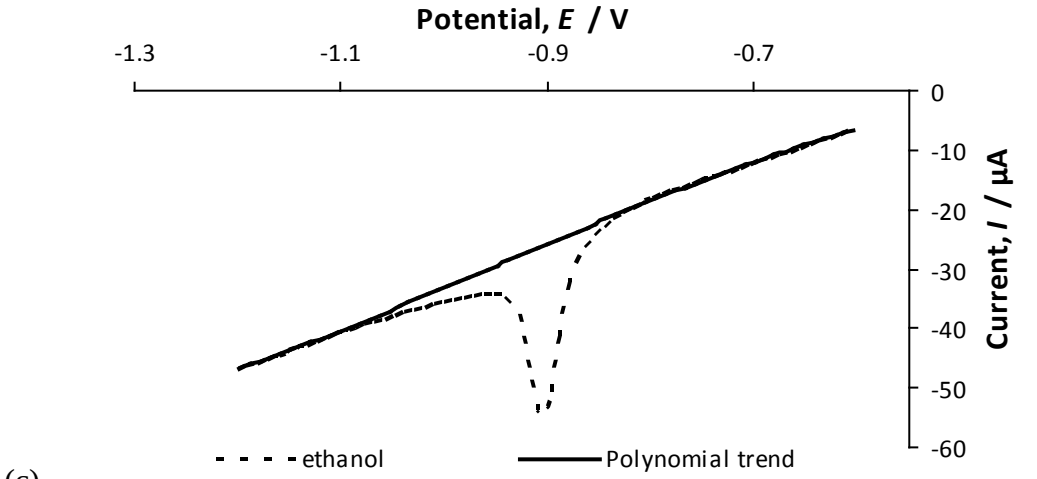

(c)

Fig. 3.46 Cathodic scans of cyclic voltammograms of (a) 7 mM ethanol and background, (b) 7 mM ethanol and background (multiplied by 1.2), and (c) 7 mM ethanol and baseline calculated from curve before and after ethanol peak, all collected at 1000 rpm electrode rotation rate and 50 mV s^{-1} potential scan rate.

3.6.4 Effect of Alcohol Concentration

As stated in Section 3.6, three of the five primary alcohols examined showed a reduction response on the lead disc electrode in the pH 8.1 aqueous phosphate buffer electrolyte solution. These three alcohols were ethanol, propanol and propan-2-ol.

The effect of the ethanol concentration was investigated by varying the bulk ethanol concentration, $[C_2H_5OH]_{bulk}$, in the electrolyte from 7 mM to 10, 15 and 20 mM. Figure 3.47 shows the cathodic sweeps of voltammograms of the four bulk ethanol concentrations in the potential range –0.60 to –1.30 V at 1000 rpm electrode rotation rate and 50 mV s^{-1} potential scan rate. The effect of the propanol and propan-2-ol concentrations was also investigated by varying the concentrations of propanol and propan-2-ol in the electrolyte from 7 mM to 10, 15 and 20 mM. Figures 3.48 and 3.49 show the cathodic sweeps of the voltammograms of the four bulk propanol and propan-2-ol concentrations respectively in the potential range –0.60 to –1.30 V at 1000 rpm electrode rotation rate and 50 mV s^{-1} potential scan rate.

The data analysis followed for the experiments was as outlined in Section 3.6.2. A polynomial trendline was fitted to the sections immediately either side of the peak C2 in the voltammograms in the presence of the alcohol. This assumed baseline was subtracted from the ethanol or propanol curves and the charge of the peak was calculated by integrating the resulting voltammetric curve. Corresponding amounts of product per m^2 and molecules m^{-2} were calculated following eqns. 3.7 – 3.10. The charges of the peak, C2, as calculated for the peaks at each bulk alcohol concentration, are recorded in Tables 3.24 (ethanol), 3.25 (propanol) and 3.26 (propan-2-ol) together with the resulting values for q_{C2}, n_{C2} and N_{C2} for each peak.

In all alcohol investigations the cyclic voltammograms are observed to have no significant differences and are within the spread of the voltammograms of any one of the concentrations observed over several identical experiments providing an uncertainty of ± 12 %. Peak C2 appeared to be reproducible in shape and size in all cyclic voltammograms for each of the alcohols, resulting in equivalent peak area for data analysis regardless of the bulk alcohol concentration. The values of N_{C2}; $(3.6 – 3.9) \times 10^{18}$ molecules m^{-2} for ethanol, $(3.9 – 4.3) \times 10^{18}$ molecules m^{-2} for propanol, and $(3.7 – 4.4) \times 10^{18}$ molecules m^{-2} for propan-2-ol, indicate that the four sets of data for each alcohol are effectively equivalent.

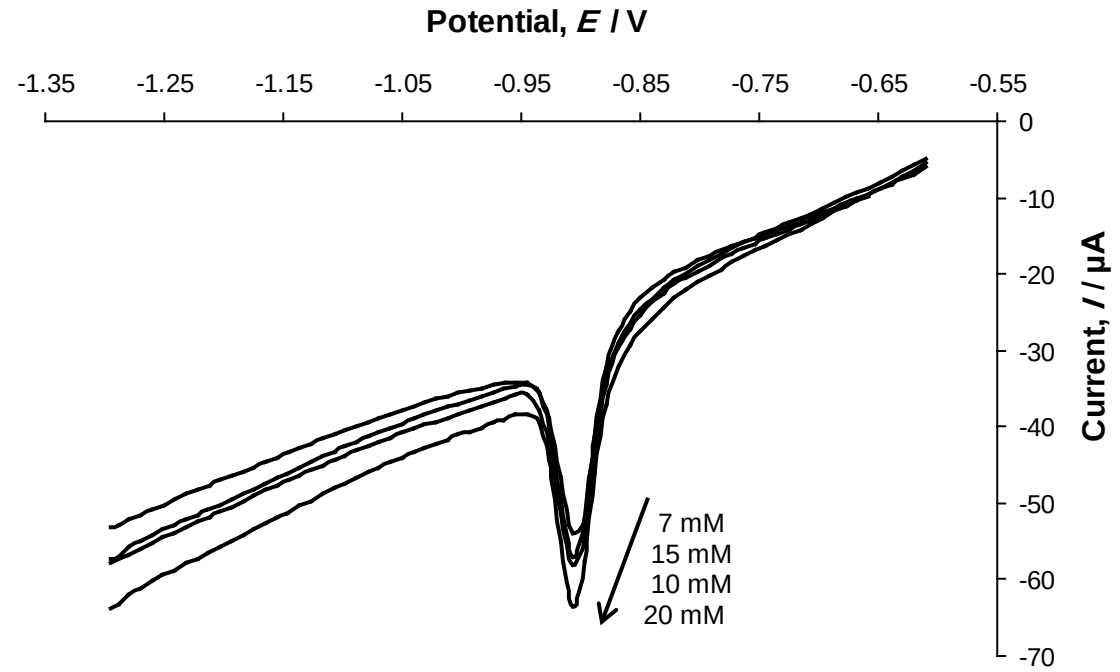

Fig. 3.47 Cathodic sweeps of cyclic voltammograms for the 4 bulk ethanol concentrations; 7, 10, 15 and 20 mM, showing the similarity of the C2 peak for all concentrations studied, with a Pb RDE collected at 1000 rpm electrode rotation rate and 50 mV s^{-1} potential scan rate.

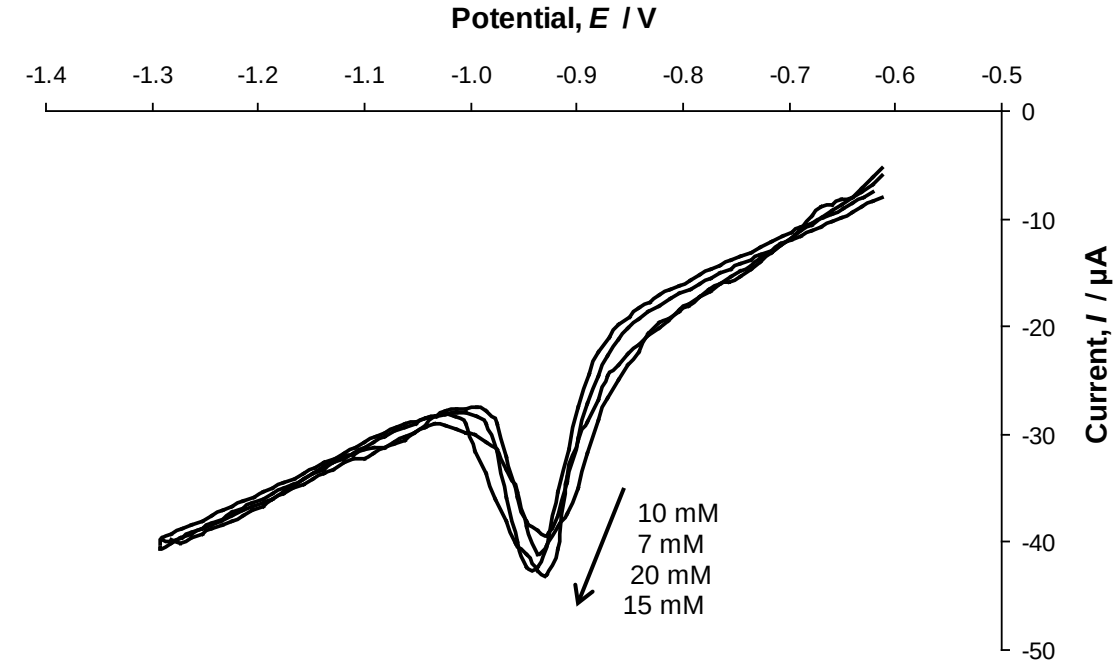

Fig. 3.48 Cathodic scans of cyclic voltammograms at four bulk propanol concentrations; 7, 10, 15 and 20 mM, showing the similarity of the C2 peak for all concentrations studied, with a Pb RDE collected at 1000 rpm electrode rotation rate and 50 mV s^{-1} potential scan rate.

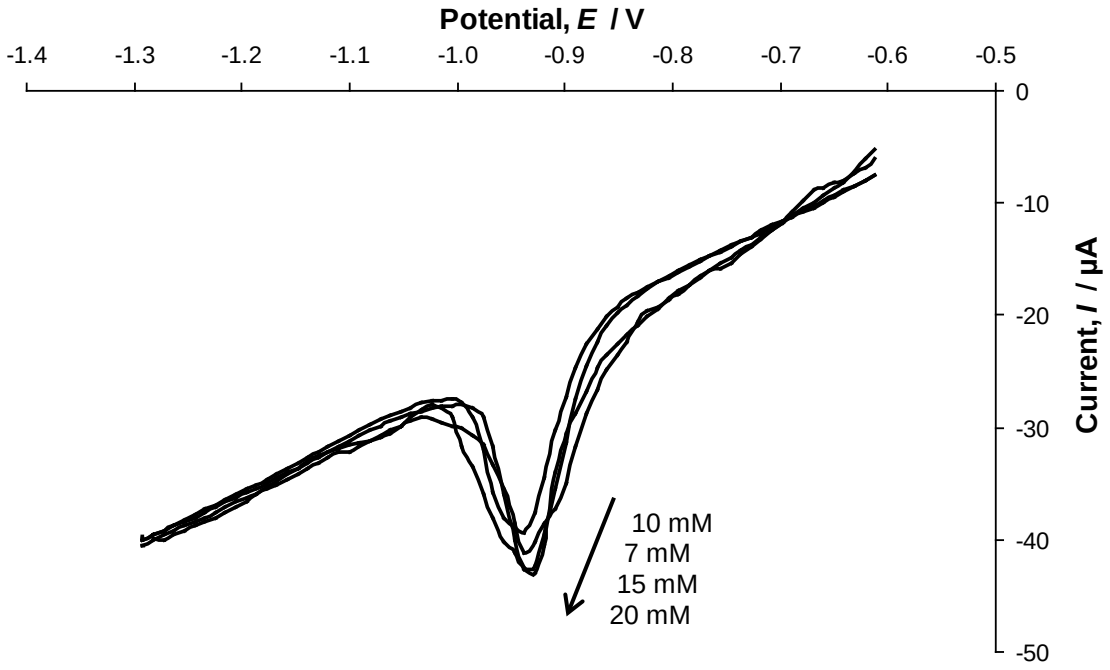

Fig. 3.49 Cathodic scans of cyclic voltammograms at four bulk propan-2-ol concentrations, showing the similarity of the C2 peak for all concentrations studied, with a Pb RDE collected at 1000 rpm electrode rotation rate and 50 mV s^{-1} potential scan rate.

Table 3.24 Analysis for the effect of varying bulk ethanol concentration with the Pb RDE. Listing the charge, Q, from the reduction peak, charge per area, q_{C2}, moles of material, n_{C2}, molecules per area, N_{C2}, and area per molecule, A_N as a function of bulk ethanol concentration.

	Bulk Ethanol Concentration / mM			
	7	10	15	20
Charge of Peak Q / μC	26.9	26.6	25.8	24.4
Charge per area q_{C2} / C m^{-2}	1.37	1.36	1.31	1.36
moles per area n_{C2} / 10^{-6} mol m^{-2}	7.10	7.02	6.82	7.06
molecules per area N_{C2} / 10^{18} m^{-2}	4.30	4.23	4.10	4.24
area per molecule A_N / nm^2	2.34	2.36	2.44	2.35

Table 3.25 Analysis for the effect of varying bulk propanol concentration with the Pb RDE. Listing the charge, Q, from the reduction peak, charge per area, q_{C2}, moles of material, n_{C2}, molecules per area, N_{C2}, and area per molecule, A_N as a function of bulk propanol concentration

	Bulk Propanol Concentration / mM			
	7	10	15	20
Charge of Peak Q / μC	24.7	26.4	25.0	27.1
Charge per area q_{C2} / C m^{-2}	1.26	1.34	1.27	1.38
Moles per area n_{C2} / 10^{-6} mol m^{-2}	6.52	6.97	6.60	7.15
molecules per area N_{C2} / 10^{18} m^{-2}	3.93	4.20	3.97	4.31
Area per molecule A_N / nm^2	2.54	2.38	2.51	2.32

Table 3.26 Analysis for the effect of varying bulk propan-2-ol concentration with the Pb RDE. Listing the charge, Q, from the reduction peak, charge per area, q_{C2}, moles of material, n_{C2}, molecules per area, N_{C2}, and area per molecule, A_N, as a function of bulk propan-2-ol concentration.

	Bulk Propan-2-ol Concentration / mM			
	7	10	15	20
Charge of Peak Q / μC	23.3	25.2	27.3	27.4
Charge per area q_{C2} / C m^{-2}	1.19	1.28	1.39	139
Moles per area n_{C2} / 10^{-6} mol m^{-2}	6.15	6.64	7.2	7.22
molecules per area N_{C2} / 10^{18} m^{-2}	3.70	4.00	4.34	4.35
Area per molecule A_N / nm^2	2.70	2.50	2.30	2.30

This suggests that the increase in alcohol concentration does not substantially alter the amount of reduction occurring. An increase in concentration would provide more reactant available for reduction and an increase in reductive response would be expected. In this case, as with the tin investigation, it is observed that there is no increase in reduction, reduction appears to be inhibited. This may suggest an insoluble insulating layer is forming on the surface of the electrode and preventing more reduction from taking place.

There is a very small difference between the ethanol and propanol values of N_{C2}. Unlike the Sn the results of the Pb disc show a slightly larger N_{C2} value for the propanol, perhaps indicative of the propanol being slightly easier to reduce.

The concentration independence suggests a possible insulating layer may be forming on the lead electrode. The thickness of this proposed layer is considered in the next section.

3.6.4.1 Insulating Layer Thickness

The thickness of the insulating layer thought to be forming on the surface of the Pb electrode was considered as in the Sn investigation. The calculations described earlier in section 3.5.3 gave values for the moles of product per area, n_{C2}, and these values can be used to calculate the possible thickness of the insulating layer using eqns. 3.13 – 3.16.

Using the molar mass of ethane, M = 30.07 g mol^{-1}, along with the assumed density of ethane, ρ = 0.65 g ml^{-1}, (explained in Section 3.5.5.1 with the tin electrodes), these calculations provide values for the thickness of the layer of approximately 0.78 nm, consistent with only a very thin layer forming before the reduction can no longer continue.

Similar calculations were carried out for the propanol and propan-2-ol investigations. As with the Sn experiments, assuming the product is propane, using the molar mass and assumed density of propane as 44.1 g mol^{-1} and 0.65 g L^{-1} (density of hexane at 25°C) respectively, values for the thickness of the layer on the surface of the electrode were calculated. The values were found to be approximately 0.80 nm, indicative of a very thin layer formed before reduction is stifled. As with the tin electrode investigation, this is not inconsistent with the possibility of a monolayer forming on the surface of the electrode.

3.6.5 Effect of Potential Scan Rate

Figure 3.50 shows the cathodic sweeps of voltammograms (anodic sweeps are not shown for clarity) at the 5 potential scan rates; 10, 20, 50, 100, and 200 mV s^{-1}, for the 10 mM ethanol response with Pb electrode in phosphate buffer pH 8.1 at 1000 rpm electrode rotation rate. It is evident in these voltammograms that the peak size (in terms of current) increases with increasing scan rate. Figure 3.51 and 3.52 show the cathodic sweeps of the cyclic voltammograms at the potential scan rates 10, 20, 50, 100 and 200 mV s^{-1}, for the 10 mM bulk propanol and propan-2-ol concentrations respectively. In these voltammograms the peak current also increases with the increasing scan rate with the voltammograms for the propanol exhibiting very similar peak currents, size and shape as the propan-2-ol.

The increase in size of the peak could be indicative of a constant amount of product being formed due to the time scale associated with the scan rates. As the scan rate is the rate at which the cyclic voltammogram is swept through the potential range the potential axis can also be represented as a time axis having an effect on the analysis of the data.

The charge of the peak was calculated for each scan rate depicted in Figs. 3.50 - 3.52 using the background subtraction method based on the polynomial trendline described previously in Section 3.6.2. The resulting values for q_{C2}, n_{C2} and N_{C2} for each alcohol are listed in Tables 3.27 (ethanol), 3.28 (propanol), and 3.29 (propan-2-ol).

For all 3 alcohols the data exhibit a trend of decreasing charge with increasing potential scan rate leading to a decrease in N_{C2} with increasing potential scan rate. This indicates that there is a formation of a smaller amount of reaction product with increasing scan rate in each alcohol case. A similar amount of material is reduced for the propanol and propan-2-ol systems. A slower scan rate allows a longer period of time at each potential permitting more reduction to take place over this extended time.

To consider the scan rate-independent nature of the reduction peak, experiments varying the scan rate at the four bulk ethanol concentrations previously examined were completed. Table 3.30 shows the values for N_{C2} calculated for each of the four concentrations at each scan rate. The values of N_{C2} recorded in Table 3.30, reported at 10 mM bulk ethanol concentration, suggest a scan rate-dependent nature of the peak.

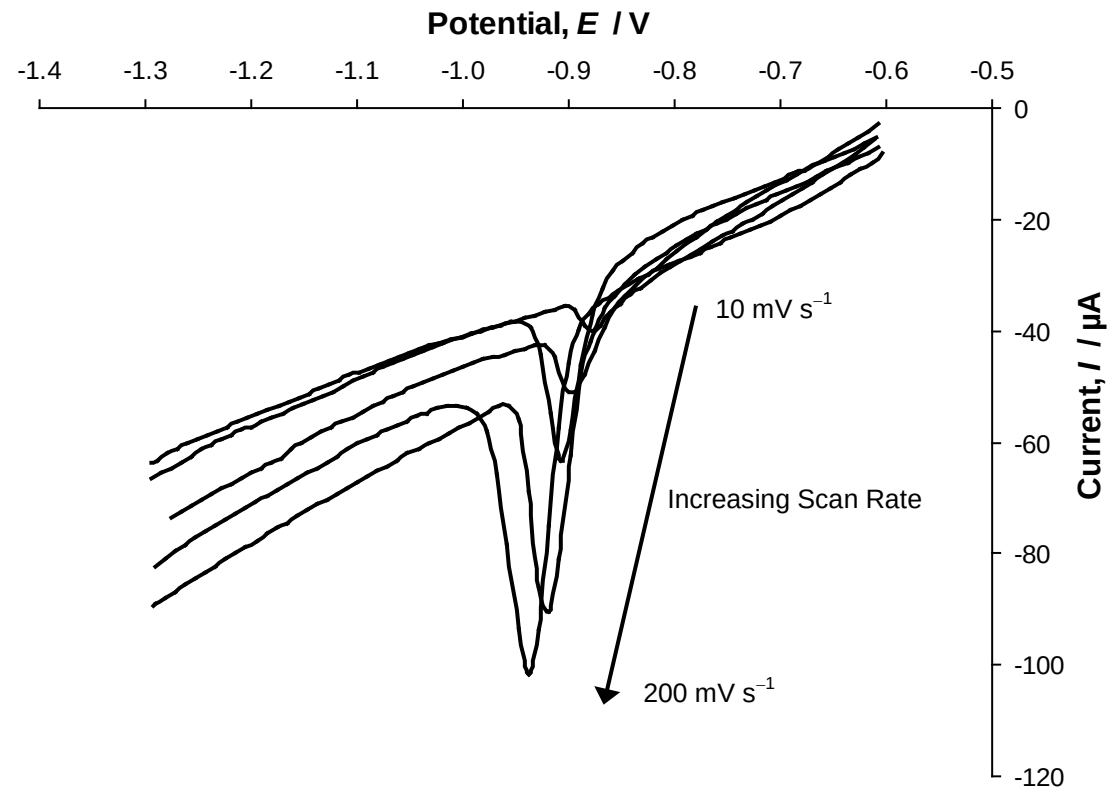

Fig. 3.50 Cathodic scans of cyclic voltammograms on the Pb RDE at varying potential scan rates; 10 – 200 mV s^{-1}, showing the increase of the size of the C2 peak with increasing scan rate, in the presence of 10 mM bulk ethanol concentration, at 1000 rpm electrode rotation rate.

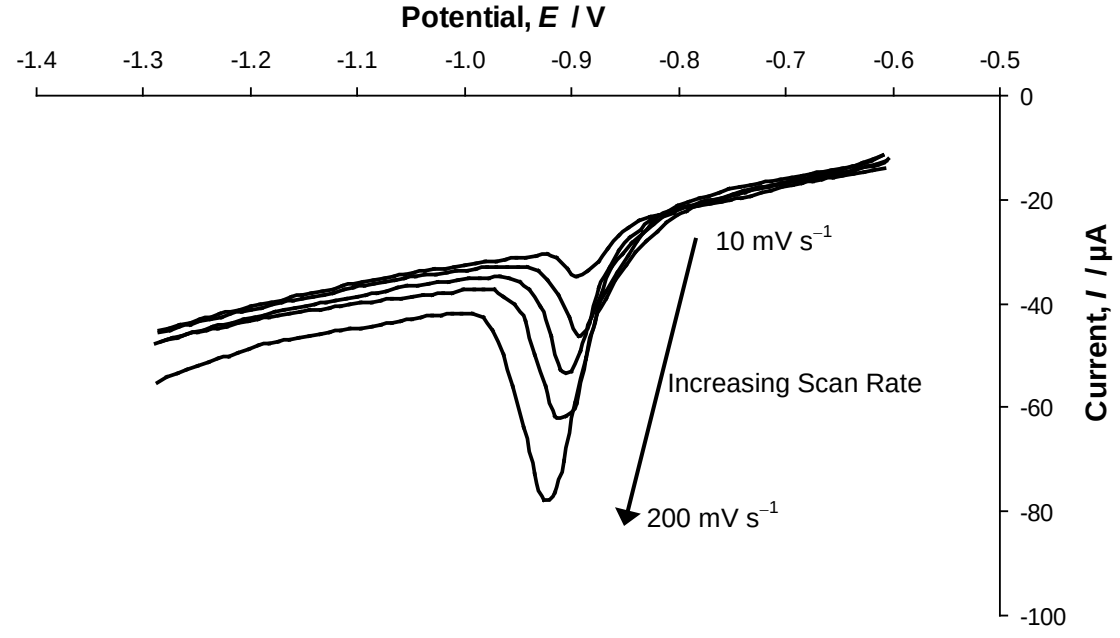

Fig. 3.51 Cathodic scans of cyclic voltammograms on the Pb RDE at varying potential scan rates; 10 – 200 mV s^{-1}, showing the increase of the size of the C2 peak with increasing scan rate, in the presence of 10 mM bulk propanol concentrations, at 1000 rpm electrode rotation rate.

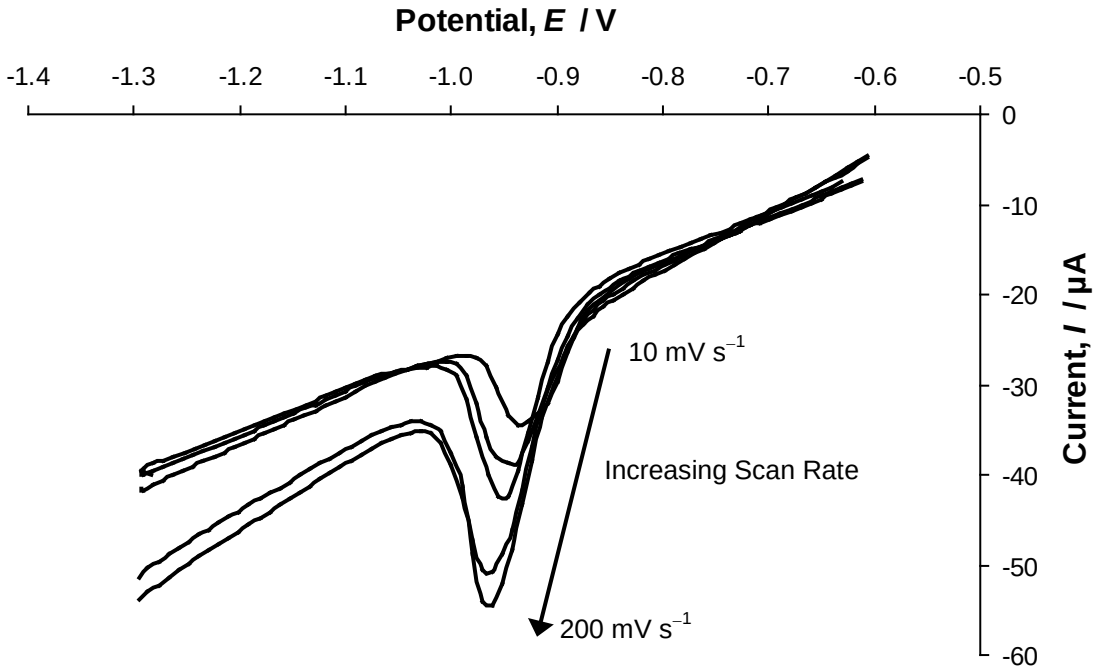

Fig. 3.52 Cathodic scans of cyclic voltammograms on the Pb RDE at varying potential scan rates; 10 – 200 mV s^{-1}, showing the increase of the size of the C2 peak with increasing scan rate, in the presence of 10 mM bulk propan-2-ol concentrations, at 1000 rpm electrode rotation rate.

Table 3.27 Analysis for the effect of potential scan rate of voltammograms for the Pb RDE in the presence of 10 mM ethanol. Listing the change, Q, from the reduction peak, charge per area, q, moles of material, n_{C2}, molecules per area, N_{C2}, and area per molecule, A_N, as a function of potential scan rate.

	Potential scan rate / mV s^{-1}				
	10	20	50	100	200
Charge of Peak Q / μC	33.5	29.9	26.6	15.8	10.9
Charge per area q_{C2}/ C m^{-2}	1.71	1.52	1.36	0.81	0.56
Moles per area n_{C2} / 10^{-6} mol m^{-2}	8.86	7.90	7.02	4.18	2.88
Molecules per area N_{C2} / 10^{18} m^{-2}	5.33	4.76	4.23	2.52	1.73
area per molecule A_N / nm^2	1.94	2.10	2.36	3.97	5.78

Table 3.28 Analysis for the effect of potential scan rate of voltammograms for the Pb RDE in the presence of 10 mM propanol. Listing the charge, Q, from the reduction peak, charge per area, q, moles of material, n_{C2}, molecules per area, N_{C2}, and area per molecule, A_N, as a function of potential scan rate.

	Potential scan rate / mV s^{-1}				
	10	20	50	100	200
Charge of Peak Q / μC	78.1	33.3	26.4	15.3	9.46
Charge per area q_{C2}/ C m^{-2}	3.98	1.70	1.34	0.78	0.48
Moles per area n_{C2} / 10^{-6} mol m^{-2}	20.6	8.79	6.97	4.03	2.50
Molecules per area N_{C2} / 10^{18} m^{-2}	12.4	5.29	4.20	2.43	1.50
area per molecule A_N / nm^2	0.81	1.89	2.38	4.12	6.66

Table 3.29 Analysis for the effect of potential scan rate of voltammograms for the Pb RDE in the presence of 10 mM propan-2-ol. Listing the charge, Q, from the reduction peak, charge per area, q, moles of material, n_{C2}, molecules per area, N_{C2}, and area per molecule, A_N, as a function of potential scan rate.

	Potential scan rate / mV s^{-1}				
	10	20	50	100	200
Charge of Peak Q / μC	77.1	35.8	25.2	15.5	9.4
Charge per area q_{C2}/ C m^{-2}	3.93	1.82	1.28	7.89	4.80
Moles per area n_{C2} / 10^{-6} mol m^{-2}	20.4	9.45	6.64	4.09	2.49
Molecules per area N_{C2} / 10^{18} m^{-2}	12.3	5.69	4.00	2.45	1.50
area per molecule A_N / nm^2	0.81	1.76	2.50	4.08	6.67

The scan rate-dependence in the presence of propanol and propan-2-ol was also considered and Tables 3.31 and 3.32 list the values for N_{C2} calculated for each of the four bulk propanol and propan-2-ol concentrations at each scan rate. The values recorded in Tables 3.30 and 3.31 reported for the 10 mM bulk alcohol concentrations, again supporting a proposed scan rate-dependent nature of the peak.

The observations here show that regardless of the bulk alcohol concentration the same amount of material appears to be reducing at the electrode at each scan rate, however, as the scan rate is increased less reduction is able to occur. Therefore, a larger amount of reduction is likely to occur at a slower potential scan rate at any bulk alcohol concentration examined. However, the lowest potential scan rate, 10 mV s^{-1}, showed a wider spread of results than other potential scan rates, with values of N_{C2} in the ranges of (5.02 – 5.32) × 10^{18} molecules m^{-2} for ethanol, (0.73 – 1.24) × 10^{18} molecules m^{-2} for propanol and propan-2-ol.

Table 3.30 Average molecules per area, N_{C2}, at each bulk ethanol concentration, 7, 10, 15, 20 mM as a function of potential scan rate.

Molecules per area, N_{C2} / 10^{18} m^{-2}					
	Potential scan rate / mV s^{-1}				
Ethanol Concentration / mM	10	20	50	100	200
7	5.15	4.72	4.30	2.73	1.65
10	5.33	4.76	4.23	2.52	1.73
15	5.02	4.77	4.10	2.59	1.69
20	5.43	4.68	4.24	2.48	1.81

Table 3.31 Average molecules per area, N_{C2}, at each bulk propanol concentration, 7, 10, 15, 20 mM as a function of potential scan rate.

Molecules per area, N_{C2} / 10^{18} m^{-2}					
	Potential scan rate / mV s^{-1}				
	10	20	50	100	200
Propanol Concentration / mM					
7	7.36	6.52	3.93	2.06	1.68
10	12.40	5.29	4.00	0.243	1.50
15	8.92	6.34	3.97	2.40	1.77
20	7.84	6.92	4.31	6.83	1.19

Table 3.32 Average molecules per area, N_{C2}, at each bulk propan-2-ol concentration, 7, 10, 15, 20 mM as a function of potential scan rate.

Molecules per area, N_{C2} / 10^{18} m^{-2}					
	Potential scan rate / mV s^{-1}				
	10	20	50	100	200
Propan-2-ol Concentration / mM					
7	7.36	6.52	3.70	2.26	1.61
10	1.23	0.569	0.420	2.46	1.50
15	0.692	0.734	0.397	2.04	1.37
20	0.784	0.692	0.431	233	1.90

3.6.6 Effect of Electrode Rotation Rate

Figure 3.53 shows cathodic scans of the cyclic voltammograms for the different rotation rates: 500, 675, 750, 1000, 1250, 1500 and 2000 rpm all at 50 mV s^{-1} potential scan rate, and in pH 8.1 phosphate buffer in the presence of 10 mM bulk ethanol concentration. The returning anodic scan segments, devoid of further reduction or oxidation peaks, are not shown for clarity. The peak areas for C2 were calculated using previously described methods and the values for Q, q_{C2}, n_{C2} and N_{C2} are recorded in Table 3.33. Figures 3.54 and 3.55 show the cathodic scans of the cyclic voltammograms for the range of rotation rates; 500, 675, 750, 1000, 1250, 1500 and 2000 rpm all at 50 mV s^{-1} potential scan rate, in the presence of 10 mM bulk propanol and propan-2-ol concentrations respectively in the pH 8.1 phosphate buffer. Table 3.34 and 3.35 lists the values for Q, q_{C2}, n_{C2} and N_{C2} for these propanol and propan-2-ol experiments.

As the rotation rate is increased through 500 to 2000 rpm the apparent product loading on the surface of the electrode decreases from approximately 7.04×10^{18} molecules m^{-2} for ethanol at 500 rpm to 4.16×10^{18} molecules m^{-2} at 2000 rpm. This effective decrease is observed for propanol and propan-2-ol also from approximately 4.3×10^{18} at 500 rpm to approximately 2.7×10^{18} at 200 rpm. Evidently, there is a progressive decrease in the peak size observed as the rotation rate is increased.

This decrease of peak size implies that the amount of alcohol required to form a passivating layer on the electrode decreases with increasing rotation rate. This is counter to what would typically be expected as increasing the rotation rate should promote the loss of any insulating materials away from the electrode as they form, particularly given the time-dependent nature discussed earlier. Here, increasing the rotation rate appears to act to complete a passivating layer.

The effect of electrode rotation rate was tested with varying bulk alcohol concentrations to determine if this phenomenon was consistent regardless of concentration. Tables 3.36, 3.37 and 3.38 list the values of N_{C2} for the ethanol, propanol and propan-2-ol investigations respectively. These data show that this interesting rotation-rate dependence phenomenon is maintained at all concentrations examined.

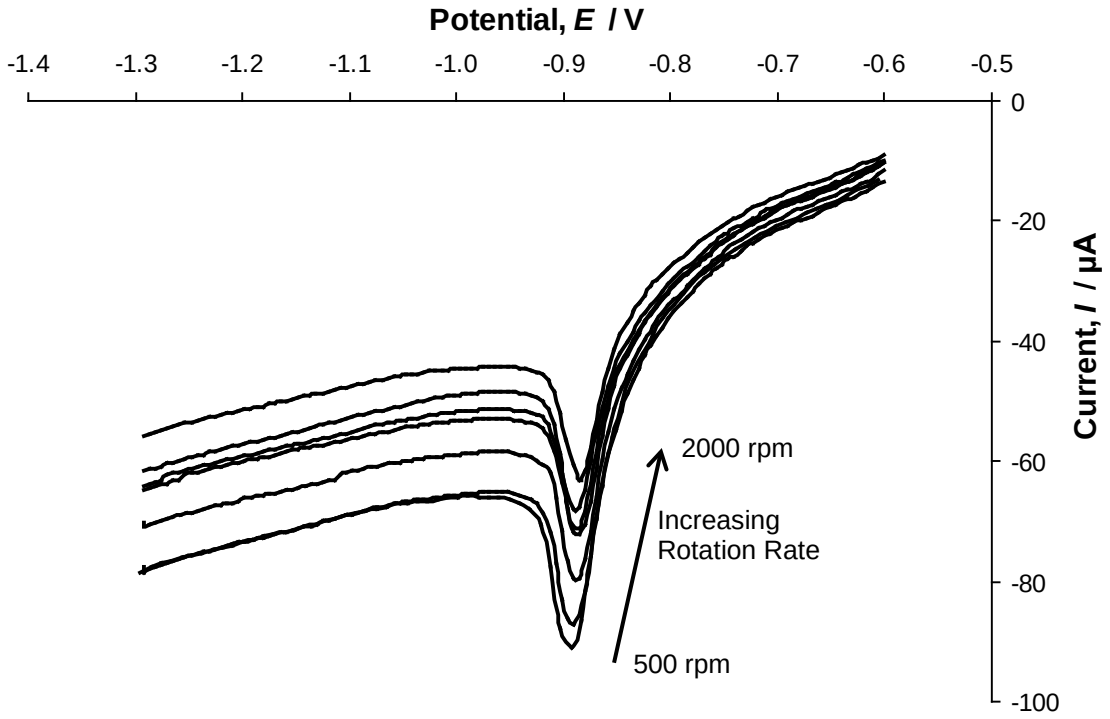

Fig. 3.53 Cathodic sweeps of cyclic voltammograms at varying electrode rotation rates; 500 – 2000 rpm, of the Pb RDE, showing the decrease of the size of the C2 peak with increasing rotation rate, in the presence of 10 mM bulk ethanol concentration, at 50 mV s^{-1} potential scan rate.

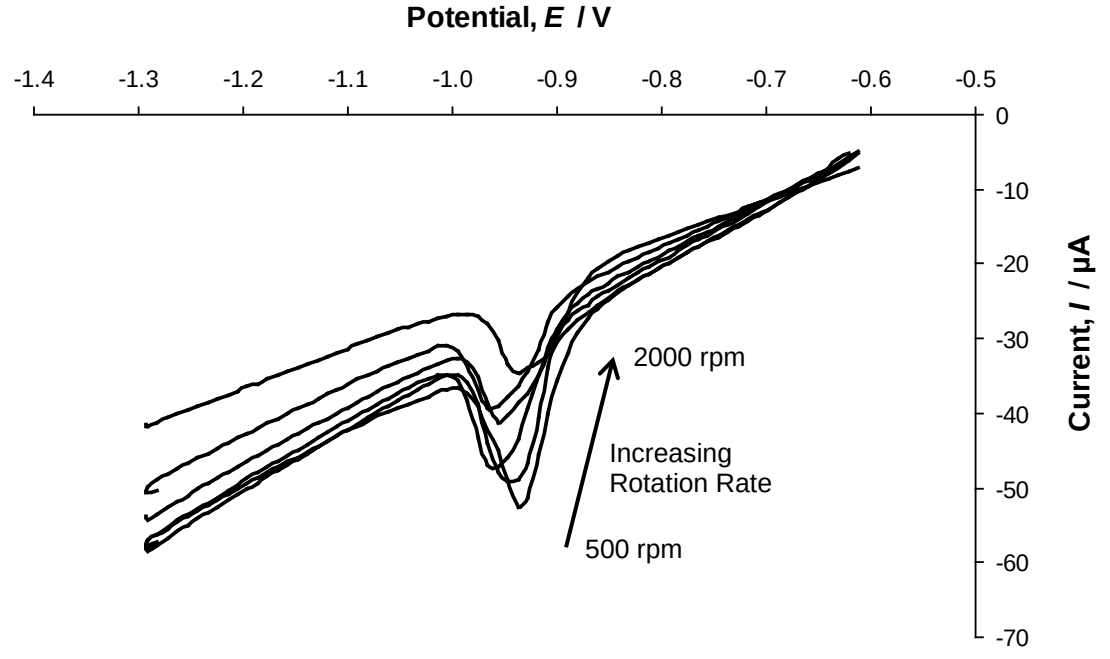

Fig. 3.54 Cathodic scans of cyclic voltammograms at varying electrode rotation rates; 500 – 2000 rpm, of the Pb RDE, showing the decrease of the size of the C2 peak with increasing rotation rate, in the presence of 10 mM bulk propanol concentration, at 50 mV s^{-1} potential scan rate.

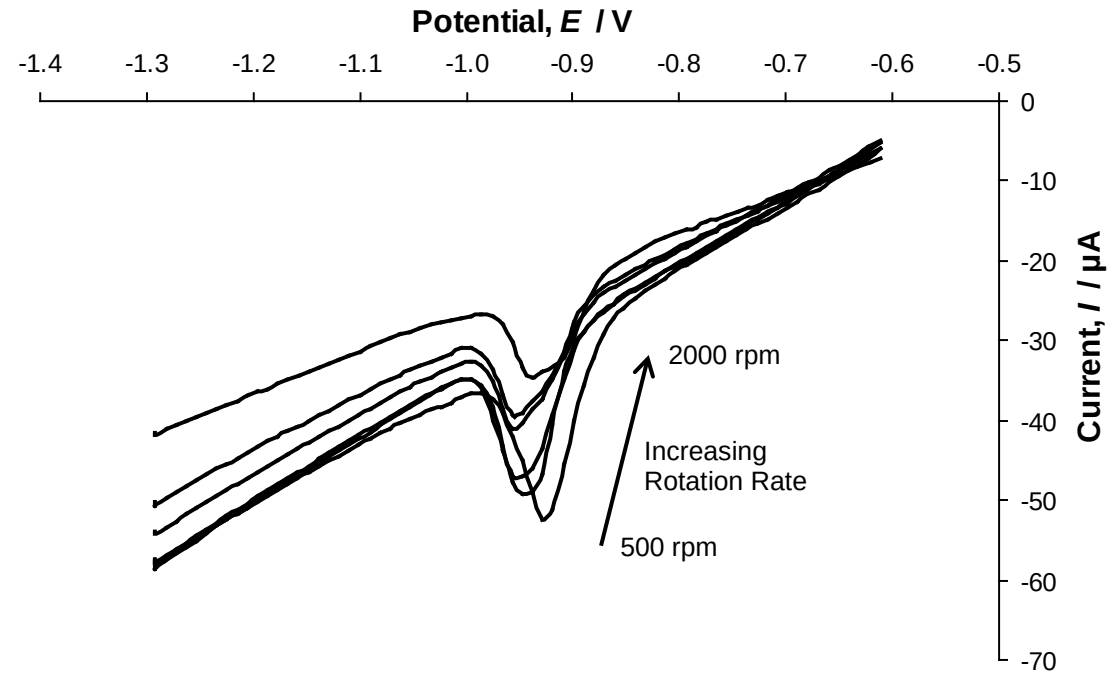

Fig. 3.55 Cathodic scans of cyclic voltammograms at varying electrode rotation rates; 500 – 2000 rpm, of the Pb RDE, showing the decrease of the size of the C2 peak with increasing rotation rate, in the presence of 10 mM bulk propan-2-ol concentration, at 50 mV s^{-1} potential scan rate.

Table 3.33 Analysis for the effect of varying the electrode rotation rate of the Pb RDE in the presence of 10 mM bulk ethanol concentration. Listing the charge, Q, from the reduction peak, charge per area, q_{C2}, moles of material, n_{C2}, molecules per area, N_{C2}, and area per molecule, A_N, as a function of electrode rotation rate.

	Electrode rotation rate / rpm						
	500	675	750	1000	1200	1500	2000
Charge of Peak Q / μC	44.3	38.4	31.5	26.6	28.3	26.7	26.2
Charge per area q_{C2} / C m^{-2}	2.26	1.95	1.61	1.36	1.44	1.37	1.33
moles per area n_{C2} / 10^{-6} mol m^{-2}	11.71	10.12	8.32	7.02	7.46	7.03	6.91
Molecules per area N_{C2} / 10^{18} m^{-2}	7.05	6.10	5.01	4.23	4.49	4.25	4.16
Area per molecule A_N / nm^2	1.42	1.64	2.00	2.36	2.23	2.34	2.40

Table 3.34 Analysis for the effect of varying the electrode rotation rate of the Pb RDE in the presence of 10 mM bulk propanol concentration. Listing the charge, Q, from the reduction peak, charge per area, q_{C2}, moles of material, n_{C2}, molecules per area, N_{C2}, and area per molecule, A_N, as a function of electrode rotation rate.

	Electrode rotation rate / rpm						
	500	675	750	1000	1200	1500	2000
Charge of Peak Q / μC	27.4	27.5	26.8	26.4	22.2	20.1	17.2
Charge per area q_{C2} / C m^{-2}	1.40	1.40	1.36	1.34	1.13	1.02	8.76
moles per area n_{C2} / 10^{-5} mol m^{-2}	7.23	7.26	7.07	6.97	5.86	5.30	4.54
Molecules per area N_{C2} / 10^{18} m^{-2}	4.35	4.37	4.26	4.20	3.53	3.19	2.73
area per molecule A_N / nm^2	2.30	2.29	2.35	2.38	2.83	3.13	3.66

Table 3.35 Analysis for the effect of varying electrode rotation rate of the Pb RDE with 10 mM bulk propan-2-ol concentration. Listing the charge, Q, from the reduction peak, charge per area, q_{C2}, moles of material, n_{C2}, molecules per area, N_{C2}, and area per molecule, A_N, as a function of electrode rotation rate.

	Electrode rotation rate / rpm						
	500	675	750	1000	1200	1500	2000
Charge of Peak Q / μC	27.6	26.9	27.3	25.2	22.0	19.2	16.7
Charge per area q_{C2} / C m^{-2}	1.39	1.37	1.39	1.28	1.12	0.982	8.49
moles per area n_{C2} / 10^{-6} mol m^{-2}	7.22	7.10	7.22	6.64	5.82	5.08	4.40
Molecules per area N_{C2} / 10^{18} m^{-2}	4.39	4.28	4.34	4.00	3.50	3.06	2.65
area per molecule A_N / nm^2	2.28	2.34	2.30	2.50	2.86	3.27	3.77

Table 3.36 Average molecules per area, N_{C2}, for each bulk ethanol concentration, 7, 10, 15, 20 mM, as a function of electrode rotation rate.

Molecules per area, N_{C2} / 10^{18} m^{-2}							
	Electrode rotation rate / rpm						
Ethanol Concentration / mM	500	675	750	1000	1200	1500	2000
7	7.12	6.01	5.03	4.30	4.44	4.18	4.07
10	7.04	6.10	5.01	4.23	4.49	4.25	4.16
15	7.01	6.06	4.92	4.10	4.42	4.19	4.12
20	7.25	6.17	5.09	4.24	4.36	4.27	4.19

Table 3.37 Average molecules per area, N_{C2}, for each bulk propanol concentration; 7, 10, 15 and 20 mM, as a function of electrode rotation rate.

Molecules per area, N_{C2} / 10^{18} m^{-2}							
	Electrode rotation rate / rpm						
Propanol Concentration / mM	500	675	750	1000	1200	1500	2000
7	4.38	4.31	4.24	3.93	3.45	2.90	2.78
10	4.35	4.37	4.26	4.20	3.53	3.19	2.73
15	4.42	4.35	4.33	3.97	3.42	3.01	2.69
20	4.32	4.27	4.28	4.31	3.35	3.10	2.72

Table 3.38 Average molecules per area, N_{C2}, for each bulk propan-2-ol concentration, 7, 10, 15 and 20 mM, as a function of rotation rate.

Molecules per area, N_{C2} / 10^{18} m^{-2}							
	Rotation rate / rpm						
Propan-2-ol Concentration / mM	500	675	750	1000	1200	1500	2000
7	4.43	4.37	4.26	3.70	3.45	2.92	2.73
10	4.39	4.28	4.34	4.00	3.50	3.06	2.65
15	4.47	4.31	4.33	4.34	3.42	2.99	2.69
20	4.32	4.35	4.28	4.35	3.35	3.10	2.73

The number of active binding sites available on an electrode is typically in the range $1.3 \pm 0.5 \times 10^{19}$ sites m^{-2}.[52] The number of molecules per area produced for the Pb-ethanol system reported in this work is approximately 4×10^{18} molecules m^{-2} (1000 rpm and 50 mV s^{-1}). This value is considerably less than the proposed available binding sites on the electrode surface indicating not all of these binding sites are required to be occupied for the electrode to be sufficiently covered inhibiting any continuing reduction. Assuming that each molecule occupies only one binding site on the electrode, binding sites on the Pb disc occupied in these experiments may be relatively isolated to be sufficiently spaced in order to cover the electrode surface and inhibit further reduction. Each molecule must effectively shield some of the electrode surface between the activated binding sites. A molecule at a single binding site on the electrode potentially occupies an area of the surface of the electrode of > 22 $Å^2$, this area is larger than the molecule itself supporting the suggestion of isolated binding sites.

There exists the possibility that while the electrode rotation facilitated removal of insulating products has been ruled out, the facilitated replenishment of ethanol (or propanol) may promote a second non-electrochemical process that is responsible for promotion of the insulating layer. One mechanism that could explain the behaviour is given by:

Step 1 $\quad ROH + 2H^+ + 2e^- \rightarrow intermediate_{(ads)}$ (3.17)

Step 2 $\quad Intermediate_{(ads)} + ROH \rightarrow insulating\ product_{(ads)}$ (3.18)

The alcohol approaching the electrode surface may react with the adsorbed intermediate before it reaches the electrode surface and is available to react electrochemically.

The hypothesis was that increasing the rotation rate of the electrode would not alter the rate of Step 1 (consistent with the forward slope of C2 being alcohol concentration-independent, Figs. 3.47 - 3.49), but that ensuring replenishment of ethanol (or propanol) at the electrode surface will promote Step 2, a non-electrochemical step.

This extremely interesting anomalous rotation rate phenomenon observed in the presence of these alcohols will be discussed and explained with product determination in Chapter 4. Elucidation of the causes of this phenomenon may yield insight into the mechanism operating in the overall reaction.

3.6.7 Lead Electrode Process Possible Products

Due to the suggestion of a two step process occurring a simple reduction to the alkane (ethane or propane) may be unlikely. The possibility of the formation of a longer chain alkane or an ether product was also considered. The possibility of the alcohol being required to adsorb to the surface of the electrode for reduction to occur could determine a two step process with an adsorbed intermediate leading to either of these possible products. The scan rate dependence and the rotation rate anomaly are also consistent with there being a two step process. Adsorption to the electrode could be through a carbon, most likely the carbon adjacent to the oxygen due to electronegativity, or through the lone pairs of electrons on the oxygen.

Possible products for the ethanol process; could be butane, butene, and diethyl ether. For the propanol process; hexane, hexane and dipropyl ether and for the propan-2-ol process; 2,3 dimethyl butane, and diisopropyl ether.

Due to the interesting and novel observations in the Pb-alcohol systems, product identification was attempted, the results of which are recorded and discussed in Chapter 4.

3.6.8 Lead Disc Summary

Using a rotating Pb disc electrode, the conditions for the reproduction of the reduction peak C2, the effect of bulk ethanol concentration, potential scan rate, and electrode rotation rate in pH 8.1, 0.1 M phosphate buffer were established. The initial hypothesis of this work was that the electrochemical reduction of alcohols would produce alkanes, *i.e.* ethanol reduces to ethane.

Using this working hypothesis of the production of alkanes, the amount of charge associated with this peak may suggest the formation of a monolayer of product on the surface of the electrode within the rotation rate, scan rate and concentration ranges considered in this work. Increasing the bulk alcohol concentration has no effect on the total charge produced; this is consistent with the reduction process being progressively stifled through the formation of an insulating layer of reaction product. Therefore, irrespective of the concentration of the ethanol in the system, it appears that the same amount of material is reducing and being deposited out on the surface. However, various other conditions of the experiments appeared to have some effect on the processes occurring at the electrode.

The anodic limit of the cyclic voltammogram had an effect on the reduction processes occurring at the electrode. There is a change in the cathodic wave of the cyclic voltammograms observed between the anodic limit of –0.65 V and –0.7 V where the reductive peak becomes substantially smaller and no longer reproducible. The absence of an accompanying oxidative wave with any if the anodic limits investigated suggests an irreversible reaction. Some inhibition of reduction on the electrode surface appears to be present with anodic limit $E < -0.7$ V. This inhibition is absent for those with anodic limit $E > -0.65$ V. Experiments with the potential hold technique suggested that the reproducibility of the peak at anodic limits $E < -0.7$ V had a time-dependent nature and by allowing enough time for the layer to be removed the reductive peak could be obtained reproducibly in subsequent scans. However, the size of the peak appears to

have a time-independent nature and the magnitude of the reductive current produced is less at the more negative potentials.

The potential scan rate also had an effect on the reduction processes. A decrease in the amount of material reducing was observed with increasing scan rate. The scan rate is the rate at which the potential is scanned through the potential range by the potentiostat. Small scan rates (i.e. 10 mV s^{-1}) pass through the potential range over longer times than larger scan rates (i.e. 200 mV s^{-1}), therefore a single scan takes a longer time, and more time is spent at each potential scanned, at a lower scan rate than at a larger scan rate. More reduction appears to be able to take place at slower scan rates indicating that the reduction process is relatively slow, allowing more time in the potential range where reduction occurs may allow for more reduction.

The rotation rate of the RDE also appears to have an effect on the reduction processes occurring. As noted in Section 3.5.5, there is a progressive decrease in observed peak size as the rotation rate is increased. An increase in rotation rate is expected to promote the loss of such insulating materials away from the electrode as they form due to hydrodynamic shear. However, in this case, increasing the rotation rate appears to promote an insulating reduction product at the electrode, therefore ruling out the facilitated removal of insulating products.

The facilitated replenishment of the alcohol at the surface of the electrode may promote a second non-electrochemical process that is responsible for formation of the insulating layer.

A two step process was suggested:

Step 1 $ROH + 2H^+ + 2e^- \rightarrow$ intermediate (3.17)

Step 2 Intermediate + $ROH \rightarrow$ insulating product (3.18)

With the hypothesis being that increasing the rotation rate will not alter the rate of Step 1 but ensuring replenishment of ethanol (or propanol) at the electrode surface will promote Step 2.

The data in this section gives values of $(7.0\text{-}4.1) \times 10^{18}$ molecules m^{-2} of product at the surface which is less than the typical values for a monolayer of adsorbates on the metal surface where the number of sites on a metal surface available for adsorption of electroactive species is typically 1.3×10^{19} sites m^{-2}.[52]

As discussed earlier, an insulating layer is not inconsistent with some of these results. The possible thickness of an insulating layer was therefore calculated, using the working hypothesis assuming the reduction products are alkanes (ethane and propane), providing values of approximately 0.78 nm, showing that only a thin layer is formed before the reduction can no longer continue. The calculated thickness is consistent with the possibility of a monolayer forming on the electrode surface. It is also suggested that the binding sites utilized in this process are isolated, spaced apart on the electrode. This is due to the number of molecules per area produced for the Pb electrode system being reported as approximately 4×10^{18} molecules m^{-2} whereas the typical number of active binding sites on an electrode is 1.3×10^{19} sites m^{-2}. This indicates that not all the possible available binding sites on the electrode surface are occupied before the electrode is sufficiently covered and further reduction is inhibited. Assuming that each molecule of product occupies only one binding site on the electrode, the molecule therefore also effectively shields or occludes some of the electrode surface area surrounding the binding site.

The possibility of the formation of a longer chain alkane or an ether product was also considered. The possibility of the alcohol being required to adsorb to the surface of the electrode for reduction to occur could determine a two step process with an adsorbed intermediate leading to either of these possible products. The electrode rotation rate anomaly is also consistent with there being a 2 step process. Adsorption to the electrode would be thought to be through a carbon, most likely the carbon adjacent to the oxygen due to electronegativity, or through the oxygen itself as a result of its lone pairs.

Possible products considered at this point were butane, butene, and diethyl ether for the ethanol investigation, hexane, hexane and dipropyl ether for propanol and 2,3 dimethyl butane, and diisopropyl ether for propan-2-ol.

The Pb electrode systems exhibit some unexpected results and novel phenomena. These results suggest that there may not be a simple alkane product from a simple reduction process. The reduction product may be an intermediate in another process giving a non-reductive final product. These novel findings require further examination to be fully understood. Therefore product identification for these Pb electrode systems were considered. Chapter 4 discusses the product identification methods and suggested products of the Pb electrode systems.

Chapter 4

Lead Electrode Product Identification

4.1 Introduction

Chapter 3 discussed the information obtained from the cyclic voltammetry investigations on three electrode materials. The results with the lead electrode described in Chapter 3 suggested an interesting and novel process may be occurring, and identification of the product was investigated. Previously in this work possible products have only been suggested or assumed for the purposes of a working hypothesis. The focus of this chapter is to investigate and discuss the product identification for the lead electrode, in 0.1 M phosphate buffer electrolyte of pH 8.1. The rotating disc electrode cyclic voltammetry studies provide some information on the processes occurring and the effect of the different conditions on the occurring reduction. However, the product of the reduction cannot be determined in the cyclic voltammetry with the rotating disc electrode.

Several methods for product identification were considered, these being NMR, Mass Spectrometry, Gas IR and Surface Enhanced Raman Spectroscopy. However, it was determined that not all of these methods would be suitable product identification methods for this work. The constraints of the work discussed here include the small volume of product due to the small scale of the experiment, significantly smaller volume due to the suggested insulating layer formation involved with the lead electrode processes, and the suggestion that the product may or may not be a gaseous product. These constraints needed to be fully considered when selecting a product identification method.

The formation of the possible insulating monolayer on the surface of the RDE electrode dictates that there is only a small amount of material being reduced. This amount of material being produced, approximately 1.30×10^{-10} moles, as reported in Chapter 3 was found to be an inadequate amount of material for most routine analytical methods. The possible alkane or ether products assumed for this are of very low molecular mass as well, requiring a system that has high sensitivity or low detection limits due to the small molecular mass and amount of product likely to be present. A method that might

possibly have the sensitivity to detect molecular mass this low would be Mass Spectrometry. However, with the added difficulty of such a small amount of product even this system may not be sufficient.[68]

Possibilities for overcoming the problem of the small amount of product being produced were considered. This small amount from one cyclic voltammetry scan on the rotating disc electrode; more would be produced if more cyclic voltammetry scans were performed. However, at the small surface area of the rotating disc electrode even several hundred scans would still produce a very small quantity of product(s). Five hundred scans would potentially produce 6.5×10^{-8} moles; if gaseous this would be 1.61×10^{-3} cm^3 at standard ambient temperature and pressure (298.15 K, 100 kPa). Along with this the experimental set up using the rotating disc electrode is not very easily modified to collect this small volume of putative gaseous sample that might depart the system. A larger surface area on which the reduction can occur would lead to a larger amount of product potentially being produced from each cyclic voltammetry scan. Therefore possible larger surface area electrodes were considered.

4.2 Large Surface Area Electrode

The rotating disc electrode provides some information on the processes occurring and the effect of the different conditions on the occurring reduction. However, as discussed above the formation of the possible insulating monolayer on the surface of the electrode precludes ready analysis; it is inadequate for detection by many techniques for product identification, or is at the low end for detection limits. Therefore it would be difficult to establish the product of the reduction using the RDE set up. An electrode with a larger surface area than the RDE offers the opportunity to increase the quantity of reaction product for detection and identification.

Consequently, a larger surface area electrode for the lead system was considered. A porous lead planar anode was extracted from a fully charged lead acid battery (to ensure Pb^0 for use as the Pb WE. This plate was carefully washed with Millipore water to remove the lead-acid H_2SO_4 electrolyte. The projected surface area (both faces) of this plate was 2.04×10^{-3} m^2. It is anticipated that the true surface area is several multiples of this area due to the porous nature of typical commercial lead –acid electrode systems. However, it is noted that given the intent is to produce gaseous products, much of this

surface area will likely become occluded. Hence, the precise surface area is not of great interest. In any event, this substantially higher projected surface area of the battery anode is nearly 100 times greater than that for the Pb RDE, and hence provides a much larger area and amount of product for detection in analytical instrumentation.

4.3 Candidate Product Identification Techniques

4.3.1 Nuclear Magnetic Resonance Spectroscopy (NMR)

NMR can provide information about structure, reaction state and dynamics of the analyte and the chemical environment in which the analyte is present.[4,24] NMR is non destructive and qualitative data can be obtained from samples weighing less than a milligram. [4,24,69] However, NMR is only suitable for liquid and solid samples.[4,24,69] The sample for analysis in this case is definitely not a solid, but is possibly a liquid or a gas. If the product is in the liquid state, the concentration of product within the electrolyte is significantly small that it would likely not be detected in an NMR spectrum. If the product is a gas, NMR is not a suitable technique for detection. There is the possibility of extracting the gas into a liquid alkane such as Hexane. However, the possible concentration of the product within the gas sample extracted will again be significantly small that only the Hexane would be detected. Therefore NMR was determined not to be a suitable method for product identification in this case.

4.3.2 Surface Enhanced Raman Spectroscopy (SERS)

Owing to its high sensitivity and specificity, SERS has a great potential for analytical chemistry and biological sensors.[4,24,70] However, SERS is sensitive to the surface on which the experiment is taking place, with good results only from specific metals such as Au, Ag, and Cu. [4,24,70,71] In this case the electrode material is lead, which is not one of the specific metals confirmed to be suitable for SERS. It could be possible to deposit a layer of lead on a gold or silver electrode. This would provide the lead for the electrochemical investigation and gold or silver for the SERS enhancement. However, this process adds extra electrochemical steps required to deposit the layer and extra care would need to be taken to obtain a suitable thickness layer so as not to inhibit the enhancement.

Due to the lack of a suitable electrode material for SERS and the difficulty in the deposition of a suitable thin Pb layer on the Ag or Au, it was determined at this point that SERS is not the best technique for product identification.

4.3.3 Mass Spectrometry

In Mass Spectrometry it is possible to record molecules with a molar mass as small as 28 g mol^{-1}.[50] The molar mass of the smallest possible product being considered here (ethane Mr = 30.07 g mol^{-1}) is within the limits, albeit at the minimum limit, of the Bruker FT–ICR mass spectrometer used in this work. However, the amount of material being produced is very small. The collected gas sample, could contain a gaseous product from the electrochemical processes. However, it will likely also contain hydrogen gas produced at the cathodic limit of the CV, as seen by the background current due to H_2 observed in Figs. 3.47 – 3.55 reported in chapter 3. Along with the gaseous product and hydrogen gas there will possibly also be some ethanol and water vapor due to vaporization as gaseous product bubbles escape the aqueous buffer.

The volume of gaseous product collected in the Pb-ethanol system is approximately 6 ml in 5 hours, therefore, the maximum collected in any one day being < 10 ml. The possible amount of product assumed to be produced on the larger surface area electrode would be 7.88×10^{-9} moles for each scan as calculated based on eqn. 3.11 described in chapter 3, section 3.5.3. Up to 900 scans could be cycled in one day, therefore up to 7.09×10^{-6} moles of product could be produced. This amount of product could possibly be detected by a mass spectrometer.[68]

The possibility of running the system for several days to collect more gas was considered. However, as discussed in chapter 3, the electrode materials are not inert substances and there may be an effect on the surface of the electrode from prolonged cathodic potentials. This effect on the electrode surface is largely unknown. Any changes to the electrode surface due to prolonged exposure to cathodic potentials may have an effect on the products forming from the alcohol reduction of interest. Therefore the length of individual experiments was limited to 8 hours, then allowing time for mechanical and electrochemical cleaning of the electrode surface.

The spectra produced contain a certain amount of noise in the background. It is recommended that detection of a sample should be 10 times the noise of the instrument.[50,51] There is only a small volume, (5 – 10 mL), of gas potentially containing up to only 7.09×10^{-6} moles of product, a response from this small sample size may be difficult to detect over the instruments noise.

There are challenges to the use of mass spectrometry, however due to its sensitivity and detection limits this technique was considered a possible product identification technique for this work.

4.3.4 Infra Red Spectroscopy

Infrared spectroscopy is the measurement of the wavelength and intensity of the absorption of infrared light by a sample.[53,54] Infrared spectroscopy has high selectivity and the examination of the twisting, bending, rotating and vibrating motions of atoms is possible. IR spectroscopy can be used for gas, liquid or solid samples.[54] Every species examined has a unique fingerprint spectrum. Since no two chemical species have the same IR spectrum FTIR is a highly effective method for analysis. The product being considered here is either in liquid or gas phase, therefore, FT–IR would be a possible product identification technique for this work.

4.4 Electrochemical Cell Set Up

A large surface area lead electrode was obtained by extracting a lead plate from a lead acid battery for use as the WE. A 2 cm by 4 cm piece of porous Ni foam was used as the CE in the cell. The porosity of the Ni foam leads to a much greater surface area than the lead plate as is necessary for a CE (section 2.4.4). An Ag/AgCl standard reference electrode was used in the cell as the RE. A 250 ml beaker was used as the cell, loaded with 150 ml of the pH 8.1, 0.1 M phosphate buffer electrolyte. The WE, CE and RE were connected to the potentiostat and placed in the beaker.

A headspace was created for collection of the gas produced only by the WE and not the other electrodes. The headspace was created in the electrochemical cell using a glass funnel, inverted over only the Pb plate WE. The end of the funnels neck was sealed

with a septum providing a space where the gaseous product could be collected and ultimately extracted from the system through the septum. The neck of the funnel was completely filled with electrolyte, as the gas was produced the liquid in the funnel neck was displaced and the gas was collected in the headspace. Both the RE and the CE in the cell were outside the glass funnel to ensure that any gas collected in the headspace was due only to the gas produced from the WE alone.

Cyclic voltammetry was conducted in the electrochemical cell, gas was produced on the electrode surface on the cathodic sweeps and as these gas bubbles escaped from the surface of the electrolyte a sample of the gas produced was collected in the headspace. The collected gas sample was extracted through the septum above the headspace using a needle and syringe and transferred to the appropriate instrument for identification.

4.5 Cyclic Voltammetry

Cyclic voltammetry was conducted using the large surface area lead plate in the pH 8.1, 0.1 M phosphate buffer with and without the presence of the three alcohols ethanol, propanol and propan-2-ol , at a potential scan rate of 50 mV s^{-1}. Figures 4.1 – 4.3 show the cyclic voltammograms of the Pb plate WE in the pH 8.1 phosphate buffer with and without the presence of 10 mM ethanol, propanol and propan-2-ol respectively, all at a potential scan rate of 50 mV s^{-1} within the potential range –0.50 to –1.3 V.

A reductive response was observed in the form of a broad peak centered at approximately the peak potential observed in the RDE experiments. The peak observed here is much broader than that observed in the rotating disc experiments. The electrode surface is larger, allowing more reduction to occur, and more porous than the RDE, with slow diffusion in and out of the thick (3 mm) porous electrode leading to a slower coverage of the surface of the electrode. The decrease in the reduction current does not occur as soon or as rapidly as in the RDE experiment due to the electrode surface not being covered as quickly. The potential range is extended slightly from that in the rotating disc experiments merely to aid in the observation of the broader reductive peak.

Gas bubbles were visible on this large surface area Pb plate electrode during the cathodic sweeps. As discussed in Chapter 3 (Section 3.6) the product from the system on the Pb electrode is possibly a gas, considering the assumed reductive products. This visible evidence of gas forming supports the possibility of a gas product.

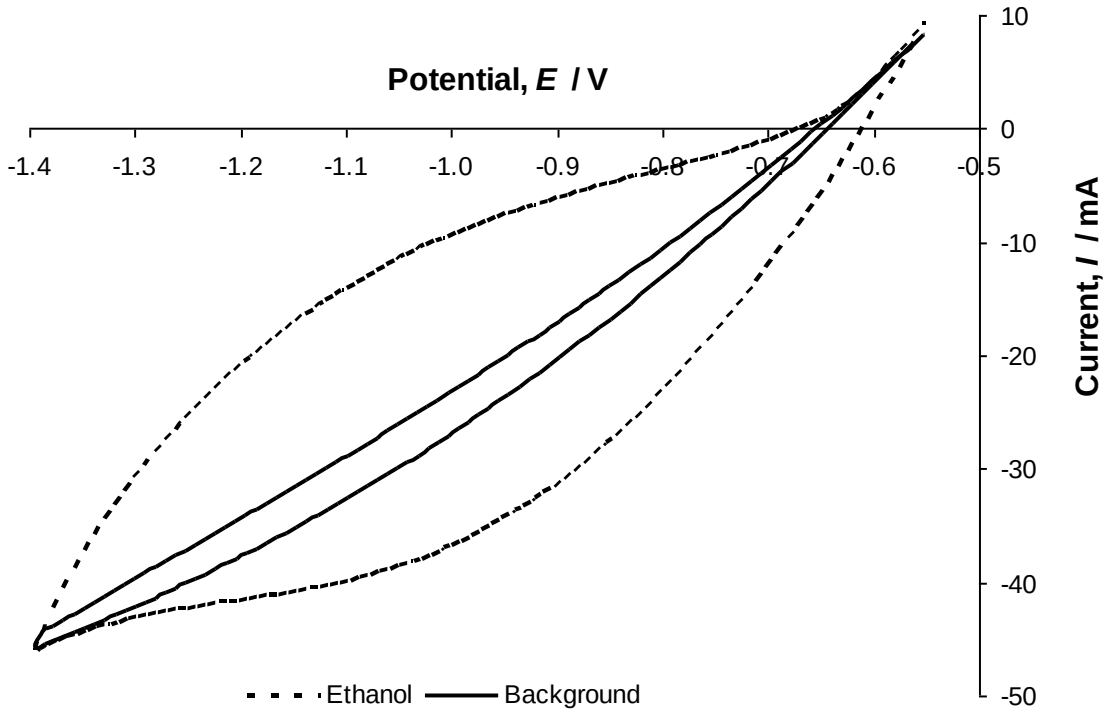

Fig. 4.1 Cyclic Voltammograms on Pb plate WE with and without the presence of 10 mM bulk ethanol concentration at 50 mV s^{-1} potential scan rate within the potential range -0.50 to -1.30 V.

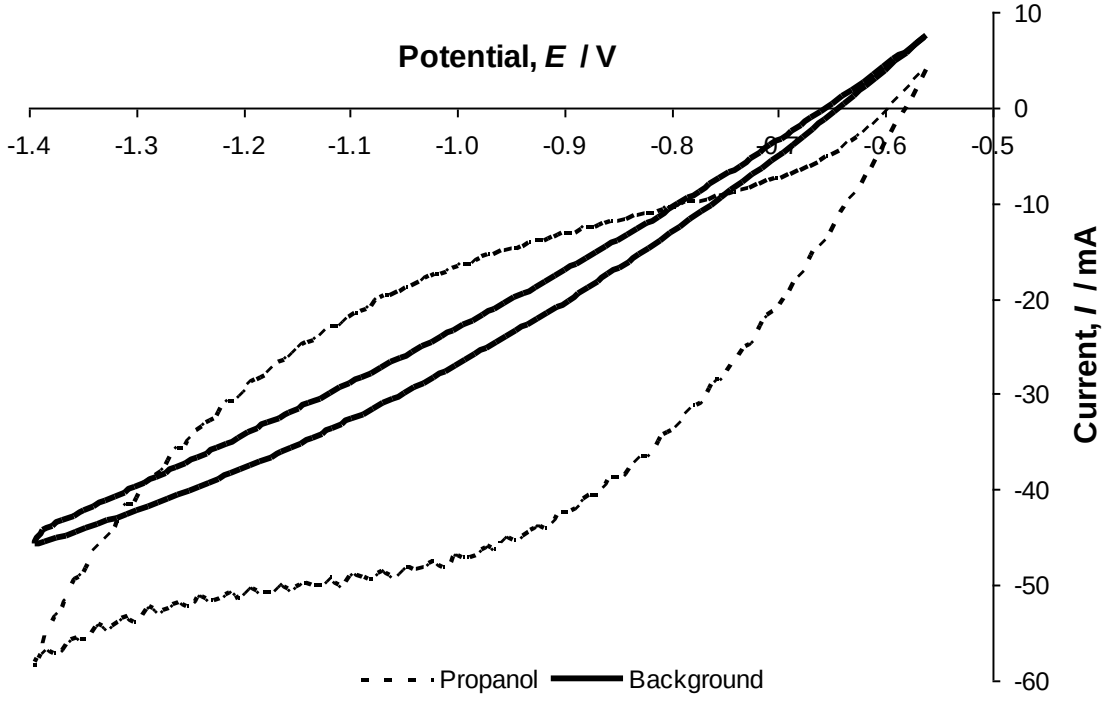

Fig. 4.2 Cyclic Voltammograms on Pb plate WE with and without the presence of 10 mM bulk propanol concentration at 50 mV s^{-1} potential scan rate within the potential range -0.50 to -1.30 V.

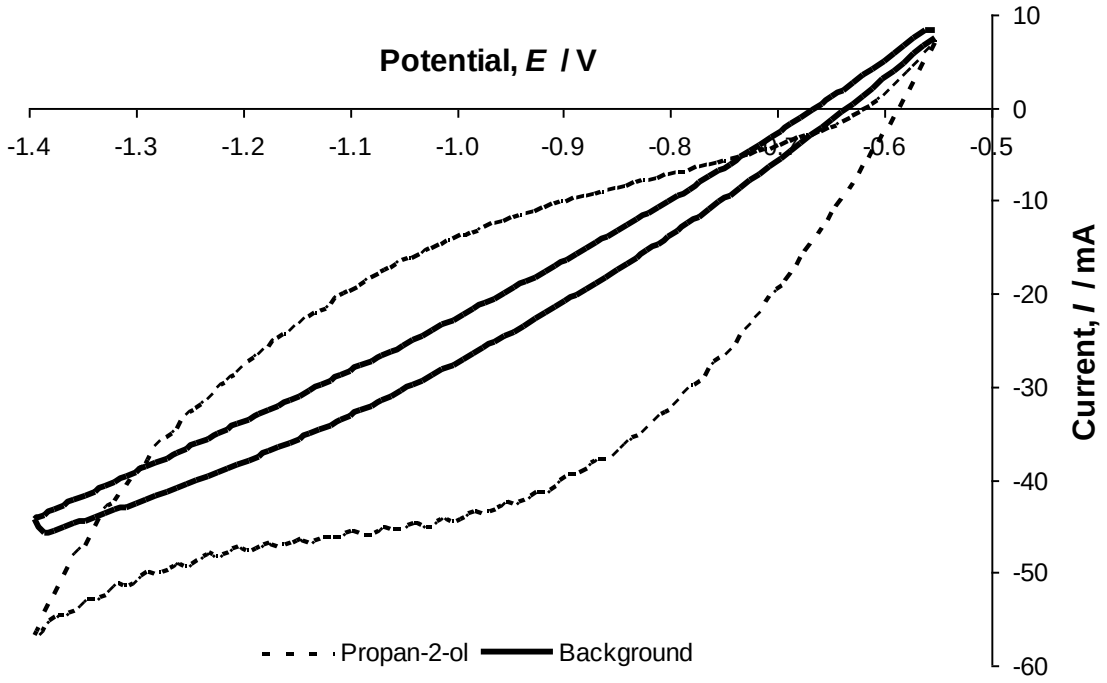

Fig. 4.3 Cyclic Voltammograms on Pb plate WE with and without the presence of 10 mM bulk propan-2-ol concentration at 50 mV s^{-1} potential scan rate within the potential range -0.50 to -1.30 V.

4.6 Identification of Ethanol Reduction Product

4.6.1 Mass Spectrometry

Initially mass spectrometry was pursued due to its high sensitivity and the ability to detect low molecular mass molecules. The 10 ml sample was extracted from the headspace of the electrochemical cell with a needle and syringe and was transferred to the mass spectrometer. The sample was injected through a septum into the carrier gas stream flowing into the ionization chamber of the mass spectrometer. However with such a small volume of gas being collected and inserted into the larger mass spectrometer quadrapole the response was not observed above the background noise of the instrument. Under the current conditions, volume of gas and amount of product, Mass Spectrometry was not and effective product identification method.

It could be possible to collect a larger sample, and therefore a larger detection, if the number of scans was increased to produce more product (as discussed in section 4.2) or if the size of the electrode was increased again. As the electrode material is not an inert substance it is unknown what changes may be occurring on the surface of the electrode over several hundred scans. At some point a change to the electrode surface may occur and this may have an effect on the processes occurring and the product forming, therefore increasing the scans from the already > 500 scans is not desirable. Also, increasing the size of the electrode again was decided to be outside the scale of this work. As such, it was determined that Mass Spectrometry was no longer considered a suitable solution for product identification.

4.6.2 Gas InfraRed Spectroscopy

Gas infrared spectroscopy was considered for identification of the products. A 200 ml gas IR cell, with path length of 100 mm was used for Gas FT-IR Spectroscopy experiments. Firstly the gas IR cell was purged with N_2 gas to ensure no contaminants in the cell. N_2 gas was used as it will not produce an FT-IR spectrum, hence will not interfere with any spectrum being recorded for a sample. The background spectrum was recorded first with the cell filled with N_2 gas. The spectrum obtained from this background experiment simply records the IR activity in the air space surrounding the gas cell due to the N_2 contained in the cell not producing an IR spectrum. The

background spectrum indicates some presence of H_2O and CO_2 in the instruments' air space.

The gaseous ethanol product samples were inserted, using the needle and syringe, through a septum on one of the collection tubes into the gas IR cell and the FT-IR spectrum for the product sample was recorded with respect to the previously recorded background. Figure 4.4 shows the FT–IR transmittance spectra for the ethanol product sample. There is a small peak present at 2350 cm^{-1} assigned to the CO_2 present in the airspace around the gas cell. This peak is present in all spectra, backgrounds and samples, and fluctuates slightly over time due to the amount of CO_2 in the chamber changing with the chamber being opened, closed and re-purged with each sample spectrum collected. There is also a large collection of peaks in the ranges, 1300 – 1900 cm^{-1} and 3500 – 3900 cm^{-1}, assigned to water vapor. This water vapor is assumed to be predominately from water vapor in the collected gas sample.

Transmittance peaks of interest for the product are observed at 1050 and 2900 cm^{-1} assigned to single C–O bond stretching and C-H bond stretching respectively.[53] There is a possibility that there are some of the starting materials present in this gas and the peaks possibly attributed to those starting materials should be noted. A gas sample of the reactants was collected by bubbling N_2 through the electrolyte and ethanol solution and collecting a headspace gas sample of equivalent volume to the product sample. Bubbling N_2 through the electrolyte mimics the product bubbles forming and escaping, breaking the surface of the electrolyte and will provide an estimation of the amount of reactants that may be vaporized into the gas phase during the process. The FT-IR spectrum of this gas sample of N_2 and the reactants of the ethanol reduction process is presented in Fig. 4.5 along with the product sample spectrum (from Fig. 4.4). There are peaks present for the reactants that are similar to the product sample; however, the product sample does have three peaks present at 2900 cm^{-1} unlike the doublet present for the reactants in Fig. 4.7 assigned to ethanol. These three peaks in the product sample spectrum are not inconsistent with the possibility that there could be two doublets, one assigned to ethanol and one assigned to the product, overlapping in a way that only three peaks are discernable.

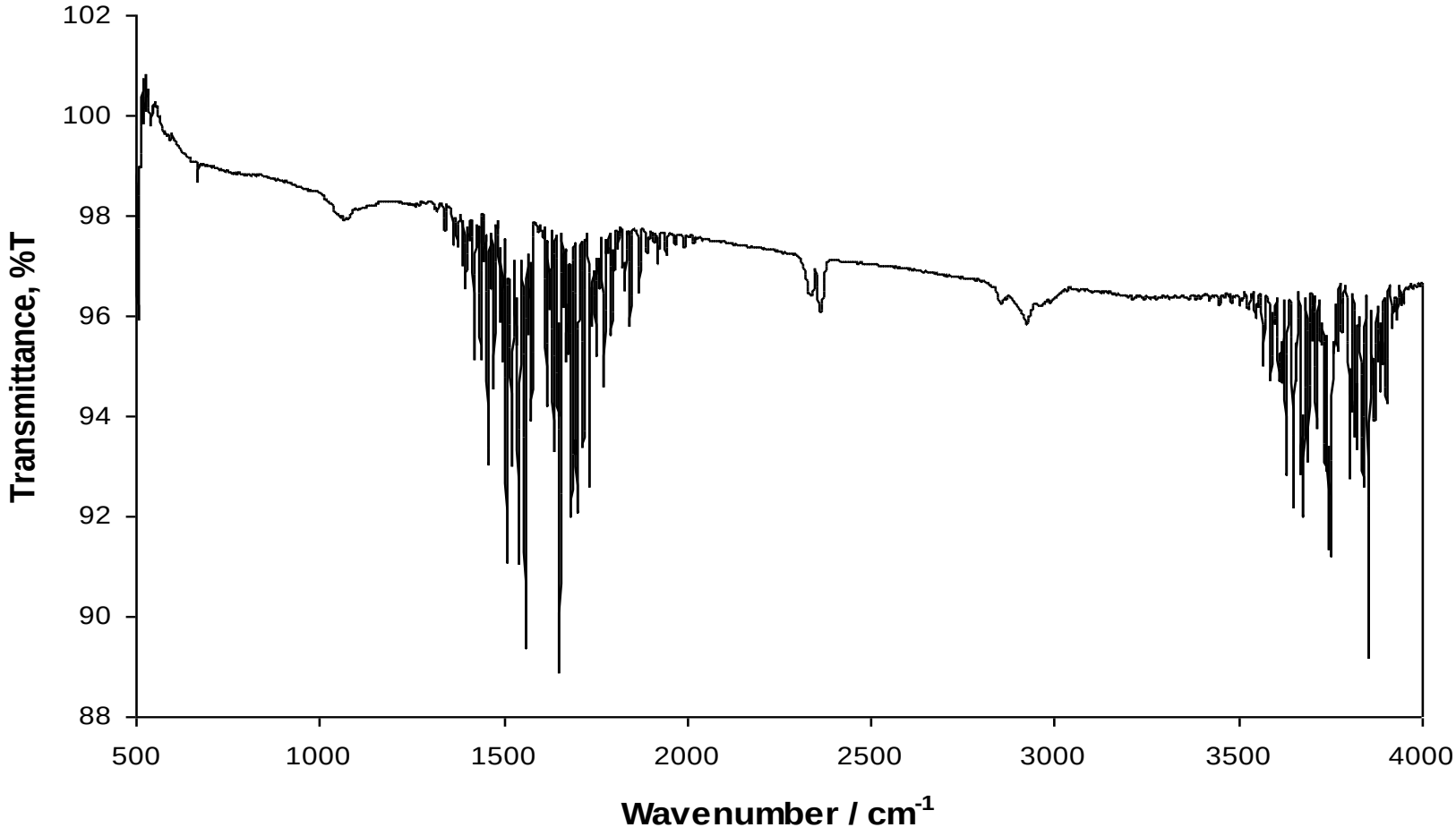

Fig. 4.4 FT-IR Transmittance Spectrum for the Ethanol Product Sample.

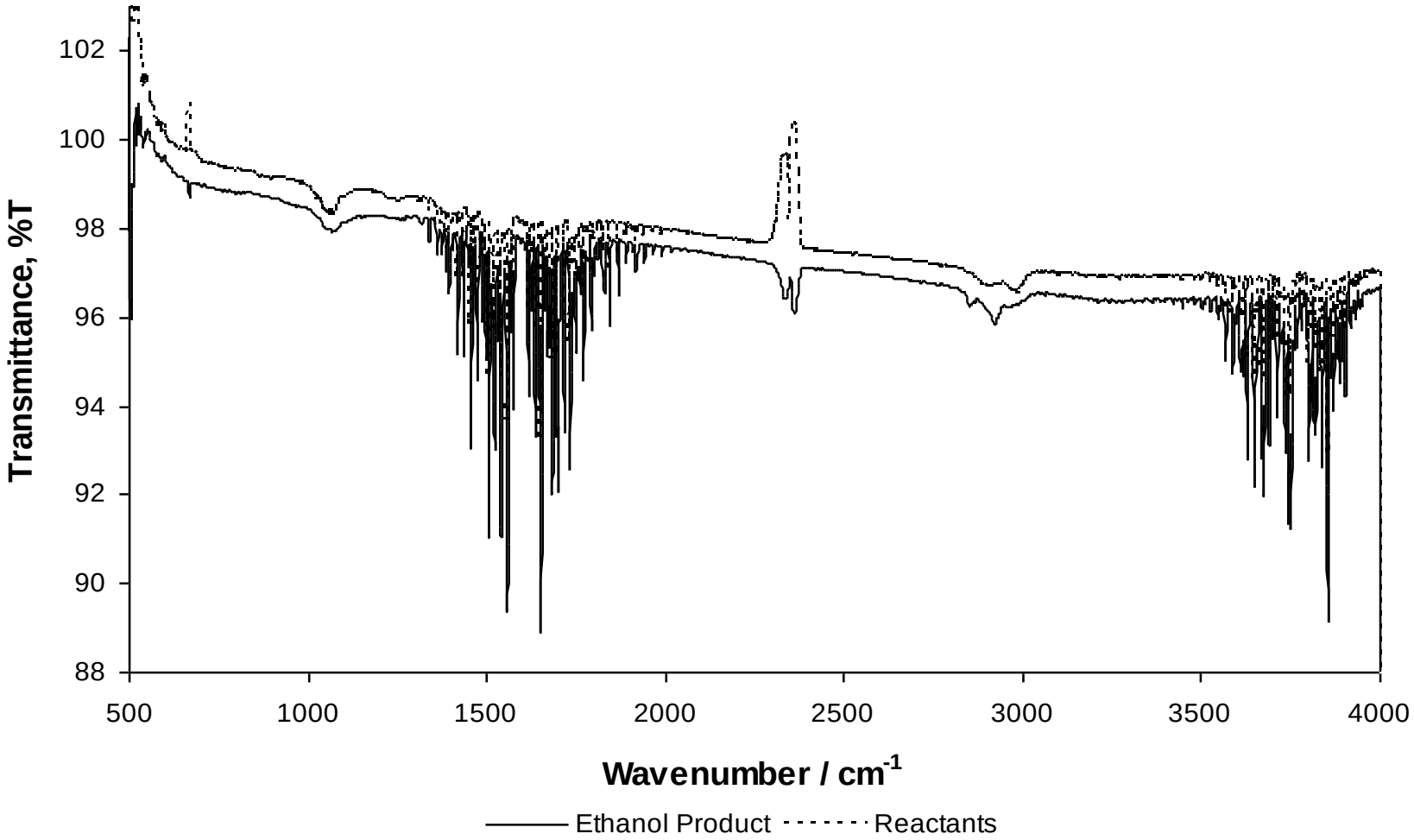

Fig. 4.5 FT-IR spectra for the reactants and products of the Pb–ethanol system.

4.6.3 Challenges

A number of challenges were experienced throughout the FT–IR spectroscopy analysis. These challenges being problems such as the small amount of sample, the size of the available gas IR cell, the observed peak intensity and the presence of a large water response.

Although there are peaks observed in the gas FT–IR spectra presented, the small amount of gas sample leads to these peaks being of a very minimal intensity creating difficulties in interpretation. With only 10 ml of gas and less than 7×10^{-6} moles of product at most, there is only a small amount of material available for detection.

The absorbance (A) of a substance is represented by eqn. 4.1,[72]

$$A = \varepsilon.c.l \qquad (4.1)$$

where ε is the absorptivity coefficient, c is the concentration of the analyte in the cell and l in the pathlength of the cell, 100 mm. The small amount of material in combination with the large volume of the IR cell gives a possible concentration of product in the 200 mL IR cell of only 3.5×10^{-5} mol L^{-1}.

The spectra reported in this work are in terms of transmittance (T). The Transmittance is related to absorbance by eqn. 4.2,

$$\log 1/T = A \qquad (4.2)$$

$$1/T = 10^{-A} = 10^{-(\varepsilon.c.l)} \qquad (4.3)$$

therefore, the transmittance decreases exponentially with increasing absorbance.[72]

If the concentration or the pathlength is increased the absorbance will increase (transmittance will decrease). However, increasing the pathlength of a cell (and keeping all other dimensions of the cell constant), will increase the volume of the cell and in doing this decrease the concentration of the analyte inside the cell. Likewise, increasing the concentration could be achieved by reducing the volume of the cell, which could decrease the pathlength. Therefore, increasing one of either the concentration or the pathlength may have a negative effect on the absorbance due to the consequence of decreasing the other.

The product of the concentration and pathlength (*c*.*l*) is important. If this product, *cl*, is increased the absorbance will increase (transmittance will decrease). The concentration and pathlength product, *cl*, could be increased three ways;

1.) increasing the concentration while the pathlength remains constant,

2.) increasing the pathlength while the concentration remains constant, or

3.) increasing both the concentration of the analyte in the cell and the pathlength of the cell.

The pathlength of the cell can be increased with no change to the concentration by employing a multipass cell of the same volume. A multipass cell is a cell of standard size which allows the IR beam to pass through the cell multiple times by the use of mirror surfaces within the cell, effectively increasing the cells pathlength by several times without a change in volume.[73]

The concentration could be increased with no change to the pathlength by reducing the volume of the cell without altering its length. By simply decreasing the diameter of the cell a smaller volume would be achieved, increasing the concentration, without affecting the pathlength. Of course a smaller volume multipass cell could be employed to increase both *l* and *c*.

Purchasing a new cell was considered, however due to the large expense of both multipass cells and smaller volume gas cells, and the time to receive the new cells, it was decided that the scope of this particular project was not sufficient for that expense. Future work related to this project may consider purchasing a new gas IR cell to provide a more accurate identification of this product.

The initial gas IR spectra collected for all the lead systems also has a very large product to water signal ratio. Due to the significantly larger signal from the water response there is difficulty in effectively interpreting the response from the actual product. It may be possible to obtain a better response from the actual product if the water was removed. Therefore the possibility of drying the collected gas sample was considered.

Size 4A molecular sieves were obtained for drying the sample. The molecular sieves were activated by placing in a furnace at 550°C for 24 hours and were stored in a dessicator after activation when not in use. The molecular sieves were placed in a test-tube with a septum seal, which was then flushed with dry N_2 gas. The collected product gas sample from the electrochemical experiments was transferred from the headspace of

the electrochemical cell to the test-tube, via a needle and syringe through the septum, displacing some of the N_2 gas within the test tube. The gas sample thought to be containing the product was left in the test-tube drying over the molecular sieves for a period of 24 hours at which time the gas was extracted from the test-tube and transferred, again via a needle and syringe, to the N_2 purged gas IR cell and the new FT–IR spectrum was recorded. Figure 4.6 shows the IR spectra of the ethanol product sample before and after drying. Some of the water response in the IR spectra is diminished. However, some of the product is also lost due to the extra transfer steps involved in this drying. Although the sample has been partially dried by the sieves, the transmittance from the sample has decreased and the ratio of the responses has not been improved substantially, therefore, the spectrum cannot be interpreted more effectively than before drying was performed.

The product determination was therefore based on the interpretation of the spectra of samples with out drying due to the larger product response.

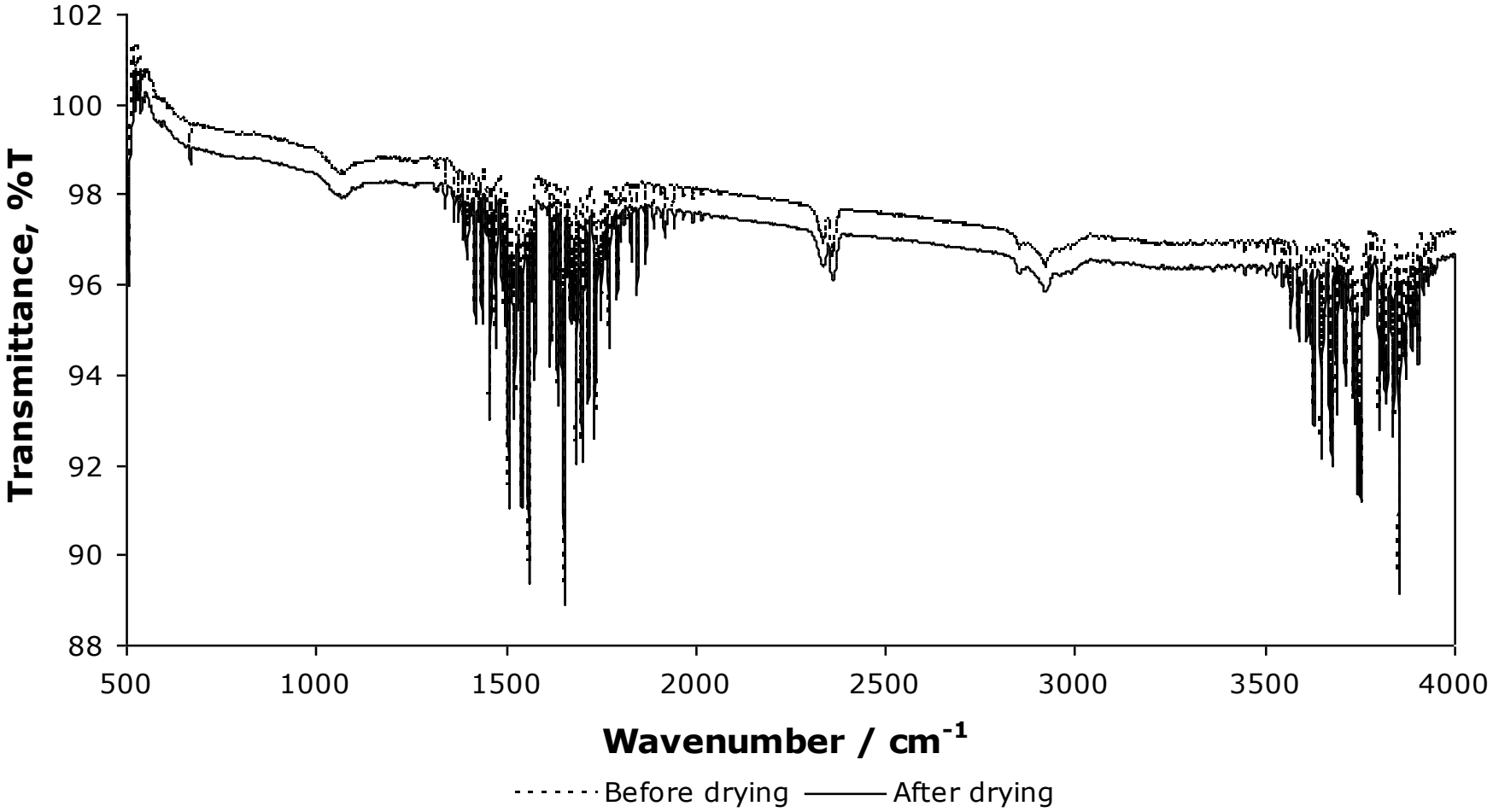

Fig. 4.6 FT-IR transmittance Spectra of the Ethanol Product Sample before and after drying over 4A molecular sieves for 24 hours.

4.6.4 Product Identification

Reference spectra and data for the possible products suggested in Chapter 3 were examined. The working hypothesis used in Chapter 3 assumed that the product would be the corresponding alkane, i.e. ethanol would produce ethane. However, from the reference spectra, it is evident that the product cannot be ethane or ethene. The ethane and ethene spectra do not have a peak at approximately 1100 cm^{-1} as in the product sample spectrum, (ethane: ~ 800 and 1500 cm^{-1}, ethene: ~900 and 1400 cm^{-1}) therefore, the ethanol reduction product is not ethane or ethene.

Reference spectra for all starting materials and all considered products are contained in Appendix 1 including ethane, ethene, ethanol, propane, propene, propanol, propandiol, butane, butene, butanol, butandiol, diethyl ether, dipropyl ether.

A possible two step process was suggested in Chapter 3 (Section 3.6.6) which led to the consideration of other possible products such as longer chain hydrocarbons; butane or butene, or ethers; diethyl ether. Butane has a doublet at 2900 cm^{-1} that could overlap with the ethanol doublet to give three observed peaks but the 1100 cm^{-1} peak present in the product sample is not observed in butane, rather a peak at 980 cm^{-1} is present. Butene does not produce a peak at 2900 cm^{-1} or at 1100 cm^{-1}. Consequently, butane and butene cannot be the product of the ethanol reduction. Diethylether has a doublet at 2900 cm^{-1}, which could overlap with the ethanol doublet to produce the 3 peaks observed in the product spectrum. Along with this a peak close to 1100 cm^{-1} is also observed in the diethyl ether spectrum. In the first instance diethyl ether appears to be a highly probable product. However, careful inspection of the 1100 cm^{-1} peaks shows the product sample and ethanol coincide at 1050 cm^{-1} but the diethyl ether peak is observed at a slightly larger wavenumber, 1150 cm^{-1}, without the presence of this significant diethyl ether peak, in the product spectrum, diethyl ether cannot be identified as the product of the electrochemical reduction of ethanol either.

Further investigation into other possible products was now required and the FT-IR spectrum of the ethanol product sample was compared to reference spectra of any molecules that could be formed from the ethanol molecules present. Two new possible products were discovered: 1,2 propandiol and 1,3-propandiol.

Figure 4.7 shows the IR spectra of the ethanol product sample, 1,2 propandiol and 1,3-propandiol. The peaks present at 1050 cm^{-1} and 2900 cm^{-1} appear to agree well across the 3 spectra. Each peak was examined more closely to compare the three spectra. Figures 4.8 and 4.9 show the 1050 cm^{-1} and 2900 cm^{-1} peak regions for each spectrum respectively.

The 1,3 propandiol peaks appear to fit the product spectra more closely than the 1,2 propandiol peaks. The 1050 cm^{-1} peak for 1,3 propandiol follows a similar shape to the product spectra whereas the 1,2 propandiol deviates from the shape of the product peak. When examining the 2900 cm^{-1} peak, again a better fit from the 1,3 propandiol peak to the product is evident. A doublet corresponding to two of the 3 peaks in the product spectrum is observed (the third peak in the product spectrum assumed to correspond to the doublet in an ethanol spectrum). These gas IR spectra suggest that the product of the processes taking place in the pH 8.1 phosphate buffer in the presence of ethanol at the lead electrode is 1,3 propandiol.

Forming 1,3-propandiol from ethanol is not a reduction process but evidently an oxidation or addition process (i.e. a new carbon-carbon bond would have to form). However, the electrochemistry observed via the cyclic voltammetry showed a reduction process in the cathodic sweep of the cyclic voltammogram. This presence of a reduction process and evidence of a non-reduction product supports the suggested two step process discussed in Chapter 3 involving an electrochemical reduction step, producing an adsorbed intermediate, followed by a non-electrochemical step to obtain the final product.

Another interesting point is this product was collected as a gas in the headspace in the electrochemical cell. 1,2 propandiol and 1, 3 propandiol are typically liquids at room temperature, with boiling points of 187ºC and 211ºC respectively.[74,75] They are therefore not expected to be found in the gas phase under the conditions of this experiment. The reason for the presence of these compounds in the gas phase is yet unknown.

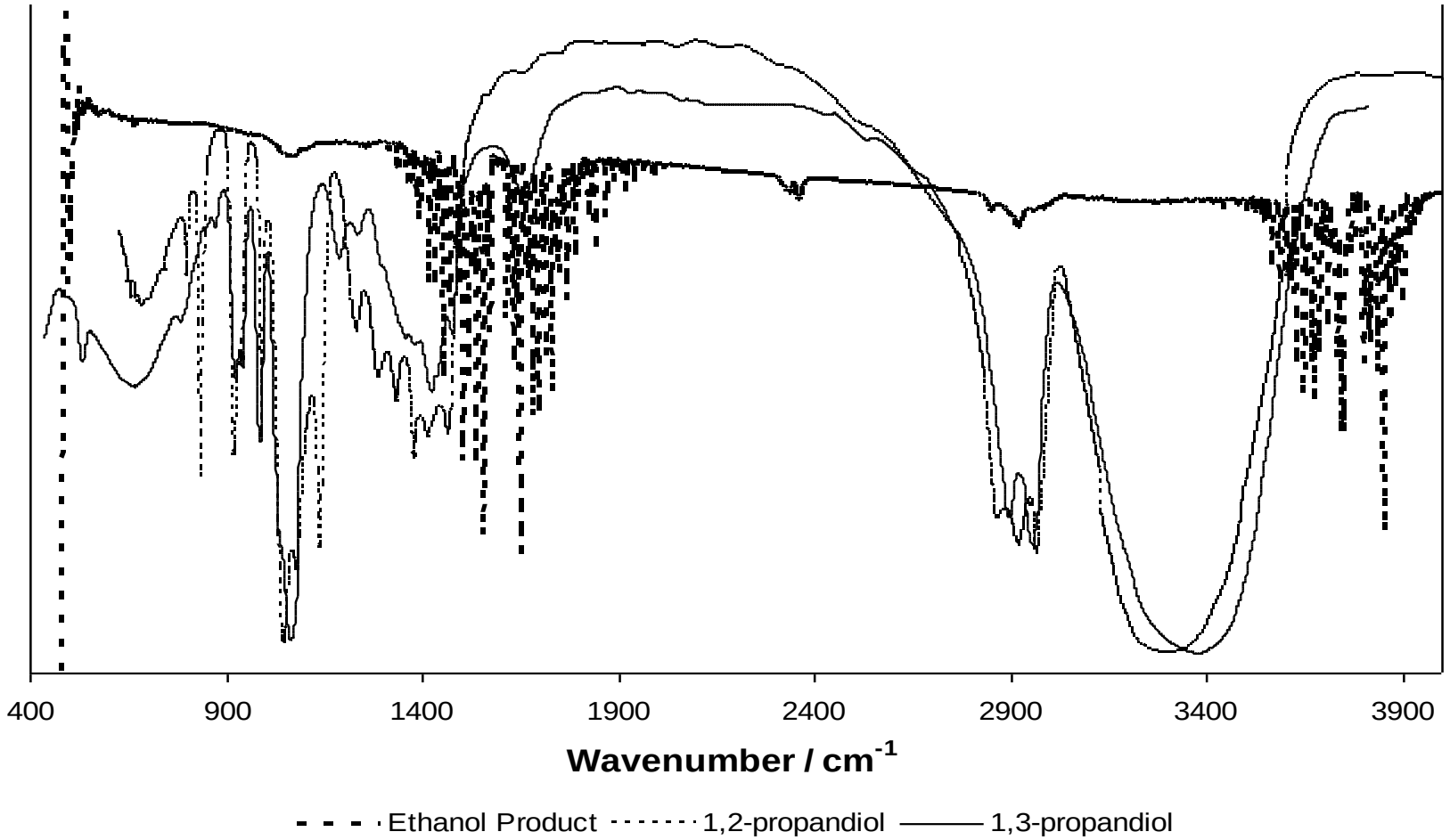

Fig. 4.7 FT-IR transmittance spectra of the Ethanol product sample and possible products, 1,2-propandiol, and 1,3-propandiol.

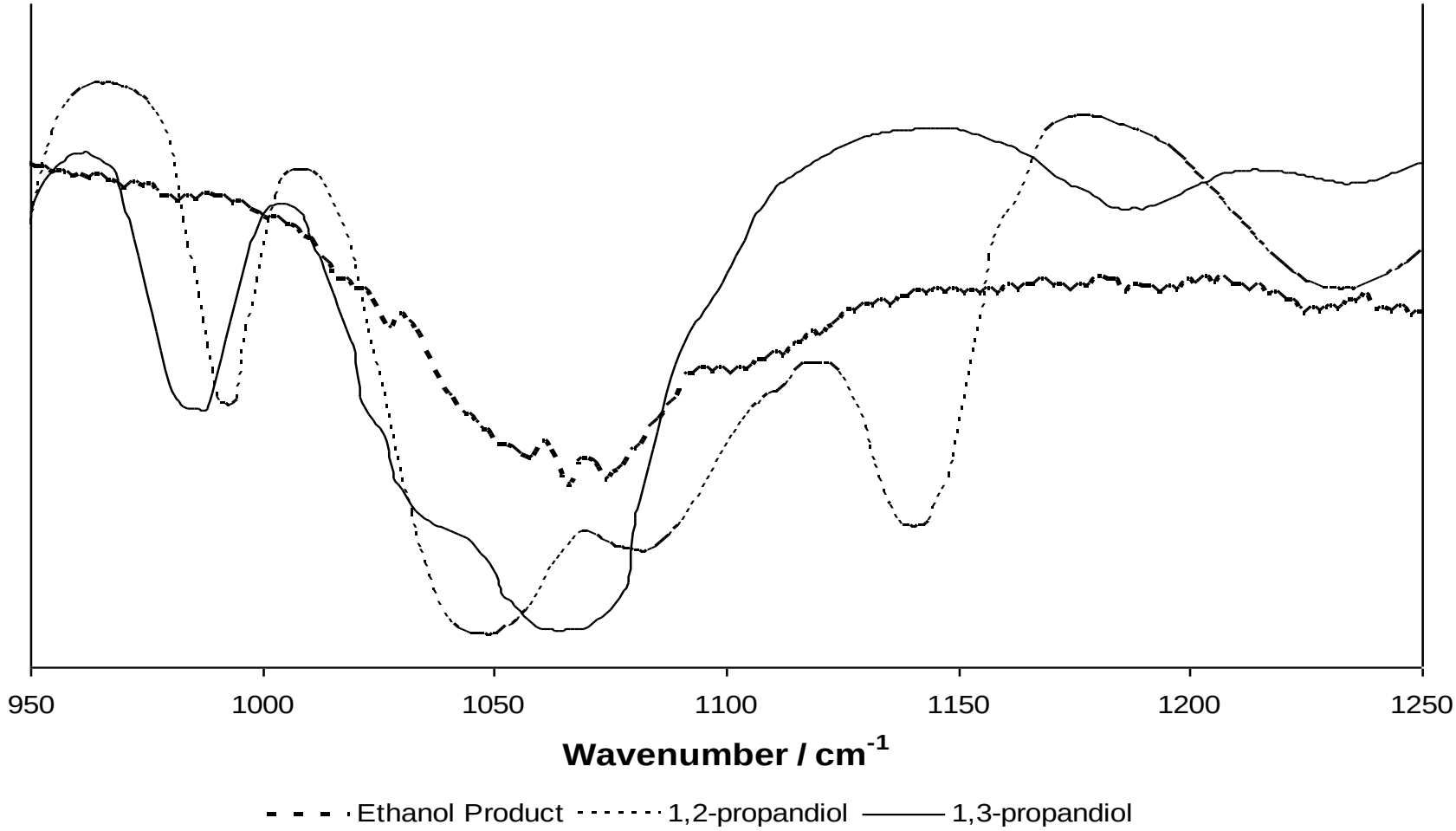

Fig. 4.8 FT-IR transmittance spectra, showing the peak at 1050 cm^{-1}, of the Ethanol product sample and possible products, 1,2-propandiol, and 1,3-propandiol.

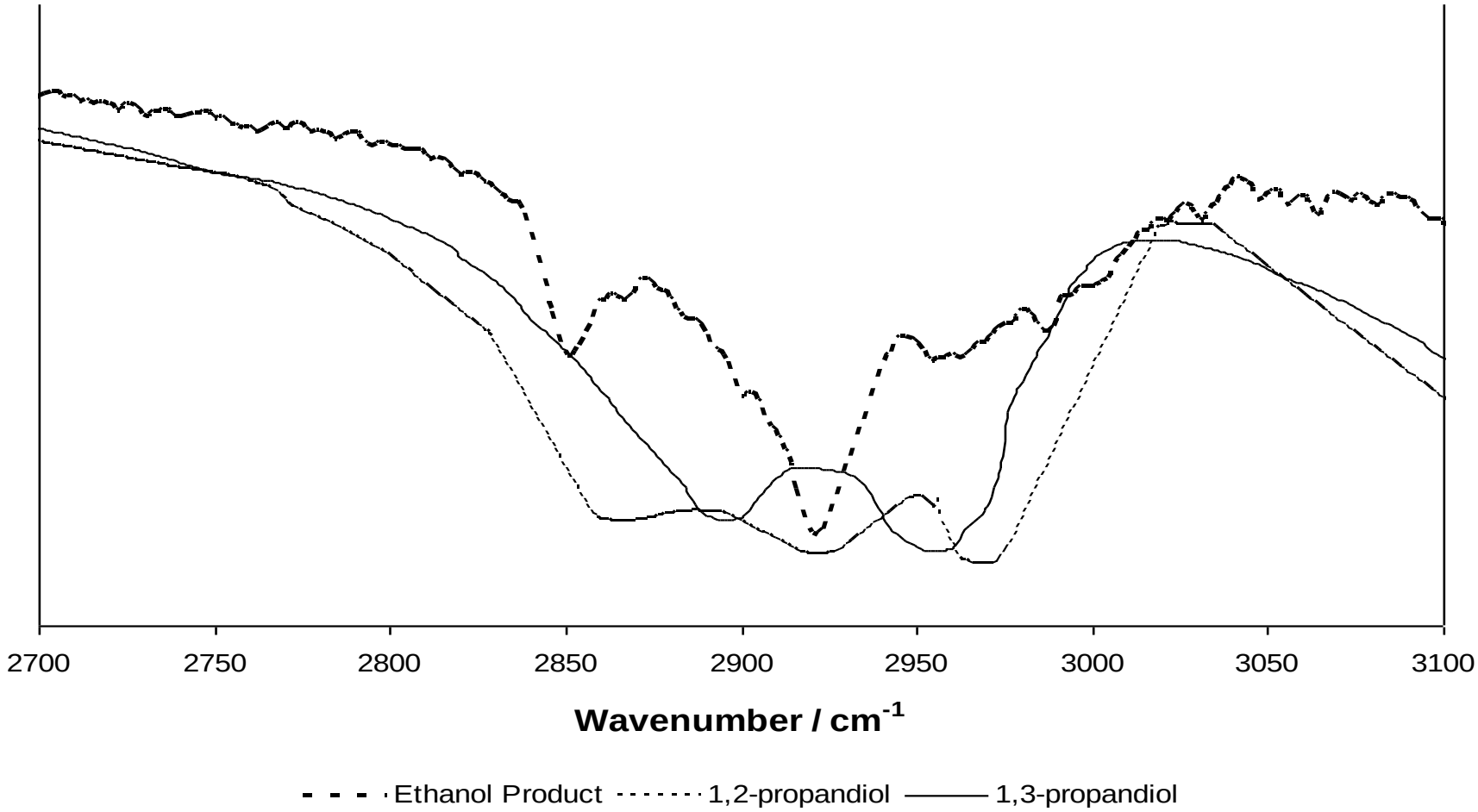

Fig. 4.9 FT-IR transmittance spectra, showing the peak at 2900 cm^{-1}, of the Ethanol product sample and possible products, 1,2-propandiol, and 1,3-propandiol.

4.6.5 Suggested Mechanism

Considering the mechanism of the processes involved is not without its own challenges. It is clearly not the assumed process for the reduction of alcohols to alkanes given by eqn. 2.1.

$$R\text{-}OH + H^+ + 2e^- \rightarrow R\text{-}H + OH^- \quad (2.1)$$

When considering the mechanism several observations need to be accounted for:

- A reduction process is occurring, as evident from the cyclic voltammograms,
- the apparent presence of C-O bonds in the product, as evident from 1050 cm^{-1} transmittance peak in FT-IR spectra, and,
- the effect on the electrochemical reduction of the potential scan rate and the electrode rotation rate observed in the cyclic voltammetry studies.

Firstly, H_2 evolution was considered. This takes place throughout the cathodic potential range used in this work and is evident in some of the cyclic voltammograms by a large increase in the reductive current of the baseline of the voltammogram. H_2 will be produced as a gas collect in the headspace with the product gas sample. H_2 evolution occurs as follows:

$$Pb_{surf} + H_2O + e^- \rightarrow Pb_{surf}\text{–}H(ads) + OH^-(aq)$$

$$2Pb_{surf}\text{–}H(ads) \rightarrow Pb_{surf} + H_2(g)$$

Next, cyclic voltammetry studies confirmed the presence of a reduction process taking place at the electrode; being the reduction of ethanol as only observed when the alcohol is present. Ethanol reduction is represented by:

$$Pb_{BS} + CH_2CH_3OH + e^- \rightarrow Pb_{BS}\text{-}CH_2CH_3 + OH^-(aq)$$

The presence of the diol as the identified product for the ethanol system indicates that there must be a new C-O bond formed. The formation of this new C-O bond has two possibilities:

$$Pb_{BS}\text{-}CH_2CH_3 + H_2O \rightarrow Pb_{BS}\text{-}CH_2CH_2OH + H_2(g)$$

and/or

$$Pb_{BS}\text{-}CH_2CH_3 + H_2O \rightarrow Pb_{BS}\text{-}CH(OH)CH_3 + H_2(g)$$

Chapter 3 discusses the potential scan rate and electrode rotation rate dependencies and the deviation from the expected observations in RDE electrochemistry. These dependencies may be explained by the following steps:

Pb_{BS}-CH_2CH_2OH + Pb_{surf}-H(ads) → Pb_{surf} + CH_3CH_2OH(aq)

and/or

Pb_{BS}-$CH(OH)CH_3$ + Pb_{surf}-H(ads) → Pb_{surf} + CH_3CH_2OH(aq)

The more efficiently that H_2 is removed, the less prevalent the above processes, therefore Pb_{BS} are filled more readily. Increasing the electrode rotation rate would aid in the removal of the H_2(g), with less availability for the above process to occur. Therefore, less of the adsorbed species ($CH(OH)CH_3$ or CH_2CH_2OH) is removed from the electrode as CH_3CH_2OH, not providing free binding sites and leading to less reduction observed than at slower electrode rotation rates. An increase in the potential scan rate allows less time per scan for processes to occur leading to less of the above process being able to occur not providing free binding sites and therefore less reduction is observed.

As the product contains a longer carbon chain than the reactants a new C-C bond must also be forming. This could occur when two adsorbed species are in close proximity to each other or when ethanol is replenished at the surface of the electrode near an adsorbed species. New C-C bond formation may occur as follows:

$2Pb_{BS}–CH_2CH_2OH$

$$\rightarrow \quad Pb_{BS} \; + \; Pb_{BS}–CH_2\bullet \; + \; HOCH_2CH_2CH_2OH(aq)$$

and/or

$Pb_{BS}–CH(OH)CH_3 \; + \; Pb_{BS}–CH_2CH_2OH$

$$\rightarrow \quad Pb_{BS} \; + \; Pb_{BS}–CH_2\bullet \; + \; HOCH_2CH(OH)CH_3(aq)$$

and/or

$$Pb_{BS}–CH_2CH_2OH \; + CH_3CH_2OH \; \rightarrow \; Pb_{BS}–CH_2\bullet \; + \; HOCH_2CH_2CH_2OH(aq) \; + \; H^+$$

followed by the removal of the $CH_2\bullet$ from the electrode to return the electrode surface to its initial state for reproducible reductive peaks.

$Pb_{BS}–CH_2\bullet + H_2O \rightarrow Pb_{BS} + CH_3OH$

or

$Pb_{BS}\text{-}CH_2\bullet + HO\text{-}CH_2CH_3 \rightarrow Pb_{BS}\text{-}CH_2CH_2CH_2OH$

and

$Pb_{BS}\text{-}CH_2CH_2CH_2OH + H_2O \rightarrow Pb_{BS}\text{-}H_{ads} + HOCH_2CH_2CH_2OH(aq)$

The step involving the formation of the new C-C bond would likely be the rate determining step. This step would be slow due to the proposed isolated binding sites. If the binding sites on the electrode surface are spaced far apart the probability of two adsorbed species meeting and reacting is less. The formation of the C-C bond relies on the chance meeting of the two adsorbed species on two binding sites close enough together to be within the reaction diameter to occur.

If the proposed methyl radical is being removed from the Pb electrode to form methanol, it would be expected that an amount of methanol equivalent to the amount of diol would be being produced and would be present in the gas sample. However, there is no evidence of methanol being present in the FT-IR spectra recorded. It is possible that the evidence of the methanol is hidden under the peaks for the diol and the water. The presence of methanol could also be affecting the width of the peaks in the product IR spectra.

Methanol, if it is produced, does not reduce in these conditions as noted in Chapter 3. As it does not reduce, the methanol will not provide any further reaction and will not compete with any of the ethanol related reactions in the mechanism. To confirm that there would be no new products from methanol reduction affecting the observed peaks in the IR spectra of the product samples, cyclic voltammetry was run on the Pb plate - methanol system and gas FT-IR analysis was performed on the gas produced. There was no evidence of any methanol reduction product present in the recorded spectrum, with peaks observed only for water and CO_2, confirming that the gas sample produced is due to H_2 evolution only. This result confirms the lack of reduction of methanol in these conditions and suggests that there is a requirement of at least a two carbon chain for reduction to take place at the Pb electrode.

The suggested mechanism for the processes occurring in the electrochemical cell for the production of 1,3-propandiol from the initial electrochemical reduction of ethanol consistent with the discussed results and observations is outlined in Fig. 4.10.

Production of 1,3-propandiol:

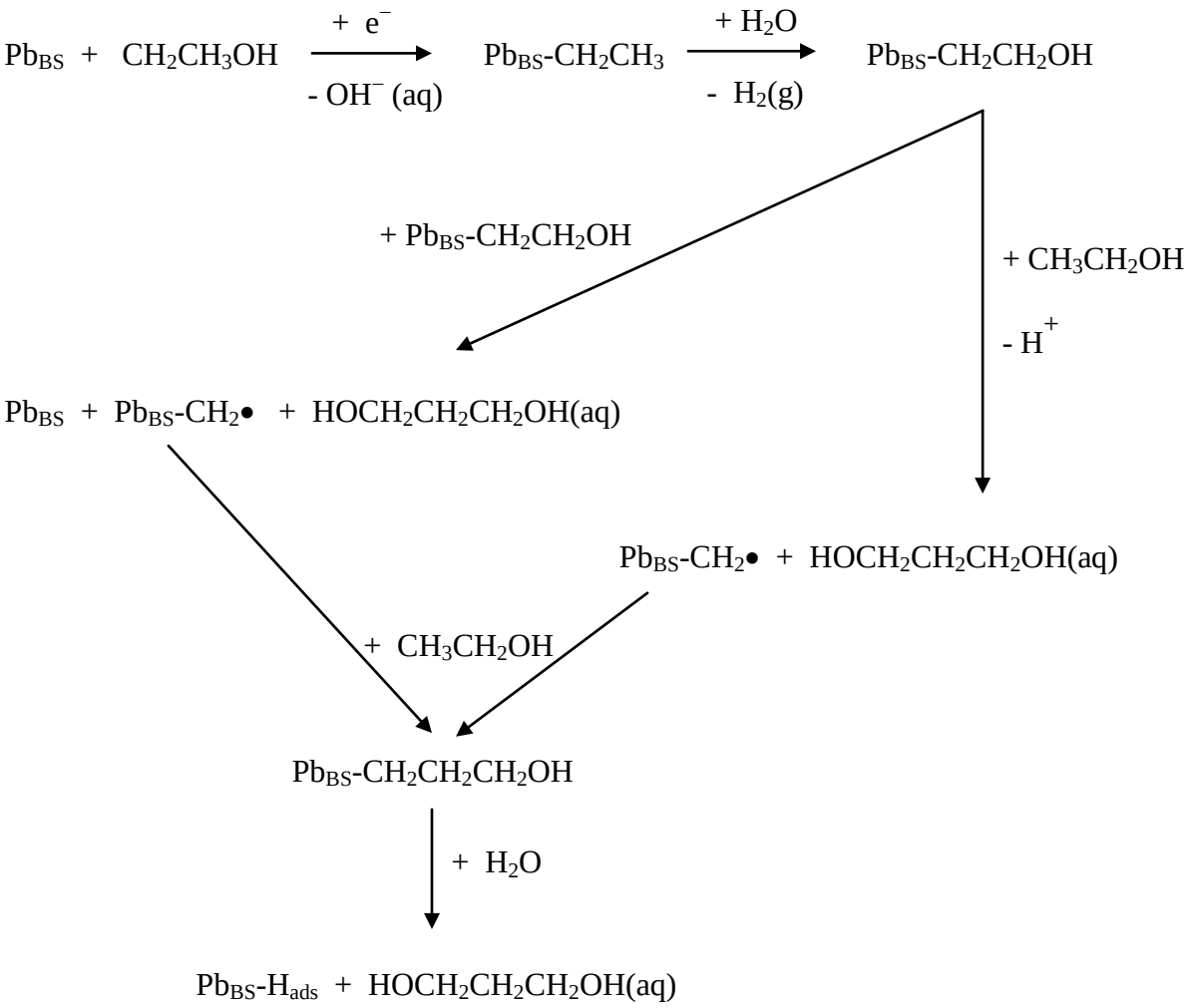

Hydrogen Evolution:

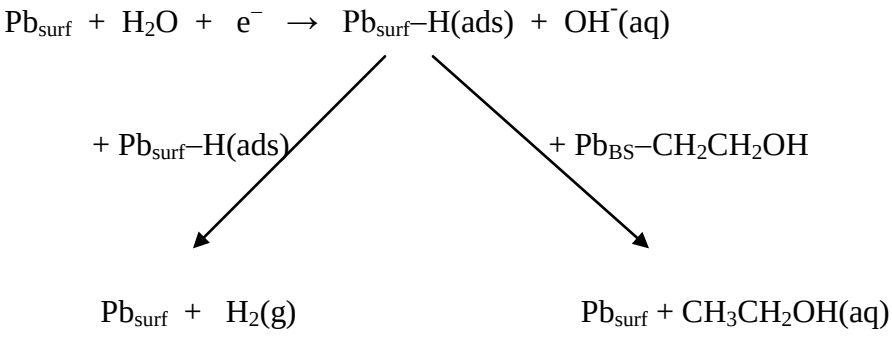

Fig. 4.10 Proposed Mechanism for the Pb-ethanol system, for the production of 1,3-propandiol.

4.7 Identification of Propanol Reduction Product

Propanol was also examined in the lead electrode system. The gaseous propanol product sample, collected and extracted as described in Section 4.6, was inserted through the septum into the gas IR cell. The FT-IR spectrum for this propanol product sample was collected with respect to a previously collected background. Figure 4.11 shows the FT-IR transmittance spectra for the propanol product sample and the reactants collected as explained in Section 4.7.2 for ethanol. Peaks assigned to CO_2 and H_2O are observed in these spectra as with the ethanol investigation. Peaks apparently associated with the product sample are observed in the 900 – 1200 cm^{-1} range (potentially four peaks in this range) and the 2800 – 3000 cm^{-1} range (potentially 3 peaks). Some comparisons are evident with the peaks in both spectra, however, the amount of transmittance observed for the reactants is much less than that of the product sample indicative of the sample spectrum being a good representation of the actual product spectrum with little influence from reactants.

In the case of the propanol investigation a larger concentration of sample was present in the cell than for the ethanol investigation. Therefore, interpretation of the spectra was improved. However there was still a significant water presence observed in the spectra, and consequently drying of the sample was attempted. As in the ethanol investigation, drying led to no significant improvement of the spectra, hence interpretation of the spectra in the absence of drying was continued.

Reference spectra and data for the possible products were examined as with the ethanol investigation. Again, hydrocarbons and ethers (propane, propene, hexane, hexene and dipropyl ether) were ruled out as possible products with a lack of peak-alignment with the product spectrum.

The proposed products for the propanol investigation were a possible mixture of 2,3-butandiol and 1,3-propandiol. Figure 4.12 shows the FT-IR spectra of the propanol product sample and the two proposed products. Ranges of peaks at 900 – 1200 cm^{-1} and 2800 – 3000 cm^{-1} are comparable across the two spectra. Figures 4.13 and 4.14 show the 900 – 1200 cm^{-1} and 2800 – 3000 cm^{-1} peaks respectively, in further detail.

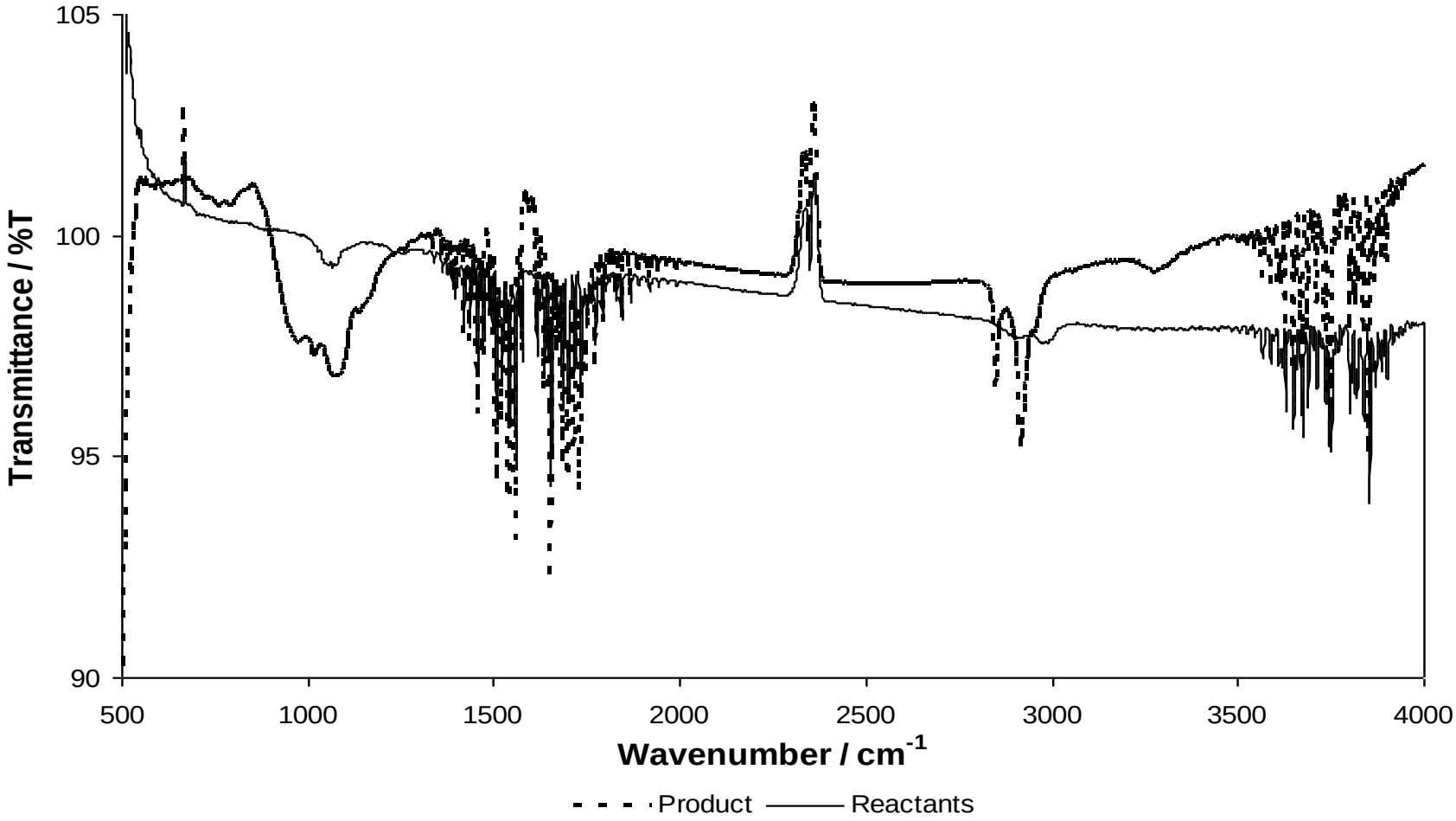

Fig. 4.11 FT-IR spectra for the reactants and products of the Pb–propanol system

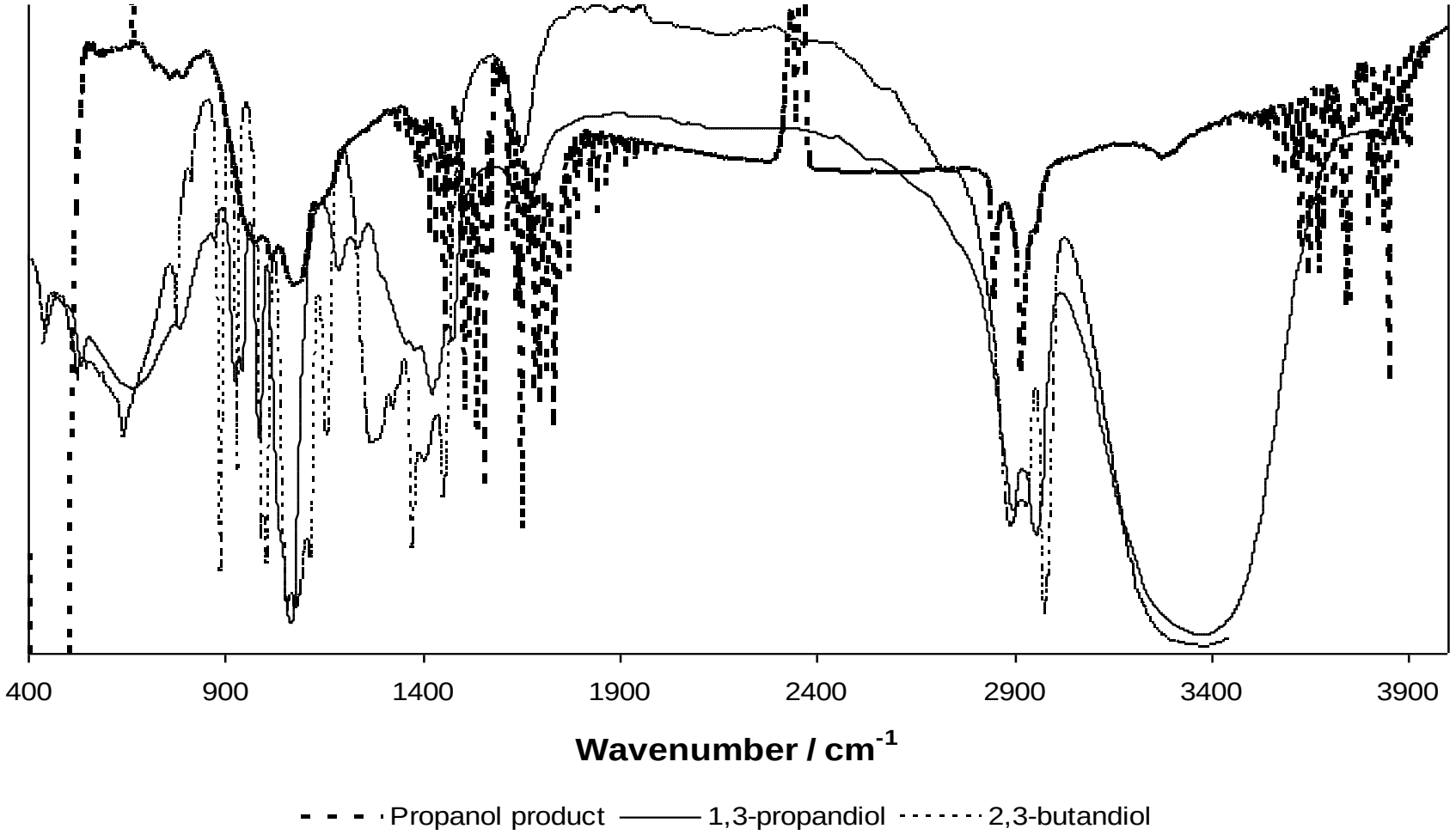

Fig. 4.12 FT-IR transmittance spectra of the Propanol product sample and the possible products, 2,3-butandiol, and 1,3-propandiol.

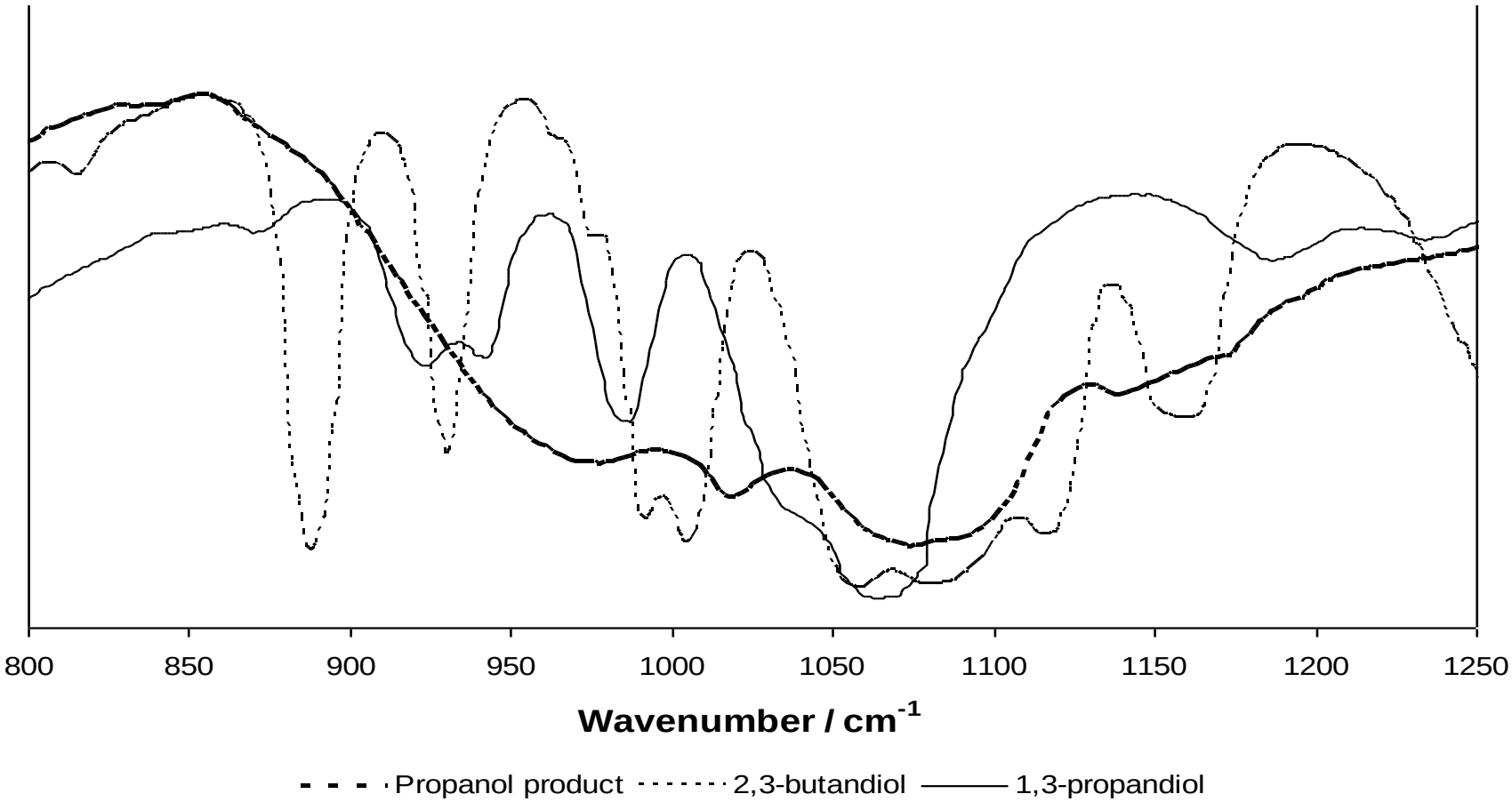

Fig. 4.13 FT-IR transmittance spectra, showing the peak at 1050 cm^{-1}, of the Propanol product sample and possible products, 2,3-butandiol, and 1,3-propandiol.

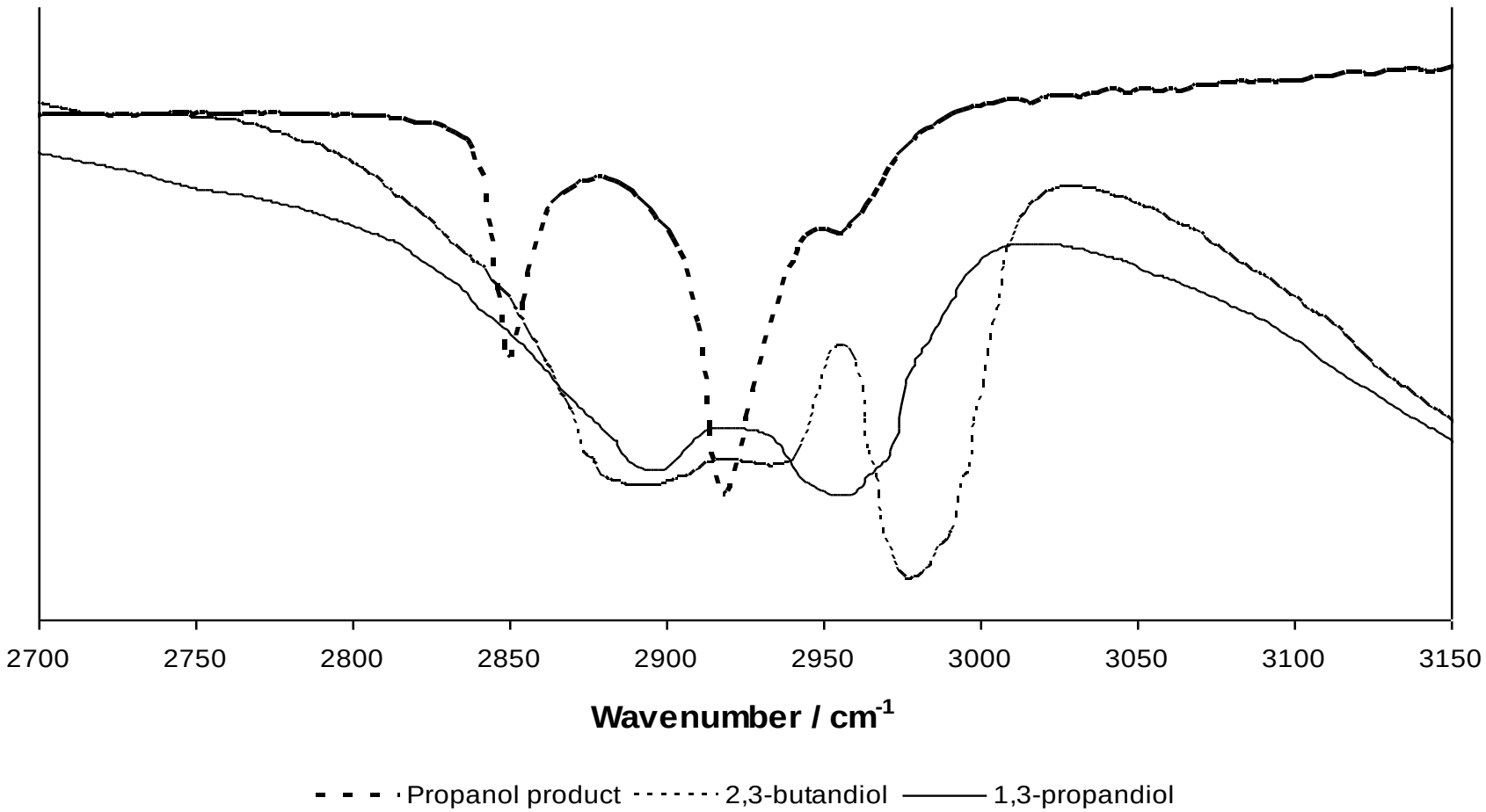

Fig. 4.14 FT-IR transmittance spectra, showing the peak at 2900 cm^{-1}, of the Propanol product sample and possible products, 2,3-butandiol, and 1,3-propandiol.

In Fig. 4.13 the peaks in the 900 - 1200 cm^{-1} range from the propanol product appear broader than the equivalent peaks for the suggested products, along with a possible 30 cm^{-1} shift in position. This broadening is not inconsistent with a heterogeneous sample where the products, 1,3-propandiol or 2,3-butandiol may be present in different phases, i.e. the presence of gaseous and liquid phases in contact. The reference spectra are from pure liquid samples of the possible products whereas the product sample is a gas mixture which may have water present. Muniz-Miranda et. al. reported that hydrogen bonding in mixtures effect the sharpness of the peaks observed in the IR spectra, where a mixture of the diol in water or some other solvent will have peaks slightly broader than the neat solution and can have a 20 cm^{-1} shift in wavenumber for the observed peaks.[76] The observed shift in position of the peaks is also observed in Fig.4.15 with the peaks in the 2800 – 3000 cm^{-1} range is approximately 30 cm^{-1} which could be partially attributed to this hydrogen bonding effect.

4.7.1 Suggested Mechanism

The proposed mechanism for the propanol processes is similar to that of the ethanol process, including H_2 evolution, alcohol reduction, formation of new C-O and C-C bonds, reaction with the $Pb_{surf}–H_{ads}$ and removal of alkyl radicals from the electrode.

H_2 evolution is occurring throughout the collection of the gaseous product:

$$Pb + H_2O + e^- \rightarrow Pb–H_{ads} + OH^-(aq)$$

$$2Pb–H_{ads} \rightarrow Pb + H_2(g)$$

Initial propanol reduction occurs on the cathodic sweep of the voltammograms:

$$Pb + CH_3CH_2CH_2OH + e^- \rightarrow Pb–CH_2CH_2CH_3 + OH^-(aq)$$

Suggested products from the interpretation of the FT-IR spectra are 1,3-propandiol and 2,3-butandiol. To form these products formation of specific C-O and C-C bonds are required.

To form 1,3-propandiol:

$$Pb\text{-}CH_2CH_2CH_3 + H_2O \rightarrow Pb\text{-}CH_2CH_2CH_2OH + H_2(g)$$

and

$Pb_{BS}–CH_2CH_2CH_2OH + H_2O \rightarrow Pb + HO–CH_2CH_2CH_2–OH(aq)$

To form 2,3-butandiol:

$Pb_{BS}\text{-}CH_2CH_2CH_3 + H_2O \rightarrow Pb_{BS}–CH_2CH(OH)CH_3 + H_2(g)$

and

$2Pb_{BS}–CH_2CH(OH)CH_3 \rightarrow 2Pb_{BS}–CH_2\bullet + CH_3CH(OH)CH(OH)CH_3$

Followed by:

$Pb_{BS}–CH_2\bullet + H_2O \rightarrow Pb + CH_3OH$

or

$Pb_{BS}–CH_2\bullet + HO–CH_2CH_2CH_3 \rightarrow Pb_{BS}–CH_2CH_2CH_2CH_2OH$

$Pb_{BS}–CH_2CH_2CH_2CH_2OH + H_2O \rightarrow Pb_{BS}–H_{ads} + HOCH_2CH_2CH_2CH_2OH(aq)$

However, there is no evidence that 1,4-butandiol or methanol are present.

Similar potential scan rate and electrode rotation rate dependence was observed in the propanol system as with ethanol. Again this dependence may be explained by the possible reaction with $Pb–H_{ads}$:

$Pb–CH_2CH_2CH_2OH + Pb–H_{ads} \rightarrow Pb + CH_3CH_2CH_2OH\ (aq)$

or

$Pb–CH_2CH(OH)CH_3 + Pb–H_{ads} \rightarrow Pb + CH_3CH_2(OH)CH_3\ (aq)$

A more effective removal of H_2 (larger rotation rate or scan rate) decreases the prevalence of this process and decreases the free binding sites available for reduction leading to less reduction occurring.

The suggested mechanism for the processes occurring in the electrochemical cell for the production of 1,3-propandiol and 2,3–butandiol from the initial electrochemical reduction of propanol consistent with the discussed results and observations is outlined in Fig. 4.15.

Production of 1,3–propandiol and 2,3–butandiol:

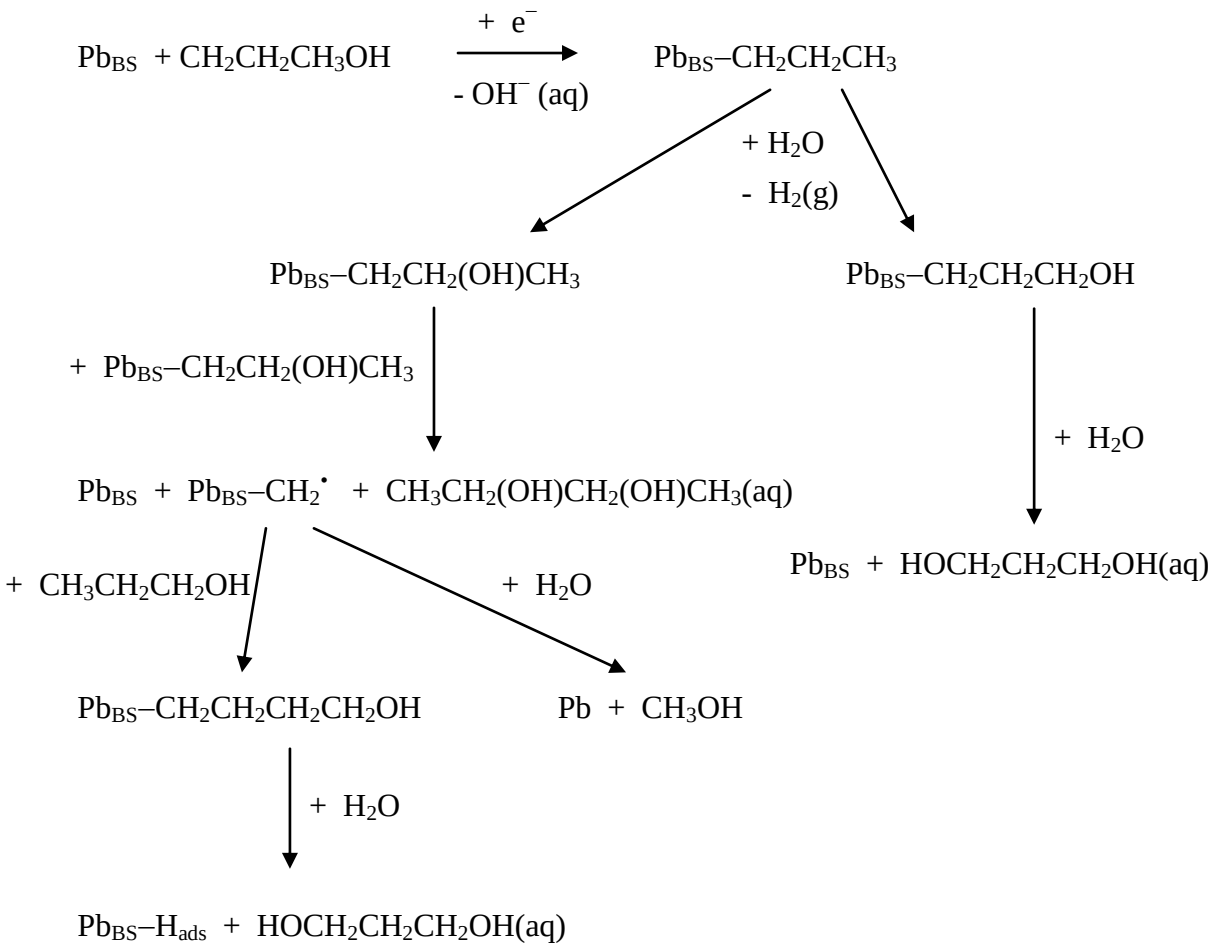

Hydrogen Evolution:

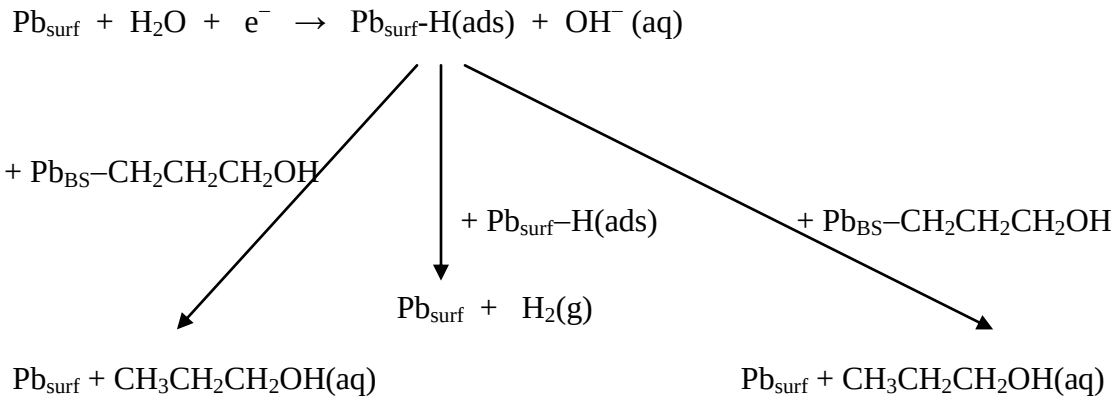

Fig. 4.15 Proposed Mechanism for the Pb-propanol system, for the production of 1,3-propandiol and 2,3-butandiol.

4.8 Identification of Propan-2-ol Reduction Product

The third alcohol examined in this lead electrode investigation was propan-2-ol. The gaseous propan-2-ol product sample, collected and extracted as described in Section 4.6, was inserted through the septum into the gas IR cell. The FT–IR spectrum for this propan-2-ol product sample was collected with respect to a previously collected background. Figure 4.16 shows the FT–IR transmittance spectra for the propanol product sample and for the reactants. Peaks assigned to CO_2 and H_2O are observed in these spectra as with previous investigations. Peaks apparently associated with the product sample are observed in the 900 – 1200 cm^{-1} range (potentially 4 peaks in this range) and the 2800 – 3000 cm^{-1} range (potentially 3 peaks). Some comparisons are evident with the peaks in both spectra; however, the peaks observed for the reactants are much smaller than that of the product sample indicative of the sample spectrum being a good representation of the actual product spectrum with little influence from reactants. It is noted here that the spectrum for the propan-2-ol product is near identical to that of the propanol product. The similarity of propan-2-ol to propanol is not inconsistent with the suggestion that the two systems are producing the same product.

For the propan-2-ol investigation there is a larger concentration of sample present in the cell as with the propanol investigation, and still a significant water presence observed in the spectra. Drying of the sample was attempted which lead to no significant improvement of the spectra. Interpretation of the spectra before drying was continued.

Reference spectra and data for the possible products were examined. As with the propanol investigation, hydrocarbons and ethers (propane, propene, hexane, hexane and dipropyl ether) were ruled out as possible products and the proposed products for the propanol investigation were a possible mixture of 2,3–butandiol and 1,3–propandiol as with propanol. Figure 4.17 shows the FT–IR spectra of the propanol product sample and the proposed products. Peaks in the ranges 900 – 1200 cm^{-1} and 2800 – 3000 cm^{-1} are comparable across the 2 spectra. Figures 4.18 and 4.19 show the 900 – 1200 cm^{-1} and 2800 – 3000 cm^{-1} peak ranges respectively, in further detail.

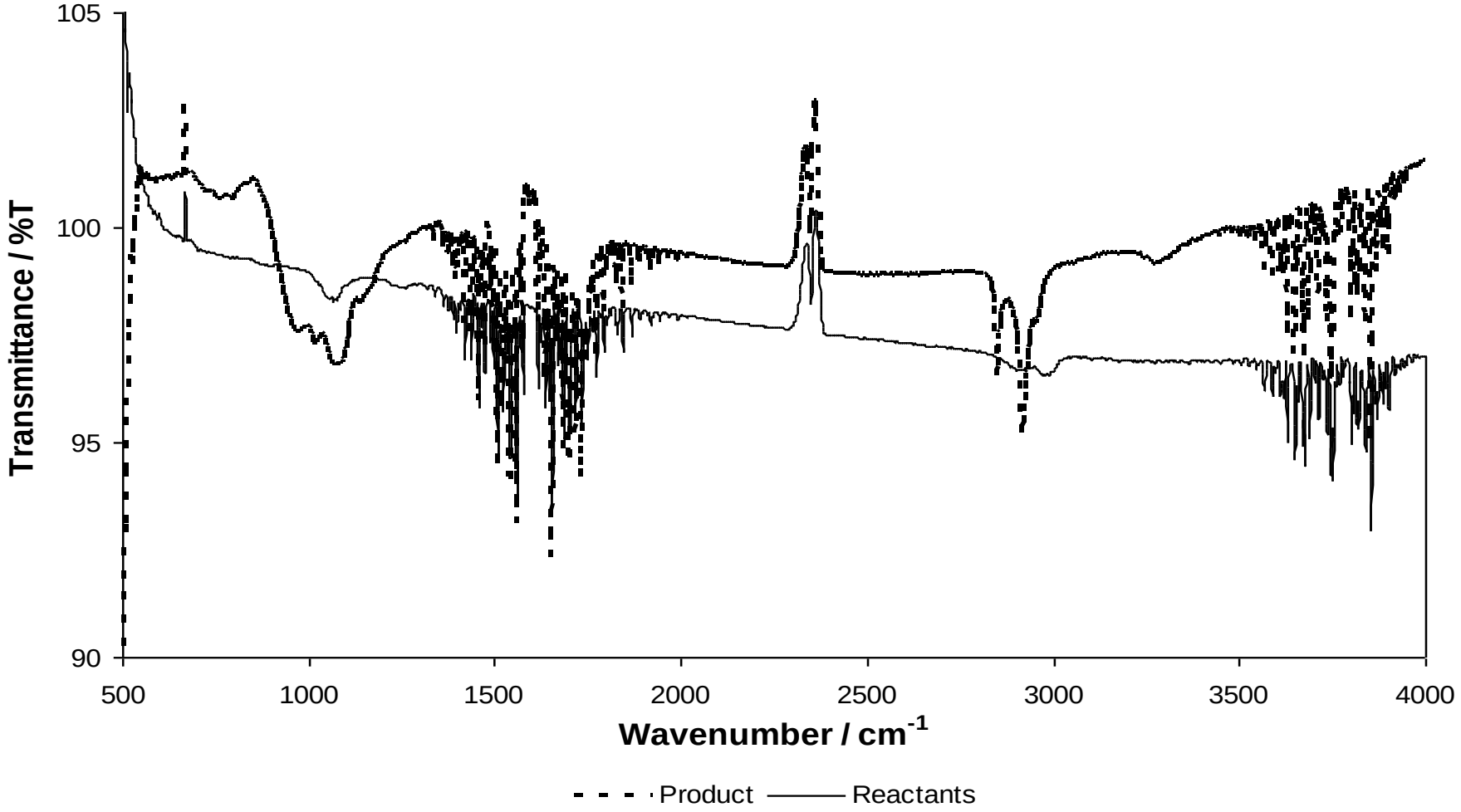

Fig. 4.16 FT–IR spectra for reactants and products of the Pb–propan-2-ol system

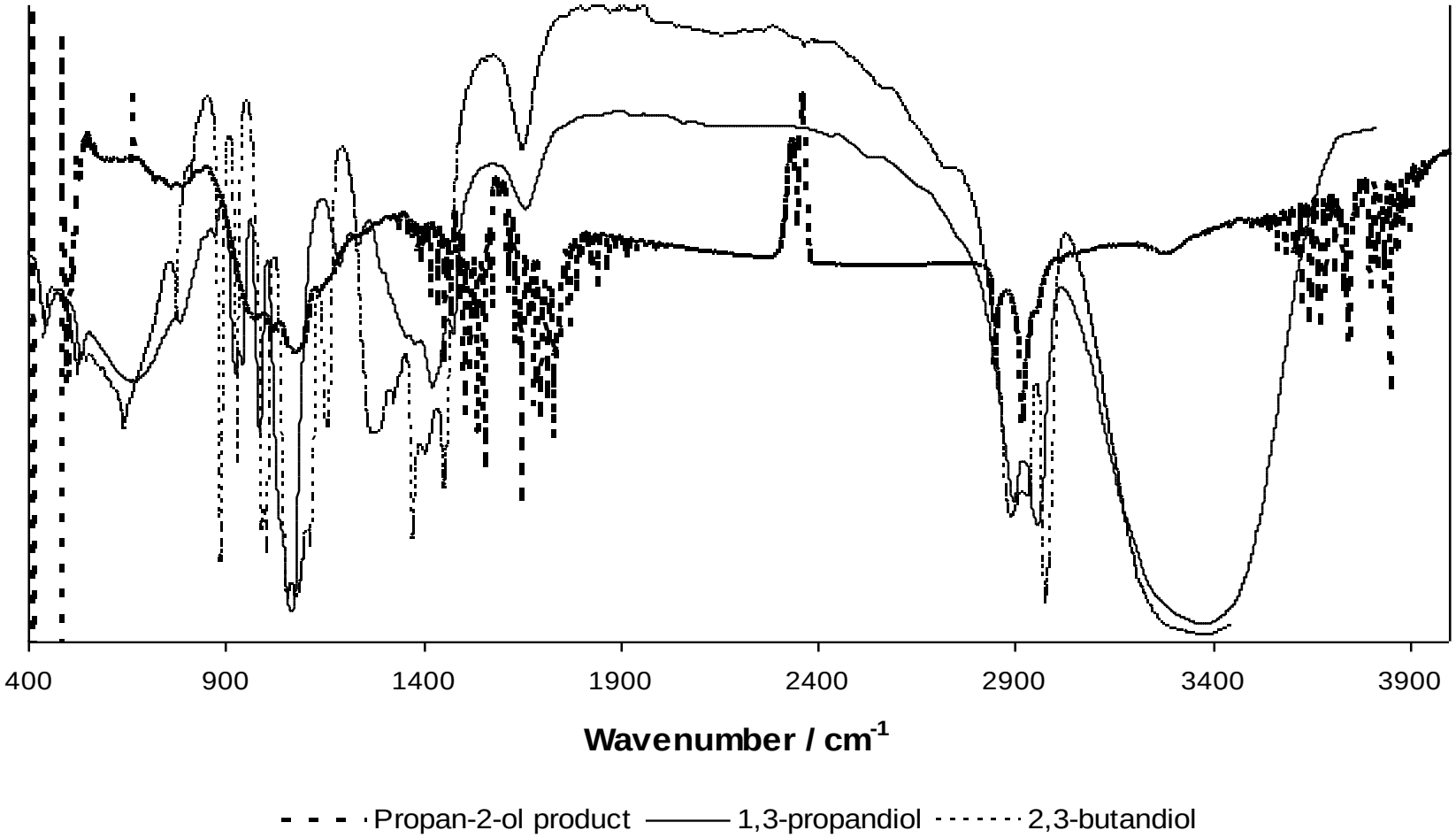

Fig. 4.17 FT–IR transmittance spectra of the Propan-2-ol product sample and the possible products, 2,3–butandiol, and 1,3–propandiol.

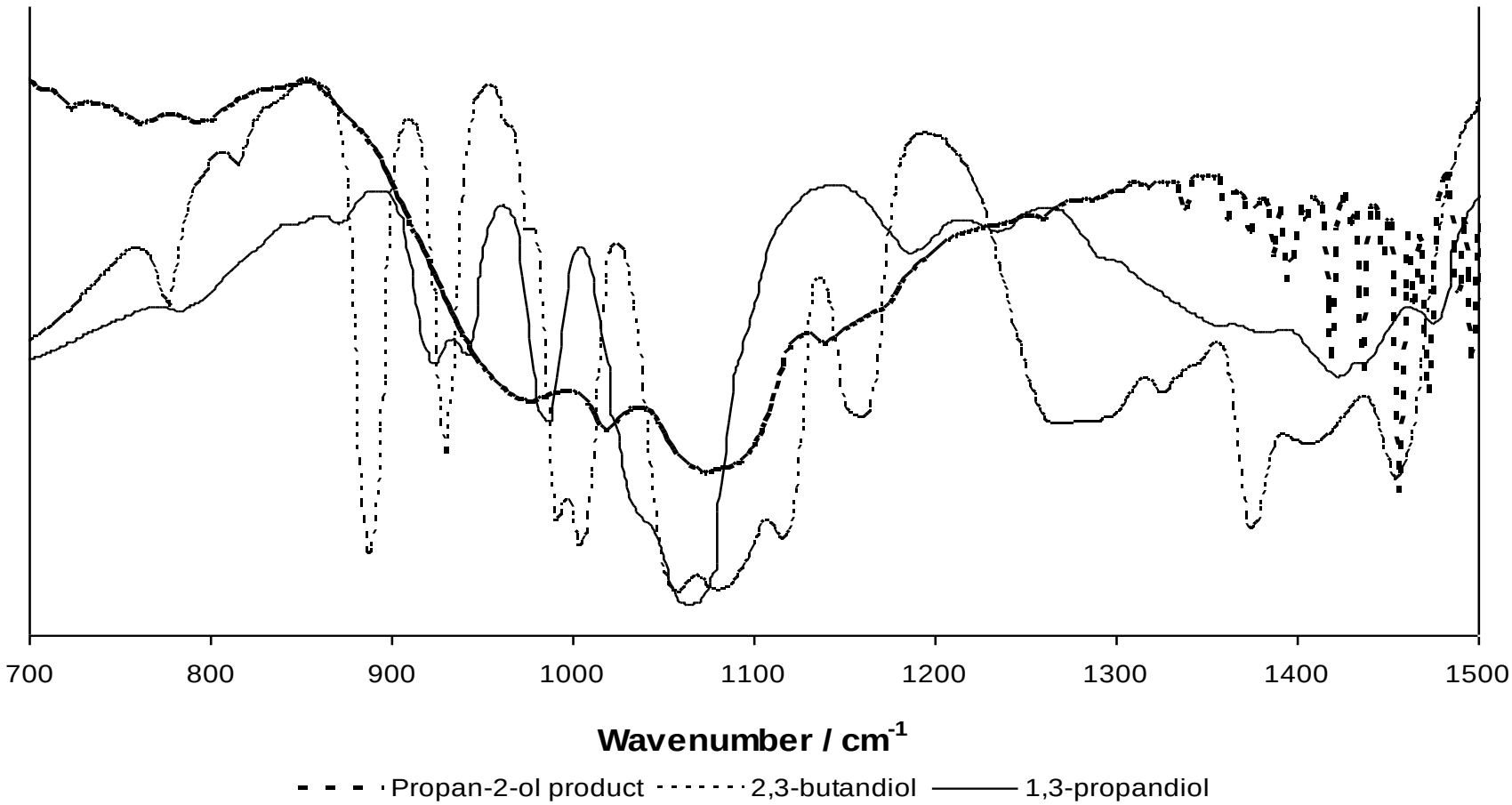

Fig. 4.18 FT-IR transmittance spectra, showing the peak at 1050 cm^{-1}, of the propan-2-ol product sample and possible products, 2,3–butandiol, and 1,3–propandiol.

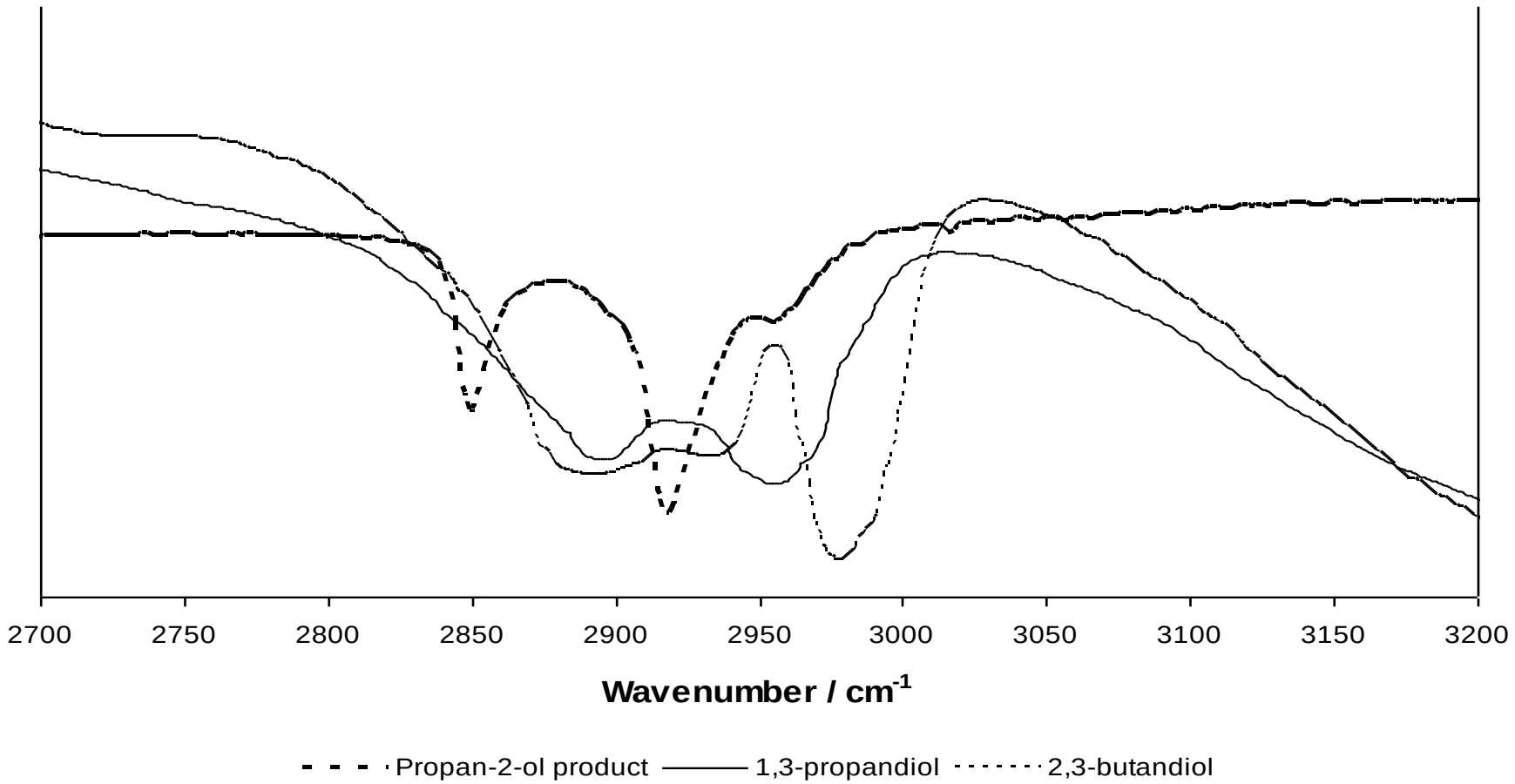

Fig. 4.19 FT–IR transmittance spectra, showing the peak at 2900 cm^{-1}, of the propan-2-ol product sample and possible products, 2,3–butandiol, and 1,3–propandiol.

In Fig. 4.18 the peaks in the 900 - 1200 cm^{-1} range from the propan-2-ol product appear broader than the equivalent peaks for the suggested products, along with a possible 30 cm^{-1} shift in position as was noted with the propanol spectra. The broadening of the peak is indicative of a heterogeneous sample where the products may be present in different phases and the shift in position is not uncommon due to the possibly different conditions surrounding the recording of the spectra and the possible hydrogen bonding effects as explained in section 4.8.[76] The observed shift in position of the peaks is also observed in Fig. 4.19 with the peaks in the 2800 – 3000 cm^{-1} range.

4.8.1 Suggested Mechanism

The mechanism for the propan-2-ol processes becomes considerably more complicated than that of the ethanol or propanol processes. The proposed product does not match the initial alcohol reduction step where it would be expected that the reduction of the alcohol would lead to the molecule being adsorbed to the electrode through the secondary carbon. The proposed mechanism as determined by the ethanol and propanol results would give the following steps for propan-2-ol:

H_2 evolution:

$$Pb + H_2O + e^- \rightarrow Pb{-}H_{ads} + OH^-(aq)$$

$$2Pb{-}H_{ads} \rightarrow Pb + H_2(g)$$

Alcohol reduction:

$$Pb + CH_3CH(OH)CH_3 + e^- \rightarrow Pb{-}CH(CH_3)CH_3 + OH^-(aq)$$

New C–O bond formation:

$$Pb{-}CH(CH_3)CH_3 + H_2O \rightarrow Pb{-}CH(CH_3)CH_2OH + H_2(g)$$

or

$$Pb{-}CH(CH_3)CH_3 + H_2O \rightarrow Pb{-}CH(CH_2OH)CH_3 + H_2(g)$$

or

$$Pb{-}CH(CH_3)CH_3 + H_2O \rightarrow Pb{-}CH(CH_3)(OH)CH_2CH_3 + H_2(g)$$

New C-C formation:

$Pb–CH(CH_3)CH_2OH + H_2O \rightarrow Pb + HO–CH_2CH(OH)CH_3$

or

$Pb–CH(CH_2OH)CH_3 + H_2O \rightarrow Pb + HO–CH_2CH(OH)CH_3$

or

$Pb–CH(CH_3)(OH)CH_3 + Pb–CH(CH_3)CH_2OH \rightarrow Pb + Pb–CH(CH_3)\bullet + HO–CH_2C(CH_3)(OH)CH_3$

And removal of the radical:

$Pb–CH(CH_3)\bullet + H_2O \rightarrow Pb + CH_3CH_2OH$

(which could go on to form 1,3-propandiol through the ethanol mechanism)

Potential reaction with $Pb\text{-}H_{ads}$:

$Pb–CH(CH_3)CH_2OH + Pb\text{-}H_{ads} \rightarrow Pb + CH_3CH_2CH_2OH$ (aq)

or

$Pb–CH(CH_2OH)CH_3 + Pb–H_{ads} \rightarrow Pb + HO–CH_2CH_2CH_3$ (aq)

or

$Pb–CH(CH_3)(OH)CH_3 + Pb–H_{ads} \rightarrow Pb + CH_3CH_2OHCH_3$ (aq)

However, when following this proposed mechanism for ethanol and propanol, adsorption of the alcohol to the electrode through the secondary carbon would produce 1,2–propandiol or 2–methyl–1,2–propandiol. 2–methyl–1,2–propandiol is not a possible product as determined by FT-IR spectroscopy, however, 1,2–propandiol could be part of the mixture of products including 1,3–propandiol and 2,3–butandiol. To explain the products determined by FT-IR there must be some form of rearrangement of the propan-2-ol to propanol. Either, when adsorbing to the electrode, or through the reaction with $Pb_{surf}–H_{ads}$ species. Propan-2-ol may rearrange when adsorbing (or while adsorbed) to the electrode, to a species adsorbed through a primary carbon rather than the secondary one. The reaction with the $Pb_{surf}–H_{ads}$ species returns propanol rather than propan-2-ol for two of the three possible reaction pathways. A rearrangement of propan-2-ol to propanol would lead to the products identified through the proposed propanol mechanism.

Therefore a mixture of 1,2−propandiol, 1,3−propandiol and 2,3−butandiol may be formed through the proposed propanol mechanism, Section 4.8.1. 1,2-propandiol could be formed by the propan-2-ol following a mechanism similar to propanol. 1,3−propandiol could be formed after rearrangement of propan-2-ol to propanol and then following the propanol mechanism or from the ethanol produced when removing the alkyl radical from the electrode. 2,3−butandiol could be formed after a rearrangement of propan-2-ol to propanol and following the propanol mechanism.

Therefore the mechanism would have 3 different pathways:

H_2 evolution occurs continuously and is present in all 3 pathways:

$$Pb + H_2O + e^- \rightarrow Pb{-}H_{ads} + OH^-(aq)$$

$$2Pb{-}H_{ads} \rightarrow Pb + H_2(g)$$

1.) Producing 1,2−propandiol:

Alcohol reduction:

$$Pb + CH_3CH(OH)CH_3 + e^- \rightarrow Pb{-}CH(CH_3)CH_3 + OH^-(aq)$$

New C-O bond formation:

$$Pb{-}CH(CH_3)CH_3 + H_2O \rightarrow Pb{-}CH(CH_3)CH_2OH + H_2(g)$$

or

$$Pb{-}CH(CH_3)CH_3 + H_2O \rightarrow Pb{-}CH(CH_2OH)CH_3 + H_2(g)$$

1,2−propandiol formation:

$$Pb{-}CH(CH_3)CH_2OH + H_2O \rightarrow Pb + HO{-}CH_2CH(OH)CH_3$$

or

$$Pb{-}CH(CH_2OH)CH_3 + H_2O \rightarrow Pb + HO{-}CH_2CH(OH)CH_3$$

2.) Producing 1,3−propandiol:

Alcohol reduction:

$$Pb + CH_3CH(OH)CH_3 + e^- \rightarrow Pb{-}CH(CH_3)CH_3 + OH^-(aq)$$

Rearrangement of adsorbed species:

$$Pb{-}CH(CH_3)CH_3 \rightarrow Pb{-}CH_2CH_2CH_3$$

(then follows the propanol mechanism (Fig. 4.15))

New C–O bond formation:

$Pb–CH(CH_3)CH_3 + H_2O \rightarrow Pb–CH(CH_3)CH_2OH + H_2(g)$

or

$Pb–CH(CH_3)CH_3 + H_2O \rightarrow Pb–CH(CH_2OH)CH_3 + H_2(g)$

Potential reaction with Pb-H_{ads}:

$Pb–CH(CH_3)CH_2OH + Pb–H_{ads} \rightarrow Pb + CH_3CH_2CH_2OH\ (aq)$

or

$Pb–CH(CH_2OH)CH_3 + Pb–H_{ads} \rightarrow Pb + HO–CH_2CH_2CH_3\ (aq)$

(then follows the propanol mechanism (Fig. 4.15))

3.) Producing 2,3–butandiol:

Alcohol reduction:

$Pb + CH_3CH(OH)CH_3 + e– \rightarrow Pb–CH(CH_3)CH_3 + OH^-(aq)$

Rearrangement of adsorbed species:

$Pb–CH(CH_3)CH_3 \rightarrow Pb–CH_2CH_2CH_3$

(then follows the propanol mechanism (Fig. 4.15))

New C–O bond formation:

$Pb–CH(CH_3)CH_3 + H_2O \rightarrow Pb–CH(CH_3)CH_2OH + H_2(g)$

or

$Pb–CH(CH_3)CH_3 + H_2O \rightarrow Pb–CH(CH_2OH)CH_3 + H_2(g)$

Potential reaction with Pb-H_{ads}:

$Pb–CH(CH_3)CH_2OH + Pb–H_{ads} \rightarrow Pb + CH_3CH_2CH_2OH\ (aq)$

or

$Pb–CH(CH_2OH)CH_3 + Pb–H_{ads} \rightarrow Pb + HO–CH_2CH_2CH_3\ (aq)$

(then follows the propanol mechanism (Fig. 4.15))

These possible mechanisms are shown in Fig. 4.20

1.) Producing 1,2−propandiol:

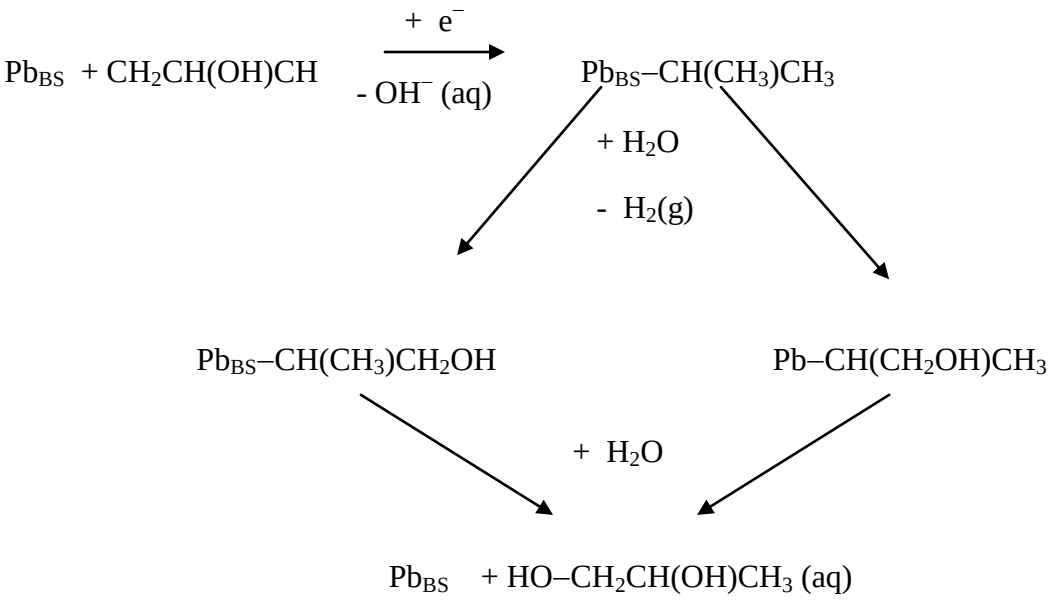

2.) Producing 1,3−propandiol:

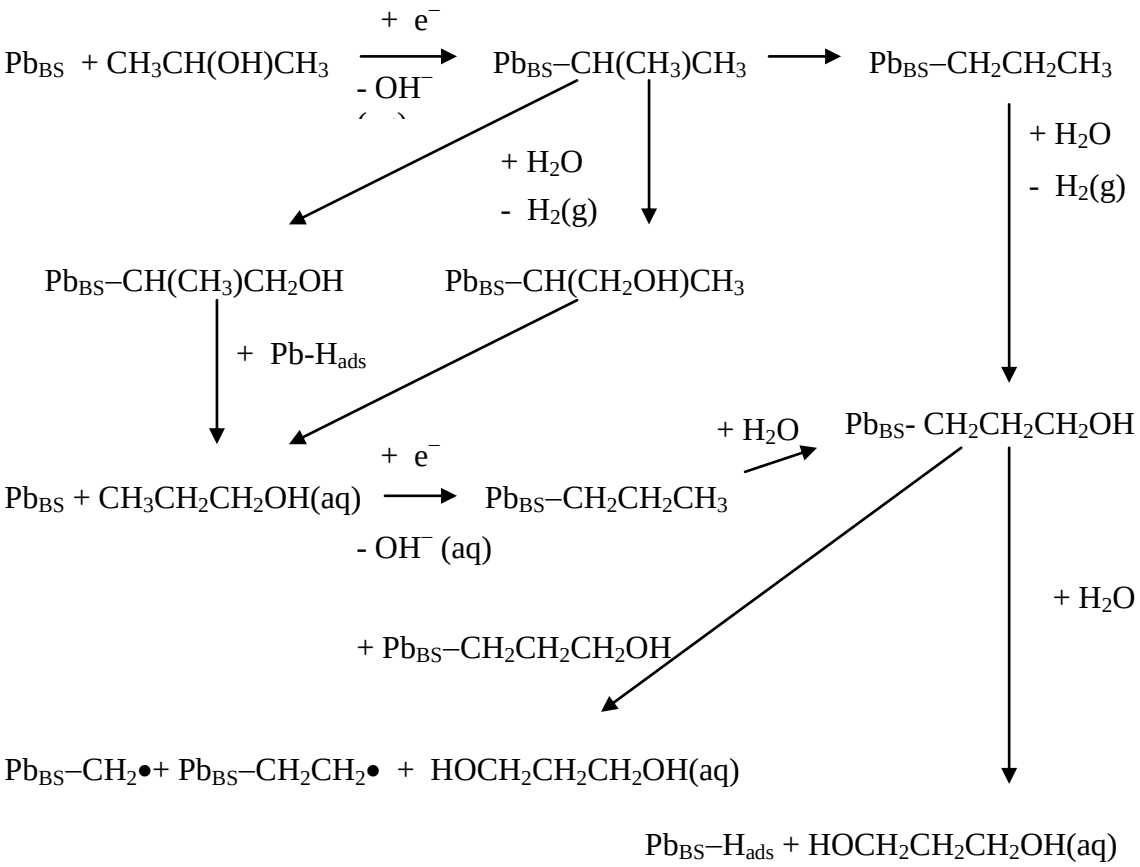

Fig. 4.20 Proposed Mechanism for the Pb−propanol system. 1.) 1,2−propandiol production, 2.) 1,3−propandiol production,

3.) Producing 2,3–butandiol:

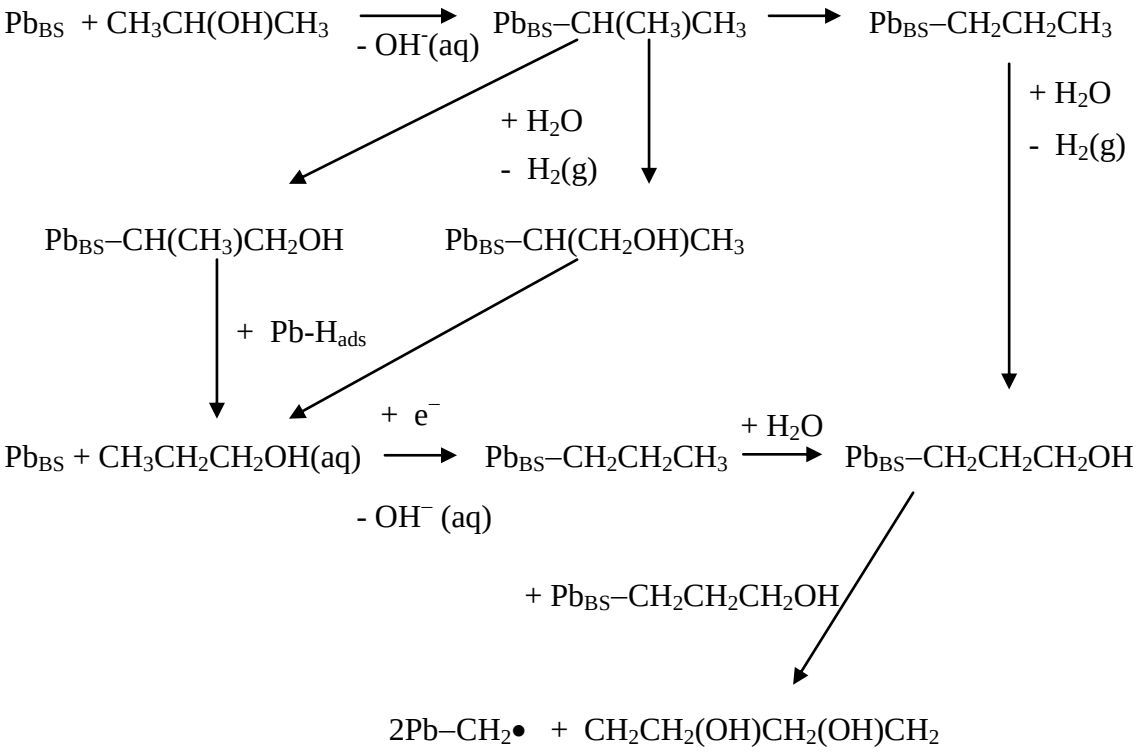

4.) Hydrogen Evolution:

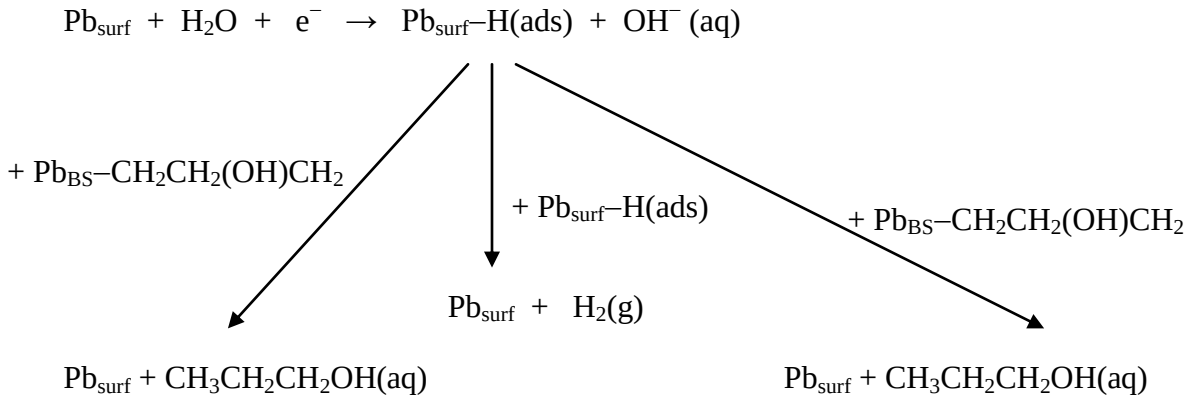

Fig. 4.20 continued Proposed Mechanism for the Pb–propanol system. 3.) 2,3–butandiol production and 4.) H_2 evolution.

4.9 Insulating Layer Thickness

Based on the calculations discussed in Chapter 3 (Section 3.6.4.1) the thickness of the proposed insulating layer can be calculated for these new proposed products. In chapter 3 the product was assumed to be the corresponding alkane (ethane or propane), however, with FT-IR spectroscopy product identification as discussed in this chapter the product is evidently not the alkane. Therefore the thickness of the insulating layer produced on the RDE calculated in Chapter 3, section 3.6.4.1, was reconsidered with the new identified diol product(s).

The proposed product for the Pb-ethanol pH 8.1 system, 1,3–propandiol, has a density of 1.053 g mL^{-1} at 25ºC, and a molar mass of 76.09 g mol^{-1}. The charge of the peak produced in one scan with the RDE was found to be 24.5°C. The moles of product, *n*, produced in one scan can be calculated from the charge, *Q*, using eqn. 3.11,

$$n = Q / zF \qquad (3.11)$$

The moles of product produced in one scan with the Pb RDE in the presence of ethanol was calculated to be 1.26×10^{-10} mol.

The mass of product produced can now be calculated from *n* using eqn. 3.13,

$$m = n\,M_r \qquad (3.13)$$

and was found to be 9.66×10^{-9} g. From this mass of product the volume of the proposed layer can be calculated using eqn. 3.14,

$$V = m / \rho \qquad (3.14)$$

found to be 9.17×10^{-9} mL. The layer forming on the RDE is considered to be of cylindrical shape and the volume of a cylinder is expressed by eqn 3.15,

$$V = \pi r^2 h \qquad (3.15)$$

where *V* is still the volume of the layer produced in mL, *r* is the radius of the RDE in cm and *h* is still the thickness of the layer. Hence, the thickness of the layer, *h*, can be calculated by rearranging eqn 3.13 to give eqn 3.14,

$$h = V / \pi r^2 \qquad (3.16)$$

Therefore the thickness of the insulating layer for the new ethanol product, 1,3–propandiol, was calculated to be 0.47 nm. The proposed insulating layer thickness

was also calculated for the propanol and propan-2-ol systems. As there is considered to be a mixture of products, the calculated thickness is only an estimation based on the average of the thickness calculated for each possible product, the actual thickness will depend on the amount of each of the products present and their orientation on the surface. The proposed products for both the Pb–Propanol and Pb–Propan-2-ol systems were 1,2–propandiol, 1,3–propandiol and 2,3–butandiol, (ρ = 1.036, 1.053 and 1.010 g mL^{-1}, and M_r = 76.09, 76.09 and 90.80 g mol^{-1} respectively). The proposed insulating layer thickness for the propanol system was approximately 0.50 nm and for the propan-2-ol system approximately 0.60 nm.

4.10 Summary

The products for the lead electrode systems were examined using a large surface area Pb plate as the WE and completing cyclic voltammetry scans continuously for a period of 6–8 hours to generate a larger volume of product for analysis. The gaseous product was collected in a headspace above the WE for analysis.

Mass spectrometry was attempted for the purpose of product identification of the system however, the small volume of sample for analysis provided little response in the mass spectrum, proving difficult to interpret and Mass Spectrometry was unsuccessful. FT–IR spectroscopy proved more successful for product identification using a 200 mL gas IR cell. Some absorption of the product sample was observed and the spectra could be interpreted.

The FT–IR spectroscopy had its challenges including the small sample volume and hence low concentration in the cell, the presence of significant amounts of water in the sample, the size of the gas IR cell and the peak intensity in the spectra. Possible solutions to some of these problems were suggested and discussed allowing for improvement in the results.

The proposed product from the FT–IR analysis for the Pb-ethanol system was 1,3–propandiol. Proposed products for the Pb–propanol and Pb–propan-2-ol systems were a mixture of 1,2–propandiol, 1,3–propandiol and 2,3–butandiol.

An insulating layer thickness for each product was determined. The insulating layer thickness was determined to be approximately 0.47 nm for the ethanol product and 0.50

and 0.60 for the propanol and propan-2-ol products respectively. As the propanol and propan-2-ol systems appear to be producing a mixture of products this insulating layer thickness is only an estimate calculated as an average of the insulating layer calculated for each of the possible products and the actual thickness will ultimately depend on the amount of each product present and their orientation.

A mechanism was proposed for the formation of these products. The proposed mechanism considered information obtained from the cyclic voltammetry discussed in Chapter 3 along with information obtained from the FT−IR product identification discussed in this chapter. The cyclic voltammetry results provided evidence of H_2 evolution present at the cathodic end of the potential range used for the cyclic voltammograms, and alcohol reduction indicated by the formation of the peak on the cathodic sweep of the cyclic voltammograms. Along with this the cyclic voltammetry investigations also showed an effect due to the variation of the potential scan rate and electrode rotation rate counter to what would be expected in RDE electrochemistry, which must be considered in the mechanism. The FT−IR analysis suggested products from the Pb−alcohol systems that required the formation of both C−O and C−H bonds throughout the processes involved. The proposed mechanism therefore involves H_2 evolution, an alcohol reduction step followed by the formation of a new C−O bond and then the new C−C bond. A competing reaction was suggested involving the adsorbed H species that could explain the interesting rotation rate− and scan rate−dependence. At increasing rotation rates or scan rates less of the reaction with the adsorbed H species can occur, decreasing the amount of free binding sites becoming available and leading to less reduction observed.

Chapter 5

Conclusions

5.1 Electrochemical Processes of Simple Alcohols

Several electrode materials and electrolyte solutions were tested with cyclic voltammetry to establish suitable conditions for the possible electrochemical reduction of range of low molecular weight alcohols. Evidence of a reproducible reductive response in the presence of ethanol in the supporting electrolyte was established for the three electrode materials, Pb, Cu and Sn, in two of the supporting electrolytes examined; 0.1 M phosphate buffer solutions, pH 7.3 and 8.1. The effect of anodic limit, concentration, potential scan rate and electrode rotation rate was examined. A product identification process was followed for establishing a likely product for the novel Pb electrochemistry.

5.2 Copper Electrode

The electrochemistry of a Cu RDE electrode in a pH 8.1, 0.1 M phosphate buffer electrolyte in the presence of ethanol, propanol, propan-2-ol and butanol was assessed. A reductive limiting current plateau was observed in the presence of the alcohols indicating the electrochemical reduction of the alcohol. The limiting current plateau observed is evident of behaviour expected when employing rotating disc electrochemistry techniques under conditions of mass-transport control. An initial increase of current was observed due to electron-transfer control, followed by a limiting current when the surface concentration of the electroactive species (in this case the alcohol) becomes zero. The plateau was reproducible with cycling and the anodic potential limit for the cyclic voltammogram had no significant effect on the limiting current plateau.

An increase in the bulk alcohol concentration caused an increase in the limiting current produced as anticipated for a system under mass-transport control. An increase in concentration provides a larger amount of electroactive species available to travel to the surface of the electrode allowing for a larger current to be produced. The potential

scan rate was increased through the range 10–200 mV s^{-1} with little change to the size of the limiting current produced. However, a very small trend was noted of increasing I_L with increasing scan rate. This is predominantly consistent with mass-transport control with some indications that there may also be some kinetic control.

Increasing the electrode rotation rate created an increase in the observed limiting current produced. In rotating disc electrochemistry a continual replenishment of analyte to the surface is produced by the laminar flow of electrolyte induced by the rotating disc allowing continual reduction leading to an observed limiting current. As the electrode rotation rate is increased, a greater rate of flow of electrolyte is induced; increasing the rate analyte is replenished to the surface of the electrode and hence increasing the reductive limiting current. As the electrode rotation rate is increased the Nernst diffusion layer thickness is decreased and diffusion can take place at an increased rate.

The Koutecky-Levich model considers a mixed control region where the current may be controlled by both electron transfer and mass transport.[47] The Koutecky-Levich model states that a plot of $1/I$ as a function of $1/\omega^{1/2}$ will provide a linear relationship for these situations. The data obtained provided a linear relationship and the intercept and slope of this linear relationship were used to calculate the electron transfer constant, k_f, and the diffusion coefficient, D, for each alcohol at the four bulk concentrations examined.

The calculated values for D across the four alcohols at each concentration were similar; however, there was an apparent increase in D with increasing bulk alcohol concentration observed. There is approximately 35 % increase in D when the bulk alcohol concentration is approximately doubled and approximately 55 % increase when the bulk alcohol concentration is approximately tripled. At 10 mM bulk alcohol concentrations the four alcohols the calculated values for D were within a small range of (1.04–1.17) x 10^{-9} m^2 s^{-1}. This value is lower than the values for the diffusion coefficient of ethanol in water reported in the literature; 1.6 x 10^{-9} m^2 s^{-1}.[67] However, as the bulk concentration of the alcohol was increased the value of D approaches this literature value, at 20 mM bulk alcohol concentration the four alcohols diffusion coefficients were within the small range of (1.41–1.53) x 10^{-9} m^2 s^{-1}.

A considerable variation is noted in the k_f values for the four alcohols with no apparent trend to the variation. The calculated values of k_f, ranging (0.91 – 2.37) x 10^9 m s^{-1} for the four bulk alcohol concentrations for the four alcohols. Further investigations would be necessary to fully interpret the mass transport and kinetic control of the processes.

The observations from the cyclic voltammetry and the Koutecky–Levich model are not inconsistent with the possible production of the corresponding alkanes for each alcohol, however, they do not provide any evidence of any particular product. Therefore, due to the observed dependencies it can only be assumed that ethanol was reduced to ethane, propanol and propan-2-ol to propane and butanol to butane.

5.3 Tin Electrode

A reductive response was observed at the Sn RDE in 0.1 M phosphate buffers at pH 7.3 in the presence of ethanol, propanol and propan-2-ol. No reduction was observed for methanol or butanol within the conditions of the cyclic voltammetry in this work. In these Sn systems, a reproducible reductive peak was observed to form at approximately –1.1 V. The formation of this peak was indicative the reduction being unable to be sustained (as it was on Cu electrodes) and the possible presence of an insoluble product forming an insulating layer on the surface of the electrode, inhibiting further reduction.

Increasing the concentration of the alcohol; ethanol, propanol or propan-2-ol, had no significant effect on the total charge of the peak, C2, produced. This supported the proposal that the reduction process was being progressively inhibited by the formation of an insoluble insulating layer. Increasing the potential scan rate of the experiment also showed no significant effect on the total charge produced from peak C2. The peak, C2, showed scan rate-independence across all bulk alcohol concentrations tested. Therefore, irrespective of the bulk concentration of the alcohol in the system and the potential scan rate applied to the system, (in the range 10 – 200 mV s^{-1}), the same amount of material appeared to be reducing and forming on the surface.

Increasing the electrode rotation rate typically increases the amount of reduction; the increase in rotation aids the removal of any product at the surface of the electrode and

replenishes the analyte to the surface at a greater rate. However, this was not the case when increasing the electrode rotation rate of the Sn disc electrode. The peak size, and hence the charge associated with the peak, remained similar with increasing electrode rotation rate. Values of N_{C2} for the ethanol experiments were within the range $(0.9–1.2) \times 10^{19}$ molecules m^{-2} and those for the propanol and propan-2-ol experiments within the range $(0.5–0.9) \times 10^{19}$ molecules m^{-2}. This was not inconsistent with the proposed formation of an insulating layer being formed. As the electrode rotation rate increases the flow rate of the electrolyte toward the electrode surface increases therefore replenishing analyte at the electrode surface at a greater rate. If the reduced product remains on the surface of the electrode as an insulating layer the continuation of reduction is inhibited regardless of how much analyte is provided to the surface. Therefore, the amount of reduction observed was restricted by the size of the electrode and the maximum amount of reduction was reached when the surface of the electrode was sufficiently covered by the insulating layer.

A simple, single step, two electron process leading to the reduction of alcohols to alkanes was initially assumed. There was no evidence within the experiments performed for the production of a more complicated product, and the formation of alkanes, not typically soluble in water, could form an insoluble product layer on the surface of the electrode. Therefore, it was assumed that the electrochemical reduction of alcohols on Sn electrodes in 0.1 M phosphate buffer electrolytes at pH 7.3 results in the production of alkanes. The electrochemical reduction of ethanol produces ethane, and that of propanol and propan-2-ol produces propane. However, if these alkanes are being produced, they would typically be present as gases at 25°C. Therefore, if alkanes were the products they would have to be adsorbed strongly (chemisorbed) to the electrode to produce an insulating layer.

The thickness of the proposed insulating layer forming was calculated. For the ethanol investigation the thickness of the proposed layer was calculated to be approximately 0.30 nm, and for the propanol and propan-2-ol investigations approximately 0.45 nm.

5.4 Lead Electrode

A reductive response was observed at the Pb RDE in 0.1 M phosphate buffers at pH 8.1 in the presence of ethanol, propanol and propan-2-ol. No reduction was

observed for methanol or butanol with the Pb RDE within the conditions of the cyclic voltammetry of this work. A reductive peak was observed to form at approximately –0.9 V, evident of the reduction being unable to continue and indicating the possible presence of an insoluble product forming an insulating layer on the surface of the electrode, inhibiting further reduction. This was similar to that found for tin electrodes.

Increasing the bulk alcohol concentration had no effect on the total charge produced; this is consistent with the reduction process being progressively stifled through the formation of a close packed insulating layer of reaction product. Regardless of how much analyte is available, reduction is still inhibited. However, several other conditions did have an effect on the amount of material being reduced.

The anodic limit of the cyclic voltammogram had an interesting effect on the processes occurring at the electrode. There was a change in the cathodic wave of the cyclic voltammograms observed between the anodic limit of –0.65 V and –0.70 V where the reductive peak became substantially smaller and no longer reproducible. The absence of an accompanying oxidative wave with any if the anodic limits investigated suggested an irreversible reaction. Some inhibition of reduction on the electrode surface appeared to be present with anodic limits $E < -0.7$ V, and absent for those with anodic limits $E > -0.65$ V. Potential hold experiments suggested the reproducibility of the peak at anodic limits $E < -0.7$ V had a time-dependent nature and by allowing enough time for the layer to be removed the reductive peak was obtained reproducibly in subsequent scans. However, the size of the peak exhibited a time-independent nature and the magnitude of the reductive current produced was less at more negative potentials.

The electrode rotation rate of the RDE also had an effect on the reduction processes occurring. There was a progressive decrease in the observed peak size as the rotation rate was increased. Increasing the rotation rate appeared to promote an insulating reduction product at the electrode. This anomaly in the rotation rate dependence suggested that the facilitated replenishment of the alcohol at the surface of the electrode may promote a second non-electrochemical process responsible for the formation of the insulating layer.

FT-IR spectroscopy identified possible products:

- 1,3-propandiol for the Pb-ethanol system,
- 2,3-butandiol and 1,3-propandiol for the Pb-propanol system and
- 2,3-butandiol, 1,3-propandiol and 1,2-propandiol for the Pb-propan-2-ol system.

Formation of these diol products cannot arise from a reduction process alone. This is despite the electrochemistry clearly showing an overall reduction process was taking place. The presence of a reduction process and evidence of a non-reduction product supported the suggested two step process involving an electrochemical reduction step, producing an adsorbed intermediate, followed by a non-electrochemical step to obtain the final product as discussed in sections 3.6.6 and 4.7.5.

Broader FT–IR peaks than the peaks for suggested products and the possible 30 cm^{-1} shift in position were observed for the propanol and propan-2-ol spectra. The broadening of the peak is indicative of a heterogeneous sample of products present in different phases and the shift in position is not uncommon due to possible hydrogen bonding effects between the alcohol groups of the product.[76]

The thickness of the proposed insulating layer was calculated from the volume of product on the surface of the electrode. The thickness of the insulating layer for the proposed ethanol product, 1,3–propandiol, was calculated to be 0.47 nm. As there is considered to be a mixture of products for the propanol and propan-2-ol systems, the calculated thickness is for these systems was estimated based on the average of the thickness calculated for each possible product, the actual thickness will depend on the amount of each of the products present and their orientation on the surface. The proposed insulating layer thickness for the propanol system was approximately 0.50 nm and for the propan-2-ol system approximately 0.60 nm.

The binding sites utilized in this process were assumed to be isolated due to the number of molecules per area produced for the Pb-ethanol system being reported as approximately 4×10^{18} molecules m^{-2} whereas the typical number of active binding sites on an electrode is 1.3×10^{19} sites m^{-2}. Assuming that each molecule of product occupies only one binding site on the electrode, the molecule therefore also effectively shields some of the electrode surface area surrounding the binding site.

The mechanism was required to account for:

- A reduction process, evident from the cyclic voltammograms,
- the presence of C–O bonds in the product, evident from the 1050 cm^{-1} transmittance peak in the FT–IR spectra, and,
- the effect on the electrochemical reduction of the potential scan rate and the electrode rotation rate observed in the cyclic voltammetry studies.

The proposed mechanisms, depicted in Figs. 4.10 (ethanol product), 4.15 (propanol products) and 4.20 (propan-2-ol products), and discussed in Sections 4.7.5 (ethanol), 4.8.1 (propanol), and 4.9.1 (propan-2-ol) contain several steps including:

Hydrogen evolution throughout the cathodic potential range used. Initial alcohol reduction resulting in an adsorbed species on the surface of the Pb electrode. Formation of a new C-O bond required to form the diol. Reaction of the adsorbed alcohol species with an adsorbed hydrogen species due to the H_2 evolution process. Formation of a new C-C chain, or removal of the adsorbed species by the addition of water.

The potential scan rate and electrode rotation rate dependencies were explained by the possible reaction of the adsorbed alcohol species with an adsorbed hydrogen species due to the H_2 evolution process. This reaction returns the alcohol to aqueous solution. The more efficiently that H_2 is removed, the less prevalent this process is and the more readily surface binding sites are filled.

The formation of a new C–C chain or removal of the adsorbed species by the addition of water provides another alcohol functional group. The step involving the formation of the new C–C bond would likely be the rate determining step. This step would be slow due to the proposed isolated binding sites and the probability of two adsorbed species meeting and reacting. The formation of the C–C bond relies on the chance meeting of the two adsorbed species on two binding sites close enough together to be within the reaction diameter to occur.

The mechanism for the propan-2-ol processes was more complicated than that of the ethanol or propanol processes. The proposed product does not match the initial alcohol reduction step where it would be expected that the reduction of the alcohol would lead to the molecule being adsorbed to the electrode through the secondary

carbon. To explain the products determined by FT–IR there must be some rearrangement of propan-2-ol to propanol. Propan-2-ol may rearrange when adsorbing (or while adsorbed) to the electrode, to a species adsorbed through a primary carbon rather than the secondary one. Concurrently, the reaction with the $Pb_{surf}–H_{ads}$ species returns propanol rather than propan-2-ol for two of the three possible reaction pathways. A rearrangement of propan-2-ol to propanol would lead to the products identified through the proposed propanol mechanism.

5.5 Future Work

Further work could be undertaken as a result of the findings presented in this thesis including:

- Identification of the Cu–alcohol system products
- Identification of the Sn–alcohol system products
- Full examination of the loss of the peak, C2, in the Pb–alcohol system with the change in anodic limit.
- Effect of Temperature.
- Effect of buffer composition.
- Effect of pH variation.
- Improvement of Pb product identification
    - Improve signal-to-noise ratio in FT–IR spectroscopy
        - Smaller volume cell
        - Multipass cell
    - Mass Spectrometry identification of Product
- Further examination of the propan-2-ol product mechanism

REFERENCES

1 J. Koryta, J. Dvorak, L. Kavan, *"Principles of Electrochemistry"*, 2nd Ed., John Wiley and Sons Ltd, New York, (1993)

2 G.H. Small, A.E. Minnella, S.S. Hall, *J. Org. Chem.*, Vol. 40, Iss. 21, (1975), p 3151-3152

3 R.D. Nimmagadda, C. McRae, *Tetrahedron Letters*, Vol. 47, (2006), p 5755-5758

4 J.B. Hendrickson, M. Singer, M. Saijat Hussoin, *J. Org. Chem.*, Vol. 58, (1993), p 6913-6914

5 Makoto Yasuda, Yoshiyuki Onishi, Masako Ueba, Takashi Miyai, Akio Baba, *J. Org. Chem.*, Vol.. 66 (2001), p 7741-7744

6 G. Horanyi, G. Vertes, P. Koenig, *Naturwissenschaften*, Vol. 60, Iss 11, (1973), p 519

7 Huang Shukun, Song Youqun, Zhang Jindong, Sun Jian, *J. Org. Chem.*, Vol. 66, (2001), p 4487-4493

8 M.C. Arévalo, J.L. Rodriguez, E. Pastor, *J. Electroanalytical Chem.*, Vol. 505, (2001), p 62-71

9 D.A. Skoog, F.J. Holler, T.A. Nieman, *"Principles of Instrumental Analysis"*, 5th Ed., Thomson Learning Inc., London, (1998)

10 J.L. Rodriguez, R.M. Souto, L. Fernández-Mérida, and E. Pastor, *Chem. Eur. J.*, Vol. 8, No. 9, (2002), p 2134-2142

11 R.M. Sauto, J.L. Rodriguez, G. Pastor, E. Pastor, *Electrochimica Acta*, Vol. 45, (2000), p 1645-1653

12 M.C. Arévalo, J.L. Rodriguez, A.M. Castro-Luna, E. Pastor, *Electrochimica Acta*, Vol. 51 (2006) p 5365-5375

13 A.J. Bard, L.R. Faulkner, *"Electrochemical Methods. Fundamentals and Applications"*, 2nd Ed., Wiley, New York. (2001)

14 J. Wang, *"Analytical Electrochemistry"*, 3rd Ed., John Wiley & Sons, Inc, New Jersey, (2006)

15 P.Y. Bruice, *Organic Chemistry*, 4th Ed. Prentice Hall: New Jersey, (2003).

16 R.G. Compton, C.E. Banks, *"Understanding Voltammetry"*, Imperial College Press, London, (2007)

17 E. Wiberg, N. Wiberg, A.F. Holleman, *"Inorganic chemistry."*, Academic Press, California, (2001)

18 H.F. Skinner, *Forensic Science International*, Vol. 48, (1990), p 128-134

19 T.S. Cantrell et. al., *Forensic Science international*, Vol. 39, (1988), p 39-53

20 G.K. Rollefson, W. Garrison, *J. Am. Chem. Soc.*, Vol. 62, (1940) p 588-590

21 H.K. Mitchel, R.J. Williams, *J. Am. Chem. Soc.*, Vol. 60, (1938), p 2723-2726

22 L.W. Trevoy, W.G. Brown, *J. Am. Chem. Soc.*, Vol. 71, (1949), p 1675-1678

23 Bohlman, Ferdinand, Enkelmann, Rudolf, Plettner, Wolfram, *Chemische, Berichte*, Vol. 97, Iss. 8, (1964), p 2118-2124

24 R.J. McMahon, K.E. Wiegers, S.G. Smith, *J. Org. Chem.*, Vol. 46, **(**1981), p 99-101

25 E.C. Ashby, A.B. Goel, *Tetrahedron Letters*, Vol. 22, Iss. 20, (1981), p 1879-1880

26 M. Gattrell, N. Gupta, A. Co. *Energy Conversion and Management*, Vol. 48, (2007), p 1255-1265

27 F. Köleli, T. Atilan, N. Palamut, A.M. Gizir, R. Aydin, C.H. Hamann. *J. App. Electrochem.*, Vol. 33, (2003), p 447-450

28 S. Pettinicchi, H. Baggetti, B.A. Lopez di Mishima, H.T. Mishima, J. Rodriguez, E. Pastor, *J. Arg. Chem. Soc.*, Vol. 91, Iss. 1/3, (2003) p 107-118

29 H. Kimuro, T. Kusayanagi, F. Yamaguchi, K. Ohtsubo, M. Morishita, *IEEE Transactions on Energy Conversion*, Vol. 9, Iss 4, (1994) p 732-735

30 K.C. Hester, P.G. Brewer, *Annu. Rev. Mar. Sci.*, Vol. 1 (2009), p 303-327

31 C.M. Rayner, *Org. Proc. Res. Dev.*, Vol. 11, **(**2007), p 121-132

32 S. Kaneco, N. Hiei, Y. Xing, H. Katsumata, H. Ohnishi, T. Suzuki, K. Ohta, *Electrochim. Acta*, Vol. 48, Iss. 1, (2002), p 51-55.

33 M. Azuma, K. Hashimoto, M. Hiramoto, M. Watanabe, T. Sakata, *J. Electrochem. Soc.*, Vol. 137, (1990), p 1772-1778

34 M. Jitaru, *Journal of the University of Chemical Technology and Metallurgy*, Vol. 42, Iss.4, (2007), p 333-334

35 T.E. Teeter, P. Van Rysselberghe, *J. Chem. Phys.*, Vol. 22 (1954) p 759-760

36 Y. Hori, R. Takahashi, Y. Yoshinami, A. Murata, *J. Phys. Chem. B*, Vol. 101, (1997), p 7075-7081

37 D.W. Dewulf, T. Jin, A.J. Bard, *J. Electrochem. Soc.*, Vol. 136, Iss 6, (1989), p 1686-1691

38 S. Wasmus, E. Cattaneo, W. Vielstich, *Electrochimica Acta*, Vol. 35, Iss 4, (1990), p 771-775

39 G. Kyriacou, A. Anagnostopoulos, *J. Electroanal. Chem.*, Vol. 322, (1992), p 233-

40 B. Jermann, J. Augustynski, *Electrochem. Acta*, Vol. 39, (1994), p 1891-1896

41 P. Friebe, P. Bogdanoff, N. Alonso-Vante, H. Tributsch, *J. Catal.*, Vol. 168, (1970), p 374-385

42 Y. Hori, H. Konishi, T. Futamura, A. Murata, O. Koga, H. Sakurai, K. Oguma, *Electrochemica Acta*, Vol. 50, (2005), p 5354-5369

43 C.M.A. Brett, A.M.O. Brett, "*Electrochemistry. Principles, methods and applications"*, Oxford University Press Inc., New York, (1993)

44 P.H. Rieger, "*Electrochemistry"*, 2nd Ed., Chapman and Hall Inc. New York, (1994)

45 V.G. Levich, "*Physiochemical Hydrodynamics"*, Prentice Hall, New Jersey, (1962)

46 P.T. Kissinger, W.R. Heinman, *"Laboratory Techniques in Electroanalytical Chemistry"*, 2nd Ed., Marcel Dekker Inc, New York, (1996)

47 O.D. Sparkman *"Mass Spectrometry Desk Reference"*, Global View Pub, Pittsburg, (2000)

48 E. De Hoffmann, V. Stroobant, *"Mass Spectrometry, Principles and Applications"*, John Wiley & Sons Ltd, London, (2007)

49 A.J. Bard, I. Rubinstein, *"Electroanalytical chemistry: a series of advances."*, Vol. 22, Marcel Dekker, Inc., New York, (2004)

50 C.N. Banwell, E.M. McCash, *"Fundamentals of Molecular Spectroscopy"*, 4th Ed., McGraw-Hill, London, (1994).

51 Personal discussion, RE: FT-IR spectroscopy, with Dr Mark Waterland, Massey University, (2012).

52 M. Nic, J. Jirat, B. Kosata, eds. (2006–). "faradaic current". *IUPAC Compendium of Chemical Terminology* (Online ed.). ISBN 0-9678550-9-8.

53 F. Scholtz (Ed.), *"Electroanalytical Methods Guide to Experiments and Applications"*, Springer, Berlin, (2002)

54 E.A. Khudaish, *"The electrochemical oxidation of hydrogen peroxide on platinum electrodes at phosphate buffer solutions"*, PhD Thesis, Massey University, New Zealand, (1999).

55 X. Li, A.A. Gewirth, *J. Raman Spectrosc.*, Vol. 36, (2005), p 715-724.

56 S. Nie, S.R. Emory, *Science*, Vol. 275, Iss. 5303, (1997), p 1102-1106

57 J. W. Schultze, D. Dickertmann, *Surf. Sci.*, Vol. 54, Iss. 2, (1976), p 489-505

58 A. Hamelin, *J. of Electroanal Chem. and Interfacial Electrochem.*, Vol. 165, Iss. 1-2, (1984), p 167-180

59 A. Hamelin, J. Lipkowski, *J. of Electroanal. Chem. and Interfacial Electrochem.*, Vol. 171, Iss. 1-2, (1984), p 317-330

60 J. Kestin, M. Sokolov, W.A. Wakeham, *J. Phys. Chem. Ref. Data.* Vol. 7, No. 3, (1978), p 941-948

61 K. R. Wehmeyer, M. R. Deakin, R.M. Wightman, *Anal.Chem.* Vol. 57, Iss 9, (1985), p 1913-1916

62 C. T. Kingzett, *J. Chem. Soc.*, Vol. 37, (1980), p 792-807

63 E. Marschall, *J.Chem.Eng.Data*, Vol. 35, (1990), p 375-381

64 H. Knapp, *Ber.Bunsen-Ges.Phys.Chem.*, Vol. 87, (1983), p 304-309

65 Personal discussion, RE: Mass Spectrometry, with Prof. Peter Derrick, Massey University, (2012)

66 J. Keeler, "*Understanding NMR Spectroscopy*." University of California, Irvine. (2007).

67 E. Smith, G. Dent, "*Modern Raman Spectroscopy: A Practical Approach.*", John Wiley and Sons, New Jersey, (2005)

68 Personal discussion, RE: SERS, with Dr Mark Waterland, Massey University, (2011).

69 C.P. Sherman Hsu, "*Handbook of Instrumental Techniques for Analytical Chemistry*", p 247-283

70 John M. Chalmers, "*Spectroscopy in process analysis*.", CRC Press LLC. (1999)

71 F. Muniz-Miranda, M. Pagliai, G. Cardini, R. Righini, *J. of Chem. Phys.*, Vol. 137, (2012), 244501 p 1-10

72 B.D. Smith, D.E. Irish, P. Kedzierzawski, J. Augustynski, *J. Electrochem. Soc.*, Vol. 144, Iss. 12, (1997), p 4288-4296

73 A. Kudelski, P. Kedzierzawski, J. Bukowska, M. Janik-Czachor. *Russian J. of Electrochem.*, Vol. 36, Iss. 11, (2000), p 1186-1188.

74 V. Sáez, M.D. Esclapez, P. Bonete, J. González-Garzía, J.M. Pérez, *Electrochimica Acta*, Vol. 53, (2008), p 3210-3217.

75 M.C. Arevalo, J.L. Rodriguez, E. Pastor. *J. of Electroanal. Chem.*, Vol. 472, (1999), p 71-82

APPENDIX 1

Reference FT-IR Spectra

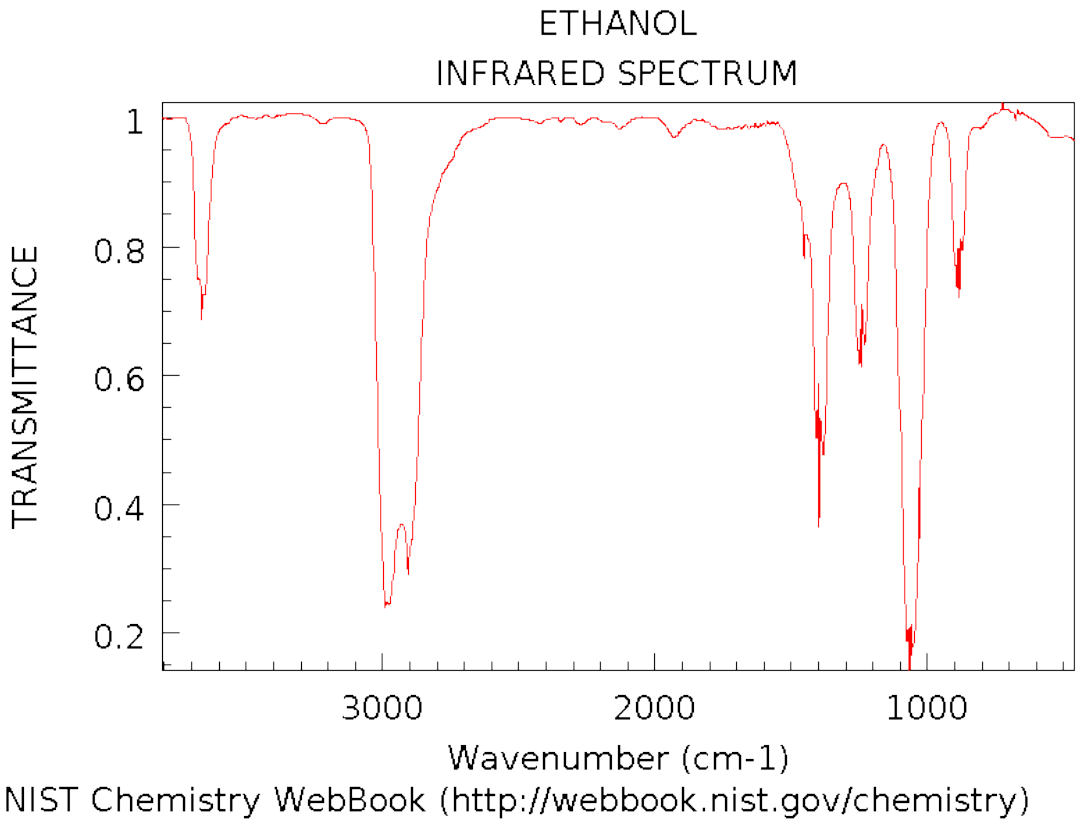

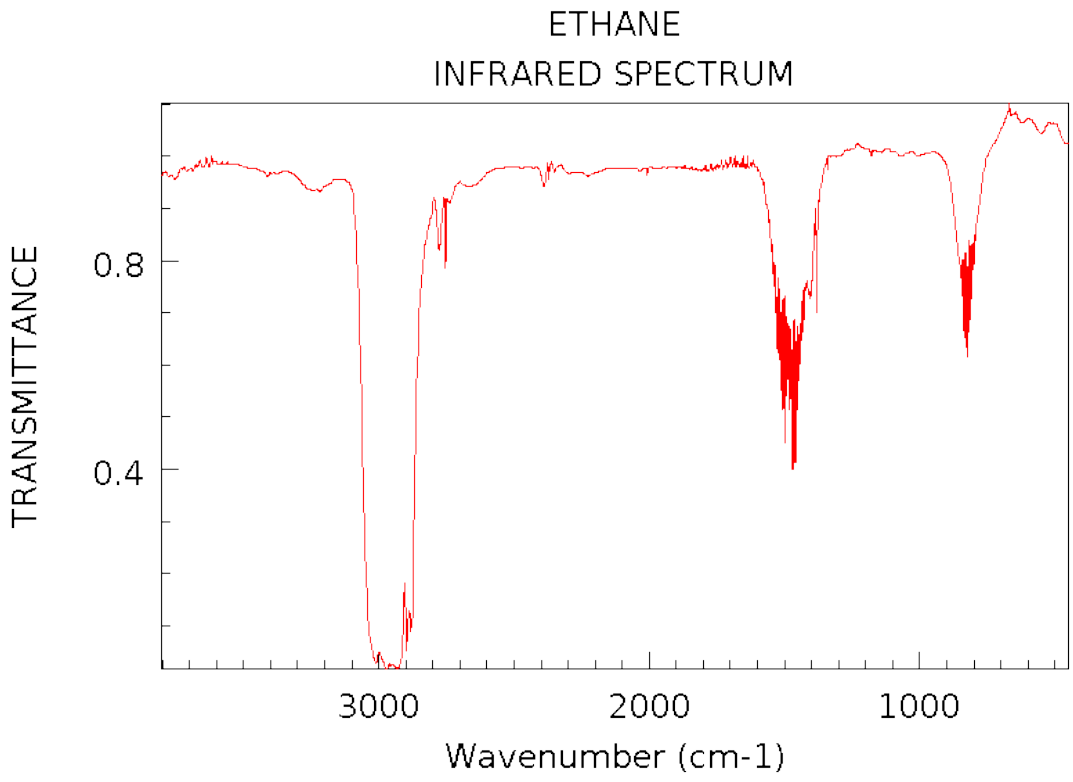

NIST Chemistry WebBook (http://webbook.nist.gov/chemistry)

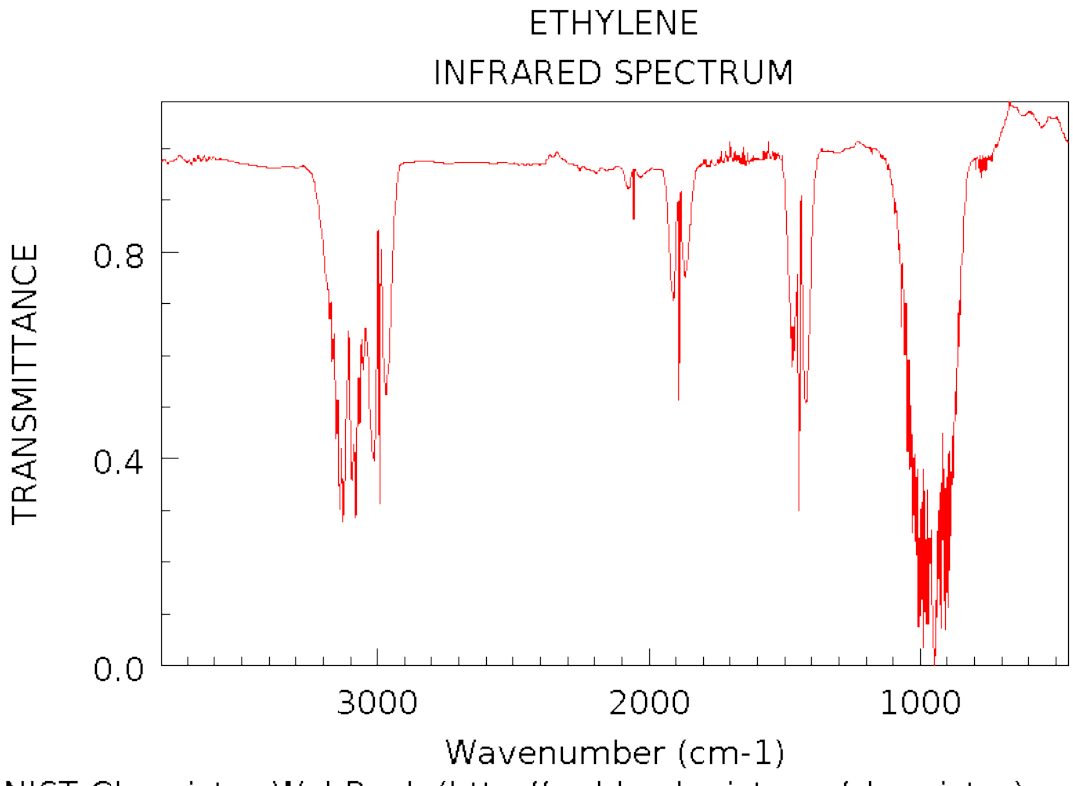

NIST Chemistry WebBook (http://webbook.nist.gov/chemistry)

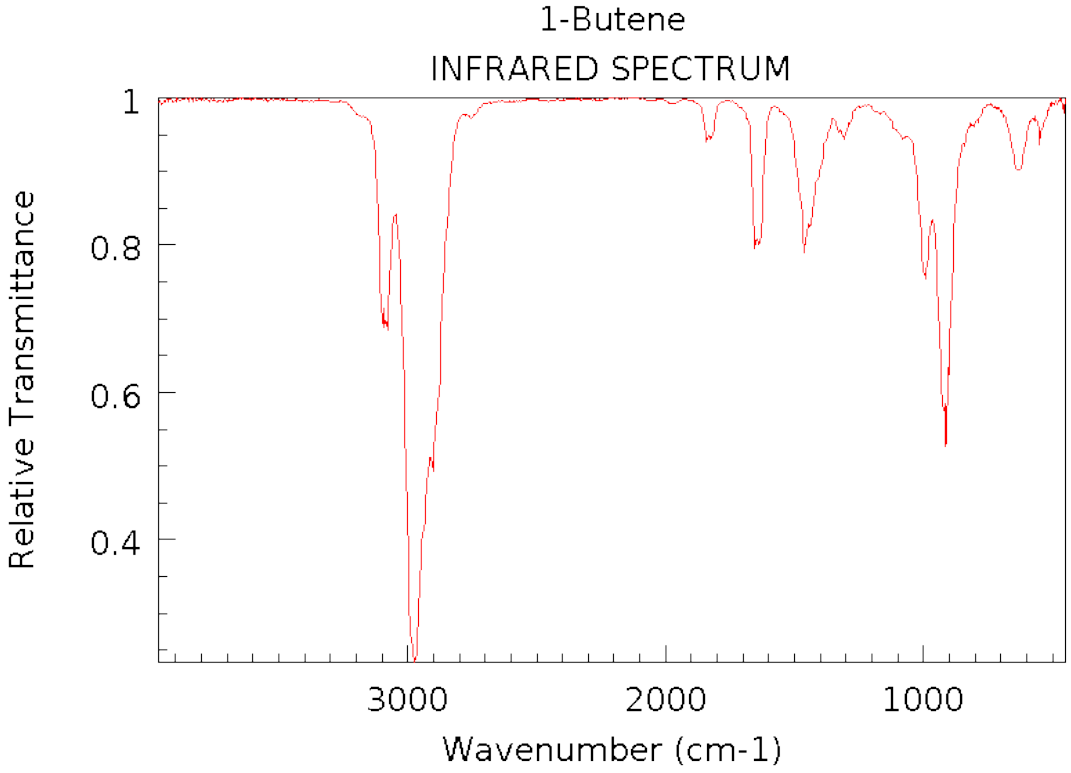

NIST Chemistry WebBook (http://webbook.nist.gov/chemistry)

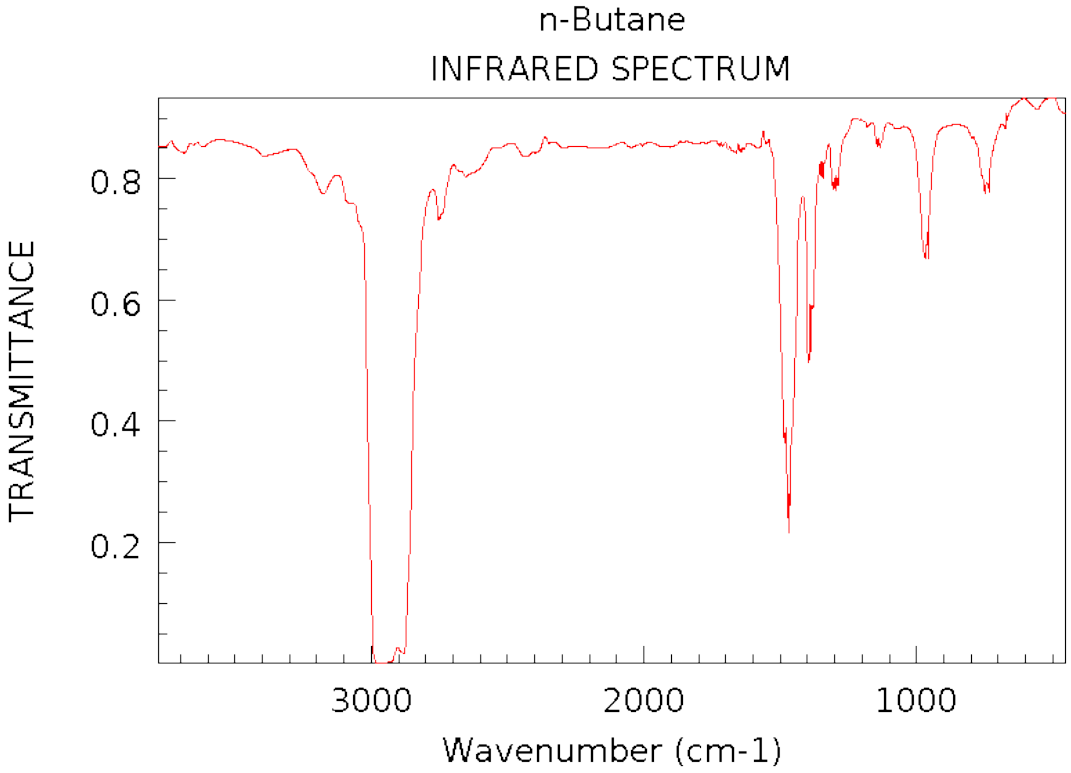

NIST Chemistry WebBook (http://webbook.nist.gov/chemistry)

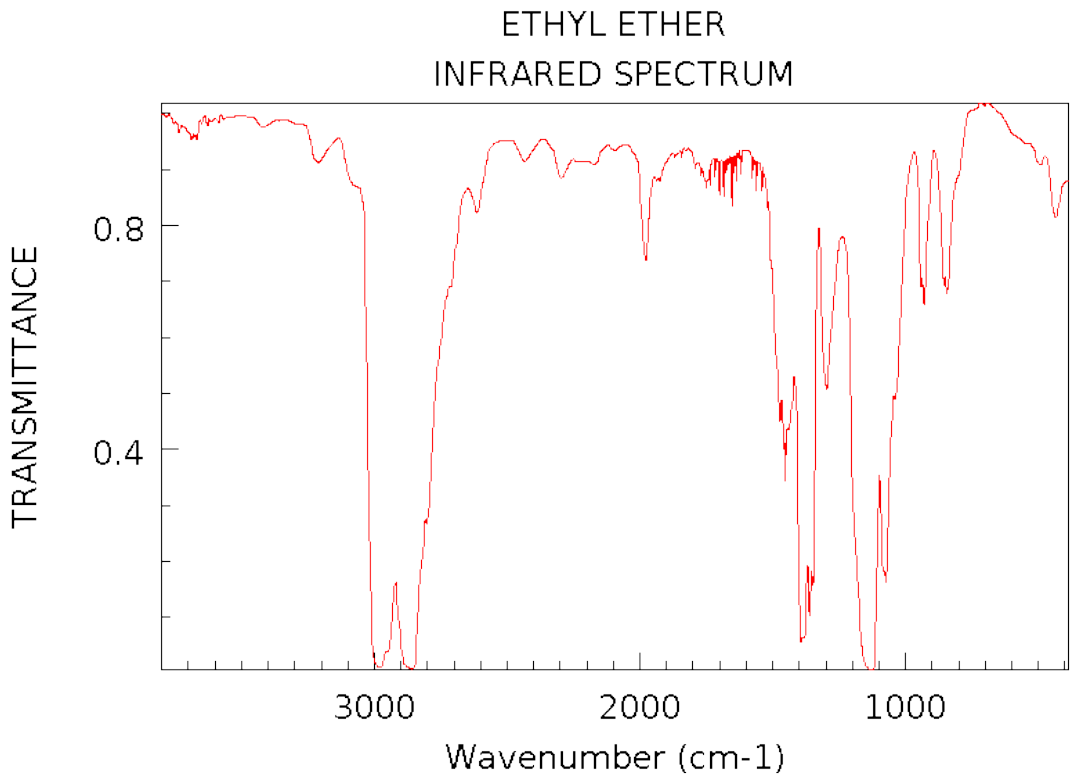

NIST Chemistry WebBook (http://webbook.nist.gov/chemistry)

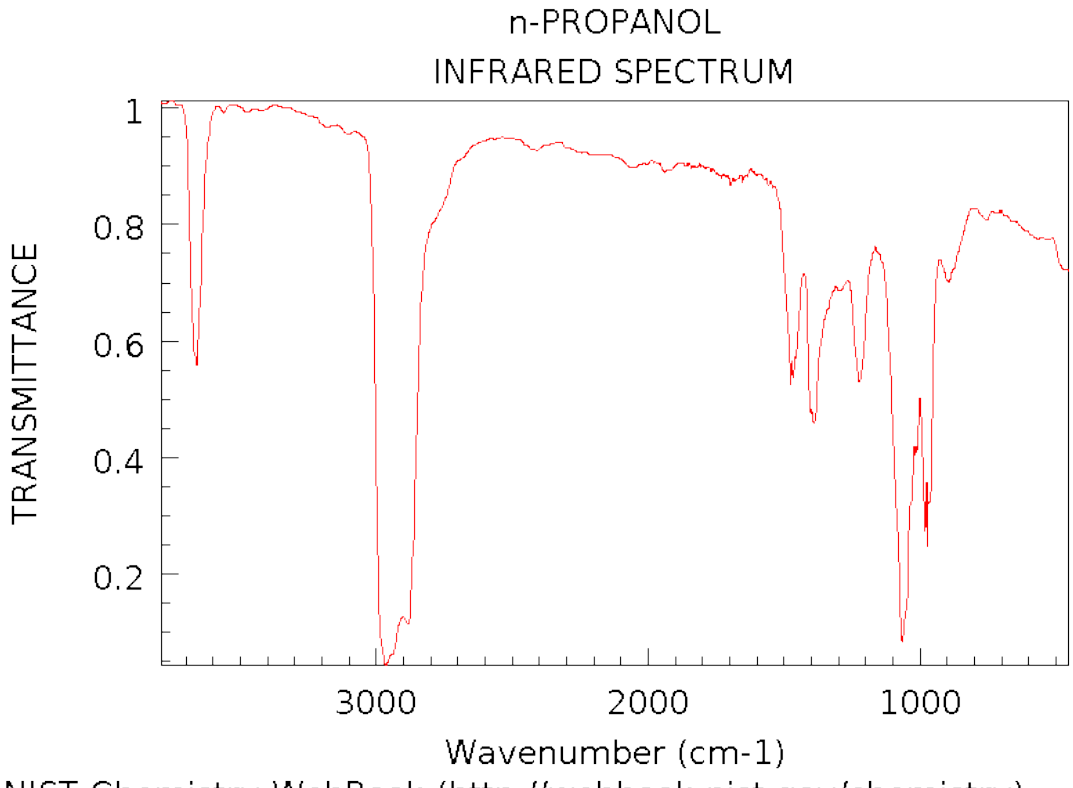

NIST Chemistry WebBook (http://webbook.nist.gov/chemistry)

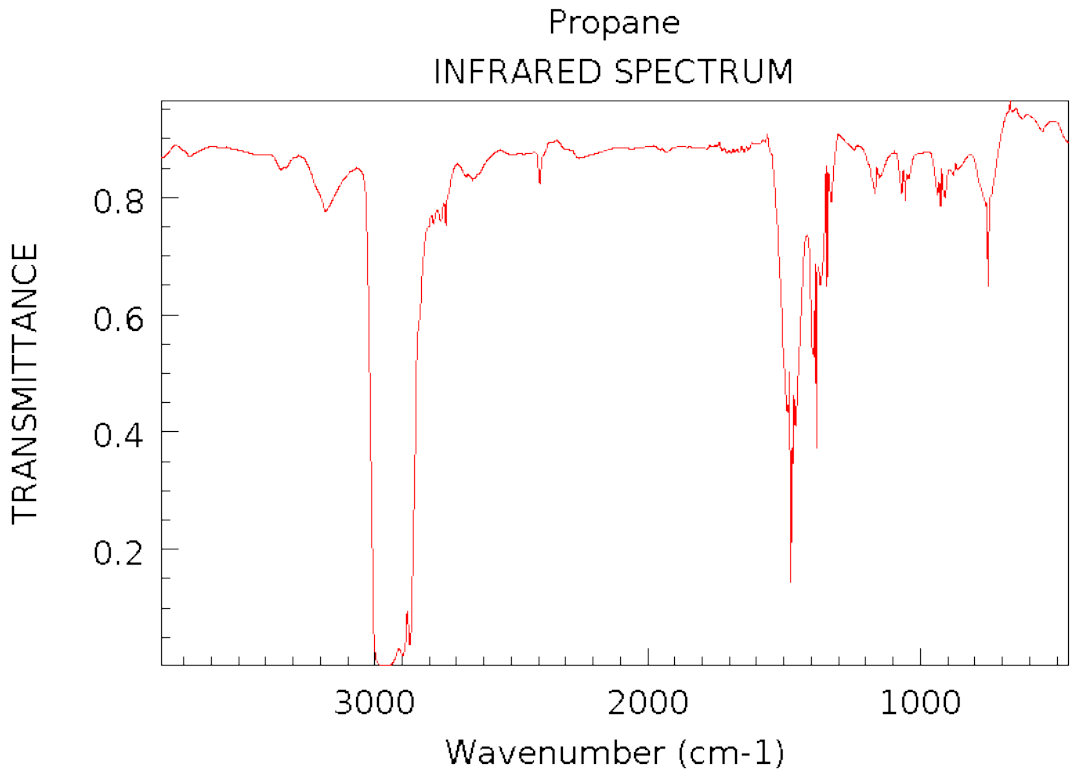

NIST Chemistry WebBook (http://webbook.nist.gov/chemistry)

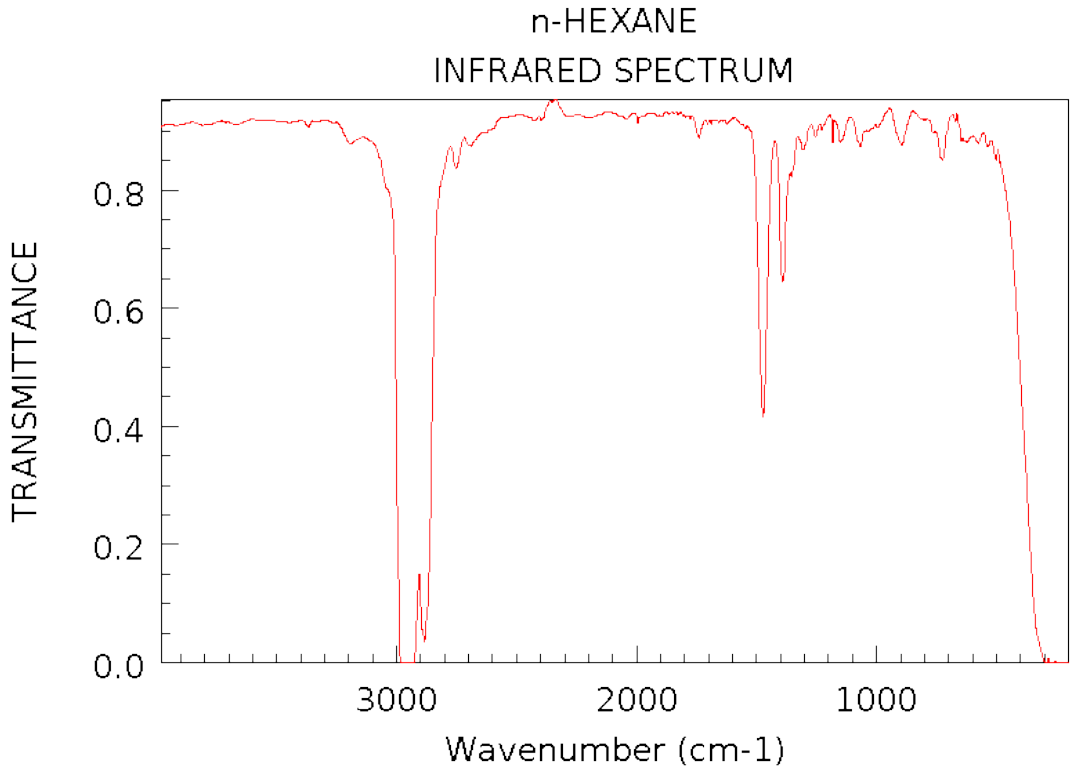

NIST Chemistry WebBook (http://webbook.nist.gov/chemistry)

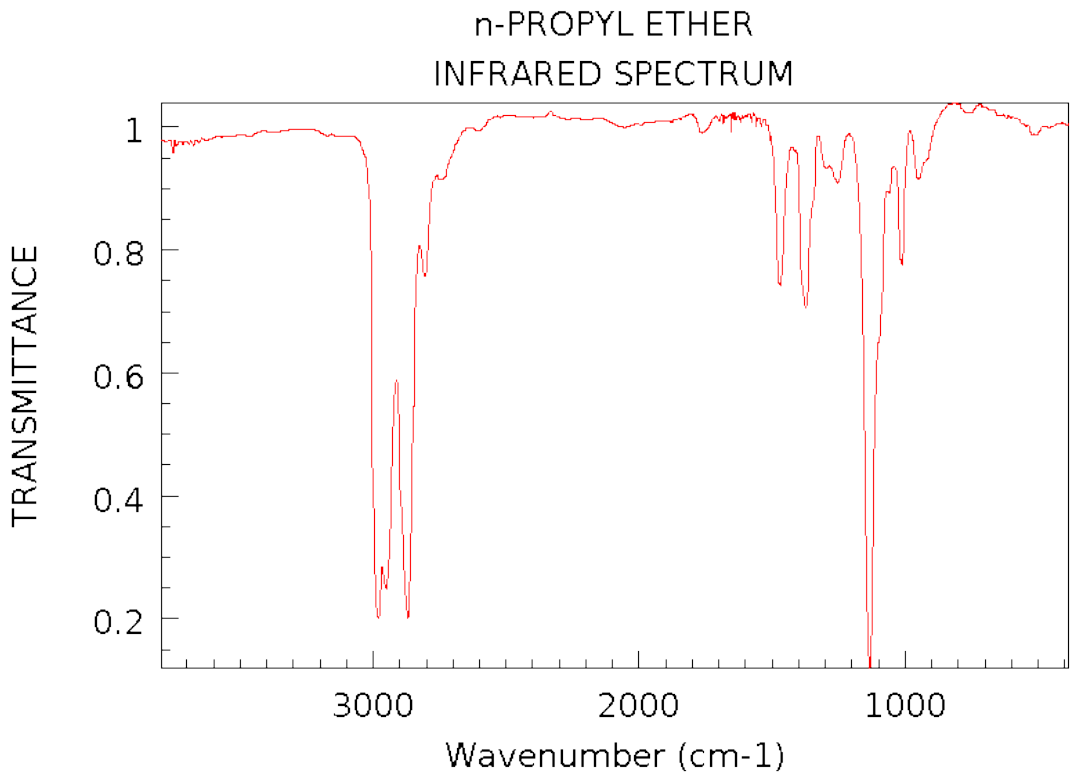

NIST Chemistry WebBook (http://webbook.nist.gov/chemistry)

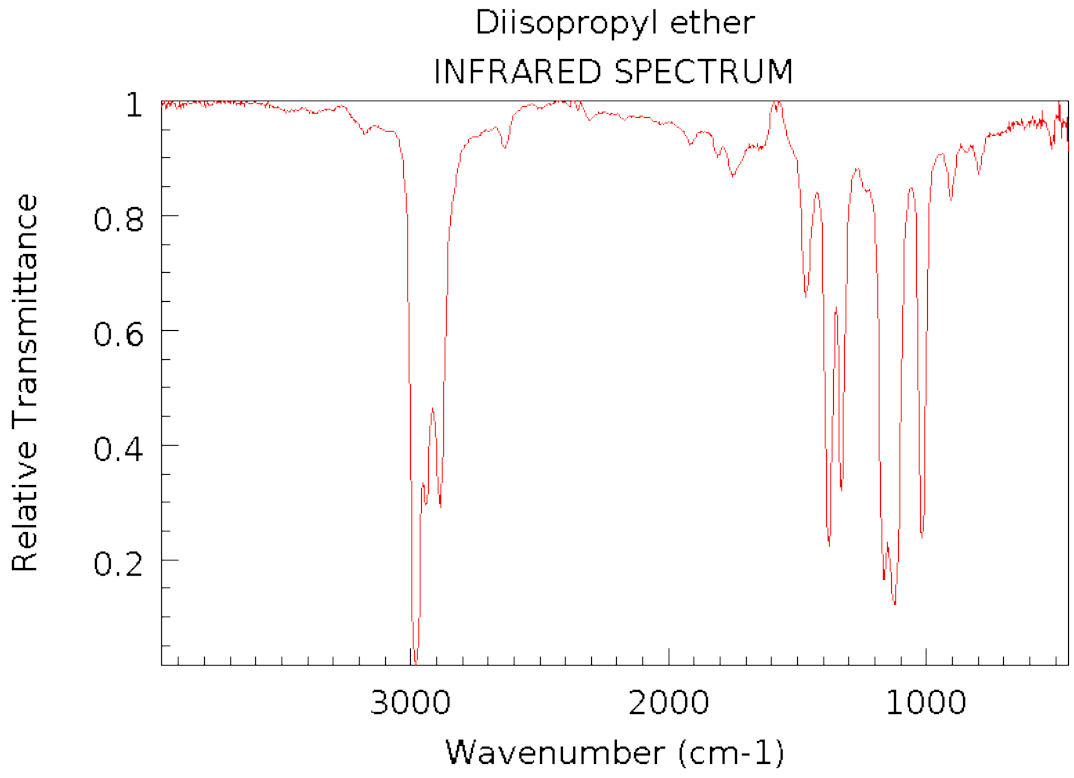

NIST Chemistry WebBook (http://webbook.nist.gov/chemistry)

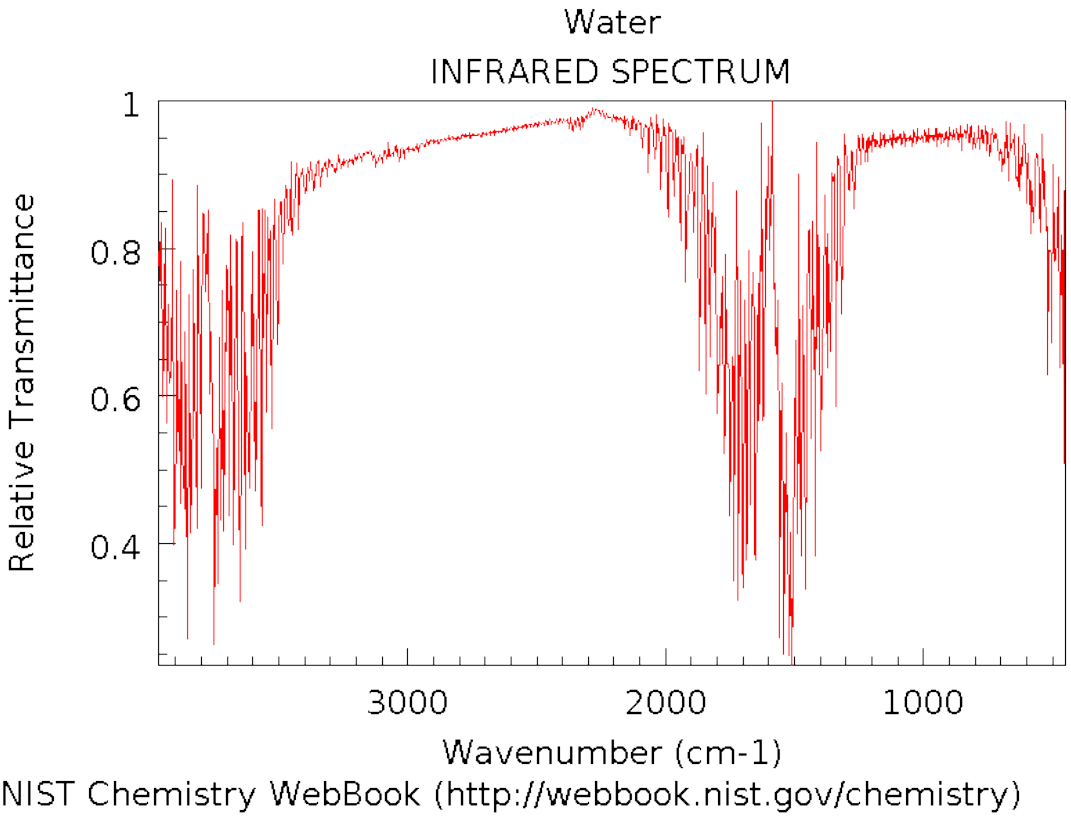
Water
INFRARED SPECTRUM
Relative Transmittance
1
0.8
0.6
0.4
3000
2000
1000
Wavenumber (cm-1)
NIST Chemistry WebBook (http://webbook.nist.gov/chemistry)